Design and Synthesis of Novel Conjugated Organic Semiconducting Materials for Organic Light Emitting Diodes

A Thesis Submitted

In Partial Fulfilment of the Requirements

for the Degree of

DOCTOR OF PHILOSOPHY

By

P. Gopikrishna

Roll No. 126153008

Centre for Nanotechnology

Indian Institute of Technology Guwahati

Guwahati-781039, Assam, India.

December, 2017

Dedicated to

My Parents and Teachers

INDIAN INSTITUTE OF TECHNOLOGY GUWAHATI

Centre for Nanotechnology

STATEMENT

I hereby declare that the matter embodied in this thesis is the result of investigations carried out by me at the Centre for Nanotechnology, Indian Institute of Technology Guwahati, Guwahati, India under the supervision of Prof. Parameswar Krishnan Iyer.

In keeping with the general practice of reporting scientific observations, due acknowledgement has been made wherever the work described is based on the findings of other investigators.

Guwahati P. Gopikrishna

December, 2017

INDIAN INSTITUTE OF TECHNOLOGY GUWAHATI

Centre for Nanotechnology

CERTIFICATE

This is to certify that Mr. P. Gopikrishna has been working under my supervision since December 2012. I am forwarding his thesis entitled "**Design and Synthesis of Novel Conjugated Organic Semiconducting Materials for Organic Light Emitting Diodes**" being submitted for the award of degree of Doctor of Philosophy of this institute. I certify that he has fulfilled all the requirements according to the rules of this institute and regarding the investigations embodied in his thesis, and this work has not been submitted elsewhere for a degree.

Guwahati — Prof. Parameswar Krishnan Iyer

December, 2017 — Supervisor

ACKNOWLEDGEMENT

My doctoral dissertation would not have come to a successful completion without help of several people. I take this opportunity to express my sincere gratitude to all of them.

First of all, I am extremely grateful to my thesis supervisor Prof. Parameswar Krishnan Iyer Sir who motivated and made me more confident and for his valuable suggestions, incisive thinking, and cogent advice throughout whole research period. His consistent encouragement, criticisms and painstaking planning have aided a long way for preparation of present thesis. His true scientific spirit, independence and self-reliance have helped me immensely to develop the quality of my research work. This feat was possible only because of the unconditional support provided by him. Whenever I went to his office, he has always made himself available to clarify my doubts despite his busy schedules. I always strongly believe that I am blessed by God to do my doctoral programme under his guidance and to learn from his research expertise. To be honest, whatever knowledge I have gained during my research period that is just because of him. Thank you very much Sir, for your unforgettable help and support. I am grateful to my supervisor and each and every member of the Interview panel for selecting me during PhD seat recruitment (2012).

I would like to thank my doctoral committee members Dr. A. S. Achalkumar, Prof. Aditya Narayan Panda and Prof. Pugazhenthi G, for their valuable suggestions and comments during all assessments of the Ph.D. program.

I take this time to express my sincere gratitude to my teachers Sudharshan Reddy, Rammohan Reddy, R. Chandrashekar Reddy, Ramesh, Dr. Pavan Kumar, Shivaprasad Achary, Swetha Gupta, Kondal Rao, Dr. Salva Reddy, Rammohan Rao, for their encouragement and motivation.

I owe my sincere thanks to my Chemistry lab mates Radhakrishna Ratha, Anamika Kalita, Akthar Hussain Malik, Arvind Sain Tanwar, Sayan Roy Chowdhury, M. Adil Afroz, Niranjan Mehar, Laxmi Raman Adil, Subrata Mondal, Maimur Hossain, Debasish Barman, Nehal Zehra, Rabindranath Garai, Retwik, Nasima Akhtar, Dr. Himani Kalita, Dr. Ekta Roy and device lab mates Ashish Singh, Dipjyoti Das, Anamika Dey, Rahul Narasimhan, Ramesh Babu Yathirajula, Indrani Medhi, Ritesh Kant Gupta, Nystha Baishya, Biki Teron, and Anwesha Choudhury, for their help and suggestions during my research period.

I would like to express my profound gratitude to my seniors in Chemistry lab Dr. Atul Kumar Dwivedi, Dr. B. Muthuraj, Dr. Suresh Vasimalla, Dr. T. Bheem Raju, Dr. Sameer

Hussain, Dr. Jupitara, Dr. Priyanka Dutta and from device lab Dr. Nimmakayala V. V. Subbarao, Dr. Murali Gedda, for their immense support, encouragement and help.

I would like to thank my friends B. Sc classmates G. Maheshwar Reddy, V. Omprakash, G. Harikrishna, Gangadhar Naidu, Rupendar Redy, Rakesh Naidu, Karunakar, Arun Kumar, Mahaboob, O. Ramulu, Anjan, Ramesh Sagar and M. Sc classmates K. Chandra Reddy, Krishna Rao, V. Ramesh, Narsing raj, Shankar, Devendar, N. Sharanya, Kumidini, Sarita and IIT-Guwahati friends Radhakrishna Gattu, Mood Mohan Chauhan, Vanaparthi Satheesh, Devulapally Mahesh, Ramanjaneyulu Unnava, Srinivas manne, Srinu Nagireddi, Upendar Reddy, Mohammad Shaad Ansari, Vamsi Krishna Sagar, Nibedita Behera, Karuna Mahato and Seniors Dr. Anil Kumar, Dr. Nani Babu Palakurthy, Dr. Krishna Chaitanya, Dr. Thalluri Kishore, Dr. Burgula Laxmi Narayana, Dr. Majji Ganesh, Dr. Kiran Indukuri, Dr. Santhosh Kumar Alla and Dr. Pradeep Sadhu, for their help throughout my life.

I would like to thank all the faculty members, research scholars, supporting staff of the Centre for Nanotechnology and Central Instruments Facility, IIT Guwahati for their kind cooperation in all respects.

No research is possible without financial support; I acknowledge DST, New Delhi DST-Max Planck Society, Germany and MHRD for fellowship for the entire period of the Ph.D. program.

In order to avoid missing any name, would like to pay gratitude to each and every emotional (human) being who helped in completing this work knowingly or unknowingly in the campus.

Finally, I want to convey my sincere gratitude to my parents and family members for their sustained help and encouragement in all my personal and academic ventures. I feel proud and blessed to have such parents my mother Mrs. Peddaboodi Nagamma garu and my father Mr. Peddaboodi Raghavulu garu. Especially my dear sisters Cheerla Sharada and Sangishetti Pusphalatha, I will be thankful to them and I promise I shall never forget their uncountable help and encouragement. Today, I am at this position that is just because of them. I do not find words to express my gratitude to them and they are always in my heart. I feel deeply indebted to them for whatever I have achieved so far.

P. Gopikrishna

Abstract

The whole thesis is divided into six chapters. Chapter 1 details short introduction of conjugated materials followed by organic light emitting diode principle and device fabrication. Chapters 2 and 3 provide synthesis of new color tuneable polymers based on polyfluorene and polycarbazole and PLED fabrication. Chapter 4 presents the procedure four novel AIEE active and dual state emitting materials synthesis and their photophysical properties. In Chapter 5, by utilizing the AIEE active and dual state emitting materials, white light emitting copolymers were synthesized and WPLEDs were fabricated. Chapter 6 provides the bridge induced AIEE active materials and photophysical properties. The contents of the individual chapters are mentioned as follows:

Chapter 1 details brief introduction of organic semiconductors materials, history of electroluminescence, basic structure of organic light emitting diode and its working principle. Recent developments conjugated materials including monomer and polymers and their OLED fabrication, followed by some most commonly used hole and electron transporting materials and brief introduction of AIE active materials and their device performances.

Chapter 2 provides a series of six new organic light emitting copolymers which were prepared from 9,9'-dioctylfluorene (DOF) and N-phenyl-1,8-naphthalimide (NPN) using palladium catalyzed Suzuki polymerization. The feed ratios of poly[2,7-(9,9'-dioctylfluorene)-co-N-phenyl-1,8-naphthalimide] (PFONPN) copolymers were 50 : 50, 65 : 35, 75 : 25, 90 : 10, 95 : 05 and 99 : 01, respectively. These copolymers have good thermal stability with an onset decomposition temperature (T_d) in the range of 340-405 °C and a glass transition temperature (T_g) in the range of 123-134 °C. All the copolymers are highly fluorescent and soluble in common organic solvents, such as chlorobenzene, chloroform, dichloromethane, THF, toluene, etc. allowing their processing from desired solvent. The electroluminescence (EL) properties of the copolymers were also studied by fabricating single layer devices with ITO/PEDOT:PSS/PFONPN/Ca:Al configuration. The photoluminescence (PL) and the EL spectra of the copolymers reveal that by changing the content of the NPN moiety in the polyfluorene main chain from 1 to 50 mol%, the emission color of the polymers can be tuned from blue to green with Commission International de l'Echairage (CIE) coordinates being (0.17, 0.22) to (0.24, 0.49). This color tuning can be attributed to the strong energy transfer from the fluorene to NPN unit in the polymer backbone. The devices made using these copolymers are

found to be very bright with PFONPN01 giving the highest brightness of 5236 cd m^{-2} with a luminous efficiency of 3.52 cd A^{-1}.

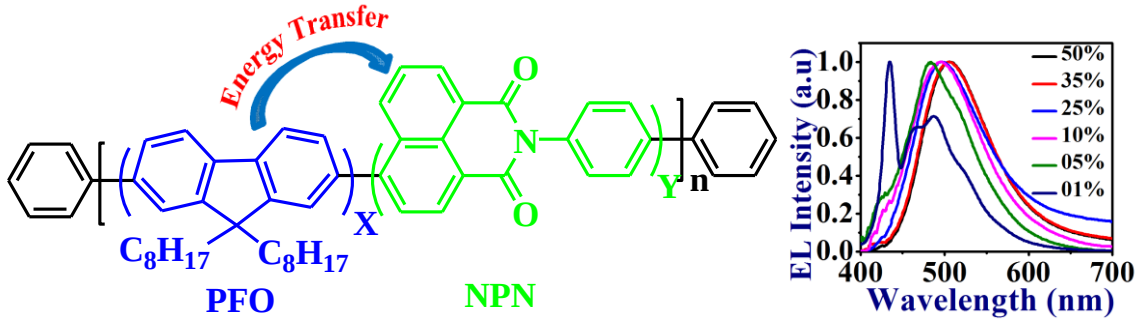

Chapter 3 mainly presents a series of novel color tunable donor-acceptor conjugated copolymers (CPs) which were developed from N-octylcarbazole (Cz-O) and N-phenyl-1,8-naphthalimide (N-PN) with a combination of feed ratios of Cz-O and N-PN (50:50, 65:35, 75:25, 90:10, 95:05 and 99:01). The copolymers exhibit desirable solubility in organic solvents, color tunability from blue to orange and desired electrochemical properties and are utilized for PLED fabrication. The new CPs are well characterized using NMR, FT-IR, TGA, DSC, UV-Vis and PL spectroscopy and their structural and photophysical properties are well correlated. The PL emissions of the CPs are red shifted steadily with increase in the N-PN content in the CP main chains. PLEDs are fabricated using these newly developed CPs as emissive layer (EML) in ITO/PEDOT:PSS/PCzN-PN/BCP/LiF/Al configuration. Among all devices, PLEDs using PCzN-PN05 copolymer as EML is found to give the best device performance with maximum brightness of 309 cd m^{-2} and 0.451 cd A^{-1} luminous efficiency.

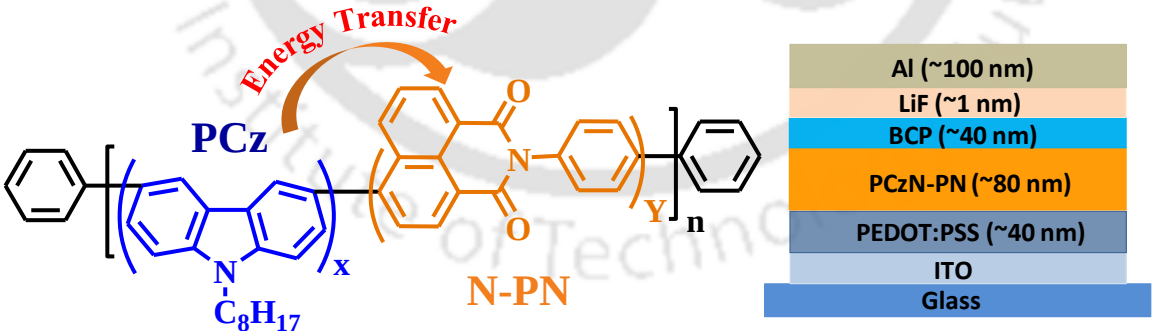

Chapter 4 discusses the observation of unusual aggregation-induced emission enhancement (AIEE) phenomenon in the deep red wavelength region, dual state emission, and intramolecular charge transfer of dibenzofulvene (DBF) derivatives is described. These consist of a series of newly synthesized donor-acceptor based M-DBF molecules (DT1, DT2, DP1, and DP2) with their cores comprising DBF molecules. Two luminogens with thiophene-substituted at the ninth position of DBF, viz. DT1 and DT2, displayed

AIEE with predominant J-type aggregation due to the effect of intramolecular planarization and formation of nanoparticles in the aggregated state. In the DP1 and DP2 luminogens, an extra phenyl ring was inserted at the ninth position of DBFs (between thiophene and DBF) that resulted in a blue-shift (~60 nm) as compared to the DT derivatives and exhibited a unique dual state emission with good quantum yields. This additional phenyl moiety reduces the effective conjugation length toward 2,1,3-benzothiadiazole from DBF and simultaneously interrupts the head to tail interaction and also prevents the J-type aggregation. All the four luminogens exhibited distinctive solvent-dependent photoluminescence (PL) behavior (solvatochromism) because of the efficient intramolecular charge transfer. The DT2 and DP2 luminogens showed heavy atom effect due to the presence of two bromine atoms. The HOMO and LUMO values of the luminogens were estimated by cyclicvoltagrams (CV) and DFT calculations.

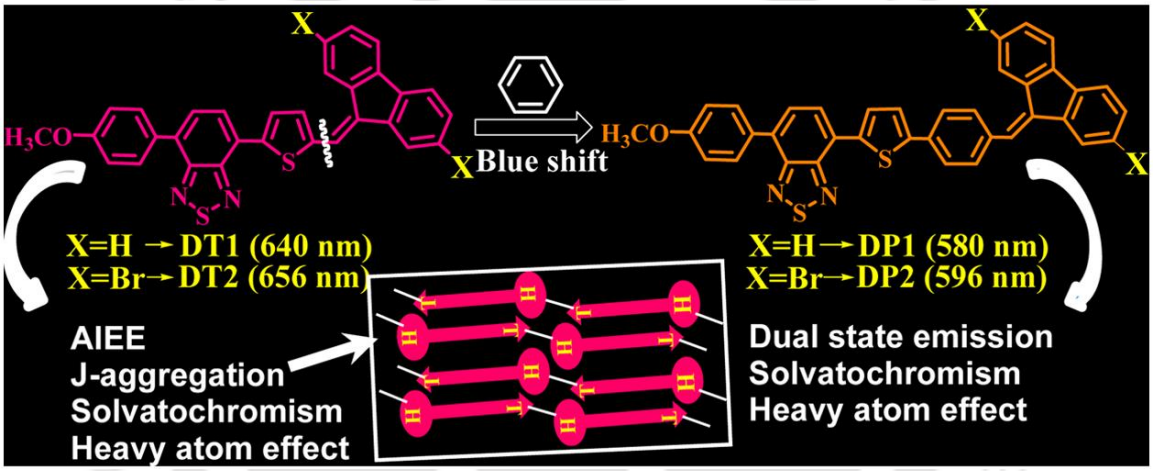

Chapter 5 highlights synthesis and WPLED fabrication of new electroluminescent copolymer based on polyfluorene and aggregation-induced emission enhancement (AIEE) active or dual state emitting, mono-substituted dibenzofulvene (M-DBF) derivatives, i.e. 4-(5-fluoren-9-ylidenemethyl- thiophen-2-yl)-7-(4-methoxy-phenyl)-benzo[1,2,5]-thiadiazole (DT) or 4-[5-(4-fluoren-9-ylidenemethyl-phenyl)- thiophen-2-yl]-7-(4-methoxy-phenyl)-benzo[1,2,5]thiadiazole (DP), as orange/red fluorophores into polyfluorene (PF) main chain is demonstrated. The mol % of these M-DBF monomer based small π-system has been optimized as low as 0.0003, 0.0006, and 0.001% in the poly[2,7-(9,9′-dioctylfluorene)- co-4-(5-fluoren-9-ylidenemethyl-thiophen-2-yl)-7-(4-methoxy-phenyl) benzo[1,2,5]thiadiazole (WDT) and poly[2,7-(9,9′- dioctylfluorene)-co-4-[5-(4-fluoren-9-ylidenemethyl-phenyl)-thiophen-2-yl]-7-(4-methoxy-phenyl)-benzo[1,2,5] thiadiazole (WDP) copolymers, respectively. Here, the utilization of "dual emission" peaks from PFO and M-DBFs in the blue and orange region that enabled the

fabrication of bias-independent WPLEDs which is fundamentally very important and highly challenging in the case of linear polymers has been reported. These copolymers showed excellent solubility in organic solvents viz. $CHCl_3$, THF, toluene, p-xylene, etc. The synthesized copolymers were characterized by UV-vis and photoluminescence (PL) spectroscopy, and WPLEDs with ITO/PEDOT:PSS/WDP or WDT/TPBi/LiF/Al configurations were also fabricated to study their electroluminescence (EL) properties. Partial energy transfer has been achieved by adjusting the PFO and DT or DP concentrations in the single polymer main chain leading to the white emission in a facile manner. The copolymers WDP-1 and WDT-1 gave saturated white emission with CIE coordinates of (0.31, 0.33) and (0.35, 0.34) between 8-14 voltages and exhibiting excellent voltage independent emission. The highest luminous efficiencies of 7.82 and 4.57 cd A^{-1} were achieved for WDP and WDT polymers with the highest brightness values of 9753 and 7436 cd m^{-2}, respectively.

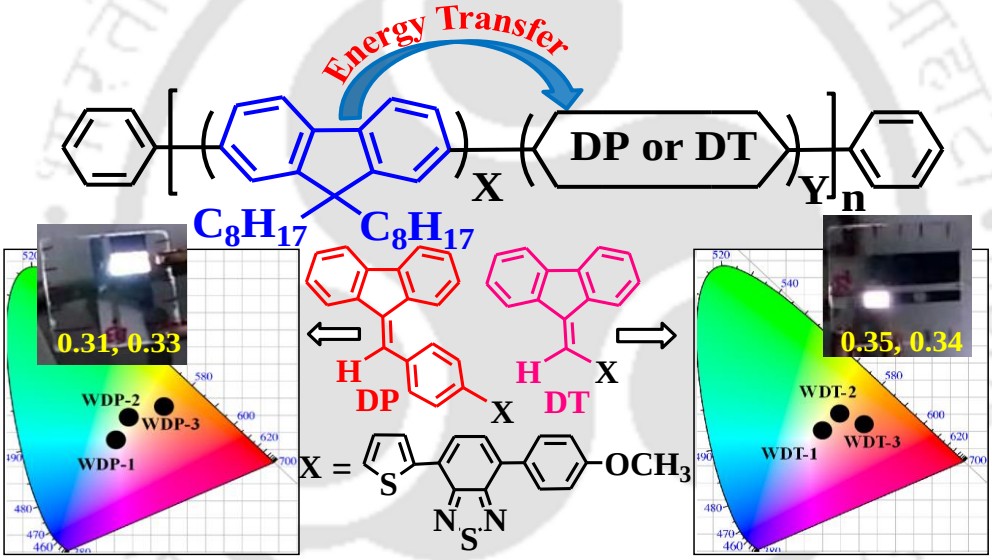

Chapter 6 provide synthesis of AIEE active and inactive materials based on 1,8-naphthalimide (NC) and mono-substituted dibenzofulvene. Two luminogens were substituted by thiophene bridge (DT1NC and DT2NC) while the two other luminogens substituted by phenyl bridge (DP1NC and DP2NC) between NC and dibenzofulvene (DBF) units. This minor structural modification makes noteworthy changes in the photophysical behavior. DT1NC and DT2NC displayed aggregation induced emission enhancement (AIEE) behaviour. They also showed orange and red emission (575 nm and 602 nm), respectively with large bathochromic shifts (35 nm and 112 nm) and high quantum yields (84.10% and 65.65%) in the aggregated state due to ladder type J-aggregation. DP1NC exhibited weak AIEE behaviour in blue region while DP2NC

showed AIE inactive nature due to the strong C-H···π intermolecular interactions. All luminogens showed positive solvatochromism caused by intramolecular charge transfer (ICT). The DT2NC and DP2NC luminogens were substituted with two extra bromine atoms at 2,7 positions of DBF moiety, but unexpectedly the DT2NC showed strong heavy atom effect. All luminogens displayed excellent thermal stabilities. Theoretical and experimental HOMO and LUMO energy levels were estimated by the density functional theory and cyclic voltammetry, respectively.

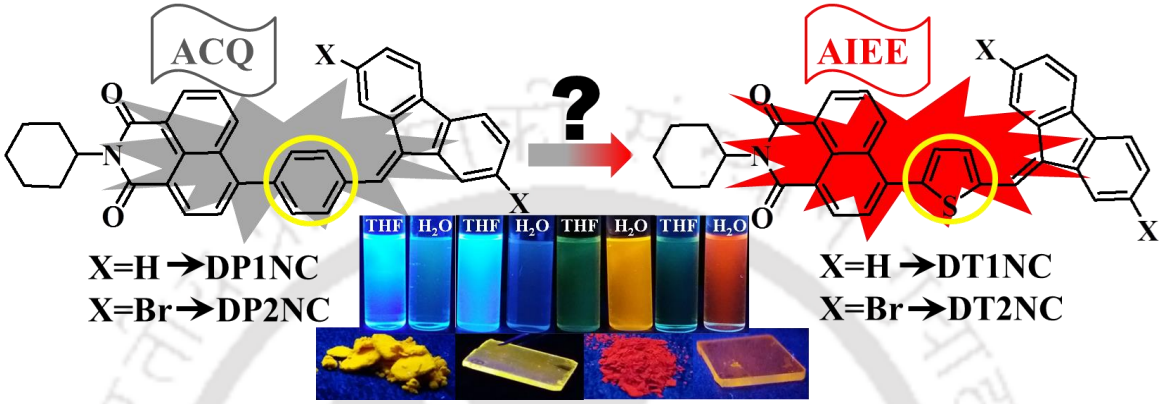

Contents

List of Figures

List of Tables

List of Symbols and Abbreviations

AIE	Aggregation induced emission
AIEE	Aggregation induced emission enhancement
ACQ	Aggregation caused quenching
BT	Benzothiadiazole
Cz-O	N-octylcarbazole
CIE	International commission on illumination
CV	Cyclic voltammetry
DBF	Dibenzofulvene
DSC	Differential scanning calorimetry
DLS	Dynamic light scattering
DFT	Density functional theory
DMSO	Dimethyl sulfoxide
d	Doublet
dd	doublet of doublet
E_g	Band gap
EL	Electroluminescence
eV	Electron Volte's
FE-SEM	Field emission scanning electron microscopy
FWHM	Full width at half maximum
GPC	Gel permeation chromatography
HOMO	Highest Occupied Molecular Orbital
Hz	Hertz
ICT	Intramolecular charge transfer
ITO	Indium tin oxide
LUMO	Lowest unoccupied Molecular Orbital
M_n	Number-average molecular weight
M_w	Weight average molecular weight
MHz	Megahertz
m/z	Mass to charge ratio
M	Multiplet
mA	Milli ampere
Mbar	Millibar

MALDI	Matrix-assisted laser desorption/ionisation
NPN	N-phenayl 1,8-naphthalimide
nm	Nanometer
NMR	Nuclear magnetic resonance
OLED	Organic light emitting diode
PLED	Polymer light emitting diode
PCzs	Polycarbazole
PFO	Polyfluorene
PL	Photoluminescence
PEDOT:PSS	poly (3,4-ethylendioxythiophene):poly(styrenesulfonate)
PDI	Polydispersity index
Q	Quartet
Rpm	Rotation per minute
RIR	Restriction of intramolecular rotation
s	Singlet
TD-DFT	Time dependent density functional theory
TPE	Tetraphenylethelene
THF	Tetrahydrofuran
TOF	Time of flight
TGA	Thermogravimetric analysis
TEM	Transmission electron microscopy
T	Triplet
TBAP	Tetrabutyl ammonium perchlorate
T_d	Degradation temperature
T_g	Glass transition temperature
T_m	Melting point
T_c	Crystallization temperature
UV-vis	Ultraviolet-visible
WPLED	White polymer light emitting diode
µm	Micrometer
Φ_F	Fluorescence Quantum yield

Chapter-1

Introduction

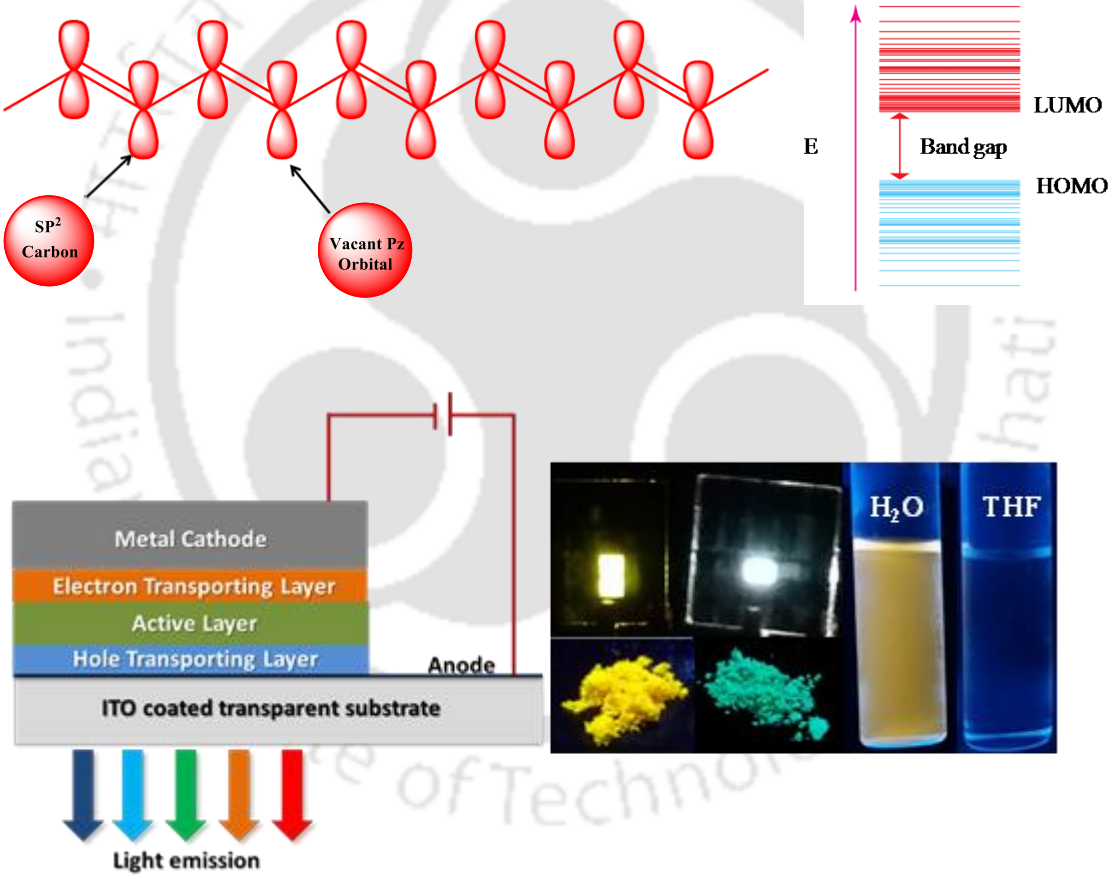

1.1. Introduction to Organic Semiconductors

Organic semiconducting materials have been used for different electronic applications since the mid-twentieth century. However, in 1977 the discovery of unusual metallic conductive properties of halogen doped polyacetylene sparked an enormous interest in this new class of organic materials.[1] Upon halogen doping, the stable charge transfer π complexes are generated and these complexes are responsible to obtain controllable/adjustable electrical properties.[2] For this noble breakthrough of the conducting organic materials, the Nobel Prize in chemistry was awarded to Alan Jay Heeger, Alan MacDiarmid and Hideki Shirakwa in 2000.[3, 4] Until then it was believed that polyacetylene, the traditional organic material was an insulator and exhibited very poor conductivity. Upon doping, the electrons are either removed or added by strong reducing or oxidizing agents, which are highly helpful to form polaron states (free electrons and free holes are called negative polarons and positive polarons, respectively) that leads to increase in the electrical conductivity of polyacetylene. The conductivity of the organic semiconducting materials is different from the conventional crystalline inorganic semiconducting materials, such as Si, GaAs and InP. The pure organic materials possess weak van der Walls forces between the molecules, unlike inorganic semiconducting materials exhibiting stronger coordinate/covalent bonds. Therefore, organic materials exhibit low melting point and show poor conductivity as compared to that of inorganic materials. It was quickly recognized that the key feature of such conjugated polymeric materials containing alternate double and single bonds results into a π-conjugated system. An important property of such system is that upon excitation, the π-electrons may become extremely mobile in the polymer backbone and improve the charge carriers. This creates a relatively small energy band gap forwarding the appearance of both metallic and semiconducting properties. In conjugated polymeric materials, the band structure can be generated by the combination of π* antibonding orbitals and π bonding orbitals. The bonding orbital levels and antibonding orbital levels can also be called as valence band and conduction band, respectively. Carbon atom (Z=6) has electronic configuration of $1S^2 2S^2 2P^2$. In conjugated materials, 2S, 2Px and 2Py orbitals of carbon are combined through SP^2 hybridization in trigonal planar form and forms covalent bond between neighboring atoms. This strong covalent bond is called a Sigma (σ) bond, which forms the backbone of the chain. Electrons in this orbital are highly localized between the atoms. The energy differences between the low energy (σ) state and the excited (σ*) state

is quite large and well beyond the visible spectral range. Thus, the electronic properties related with this bond are that of an insulating material. The fourth orbital (2Pz) does not take part in this hybridization and is perpendicular to the σ bond. Electrons in this bond are delocalized to the carbon atoms and become more mobile. The coupling of two degenerate 2Pz orbitals of adjacent carbon atoms generates two new energetically different orbitals called bonding (π) which is lower in energy compared to original 2Pz orbital and anti-bonding (π*) which is higher in energy compared to the isolated 2Pz orbital. Because of lower energy of the bonding (π) orbital both of the 2Pz electrons will occupy this orbital, leaving the anti-bonding (π*) orbital devoid of electrons. In this case, the bonding orbital is the highest energy occupied molecular orbital (HOMO), while the anti-bonding orbital is the lowest unoccupied molecular orbital (LUMO). In addition, the energy difference between π orbital and π* orbital is known as the band gap, which has absorption in the visible range and the delocalized nature of the π orbital is responsible for semiconductor properties. Conjugated polymers (CPs) are chain type structures which consist of alternating single and double bonds. CPs can show excellent optoelectronic properties due to the excess amount of charges on the polymer, and these charges can easily move throughout the conjugated main chain. The simplest CP is polyacetylene

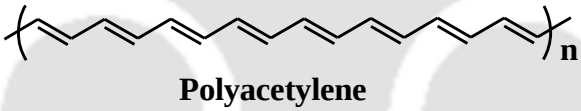

Figure 1.1: Chemical structure of polyacetylene

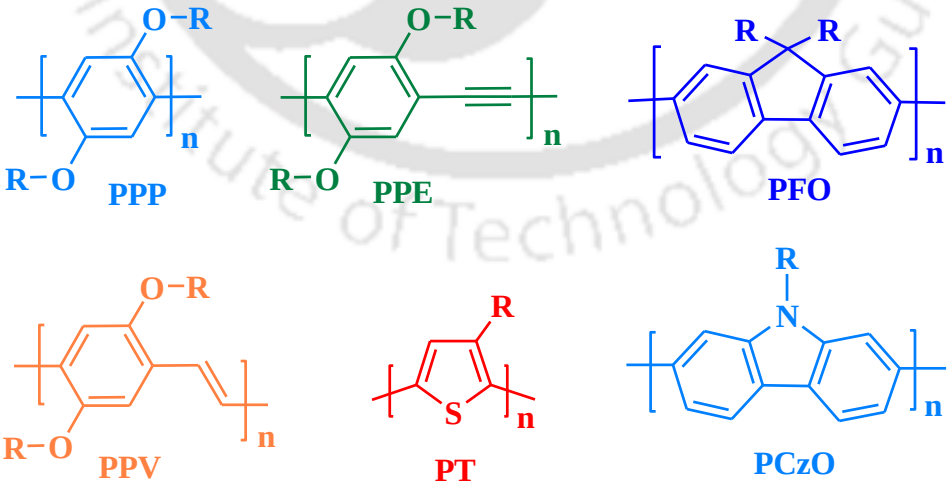

Figure 1.2: Examples of Conjugated Polymers: Poly(para-phenylene) (PPP), Poly(para-phenylene ethynylene) (PPE), Poly(para-phenylene vinylene) (PPV), Polyfluoreneoctyl (PFO), Polythiophene(PT), Polycarbazoleoctyl (PCzO)

is shown in Figure 1.1. Generally, neutral CPs are wide bandgap organic semiconductors and they show excellent absorption or emission properties at the band edge. The bright emission mainly depends on the delocalization of polarization of the electronic structure. By chemical doping of the CPs, the photophysical and electrochemical properties can be improved and as shown in the Figure 1.2, many derivatives of CPs are synthesized and investigated. Conjugated organic materials entail great advantages as compared to the inorganic counterparts, such as structural modifications, low cost, less time and ease of fabrication, flexibility and less weight.[5, 6] Organic semiconducting materials can be used in wide range of electronic applications, such as organic light emitting diodes (OLEDs),[7, 8] organic field-effect transistors (OFETs),[9-12] organic photovoltaic devices (OPVs)[13-15] and bio-sensors.[16] There are certain challenges to be met in terms of high photoluminescence (PL) quantum yields mainly in solid state and environmental stabilities of the organic semiconductors. To overcome these difficulties during the past few decades, this subject has been of intensive academic and commercial interest. In the later sections, the main discussion consists of the development of organic semiconducting materials for the fabrication of efficient OLEDs/PLEDs.

1.2. Invention of Light Bulb

The incandescent bulb has been discovered by Thomas A. Edison in 1880. This is the first artificial light that came into everyday lives of people. The mechanism of the Edison's bulb is thermal radiation where a thin filament is heated till the point of incandescence by passing an electric current through it. However, the efficiency of the incandescent bulb is very poor, converting only 5% of the applied energy into visible light and remaining 95% is emitted as heat in the range of infrared.[17] In 1937, fluorescent tube has been demonstrated as an alternate lighting element for the incandescent bulb. The mechanism of a fluorescent tube is similar to that of an incandescent bulb. In a fluorescent tube, an electric current is passed through an inert gas containing a small amount of mercury and it excites the mercury which consequently emits UV light. The phosphors that is coated on the surface of the fluorescent tube can convert UV light to visible light. The efficiency of fluorescent tubes is very high as compared to that of incandescent light. The fluorescent lamps have several drawbacks, i.e. even small amount of mercury is very toxic if released in to the environment and if not carefully disposed. Considering the low efficiency of incandescent light bulbs, and the low color-rendering index (CRI) of the fluorescent lamp, it is evident that there is the potential for a

substantial energy saving by switching to a highly energy efficient, large area and eco-friendly lighting solutions. In the past few decades a new research field has emerged referred to as solid-state lighting (SSL). Unlike conventional incandescent bulbs and Compact fluorescent lamps (CFLs), SSL uses a semiconductor light emitting diode (LED), where light is produced directly by the principle of electroluminescence (EL). The first LED emitting visible light was demonstrated in 1962[18] and since then the technology has evolved rapidly. Only in 1993, the first practical blue emitting LED was demonstrated by Shuji Nakamura[19] paving the way for the development of white emitting LEDs. Efficient semiconducting LEDs have the ability to substitute the incandescent and fluorescent lamps. LEDs are environmental friendly, not having any Hg vapors and more efficient than that of fluorescent and incandescent lamps. Also, they have unique properties, i.e. they can electrically control emission properties.

The OLED is a special class of LEDs where the active layer is an organic material having semiconducting properties.[20-23] Since organic materials can be solution processed, OLEDs are relatively easy to fabricate and promises of enabling inexpensive large area lighting, devices and displays. Furthermore, since OLEDs are broadband emitters, they have the ability to exhibit a very good CRI, which is not the case for cheap inorganic LEDs.

1.3. Organic Light Emitting Diode (OLED)

The simple OLED consists of several organic thin films deposited between two electrodes. The strong light emission can be realized by applying the electrical current to the device. OLEDs are unconventional, large area thin films, nearly two-dimensional devices. They are distributed light sources, distinctly different from point sources, such as light bulbs. Also, OLEDs can be operated at very low voltages, (3-5 V). Therefore, the introduction of OLEDs as sources of light for general lighting applications will cause a major achievement in the lighting industry. While significant research is still required, OLEDs will soon realize the efficiency to compete directly with incandescent sources.

1.4. History of Electroluminescence

Electroluminescence (EL) is the emission of light from material when a potential energy is applied. A. Bernanose and co-workers discovered EL in the organic materials for the first time in early 1950s[24] in acridine orange. This material was either deposited or spin-coated by dissolving in cellulose to make thin films. Also in 1960, M. Pope and his coworkers brought forward the importance on the work functions of the contacts for

efficient hole and electron injection. In addition, the same group also reported EL in a small molecule anthracene crystal with a thickness ranging from 10 µm to 5 mm for a voltage of bias several hundred volts applied across it.[25] Later in the year 1983, P. S. Vincent et al. was able to achieve blue light from an anthracene thin film of 0.6 µm thickness for a voltage bias of little less than 100 V.[26]

The major breakthrough in the field of OLED was achieved later in the year 1987 when Ching W. Tang and Steven Van Slyke reported low voltage OLED fabricated at Eastman Kodak which gave way for the possibility of commercializing the OLED. The OLED was fabricated as a combination of a hole-transporting aromatic diamine (N, N'-diphenyl-N,N'-bis(3-methylphenyl) 1,1'-biphenyl-4, 4' diamine) and the green fluorescent tris(8-hydroxyquinoline) (Alq_3).[27] The device used a novel bilayer structure, a hole transporting layer and an electron transporting layer with the recombination happening at the middle, exhibiting a very bright green emission with brightness higher than 1000 cd/m^2 and an external quantum efficiency of ~1% for a bias of only 10 V. Following the success of fabricating small molecular OLEDs, J. H. Burroughs et al. in 1990 reported the first yellowish green polymer light emitting diodes (PLEDs) by spin coating the poly(para-phenlene vinylene) (PPV) onto an ITO coated glass with ~100 nm thickness. Initially PLEDs research concentrated on PPV[28] and poly(para-phenylene) (PPP) systems with several potential advantages like solution processing method (spin coating or inkjet printing). This flexibility because of solution processing method creates a new challenge in the solubility of the polymers which was solved by introducing the less polar alkyl chains on the backbone of the polymers. The soluble polymers can be spin coated into high quality uniform thin films over solid substrates. Two most widely studied class of CPs are based on i) PPV derivatives i.e. MEH-PPV which emits orange-red and super yellow color. ii) Blue emitting polyfluorenes (PFs) and its derivatives. Afterwards, many types of CPs have been synthesized and utilized in the OLEDs fabrication.

1.5. Advantages and Disadvantages of OLEDs

OLEDs are already commercialized and they are making ways to the display markets. Currently, OLEDs are used in displays with limited size, such as mobile phones, personal digital assistants, MP3 players, digital cameras and some laptop cameras.

1.5.1. Advantages

- ***Self-luminous:*** The efficiency of OLEDs is better than that of other display technologies without the use of backlight, diffusers, and polarizers.

- ***Low cost and easy fabrication:*** Roll-to-roll manufacturing process, such as, inkjet printing and screen printing, are possible for PLEDs.
- ***Color selectivity:*** There are abundant organic materials to produce blue to red light.
- ***Lightweight, compact and thin devices:*** OLEDs are generally very thin, measuring only ~100 nm.
- ***Flexibility:*** OLEDs can be easily fabricated on plastic substrates paving the way for flexible electronics.
- ***High brightness and high resolution:*** OLEDs are very bright at low operating voltage (White OLEDs can be as bright as150,000 cd/m^2).
- ***Wide viewing angle:*** OLED emission is lambartian and so the viewing angle is as high as 160 degrees.

1.5.2. Disadvantages

- Highly susceptible to degradation by oxygen and water molecules. [29]
- The main disadvantage of an OLED is the lifetime. With proper encapsulation, lifetimes exceeding 60,000 hrs have been demonstrated. In our laboratory itself, we have increased the life time of green Alq_3 based OLEDs, from few days to almost a year.
- Low glass transition temperature T_g for small molecular devices (>70 °C). Hence, the operating temperature cannot exceed the glass transition temperature.
- Low mobility due to amorphous nature of the organic molecules.

1.6. Basic Structure of OLED and EL Mechanism

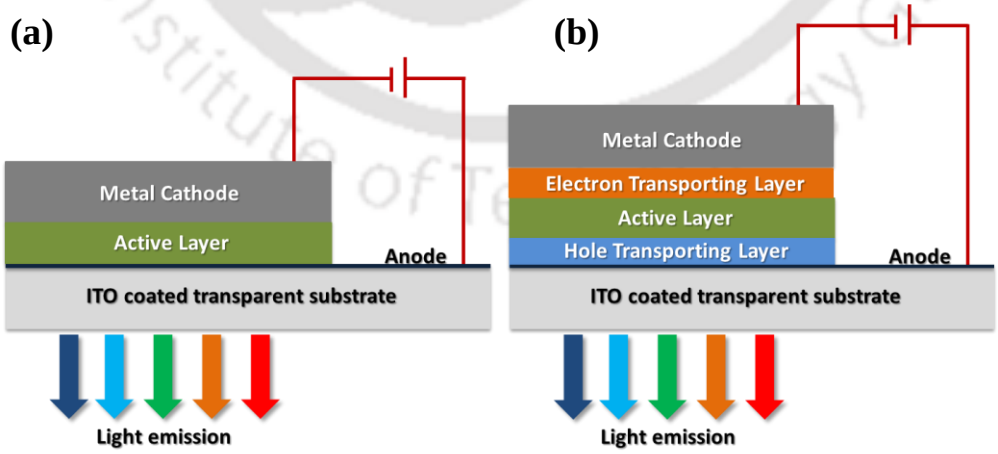

Figure 1.3: Basic structure of the (a) single layered and (b) multi layered OLED

Single layer device is the simplest OLED structure (Figure 1.3). In this device the active material is deposited between two metal electrodes (anode and cathode). In a single layer device, the active material acts as charge transporting material as well as emitting material. Small molecular active materials are normally deposited by thermal evaporation, whereas polymers are deposited by spin coating technique on the indium tin oxide (ITO) coated substrate.[30] The ITO is made up of indium oxide (In_2O_3) and 5 % of tin oxide (SnO_2). Till date, many of the OLEDs consists of ITO as anode, due to high transparency (90 %) and its high work function.[31] On the other hand, Ca (~3 eV), Mg (~3.7 eV), Al (~4.3 eV) materials are used as low work function cathodic materials to reduce the energy barrier from the LUMO of the organic compounds. Ca and Mg are very reactive in nature to the oxygen and moisture, hence, it is necessary to protect them by another layer, like Al. Along with that there is another method to reduce the energy barrier from the organic material by inserting the thin layer (1 nm) of LiF, CsF or AlOX. Similarly, for the hole-injection material, arylamines are utilized for OLED and water soluble polymer, poly(3,4-ethylenedioxythiophene):poly(styrenesulfonate) (PEDOT:PSS) for PLED. By applying the voltage to the device, the electrons and holes are injected to the LUMO and HOMO of the organic material from the cathode and anode, respectively (Figure 1.4). These injected charge carries can move throughout the organic material and recombine through the electrostatic interaction leading to the formation of exciton that decays radiatively to ground state from its excited state.

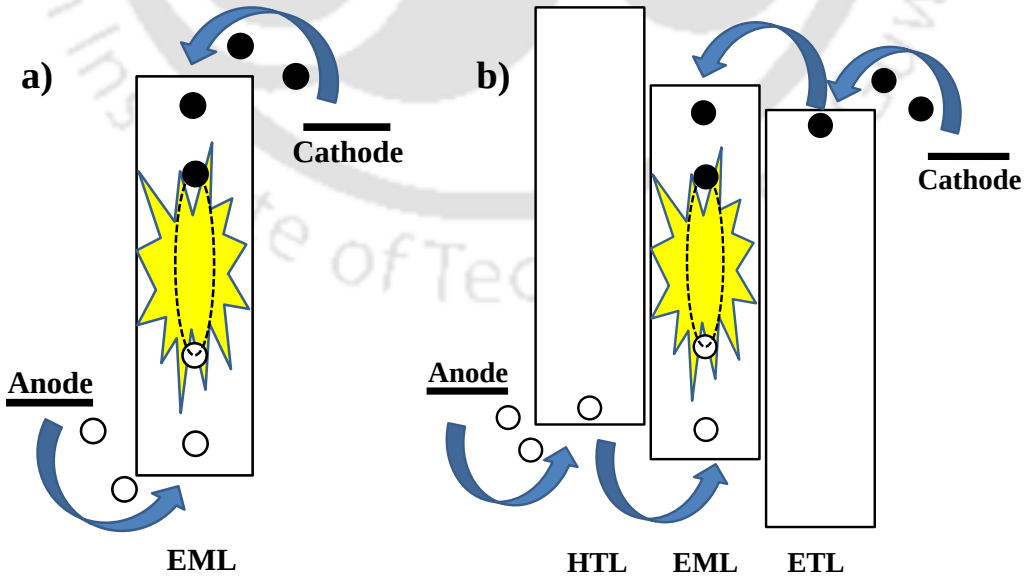

Figure 1.4: Graphical representation of the working principle of a) Single layer device and b) Multi-layer device

The most important point is that the exciton zone must be at the center of the active layer (emissive layer), therefore, it is necessary that organic materials should have identical mobility of electrons and holes. The efficiency of the device mainly depends on number of charges inserted into active materials and number of electrons and holes recombining. However, balanced charge carries are not possible in the single layer OLED architecture, since it leads to reduce the device efficiency. Due to quenching of the exciton they must recombine non-radiatively close to the electrodes. This is due to the fact that most of the organic materials which are used in single layer devices usually have better hole mobility than electron mobility. As holes move faster through the active layer than electrons, the recombination zone of the electrons and holes can move towards cathode and it leads to increase the non-radiative decay, leading to decreased device efficiency. To overcome these problems, multilayer devices were fabricated by inserting extra layers below and above the active layer, such as hole and electron transporting layers (Figure 1.3). These inserted layers can facilitate efficient injection and enhance the exciton formation, due to the well balanced charge carries the recombination zone also shifted to middle of the active layer. The multi-layer devices have more advantages to adjust the HOMO and LUMO energy levels of the organic materials leading to achieve excellent device performance.

1.7. Characterization Parameters for Organic Light Emitting Diodes

The performance of any OLED is determined by the following parameters

i) Efficiency: The efficiency of OLEDs is characterized by its luminous efficiency (LE) and power efficiency (PE), of which, LE is important for material evaluation while PE is important for device evaluation and engineering design.

a) *Luminous efficiency (LE):* LE is measured in candela per ampere (cd A^{-1}) and obtained on the basis of measurement of luminous intensity (in candela, cd), or luminance (L, in candela per meter square, cd m^{-2}) at a given current density (J). i.e.

$$\text{LE (cd/A)} = \text{Luminous Intensity (in candela)} / \text{Current Density (A/m}^2\text{)}$$

b) *Power efficiency (PE):* This is the most important parameter describing the performance of any OLED and is typically measured in lumen per watt. PE is defined as the luminous flux output (in lumen) per input power of the device. It is also termed as luminous efficacy.

$$\text{PE (lm/W)} = \text{Luminous flux output (in lumen)} / \text{Input power (W)}$$

ii) International Commission on Illumination (CIE): The CIE coordinates describe how the human eye perceives the emission color of any light using a pair of two numbers (x, y). The CIE coordinates of pure blue, green and red light are (0.14, 0.08), (0.21, 0.71) and (0.67, 0.33), respectively, whereas the same for white light is (0.33, 0.33).

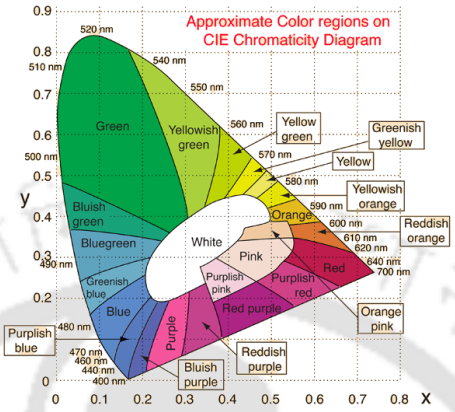

Figure 1.5: CIE chromaticity diagram (Source: http://hyperphysics.phy-astr.gsu.edu/hbase/vision/cie.html)

iii) Correlated Color temperature (CCT): The correlated color temperature of a light source is defined as the temperature [usually measured in Kelvin (K)] at which the heated black-body radiator matches the color of the light source. Higher Kelvin temperatures (5,000 K or more) are said to be "cool" (green-blue) colors, whereas lower color temperatures (2,700-3,000 K) are called "warm" (yellow-red) colors. Cool-colored light is considered better for visual tasks and warm-colored light is preferred for living spaces because it is considered more flattering to skin tones and clothing.

iv) Color Rendering Index (CRI): The color rendering index (CRI) is a quantitative measure of the ability of a light source to reveal the colors of various objects faithfully in comparison with an ideal or natural light source. It is represented by a number between 0 and 100. Natural sunlight is assumed to have a CRI value of 100. To be used for indoor lighting, a light source should have a minimum CRI value greater than or equal to 80.

1.8. Materials for the OLED

To improve all the above parameters, many research groups have been focusing on particular layers, such as modification of anodes, EML, HTL, ETL and cathodes. The emission color of the OLED device is mainly dependent on active material. It should emit light with suitable color coordinates of the CIE-system and sufficient transport of charge carriers. Active material should also have good chemical, thermal and electrochemical stability. Additionally, the materials should show good film forming properties.

Generally, small molecular materials have crystalline nature in thin films which may reduce the mobility of charge carriers and finally it can short the device.[32,33] To address this issue, small molecules with bulky side groups were introduced. These low molecular weight materials can help achieve homogeneous thin films by vacuum deposition. The substituted bulky groups can effectively reduce crystallization.[34] Generally, electron donating materials are used in OLEDs as hole transporting materials. The hole transporting layer (HTL) helps in injecting holes from the anode and transporting into the active layer. The HTL also acts as the electron blocking layer (EBL) that can stop electrons from reaching the active layer. The hole transporting materials should have the HOMO levels matched with the work function of ITO. Some of the aromatic amines like N,N'-di(naphthalen-1-yl)-N,N'-diphenyl-biphenyl-4,4'-diamine (NPD), bis-(4-carbazol-9-yl)-biphenyl (CBP) N,N′-Bis(3-methylphenyl)-N,N′-diphenylbenzidine (TPD) and tris-(4-carbazol-9-yl-phenyl)-amine (TCTA) (Figure 1.6) are typical hole transporting materials for OLED applications. Similarly, the electron-accepting materials are used as electron-transporting materials in OLEDs. The electron transporting layer (ETL) plays the role of injecting electrons from the cathode and transporting injected electrons into the active layer. ETL also acts as hole-blocking layer that can block holes from the active layer. Alq_3 (Figure 1.7) has been widely used as a good electron transporting material. Along with that some of the commonly used ETL are presented in Figure 1.7, such as 2,2′,2"-(1,3,5-Benzinetriyl)-tris(1-phenyl-1-H-benzimidazole) (TPBI), 2-(4-tert-Butylphenyl)-5

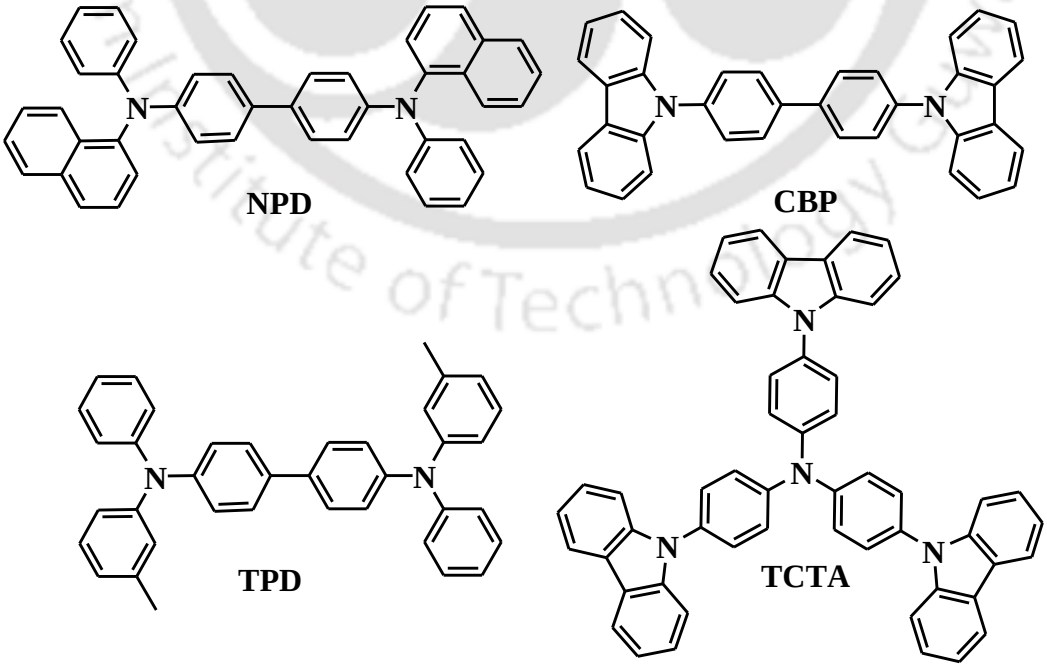

Figure 1.6: Typical examples for hole transport materials in OLED devices

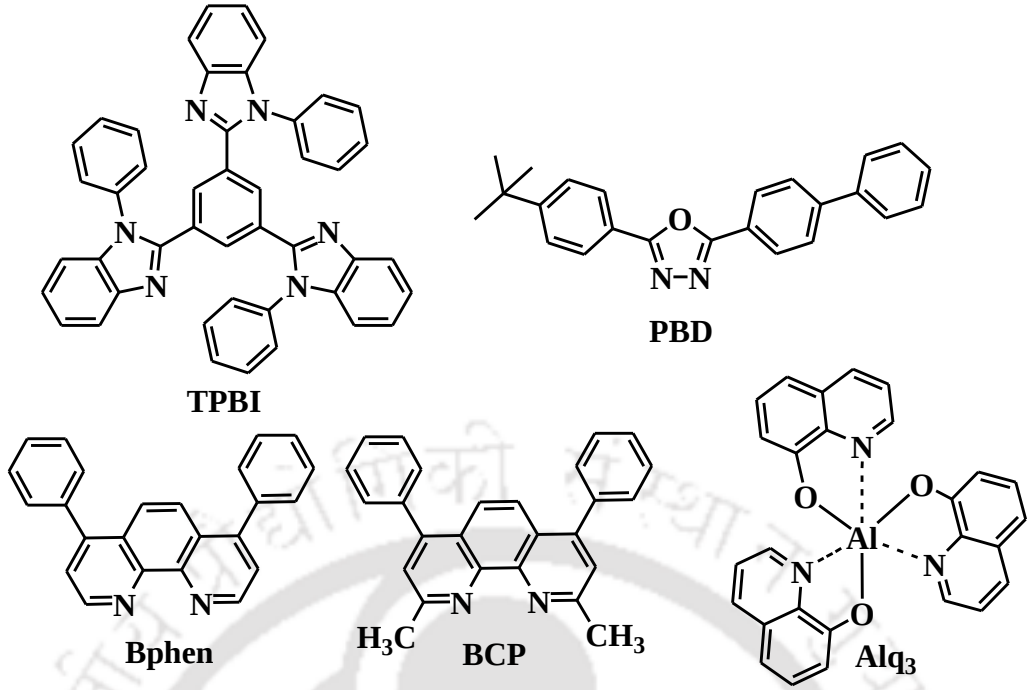

Figure 1.7: Typical examples for electron transport materials in OLED devices

-(4-biphenylyl)-1,3,4-oxadiazole (PBD), 4,7-Diphenyl-1,10-phenanthroline (Bphen) and 2,9-Dimethyl-4,7-diphenyl-1,10-phenanthroline, (BCP). To date, many research groups have developed different emission color emitting polymers and small molecules. Based on the EML, the OLEDs have been classified into two types, i) Small molecule OLEDs (SMOLEDs) and ii) Polymer LEDs (PLEDs).

1.9. Small Molecules as Active Materials

Typical small molecule materials consist of metallic complex and small molecular organic material. The chemical structures of the metallic complex and organic compounds are displayed in Figure 1.8. These materials have good thermal and chemical stability. Most important property of small molecules is that, they can have facile molecular design as doping material. Generally, in dopant and host system the dopant materials show poor film forming ability and good luminous property. On the other hand, the host material should have good film forming ability and poor luminous property. When they are doped together, balanced charge transport, thermal/chemical stability and good film properties can be achieved for better OLED performances.

1.10. Polymers as Active Materials

Recently, commercialization of conjugated polymers have received great interest due to their potential applications in large area flat panel displays[35] and other optoelectronic

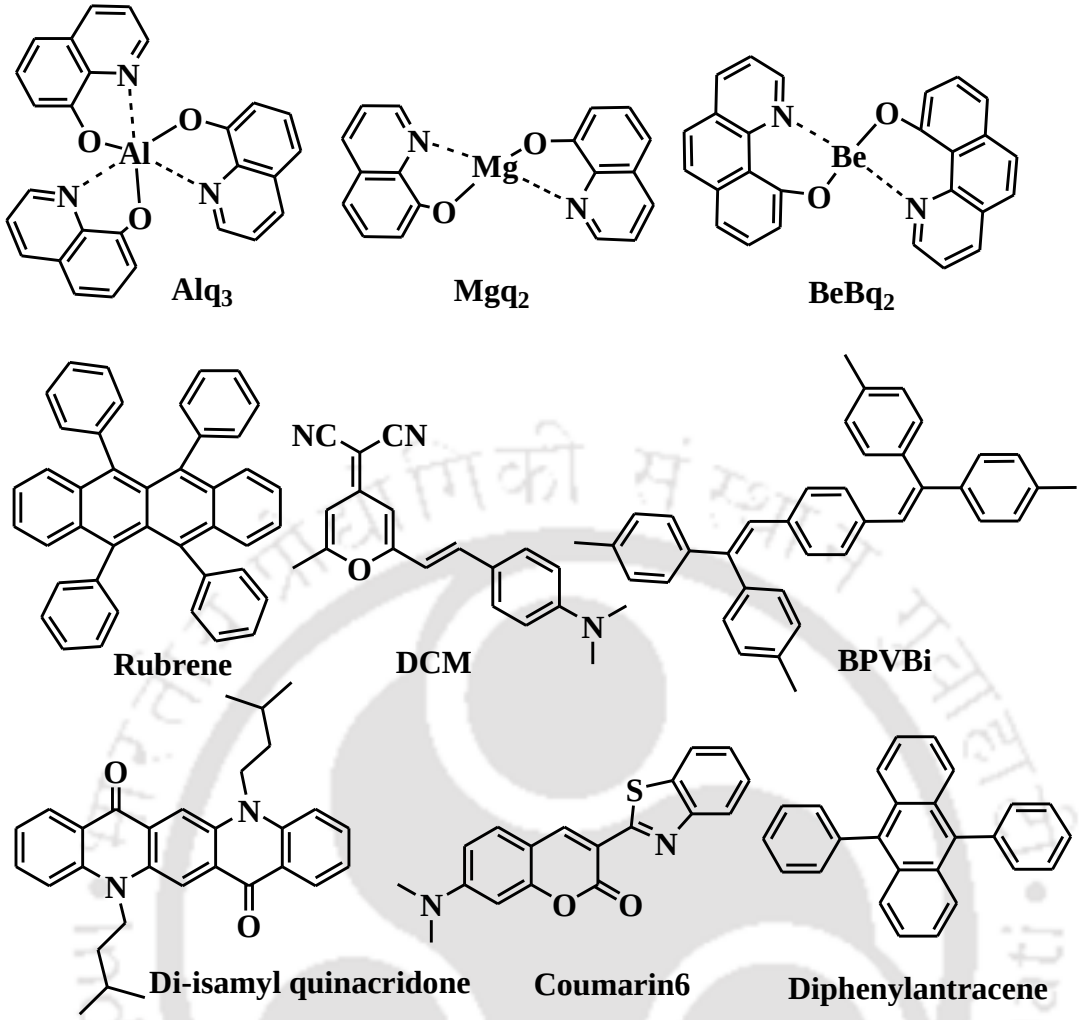

Figure 1.8: Typical examples of the small molecule based active materials

applications.[36] In the last few decades, many conjugated polymers as emissive layers such as PPVs,[37,38] polythiophenes,[39] polycarbazoles[40] and polyfluorenes[41] have been synthesized and studied to achieve highly efficient RGB emitters. Among all polymers, polyfluorene (PF) and its analogues have also been developed. Of all PF derivatives, in 1991, Yoshino et al. developed poly(9,9-di-n-hexylfluorene) (PDHF) based blue light emitting polymer.[42] The major advantages of PF and its derivatives are their high solid state PL quantum yield (0.55%), good chemical and thermal stability. Also, easy synthesis and high solubility in organic solvents due to nonpolar alkyl groups are added properties.[43] Because of the above advantages, these materials have emerged as very promising candidates for PLEDs.[44] The homo polymer of the PF is p-type (electron donor) blue emitting material with ~3.1 eV band gap, a high ionization potential (IP =5.6 eV) and a low electron affinity (EA = 2.5 eV).[45] PF has good hole-transport properties, with 10^{-3} cm^2/Vs[46] hole mobility. On the other hand, the electron transport property of PF

is poor. Therefore, due to this reason it is difficult to inject both electrons and holes into it from the cathode and anode, respectively in OLEDs. To solve this problem, a common strategy that can be applied is inserting electron acceptors into the PF main chain using a chemical reaction. Due to the large band gap of PFs, the emission color (blue) can be tuned from blue to red (400 to 800 nm) region by incorporating narrow band gap or acceptor monomer into the PF main chain. The most commonly used narrow bandgap monomers are N or S atom containing aromatic heterocycles compounds, such as thiophene,[47] bithiophene,[48] 2,1,3-benzothiadiazole,[49] 2,1,3-naphthaselenadiazole,[50] cyanovinyl-containing units,[51] 2-pyran- 4-ylidene-malononitrile.[52]

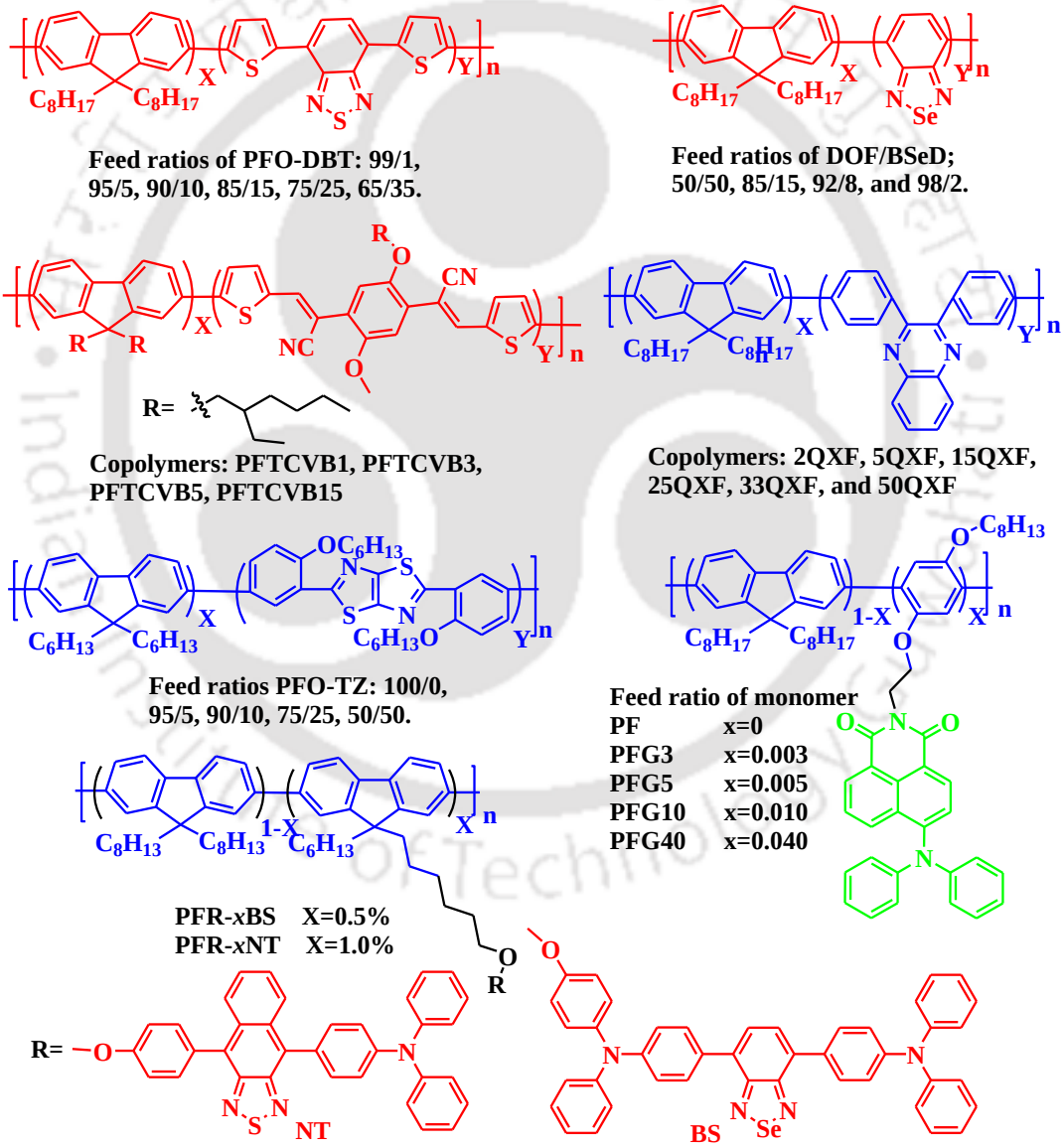

Figure 1.9: Chemical structures of the copolymers

The donor-acceptor (D-A) copolymers often results in intramolecular charge transfer (ICT)[53] from D to A monomers. When acceptor moiety is inserted into PF main chain, the electronic structures of the homo polymers will change, which leads to narrow band gaps,[54,55] broad absorption bands with bathochromic shift and ambipolar charge transport.[56] Based on this strategy, the researchers have shown a great interest in developing single layer white OLEDs using fluorene based copolymers. These white light emitting copolymers can be prepared with small quantities of green and orange or red emitting monomers incorporated into the PF main chain.

In 2002, Yong Cao and co-workers[49] synthesized a series of conjugated copolymers from 4,7-di-2-thienyl-2,1,3-benzothiadiazole (DBT) and 9,9'-dioctylfluorene (DOF) using well-known Suzuki polymerization by changing the DOF and DBT feed ratios. The chemical structures of the copolymers are shown in Figure 1.9.

The PF emission (Blue) was completely quenched having DBT concentration as low as 01% in the solid state. EL devices were fabricated using the ITO/PEDOT:PSS/PFO-DBT/Ba/Al configuration and devices exhibited red light. The emission peaks red-shifted from 628 nm to 674 nm when DBT feed ratio increased from 01 to 35%. The 1.4% of highest external quantum efficiency (EQE) was achieved for the copolymer with 15% DBT content. In 2001, Hong-Ku Shim et al.[57] developed color tuning copolymers based on PF. Poly{9,9-bis(2-ethylhexyl)fluorene-2,7-diyl-*co*-2,5-bis(2-thienyl-1-cyanovinyl)-1-(2-ethylhexyloxy)-4-methoxybenzene-5,5-diyl} (PFTCVB) synthesized from the monomers of 2,5-bis(2-(5-bromothienyl)-1-cyanovinyl)-1-(2-ethylhexyloxy)-4-methoxybenzene (BTCVB) and 2,7-dibromo-9,9-bis(2-ethylhexyl) fluorene by Ni(0) catalysed polymerization. The PL of the synthesized copolymers red-shifted as the fraction of BTCVB increased in the PF main chain and negligible variation observed in UV-vis spectra. EL devices were fabricated with ITO/PEDOT:PSS/copolymer/LiF/Al configuration. Among all copolymers, 15 mol% of BTCVB containing copolymer showed bright red emission. Another PF derivative was synthesized by Yong Cao in 2003.[58] The copolymers were synthesized from 2,1,3-benzoselenadiazole (BSeD) and DOF by Suzuki polymerization using different feed ratios of DOF and BSeD, such as 98:2, 92:8, 85:15, and 50:50, respectively. All copolymers were highly fluorescent in solid state and found good solubility in common organic solvents. The emission colors of the devices exhibited orange to red light (570-600 nm) and they were slightly red-shifted gradually with increasing BSeD concentrations in the PF main chain. The maximum EQE

of the PLED reaches 1.0%, and indicates that seleno containing polymers are promising candidates for fabricating PLEDs. Samson A. Jenekhe and co-workers synthesized six copolymers of DOF and 2,3-bis (*p*-phenylene) quinoxaline using Suzuki polymerization and used as blue emitting materials in OLEDs. All the copolymers emitted blue color in dilute toluene solution (417 nm to 423 nm) and thin films (429 nm to 439 nm) with PL quantum yields that decreased from 72% to 26% with increasing quinoxaline content. The EQE obtained was up to 1% at 100 cd/m^2 brightness.[59] These results show that composition control can be used to optimize the emission properties of copolymers. The combination of fluorene and quinoxaline based copolymers are useful materials for achieving stable blue PLEDs. In 2005, Yong Cao et al. reported new copolymers based on 2,5-di(2 hexyloxyphenyl) thiazolothiazole (TZ) and 9,9-dihexylfluorene (DHF). The copolymers were synthesized by Suzuki polymerization by changing the TZ concentration from 05 to 50 mol % in the PF main chain. All copolymers displayed excellent thermal stability and good solubility in common organic solvents. All copolymers showed strong blue emission in $CHCl_3$ solution (~416-420 nm) and solid state (446-451 nm). The EL devices were fabricated with these copolymers and exhibited EQEs in the range of 0.06 to 0.44%. Among all copolymers, the copolymer with 50% of TZ content showed more than 3 times higher EL efficiency than that of the PF homo polymer.[60] In 2006, Fosong Wang et al. developed the dopant/host methodology[61] and it allows efficient tuning of emission color and improvement of the EL efficiency of OLEDs. The copolymers were obtained by covalently attaching with 0.3 to 1.0 mol % of a green emitting monomer, i.e. 4-(N,N-diphenyl)amino-1,8-naphthalimide (DPAN) to the side chain of PF. These copolymers exhibited green color emission with high solid state PL quantum yield (0.96%), due to the efficient energy transfer from the PF to the DPAN. Single layer PLEDs were fabricated with ITO/PEDOT:PSS/copolymer/Ca/Al configuration. The copolymers exhibit low turn on voltage, maximum luminous efficiency and power efficiency of 4.8 V, 7.43 cd A^{-1} and 2.96 lm W^{-1}, respectively, with CIE coordinates of (0.26, 0.58). In 2011, the same group has reported 2,1,3-naphthothiadiazole and 2,1,3-benzoselenadiazole based highly efficient D-A-D-type derivatives to the side chain of PF. They have synthesized two series of red emitting copolymers, PFR-*x*BS and PFR-*x*NT by changing the concentrations of dopants. The efficient energy transfer was observed from the PF host to the red emitting monomers. Single layer PLED devices were fabricated with ITO/PEDOT:PSS/copolymer/Ca/Al configuration and obtained saturated red light with a peak at 620 nm with CIE coordinates

of (0.62, 0.36) and maximum luminous efficiency of 2.91 cd A^{-1} for PFR-10B. Similarly, saturated red emission with peak at 632 nm, CIE coordinates of (0.63, 0.35) and maximum luminous efficiency of 3.04 cd A^{-1} for PFR-10NT, respectively. The emission colors of the device showed predominantly red emission which was attributed to the red emitting monomers.[62]

In the past few decades, the development of white polymer light emitting diodes (WPLEDs) based on conjugated copolymers has received great interest as promising candidates due to it's potential applications in full color flat panel displays and also lighting. The WPLEDs have great advantages of fabrication and solution processing. White emission can be obtained by following conventional approaches, by mixing three primary colors (Red, Green and Blue) and also by mixing complementary colors (Yellow/Orange and Blue) as the emissive layer. The blend contains of such polymer-small molecule systems,[63] polymer-polymer systems,[64] and polymer-organometallic complex systems.[65] The WPLEDs with blends have achieved good EL efficiency. However, these blended devices have major disadvantages like phase behavior, it is sensitive to driving voltages and operational conditions, thus causing unstable EL spectra and color coordinates. Moreover, it is still challenging to develop the bias-dependent EL spectra, due to the phase separation which is limiting their practical applications. To overcome these problems, great efforts have been made towards single layer polymers and thereby established a promising candidate due to their potential advantage over conventional methods. These single layer emissive polymers were developed based on incomplete energy transfer to suppress the phase separation of chromophores by incorporating primary colors (R, G & B) or complementary colors (O/Y & B) emissive units into single polymer main chain. Based on this idea, many research groups have started working on linear single layer polymers to realize white emission by introducing various emissive units into polymer chain and maintaining the proper feed ratios of the monomers for an incomplete energy transfer.

Most of the linear single polymers are effectively suffering from unsaturated white EL with poor color stability. This is due to strong intermolecular π-π interactions between linear polymer chains in the thin film state. Therefore, it is challenging to control the insufficient energy transfer from PF to chromophores. To address these problems, hyper branched single layer polymers have been developed. Due to the non-planarity, these polymers are less experienced by π-π interactions, resulting in saturated white EL.[66]

The first single polymer layer based WPLED was reported by H. K. Shim et al. in 2005 (Figure 1.10). The synthesized emissive units linearly attached to polymer main chain by Ni(0) catalyzed coupling reaction. The fabricated WPLEDs had CIE coordinates of (0.31, 0.34) at 9 V bias and maximum brightness of 410 cd/m^2.[67] PFO, 2-(2-[2{4-bis (phenylamino)phenyl)-vinyl]-6-tert-butyl-pyran-4-ylidene)malononitrile (TPDCM) and{4-(2-[4-{2-(4-diphenylamino-phenyl)-vinyl}-phenyl]-vinyl)phenyl}diphenylamine (DTPA) have been used as a blue (412 nm), red (595 nm) and green (508 nm) emissive units, respectively. To reduce the large energy barrier of PF derivatives from ITO, two triphenyl units were incorporated as a side chain, which allows the efficient hole transport. Similarly, another set of WPLEDs were synthesized by Lixiang Wang et al. in 2005 (Figure 1.10),[68] by introducing less amount of green emitting unit, 4-diphenylamino-1,8-naphthalimide (DPAN, EL λ_{max}= 515 nm Φ_{PL} = 0.91) into the side chain and less amount of red emitting unit 4,7-bis(5-(4-(N-phenyl-N-(4-methylphenyl) amino)phenyl)-thienyl-2-)-2,1,3-benzothiadiazole (TPABT, EL λ_{max} = 624 nm Φ_{PL} = 0.37) into chain of PF.

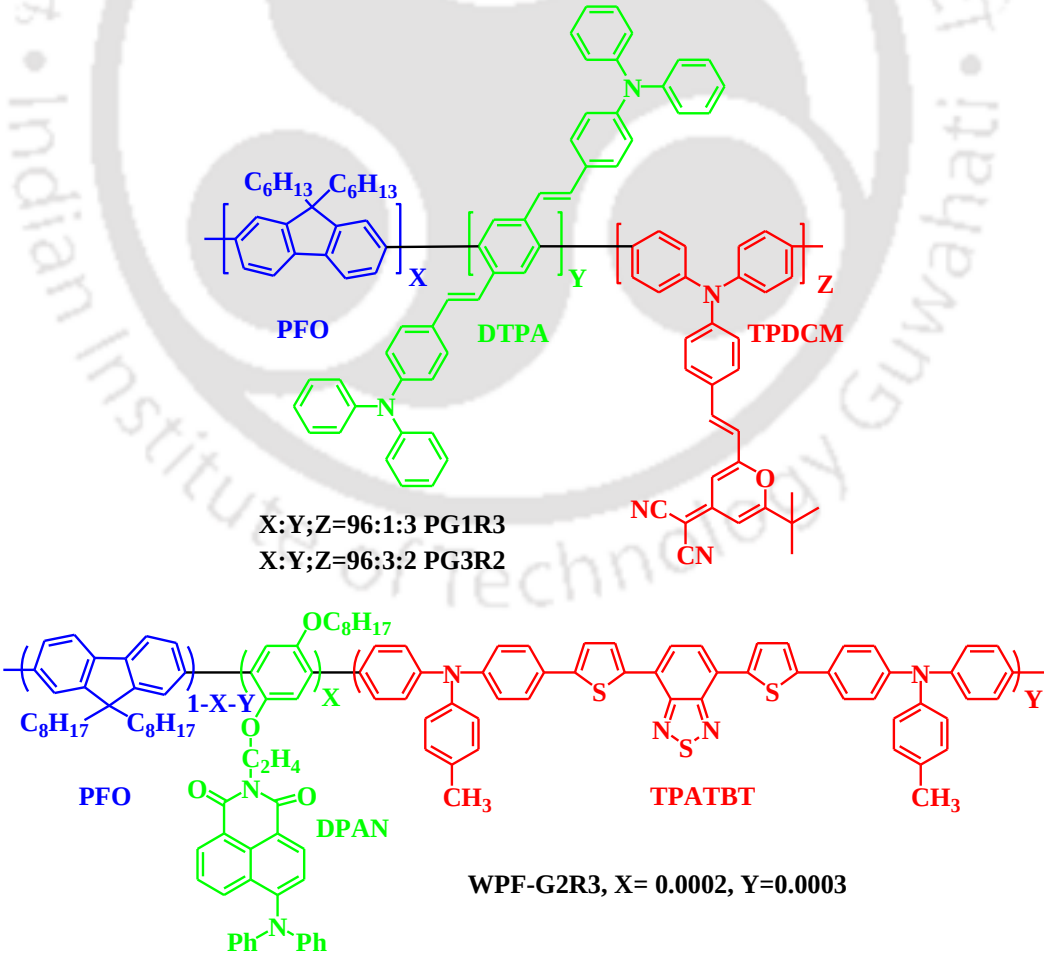

Figure 1.10: Examples of single layer white light emitting polymers

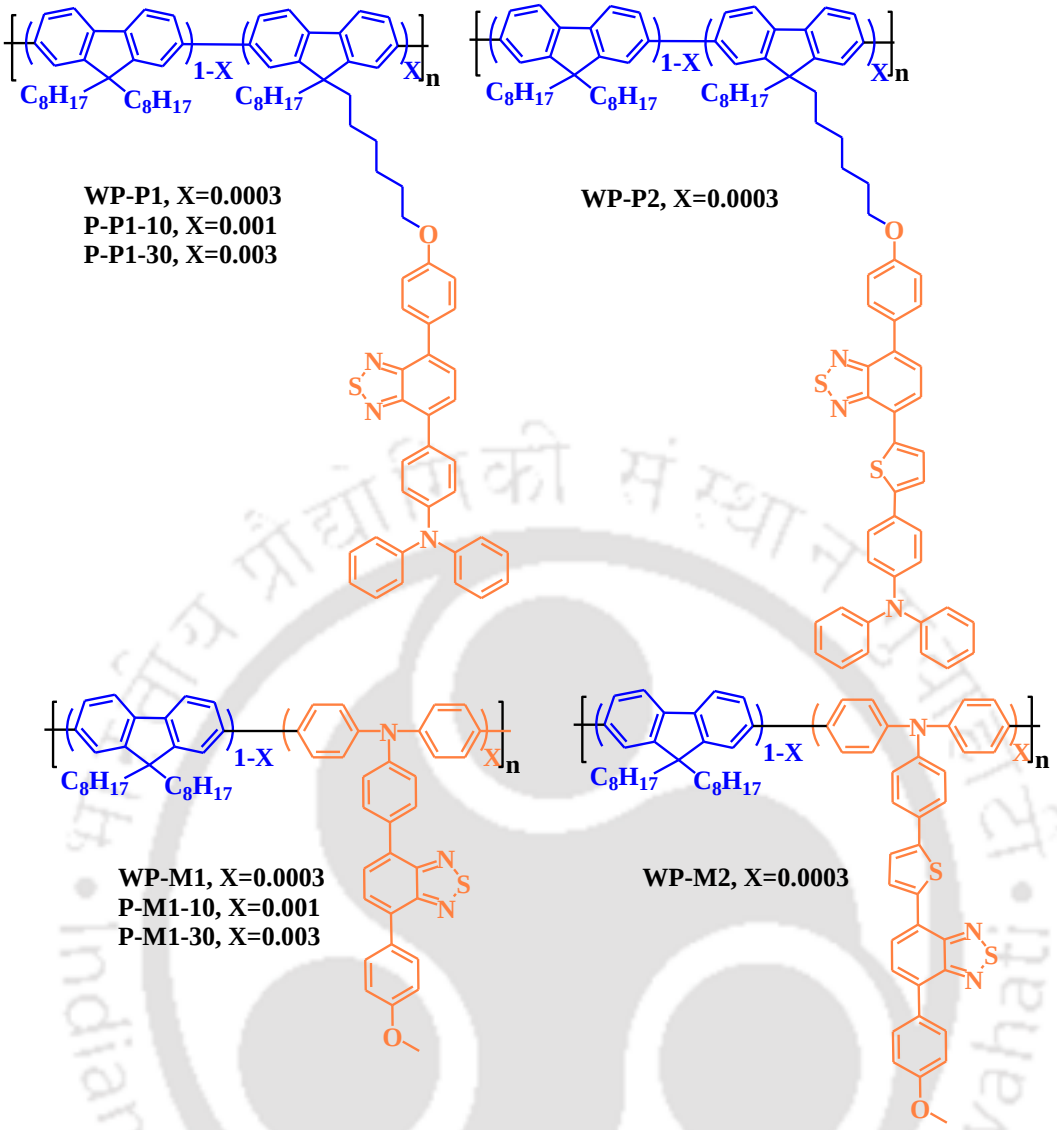

Figure 1.11: Examples of single layer white light emitting polymers.

Attaching one emissive component to the side chain reduces the energy transfer from PF to green dopant, leading to balanced incomplete energy transfer. White EL devices have been fabricated with configuration of ITO/PEDOT:PSS (50 nm)/ polymer (70 nm)/ Ca (10 nm)/Al (100 nm), achieving white light having full width at half maxima (FWHM) of 230 nm, CIE of (0.31, 0.34) and luminous efficiency of 1.59 cd/A. Fosong Wang et al.[69] in 2007 reported four single layer white light emitting copolymers by the combination of complementary colors. Orange emitting monomers were introduced into PF backbone as side chain dopant and main chain dopant (Figure 1.11). Single layer PLEDs were fabricated with ITO/PEDOT:PSS/copolymer/Ca/Al configuration. Compared to main chain copolymers, the side chain based copolymers exhibited more efficient white EL properties. Among all copolymers, the side chain dopant copolymer (WP-P1) exhibited

white light with CIE coordinates of (0.30, 0.40), with a turn-on voltage of 3.5 V, luminous efficiency of 10.66 cd A^{-1}, power efficiency of 6.68 lm W^{-1}, and a highest brightness of 21240 cd m^{-2}. Finally they have concluded that covalently attaching orange dopant unit to the side chain of blue emissive PF gives better results.

1.11. Aggregation Induced Emission Luminogens as Active Materials

Most of the research groups are developing conventional organic molecules as dopants and successfully utilized for the WPLEDs/OLEDs. The major problem with conventional fluorophores is that they are either less emissive or non-emissive in solid or aggregate state because of strong dipole-dipole interactions and effective intermolecular π-π interactions due to planar strucutes.[70, 71] This phenomenon is called aggregation-caused quenching (ACQ). These fluorophores have limited scope for practical applications. Therefore, developments of fluorophores that overcome the ACQ behavior are necessary. Recently, organic molecules exhibiting strong emission in their aggregated or solid state have been developed which is quite opposite to the ACQ. This phenomenon is termed as aggregation-induced emission (AIE) and was first reported by Tang's group in 2001.[72] AIE property can be realized in propeller-like molecules, such as tetraphenylethene (TPE) and silole. The AIE luminogens are non-emissive or less emissive in solution state but become highly emissive in aggregate state. By systematic experimental and theoretical studies, it has been concluded that the intramolecular rotations, vibrations, stretching etc. are responsible for the AIE effect. In solution state, after absorbing the energy, the molecules go to the excited state and while coming back to ground state they decay non-radiatively due to relaxation of intramolecular motions. On the other hand, in aggregated state, these intramolecular motions can be suppressed strongly due to the spatial restriction, which reduces the non-radiative decay and promotes the radiative decay of the excited state. Till date, numerous AIE systems have been developed with different cores, such as siloles,[73] cyanostilbenes,[74] pyrazine derivatives,[75] tetraphenylethenes,[76] diphenyldibenzofulvenes,[77] pyrrole,[78] anthracene derivatives,[79] diketopyrrolopyrrole derivatives,[80] metal complexes,[81] phosphole and phosphindole oxides,[82] o-carborane dyes,[83] organoborons.[84] Chemical structures of some commonly used AIE active materials are shown in Figure 1.12. In 2002, another interesting aggregation induced emission enhancement (AIEE) phenomena has been reported by Park et al.[85] AIEE materials have the ability to emit in both solution and

aggregated state, but the solution state emission is much lesser than their aggregated state. Generally, the AIEE active materials on aggregation show fluorescence enhancement than that of solution state with large bathochromic shifts in their emission wavelength. Due to this shift the electronic properties of the luminogens can be changed. These changes might be obtained via J-aggregation,[86] activated phosphorescence,[87] excimer formation,[88] and aurophilic interactions.[89] However, as compared to AIE materials, the AIEE materials are scarcely reported in literature. Many research groups have concentrated in synthesizing the new AIE materials for practical applications.

The first reported AIE active compound was hexaphenylsilole (HPS) in 2001 (Figure 1.12). HPS has good conjugation with phenyl groups and it is estimated to be highly emissive. However, on thin layer chromatography (TLC), the spot corresponding to HPS compound could hardly be seen once it is taken out from the TLC chamber. After evaporating the solvent on the TLC plate, the strong green emitting spot becomes visible. The fluorescence of HPS is quenched in wet plate and is highly emissive in dry plate, suggesting that HPS is non-emissive in solution state and possesses fluorescence in aggregated state.[72] The PL spectra of HPS has been studied by dissolving in acetonitrile solution (Φ_F = 0.22%). No significant change was observed until the solution mixture reaches to 50% water. Further, on increasing water content in acetonitrile, the fluorescence intensity increased. When water ratio reached 99% (Φ_F = 56%), fluorescence increased by ~255-fold as compared to that of pure acetonitrile solution. From this result, it can be concluded that the fluorescence enhancement is attributed to aggregation in water.

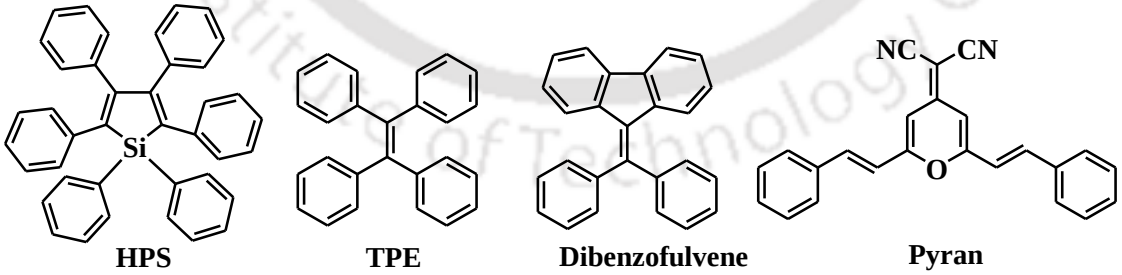

Figure 1.12: Most commonly used examples of the AIE active cores

The entire visible region emitting AIE active materials have been designed and synthesized to achieve the full color displays. Most of the EL devices consists of TPE and its derivatives as emitting layers. Some of the examples are discussed below.

1.11.1. Blue Emitting AIE Active Materials

Simple TPE compound emits deep blue EL emission color at ~445 nm. This device exhibited maximum brightness, EQE and current efficiency of 1800 cd m^{-2}, 0.4% and 0.45 cd A^{-1}, respectively. TPEBPh, having improved device properties, has been synthesized by introducing the two phenyl units to TPE molecule. The EL device of TPEBPh was fabricated with a configuration of ITO/NPB/TPEBPh/BCP/Alq_3/LiF/Al and it exhibits blue EL at ~476 nm with 10680 cd/m^2 of brightness, 5.15 cd A^{-1} of current efficiency and 2.56 % of EQE. Another similar compound was synthesized, i.e. TPTPE, that exhibits slightly better device properties than TPEBPh. The EL device of the TPTPE exhibits sky blue color at ~488 nm with highest brightness, current efficiency and EQE of 10800 cd m^{-2}, 5.8 cd A^{-1} and 2.7%, respectively. The EL of the BTPTPE emits blue color at ~448 nm and exhibits lower EL properties (2.8 cd A^{-1} and 1.6%).[90] This is due to low conjugation caused by steric crowding between the triphenylvinyl units. Compared to all luminogens, BTPE luminogen displays the best device performance. The EL device was fabricated with ITO/NPB/BTPE/TPBi/Alq_3/LiF/Al configuration and it exhibits the emission at ~488 nm with highest brightness of 11180 cd m^{-2}, current efficiency of 7.26 cd A^{-1} and EQE of 3.17%.[91] The devices displayed low turn on voltage (4 V) clearly indicating that BTPE is a promising active material for OLEDs (Figure 1.13).

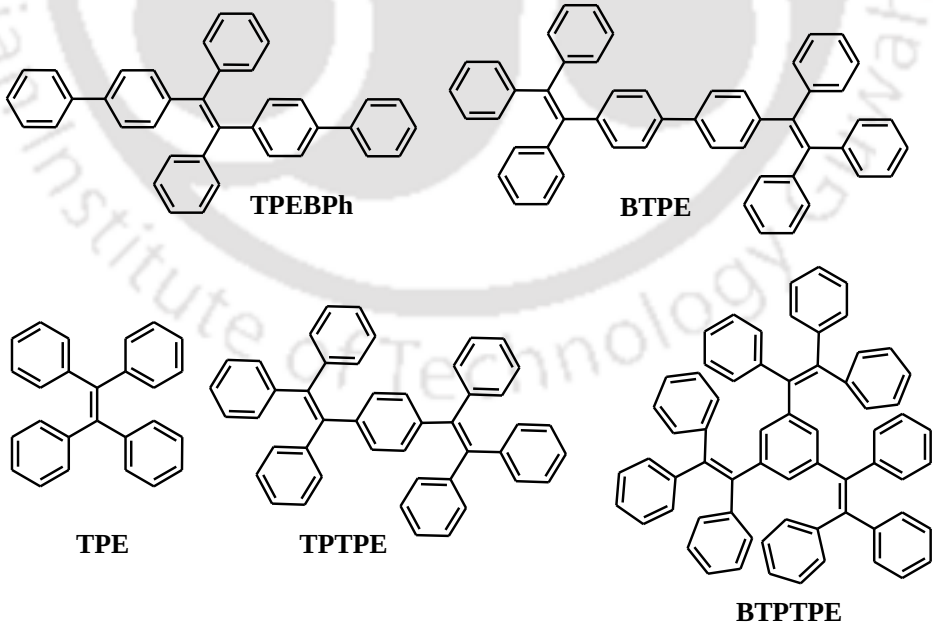

Figure 1.13: Some examples of blue emitting AIE active materials

1.11.2. Green Emitting AIE Active Materials

The starburst type EL compound has been synthesized by introducing triphenylamine (TPA) groups to achieve good charge transport properties and device performance. A multilayer non-doped EL device was fabricated in ITO/NPB/4TPAE/TPBi/LiF/Al configuration. The device shows EL emission at ~538 nm with turn-on voltage, highest brightness, EQE and current efficiency of 3.4 V, 14550 cd m^{-2}, 3.5% and 11.7 cd A^{-1}, respectively. Due to the efficient hole transporting character of the molecule, they have also fabricated OLED without NPB with same device configuration for comparison. The EL device was turned on at 6.0 V, and the EL spectra showed two peaks at 544 and 659 nm, which corresponds to the monomer and exciplex emissions, respectively. The OLED devices exhibited maximum brightness, current efficiency and EQE of 7575 cd m^{-2}, 12.2 cd A^{-1} and 4.9%, respectively.[92] Three TPE core containing luminogens were synthesized by substituting the TPE, triphenyl and multi-layer non-doped OLEDs with a configuration of ITO/NPB/emitter/TPBI/LiF/Al being fabricated.

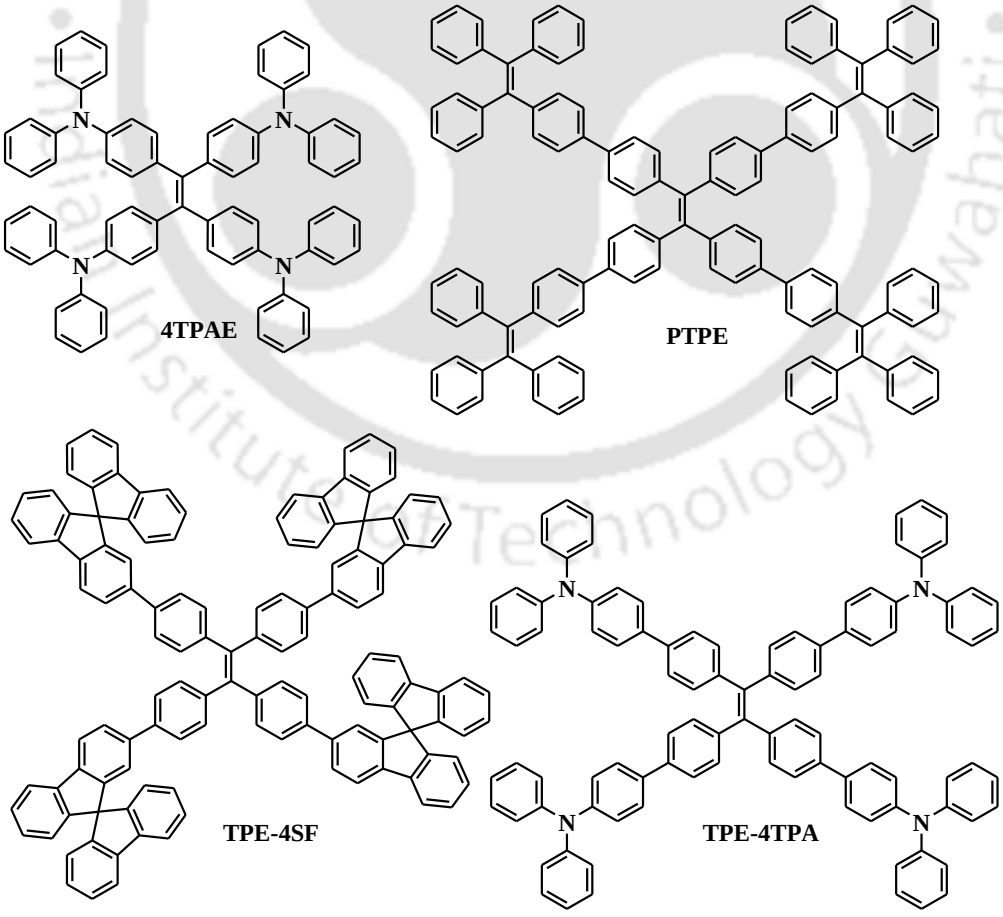

Figure 1.14: Some examples of green emitting AIE active materials

The PTPE compound exhibits the green EL at ~520 nm, which is quite similar to the PL spectra. The OLED device of PTPE exhibited low turn on voltage (4.6 V) and highest brightness of 13700 cd m^{-2} was achieved at 15 V. The highest power, current and EQEs were obtained by the device was 6.4 lm W^{-1}, 11 cd A^{-1} and 3.5%, respectively. Remaining two compounds (TPE-4TPA and TPE-4SF) showed similar EL spectra of ~536 nm. The EL devices exhibited turn on at 3.4 V for TPE-4SF and 4.4 V for TPE-4TPA. The device performance of these compounds improved as compared with PTPE compound. These compounds displayed good results with highest brightness of 14100 cd m^{-2}, highest current efficiency of 8.8 cd A^{-1} and power efficiency of 7.8 lm W^{-1} for TPE-4TPA. Whereas highest brightness of 25000 cd m^{-2} and highest power, current and EQE of 5.8 lm W^{-1}, 10 cd A^{-1} and 3.1%, respectively for TPE-4SF (Figure 1.14).[93]

1.11.3. Red Emitting AIE Active Materials

Two red emitting compounds (TTB and TNB) with high solid state emission and efficient hole transporting characteristics were also reported (Figure 1.15).[94] Non-doped OLEDs devices were fabricated with a configuration of ITO/NPB/TTB or TNB/TPBi/LiF/Al. The TTB based devices showed EL emission at 604 nm and low turn on voltage at 3.2 V. The device displayed maximum brightness of 15584 cd m^{-2} and maximum current, power and external quantum efficiencies were 6.4 cd A^{-1}, 6.3 lm W^{-1} and 3.5%, respectively. TNB based device achieved even better results than that of TTB with low turn on voltage at 3.2 V. The device performance improved with maximum brightness, current, power and EQE of 16396 cd m^{-2}, 7.5 cd A^{-1}, 7.3 lm W^{-1} and 3.9%, respectively.

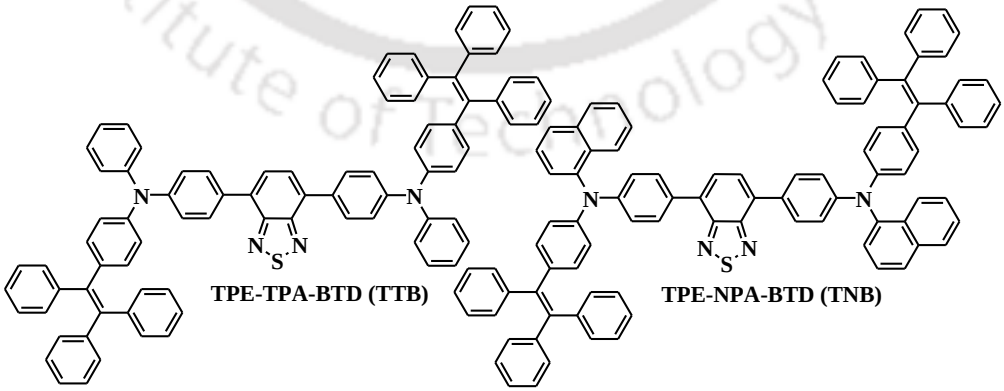

Figure 1.15: Some examples of red emitting AIE active materials

Novelty of the Thesis and Future Scope: The device efficiency and emission color mainly depends on the active material, which aids as emitting layer in the OLEDs. The

research has been carried out towards developing the efficient active materials, owing to the flexible properties of organic materials, such as easy structural modification and tuning the emission color etc. To synthesize the efficient active materials, numerous methods have been introduced and reported. However, still there is a large scope and need to develop the organic materials with better solid state quantum yields. In this thesis, it was mainly focussed and developed highly efficient materials (monomers and polymers) by utilizing the donor-acceptor monomers and AIE active compounds. The 1,8-naphthalimide monomer has been inserted as acceptor into the donor polyfluorene and polycarbazole main chain. The well charge balanced or efficient materials have been established by changing the feed ratios of acceptor mol % in the donor polymers. In addition, the emission properties of the copolymers have been tuned from blue to green for polyfluorene and blue to red for polycarbazole. Based on the observed results it was concluded that the red-shift of the emission peak is mainly dependent on the donating capacity of the donor molecules and, selection of donor and acceptor monomers are very important to achieve the efficient device performance. The AIE active monomers have been synthesized based on the mono-substituted dibenzofulvene (M-DBF) derivatives. For the first time the M-DBF derivatives have been introduced as AIE active monomers, further, the heavy atom effect on the organic molecules is also addressed. Since the M-DBFs are fluorene analogues, dibrominated M-DBFs and its derivatives can be easily synthesized with better yield by the readily available starting material (2,7-dibromofluorene). These synthesized monomers are introduced into the polyfluorene main chain by Suzuki coupling reaction and tuned the emission color. The major limitation with existing methods or molecules is that after synthesizing the efficient monomers, they have to be inserted in to the polymer back bone by metal catalysed reactions that (monomers) should have the halogens (bromine or iodine) to develop multicolor emitting polymers. It is well known in the literature that introduction of the halogen atoms at particular position of organic molecules is very difficult. This M-DBF and its derivatives open the easy way to synthesize the organic molecules. White light emitting polymers were synthesized by incorporating AIEE active monomers as orange or red emitting dopants into polyfluorene host. The newly developed materials showed high solubility, which is very important parameter to obtain better film forming properties during the device fabrication. In addition, incorporation of the AIEE active monomers into the polymer host, the voltage independent EL spectra was easily achieved. This is due to the non-planarity of the AIEE active molecules which can effectively reduce the

intermolecular interactions in the condense state. Therefore, the stable EL spectra can be achieved by this method, which has high demand for the display technology. The OLED device is a solid state device that requires high solid state quantum yields with well charge balanced organic materials. Introduction of donor-acceptor moieties into the AIE active core may display high solid state quantum yields and achieve the better device performance, which has a large scope for future developments. The multi-color emitting organic AIE molecules can be obtained by introduction of various donor and acceptor units into the AIE cores. The AIEE active white emitting polymers are still at preliminary development stage, yet AIEE active polymers (multi-color emitting materials) exhibit better OLED performance and are likely to be in focus over the next few years.

1.12. References

1. Chiang, C. K.; Fincher, C. R.; Park, Y. W.; Heeger, A. J.; Shirakawa, H.; Louis, E. J.; Gau, S. C.; Macdiarmid, A. G. *Phys. Rev. Lett.* **1977,** *39,* 1098-1101.
2. Shirakawa, H .; Louis, E. J.; Macdiarmid, A. G.; Chiang, C. K.; Heeger, A. J. *J. Chem. Soc. Chem. Comm.* **1977,** 578-580.
3. http://nobelprize.org/chemistry/laureates/2000/index.html.
4. Shirakawa, H. *Angew. Chem. Int. Edit.* **2001,** *40,* 2575-2580.
5. Arias, A. C.; Ready, S. E.; Lujan, R.; Wong, W. S.; Paul, K. E.; Salleo, A.; Chabinyc, M. L.; Apte, R.; Street, R. A.; Wu, Y.; Liu, P.; Ong, B. *Appl. Phys. Lett.* **2004,** *85,* 3304-3306.
6. de Gans, B. J.; Duineveld, P. C.; Schubert, U. S. *Adv. Mater.* **2004,** *16,* 203-213.
7. Chen, M. X.; Perzon, E.; Robisson, N.; Jönsson, S. K. M.; Andersson, M. R.; Fahlman, M.; Berggren, M. *Synth. Met.* **2004,** *146,* 233-236.
8. Kulkarni, A. P.; Kong, X.; Janekhe, S. A. *Macromolecules* **2006,** *39,* 8699-8711.
9. Steckler, T. T.; Zhang, X.; Hwang, J.; Honeyager, R.; Ohira, S.; Zhang, X. H.; Grant, A.; Ellinger, S.; Odom, S. A.; Sweat, D.; Tanner, D. B.; Rinzler, A. G.; Barlow, S.; Brédas, J. L.; Kippelen, B.; Marder, S. R.; Reynolds, J. R. *J. Am. Chem. Soc.* **2009**, *131,* 2824-2826
10. Usta, H.; Facchetti, A.; Marks, T. J. *J. Am. Chem. Soc.* **2008,** *130,* 8580-8581.
11. Zaumseil, J.; Sirringhaus, H. *Chem. Rev.* **2007,** *107,* 1296-1323.
12. Zhu, Z.; Waller, D.; Gaudiana, R.; Morana, M.; Mühlbacher, D.; Scharber, M.; Brabec, C. *Macromolecules* **2007,** *40,* 1981-1986.
13. Blouin, N.; Michaud, A.; Gendron, D.; Wakim, S.; Blair, E.; Neagu-Plesu, R.; Belletête, M.; Durocher, G.; Tao, Y.; Leclerc, M. *J. Am. Chem. Soc.* **2008,** *130,* 732-742.
14. Bundgaard, E.; Krebs, F. C. *Sol. Energy Mater. Sol. Cells* **2007,** *91,* 954-985.
15. Wienk, M. M.; Turbiez, M.; Gilot, J.; Janssen, R. A. J. *Adv. Mater.* **2008,** *20,* 2556-2560.
16. McQuade, D. T.; Pullen, A. E.; Swager, T. M. *Chem. Rev.* **2000,** *100,* 2537-2574.
17. Humphreys, C. J. *Mrs. Bull.* **2008,** *33,* 459-470.

18. Holonyak. N.; Bevacqua, S. F. *Appl. Phys. Lett.* **1962**, *1*, 82.
19. Nakamura, S.; Mukai, T.; Senoh, M. *Appl. Phys. Lett.* **1994,** *64*, 1687-1689.
20. Sheats, J. R.; Antoniadis, H.; Hueschen, M.; Leonard, W.; Miller, J.; Moon, R.; Roitman, D.; Stocking, A. *Science* **1996,** *273*, 884-888.
21. Misra, A.; Kumar, P.; Kamalasanan, M. N.; Chandra, S. *Semicond Sci. Tech.* **2006,** *21*, R35-R47.
22. Kamtekar, K. T.; Monkman, A. P.; Bryce, M. R. *Adv. Mater.* **2010,** *22*, 572-582.
23. Gather, M. C.; Kohnen, A.; Meerholz, K. *Adv. Mater.* **2011,** *23*, 233-248.
24. Bernanose, A.; Comte, M.; Vouaux, P. *J. Chim. Phys.* **1953,** *50*, 64.
25. Pope, M.; Kallmann, H. P.; Magnante. P. *J. Chem. Phys*. **1963,** *38*, 2042.
26. Vincett, P. S.; Barlow, W. A.; Hann, R. A.; Roberts, G. G. *Thin Solid Films* **1982,** *94*, 171-183.
27. Tang, C. W.; Vanslyke, S. A. *Appl. Phys. Lett.* **1987,** *51*, 913-915.
28. Burroughes, J. H.; Bradley, D. D. C.; Brown, A. R.; Marks, R. N.; Mackay, K.; Friend, R. H.; Burn, P. L.; Holmes, A. B. *Nature* **1990,** *347*, 539-541.
29. Sugiyama, K.; Ishii, H.; Ouchi, Y.; Seki, K. *J. Appl. Phys.* **2000**, *87*, 297.
30. Jen, A. K-Y.; Liu, Y.; Hu,Q. S.; Pu, L. *Appl. Phys. Lett.* **1999**, *75*, 3745-3747.
31. Wang, P. W.; Lui, Y. J.; Devadoss, C.; Bharathi, P.; Moore, J. S. *Adv. Mater.* **1996**, *8*, 237-241.
32. Forrest, S. R., Burrows, P. E., *Org. El. Mater. Dev.* **1997**, 415-458.
33. Deussen, M., Bässler, H. *Chiuz*, **1997**, *31*, 76-86.
34. Shirota, Y., *Opt. Eng.* **2005**, *94*, 147-178.
35. Kraft, A.; Grimdale, A. C.; Holmes, A. B. *Angew. Chem. Int. Ed.* **1998**, *37*, 402-428.
36. Friend, R. H.; Gymer, R. W.; Holmes, A. B.; Burroughes, J. H.; Marks, R. N.; Taliani, C.; Bradley, D. D. C.; Dos Santos, D. A.; Bre`das, J. L.; Logdlund, M.; Salaneck, W. R. *Nature* **1999**, *397*, 121-128.
37. Kang, I. N.; Hwang, D. H.; Shim, H. K.; Zyung, T.; Kim, J. J. *Macromolecules* **1996**, *29*, 165-169.
38. Ahn, T.; Ko, S. W.; Lee, J.; Shim, H. K. *Macromolecules* **2002**, *35*, 3495-3505.
39. Yamamoto, T.; Arai, M.; Kokubo, H.; Sasaki, S. *Macromolecules* **2003**, *36*, 7986-7993.
40. Mori, T.; Shinnai, T.; Kijima, M. *Polym. Chem.* **2011,** *2*, 2830-2834.
41. Cho, N. S.; Hwang, D. H.; Lee, J. I.; Jung, B. J.; Shim, H. K. *Macromolecules* **2002**, *35*, 1224-1228.
42. Ohmori, Y.; Uchida, M.; Muro, K.; Yoshino, K. *Jpn. J. Appl. Phys.* **1991,** *30*, L1941.
43. Pei, Q.; Yang, Y. *J. Am. Chem. Soc.* **1996**, *188*, 7416-7417.
44. Chen, X.; Liao, J. I.; Liang, Y.; Ahmed, M. O.; Tseng, H. E.; Chen, S. A. *J. Am. Chem. Soc.* **2003**, *125*, 636-637.
45. Liao, L. S.; Fung, M. K.; Lee, C. S.; Lee, S. T.; Inbasekaran, M.; Woo, E. P.; Wu, W. W. *Appl. Phys. Lett.* **2000**, *76*, 3582-3584.
46. Babel, A.; Jenekhe, S. A. *Macromolecules* **2003**, *36*, 7759-7764.
47. Blondin, P.; Bouchard, J.; Beaupre´, S.; Bellete^te, M.; Durocher, G.; Leclerc, M. *Macromolecules.* **2000**, *33*, 5874-5879.
48. Sun, D.; Rosokha, S. V.; Koich, J. K. *J. Am. Chem. Soc.* **2004**, *126*, 1388-1401.

49. Hou, Q.; Xu, Y. S.; Yang, W.; Yuan, M.; Peng, J. B.; Cao, Y. *J. Mater. Chem.* **2002**, *12*, 2887-2892.
50. Yang, J.; Jiang, C. Y.; Zhang, Y.; Yang, R. Q.; Yang, W.; Hou, Q.; Cao, Y. *Macromolecules* **2004**, *37*, 1211-1218.
51. Cho, N. S.; Park, J. H.; Lee, S. K.; Lee, J.; Shim, H. K.; Park, M. J.; Hwang, D. H.; Jung, B. J. *Macromolecules* **2006,** *39*, 177-183.
52. Cheon, C. H.; Joo, S. H.; Kim, K.; Jin, J. I.; Shin, H. W.; Kim, Y. R. *Macromolecules* **2005,** *38*, 6336-6345.
53. Jenekhe, S. A.; Lu, L.; Alam, M. M. *Macromolecules* **2001**, *34*, 7315-7324.
54. Brabec, C. J.; Winder, C.; Sariciftci, N. S.; Hummelen, J. C.; Dhanabalan, A.; Van Hal, P. A.; Janssen, R. A. J. *Adv. Funct. Mater.* **2002**, *12*, 709-712.
55. Sonmez, G.; Shen, C. K. F.; Rubin, Y.; Wudl, F. *Adv. Mater.* **2005,** *17*, 897-900.
56. Yamamoto, T.; Yasuda, T.; Sakai, Y.; Aramaki, S. *Macromol. Rapid. Commun.* **2005**, *26*, 1214-1217.
57. Cho, N. S.; Hwang, D. H.; Lee, J. I.; Jung, B. J.; Shim, H. K. *Macromolecules.* **2002**, *35*, 1224-1228.
58. Yang, R. Q.; Tian, R. Y.; Hou, Q.; Yang, W.; Cao, Y. *Macromolecules.* **2003**, *36*, 7453-7460.
59. Kulkarni, A. P.; Zhu, Y.; Jenekhe, S. A. *Macromolecules* **2005**, *38*, 1553-1563.
60. Peng, Q.; Peng, J. B.; Kang, E. T.; Neoh, K. G.; Cao, Y. *Macromolecules* **2005**, *38*, 7292-7298.
61. Liu, J.; Tu, G.; Zhou, Q.; Cheng, Y.; Geng, Y.; Wang, L.; Ma, D.; Jing, X.; Wang, F. *J. Mater. Chem.* **2006**, *16*, 1431-1438.
62. Chen, L.; Tong, H.; Xie, Z.; Wang, L.; Jinga, X.; Wang, F. *J. Mater. Chem.* **2011**, *21*, 15773-15779.
63. Kim, J. H.; Herguth, P.; Kang, M. S.; Jen, A. K. Y.; Tseng, Y. H.; Shu, C. F. *Appl. Phys. Lett.* **2004,** *85*, 1116- 1118.
64. Granstrom, M.; Inganas, O. *Appl. Phys. Lett.* **1996,** *68*, 147-149.
65. Kim, T. H.; Lee, H. K.; Park, O. O.; Chin, B. D.; Lee, S. H.; Kim, J. K. *Adv. Funct. Mater.* **2006,** *16*, 611-617.
66. Liu, C. F.; Jiu, Y. D.; Wang, J. Y.; Yi, J. P.; Zhang, X. W.; Lai, W. Y.; Huan, W. *Macromolecules* **2016,** *49*, 2549-2558.
67. Lee, S. K.; Hwang, Do. H.; Jung., G. J.; Cho, N. S.; Lee, J.; Lee, J. D.; Shim, H. Ku. *Adv. Funct. Mater.* **2005**, *15*, 1647-1655.
68. Liu, J.; Zhou, Q.; Cheng, Y.; Yanhou, G.; Wang, L.; Ma D.; Jing , X.; Wang , F. *Adv. Mater*. **2005**, *17*, 2974-2978
69. Liu, J.; Guo, X.; Bu, L. J.; Xie, Z. Y.; Cheng, Y. X.; Geng, Y. H.; Wang, L. X.; Jing, X. B.; Wang, F. S. *Adv. Funct. Mater.* **2007,** *17*, 1917-1925.
70. W. Verbouwe, M. Van der Auweraer, F. C. De Schryver, J. J. Piet and J. M. Warman, *J. Am. Chem. Soc.* **1998,** *120*, 1319-1324.
71. Jenekhe, S. A.; Osaheni, J. A. *Science* **1994,** *265*, 765-768.
72. Luo, J. D.; Xie, Z. L.; Lam, J. W. Y.; Cheng, L.; Chen, H. Y.; Qiu, C. F.; Kwok, H. S.; Zhan, X. W.; Liu, Y. Q.; Zhu, D. B.; Tang, B. Z. *Chem. Commun.* **2001,** 1740-1741.

73. Chen, J. W.; Law, C. C. W.; Lam, J. W. Y.; Dong, Y. P.; Lo, S. M. F.; Williams, I. D.; Zhu, D. B.; Tang, B. Z. *Chem. Mater.* **2003,** *15*, 1535-1546.
74. An, B. K.; Lee, D. S.; Lee, J. S.; Park, Y. S.; Song, H. S.; Park, S. Y. *J. Am. Chem. Soc.* **2004,** *126*, 10232-10233.
75. Chen, M.; Li, L. Z.; Nie, H.; Tong, J. Q.; Yan, L. L.; Xu, B.; Sun, J. Z.; Tian, W. J.; Zhao, Z. J.; Qin, A. J.; Tang, B. Z. *Chem. Sci.* **2015,** *6*, 1932-1937.
76. Huang, J.; Yang, X.; Li, X. J.; Chen, P. Y.; Tang, R. L.; Li, F.; Lu, P.; Ma, Y. G.; Wang, L.; Qin, J. G.; Li, Q. Q.; Li, Z. *Chem. Commun.* **2012,** *48*, 9586-9588.
77. Tong, H.; Dong, Y. Q.; Hong, Y. N.; Haussler, M.; Lam, J. W. Y.; Sung, H. H. Y.; Yu, X. M.; Sun, J. X.; Williams, I. D.; Kwok, H. S.; Tang, B. Z. *J. Phys. Chem. C* **2007,** *111*, 2287-2294.
78. Liu, G. G.; Chen, D. D.; Kong, L. W.; Shi, J. B.; Tong, B.; Zhi, J. G.; Feng, X.; Dong, Y. P. *Chem. Commun.* **2015,** *51*, 8555-8558.
79. Song, N.; Chen, D. X.; Xia, M. C.; Qiu, X. L.; Ma, K.; Xu, B.; Tian, W. J.; Yang, Y. W. *Chem. Commun.* **2015,** *51*, 5526-5529.
80. Gao, Y. T.; Feng, G. X.; Jiang, T.; Goh, C. C.; Ng, L. G.; Liu, B.; Li, B.; Yang, L.; Hua, J. L.; Tian, H. *Adv. Funct. Mater.* **2015,** *25*, 2857-2866.
81. He, G.; Delgado, W. T.; Schatz, D. J.; Merten, C.; Mohammadpour, A.; Mayr, L.; Ferguson, M. J.; McDonald, R.; Brown, A.; Shankar, K.; Rivard, E. *Angew. Chem. Int. Edit.* **2014,** *53*, 4587-4591.
82. Sanji, T.; Shiraishi, K.; Tanaka, M. *ACS Appl. Mater. Inter.* **2009,** *1*, 270-273.
83. Kokado, K.; Chujo, Y. *Macromolecules,* **2009,** *42*, 1418-1420.
84. Fu, Y. B.; Qiu, F.; Zhang, F.; Mai, Y. Y.; Wang, Y. C.; Fu, S. B.; Tang, R. Z.; Zhuang, X. D.; Feng, X. L. *Chem. Commun.* **2015,** *51*, 5298-5301.
85. An, B. K.; Kwon, S. K.; Jung, S. D.; Park, S. Y. *J. Am. Chem. Soc.* **2002,** *124*, 14410-14415.
86. Zhang, Y.; Wang, J. H.; Zheng, W. J.; Chen, T. F.; Tong, Q. X.; Li, D. *J. Mater. Chem. B* **2014,** *2*, 4159-4166.
87. Yuan, W. Z.; Shen, X. Y.; Zhao, H.; Lam, J. W. Y.; Tang, L.; Lu, P.; Wang, C. L.; Liu, Y.; Wang, Z. M.; Zheng, Q.; et al. *J. Phys. Chem. C* **2010,** *114*, 6090-6099.
88. Huang, K. W.; Wu, H. Z.; Shi, M.; Li, F. Y.; Yi, T.; Huang, C. H. *Chem. Commun.* **2009,** 1243-1245
89. Ni, W. X.; Li, M.; Zheng, J.; Zhan, S. Z.; Qiu, Y. M.; Ng, S. W.; Li, D. *Angew. Chem. Int. Ed.* **2013,** *52*, 13472-13476.
90. Zhao, Z. J.; Chen, S. M.; Shen, X. Y.; Mahtab, F.; Yu, Y.; Lu, P.; Lam, J. W. Y.; Kwok, H. S.; Tang, B. Z. *Chem. Commun.* **2010,** *46*, 686-688.
91. Hong, Y. N.; Lam, J. W. Y.; Tang, B. Z. *Chem. Commun.* **2009**, 4332-4353.
92. Zhao, L. F.; Lin, Y. L.; Liu, T.; Li, H. X.; Xiong, Y.; Yuan, W. Z.; Sung, H. H. Y.; Williams, I. D.; Zhang, Y. M.; Tang, B. Z. *J. Mater. Chem. C* **2015,** 3, 4903-4909.
93. Chang, Z. F.; Jiang, Y. B.; He, B. R.; Chen, J.; Yang, Z. Y.; Lu, P.; Kwok, H. S.; Zhao, Z. J.; Qiu, H. Y.; Tang, B. Z. *Chem. Commun.* **2013,** *49*, 594-596.
94. Qin, W.; Lam, J. W. Y.; Yang, Z. Y.; Chen, S. M.; Liang, G. D.; Zhao, W. J.; Kwok, H. S.; Tang, B. Z. *Chem. Commun.* **2015,** *51*, 7321-7324.

Chapter-2

Synthesis and Characterization of Color Tunable, Highly Electroluminescent Copolymers of Polyfluorene by Incorporating the N-Phenyl-1,8-Naphthalimide Moiety into the Main Chain

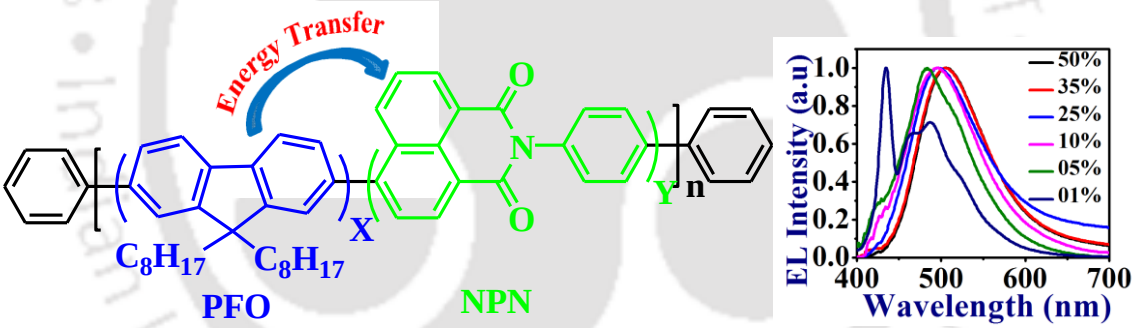

Gopikrishna, P.; Das, D.; Iyer, P. K. *J. Mater. Chem. C.* **2015,** *3*, 9318-9326.

Abstract

A series of six new organic light emitting copolymers were prepared from 9, 9'-dioctylfluorene (DOF) and N-phenyl-1,8-naphthalimide (NPN) using palladium catalyzed Suzuki polymerization. The feed ratios of poly[2,7-(9,9'-dioctylfluorene)-co-N-phenyl-1,8-naphthalimide] (PFONPN) copolymers were 50 : 50, 65 : 35, 75 : 25, 90 : 10, 95 : 05 and 99 : 01, respectively. These copolymers have good thermal stability with an onset decomposition temperature (T_d) in the range of 340-405 °C and a glass transition temperature (T_g) in the range of 123-134 °C. All the copolymers are highly fluorescent and soluble in common organic solvents such as chlorobenzene, chloroform, dichloromethane, THF, toluene, etc. allowing their processing from desired solvent. The electroluminescence (EL) properties of the copolymers were also studied by fabricating single layer devices with ITO/PEDOT:PSS/PFONPN/Ca:Al configuration. Photoluminescence (PL) and EL spectra of the copolymers reveal that by changing the content of the NPN moiety in the polyfluorene main chain from 01 to 50 mol%, the emission color of the polymers can be tuned from blue to green with Commission International de l'Echairage (CIE) coordinates being (0.17, 0.22) to (0.24, 0.49). This color tuning can be attributed to the strong energy transfer from the fluorene to NPN unit in the polymer backbone. The devices made using these copolymers are found to be very bright with PFONPN01 giving the highest brightness of 5236 cd m^{-2} with a luminous efficiency of 3.52 cd A^{-1}.

2.1. Introduction

Since the discovery of polymer light-emitting diodes (PLEDs) based on poly(p-phenylenevinylene) (PPV) in 1990,[1] conjugated polymers (CPs) have attracted significant attention towards PLEDs due to their potential application in large-area, flat-panel displays. This is because of their wide structural variety, low cost, very high flexibility and ease of processing.[2-5] In the past few decades, polyfluorenes (PFs) have been extensively used as active materials for multicolor PLEDs because of their excellent thermal & chemical stability, good solubility in common organic solvents, easy functionalization at the C-9 position of fluorene and high PL quantum yields in solid films.[6] Generally PFs are p-type (electron donor) materials with large band gaps[7] and emit blue light. However, the emission color of PFs can be judiciously tuned over the entire visible region by introducing narrow band gap units into the PF backbone as reported in few examples earlier.[8-20] The most commonly used narrow band gap units are aromatic heterocyclic derivatives such as benzothiadiazole,[8-10] bithiophene[15] and naphthoselenadiazole.[13] Recently organic molecules[21] and polymers[22-24] containing 1,8-naphthalimide (NI) and its derivatives have generated a lot of research interest as luminescent materials in organic EL devices due to their superior thermal, chemical and optical properties and high PL quantum yields. Generally NI derivatives have high electron affinities (because they possess carbonyl groups) and demonstrate good electron transporting or hole blocking capabilities that can help in charge balance in PLEDs.[25] Introduction electron donating substituents at the 4-position of NI derivatives makes them highly fluorescent.[26-28] Unlike NI containing side chain non-conjugated polymers which have the disadvantage of low light-emitting efficiency,[29-31] CPs containing NI derivatives have emerged as very promising potential candidates for PLED applications owing to the possibility of efficient energy transfer from the conjugated backbone to the low band-gap NI moieties.[22,32,33] Indeed, numerous organic light emitting homopolymers have been synthesized by incorporation of N-phenyl-1,8-naphthalimide (NPN) derivatives into PF by end capping method.[34,35] Recently, few studies have reported that when N-aryl-1,8-naphthalimide derivatives were incorporated into the CP the resulting polymer could show large EL and PL efficiency.[33,35]

In this chapter, the synthesis, characterization and color tuning of a series of new donor and acceptor based, highly electroluminescent conjugated random copolymers derived from 9,9'-dioctylfluorene (DOF) and NPN by Suzuki cross coupling reaction (Scheme 2.1) is discussed. The NPN co-monomer was inserted into the PF main chain as

an acceptor to enhance the electron transporting properties and for improved recombination of holes and electrons. This was the first time, when a block copolymer was synthesized using the NPN unit and PF by Suzuki coupling reaction. By controlling the NPN unit in the polymer main chain the emission color of the polymer was tuned efficiently from blue to green. The emission color of copolymer changes when the NPN content increases from 1-50 mol% in the PF main chain. It was observed that in solid state PL, the PF fluorescence completely quenched even for 1 mol% of NPN content. One can thus predict that the NPN unit allows efficient intramolecular energy transfer from the fluorene segment to the NPN unit. The EL spectra of these polymers showed excellent color tuning and except PFONPN01, all copolymers showed only a single peak because of strong energy transfer from the fluorene backbone to NPN unit. The emission spectra of the polymers were highly red shifted with a gradual increment of the NPN content in the polymer backbone. The devices made using these copolymers are found to be very bright with PFONPN01 giving the highest brightness of 5236 cd m^{-2} with a luminous efficiency of 3.52 cd A^{-1}.

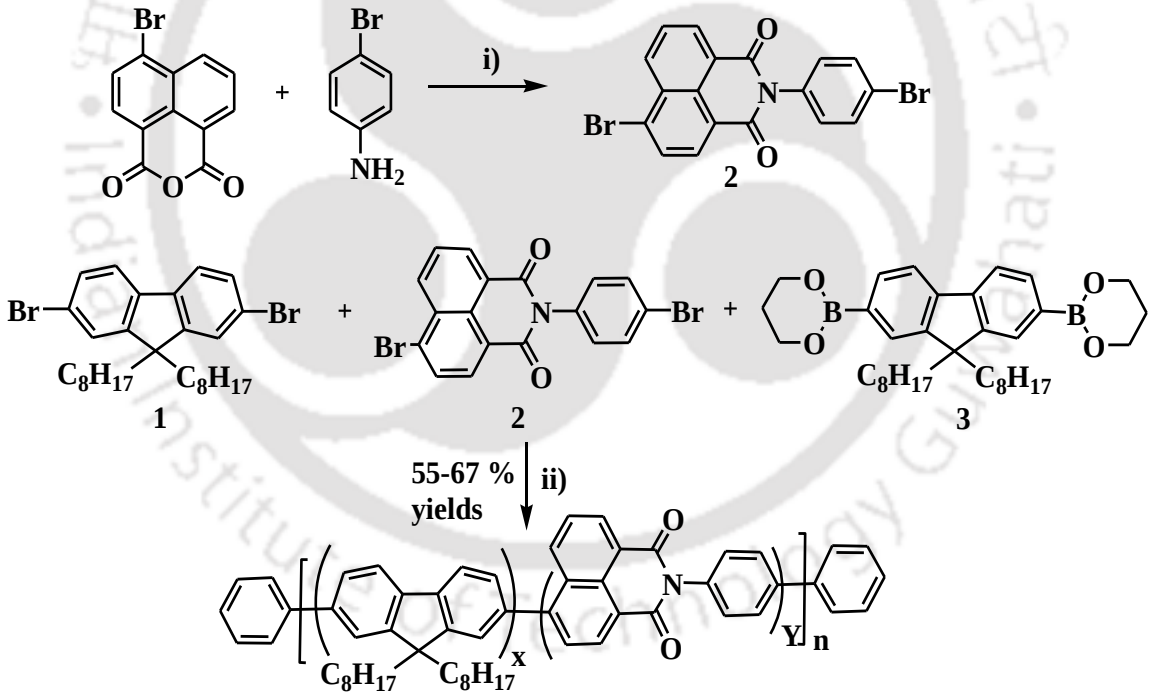

Scheme 2.1. Synthetic route for monomer and copolymers. Feed ratio of Monomers: 99/01 (PFONPN01), 95/05 (PFONPN05), 90/10 (PFONPN10), 75/25 (PFONPN25), 65/35 (PFONPN35), 50/50 (PFONPN50). i) Glacial acetic acid, Reflux, 12 hrs. ii) $Pd(PPh_3)_4$, Aliquat 336, 2M K_2CO_3, THF, 48 hrs, Benzene boronicacid, Iodobenzene.

2.2. Experimental section

2.2.1. Materials and measurements

2,7-Dibromofluorene, 1-bromooctane, 4-bromo-1,8-naphthalicanhydride, 9,9'-dioctylfluorene-2,7-diboronic acid bis(1,3-propanediol)- ester (3), 4-bromoaniline, glacial acetic acid (99.85%), tetrakis(triphenylphosphine)palladium(0) ($Pd(pph_3)_4$), and aliquat 336 were purchased from Sigma-Aldrich and used without further purification unless specified. Chloroform, dichloromethane and toluene were distilled over calcium chloride and anhydrous tetrahydrofuran was dried over sodium benzophenone. 2,7-dibromo-9,9'-dioctylfluorene (1) was prepared by following published procedures.[36]

^{1}H NMR and ^{13}C NMR spectra were recorded on Varian AS 400 MHz and Bruker 600 MHz NMR spectrometers. UV-visible spectra were recorded using a PerkinElmer, Model Lambda-25 spectrometer. PL spectra were recorded using a Varian Cary Eclipse spectrometer. Electrochemical measurements were carried out under argon atmosphere on a deoxygenated solution of 0.1 M tetra butyl ammonium hexafluorophosphate (Bu_4NPF_6) in acetonitrile by using a CH instrument (Model 700D series). Glassy carbon was used as a working electrode, platinum as a counter electrode, and Ag/Ag^+ as a reference electrode. Thermogravimetric analysis (TGA) was performed on a Mettler Toledo, model TG/SDTA 851 e, and differential scanning calorimetry (DSC) was performed on a Mettler Toledo, model DSC1, stare system. The gel permeation chromatography (GPC) measurements were recorded on a Waters 515 chromotograph connected to Waters 2414 refractive index detectors by using tetrahydrofuran as an eluent and the calibration curve of PMMA standards. FT-IR analysis was carried out using a Perkin-Elmer-Spectrum with samples prepared as KBr pellets.

2.2.2. Synthesis of 4-bromo-9-N-4-bromophenyl-1,8-naphthalimide (2)

4-Bromo-1,8-naphthalicanhydride (0.500 g, 1.80 mmol), 4-bromo aniline (0.4649 g, 2.67 mmol) and 15 mL of glacial acetic acid were added into a 50 mL round bottom flask at room temperature and refluxed for 12 hours. The reaction mixture was then cooled to room temperature and poured into distilled water (100 mL) the resultant solid was collected by filtration and recrystallized from acetone. (Yield 0.572 g, 73%). ^{1}H NMR (400 MHz, DMSO-d_6) δ (ppm): 8.62-8.58 (m, 2H), 8.36-8.34 (d, 1H) 8.27-8.25 (d, 1H), 8.06-8.04 (t, 1H), 7.74-7.72 (d, 1H), 7.39-7.37 (d, 1H); ^{13}C NMR (150 MHz, DMSO-d_6) δ (ppm): 163.0, 163.0, 135.1, 133.6, 132.5, 131.7, 131.6, 131.4, 131.3, 131.0, 129.2, 129.1, 122.5, 121.5; electrospray ionization mass spectrum (ESI-MS): $[M + H]^+$: calcd: 432.08; found: 432.2.

2.2.3. General polymerization procedure

9,9-Dioctylfluorene-2,7-diboronic acid bis(1,3-propanediol) ester, dibromo compounds (2,7-dibromo-9,9-dioctylfluorene and 4-bromo-9-N-4-bromophenyl-1,8-naphthalimide), 12 mL of Tetrahydrofuran (THF) and $Pd(PPh_3)_4$ (0.015 mmol) were added into a dry two neck round bottom flask. Subsequently 5 mL of 2 M aqueous K_2CO_3 and aliquat 336 (0.025 mmol) were added to the flask. The reaction mixture was degassed thrice by freeze- thaw cycles to remove trace amounts of oxygen completely. The reaction mixture was stirred at 80 °C for 2 days, and iodobenzene was added as an end capper. After 4 hours, benzene boronic acid was dissolved in 1mL of THF and added into the reaction mixture as another end capper and stirring continued further for 4 hours. The reaction mixture was then cooled to room temperature, poured into 100 mL of methanol and further stirred at room temperature for 4 hours. The desired polymer was collected by filtration and reprecipitated twice from methanol and acetone. The polymers were further purified by soxhlet filtration with acetone to remove oligomers and catalyst residues. Yield of 55-67% were obtained after drying the polymers. The resulting polymers were soluble in common organic solvents. The reactivity of the three different types of aryl-bromides differs under the reaction conditions reported here. The fluorene unit has two identical bromides, whereas, the NPN unit has two different types of bromides, viz. attached to napthyl and phenyl rings. As compared to the NPN bromides the fluorene bromides are more reactive due to the absence of electron withdrawing groups as well as their high electron density and there is a high possibility of oxidative addition predominantly. On the other hand, among the NPN bromides, the napthyl bromide is more reactive than the phenyl bromide since the napthyl moiety has more electron density. Hence, it has more feasibility to oxidative addition with palladium. In the case of PFONPN01 to PFONPN35 three monomers viz. fluorene boronic ester, 2,7-dibromo-9,9'-dioctylfluorene and 4-bromo-9-N-4-bromophenyl-1,8-naphthalimide were used. In these copolymers, due to the high reactivity of fluorene bromide, there is a probability that it will react first with fluorene boronic ester forming a polyfluorene block. Similarly, the remaining fluorene boronic ester will react with 4-bromo-9-N-4-bromophenyl- 1,8-naphthalimide forming another block. When they undergo polymerization, they may form copolymers containing long oligofluorene segments. However, in the case of PFONPN50, as only two monomers were used, viz. fluorene boronic ester and 4-bromo-9-N-4-bromophenyl-1,8-naphthalimide, it will form only alternating copolymers.

2.2.4. Poly[2,7-(9,9'-dioctylfluorene)-co-N-phenyl-1,8-naphthalimide] (PFONPN50)

9,9-Dioctylfluorene-2,7-diboronic acid bis(1,3-propanediol) ester (3) (0.2792 g, 0.50 mmol) and 4-bromo-9-N-4-bromophenyl- 1,8-naphthalimide (2) (0.2155 g, 0.50 mmol) were used in this polymerization. ^{1}H NMR (600 MHz, $CDCl_3$) δ (ppm): 8.75 (br, 2H), 8.42 (br, 1H), 7.86 (br, 2H), 7.69 (br, 4H), 7.59 (br, 1H), 7.48 (br, 1H), 7.38 (br, 1H), 6.88 (br, 1H), 2.10 (br, 4H), 1.15 (br, 24H), 0.82 (br, 6H); ^{13}C NMR (150 MHz, $CDCl_3$) δ (ppm): 164.6, 151.8, 140.7, 140.2, 131.6, 130.3, 129.3, 128.7, 128.2, 127.1, 124.9, 120.5, 55.8, 40.6, 31.9, 30.2, 29.4, 24.3, 22.8, 14.2; FT-IR (KBr pellets, cm^{-1}): 2953, 2922, 2850, 1710, 1669, 1585, 1466, 1357, 1237, 810.

2.2.5. Poly[2,7-(9,9'-dioctylfluorene)-co-N-phenyl-1,8-naphthalimide] (PFONPN35)

9,9-Dioctylfluorene-2,7-diboronic acid bis(1,3-propanediol) ester (3) (0.2792 g, 0.50 mmol), 2,7-dibromo-9,9-dioctylfluorene (1) (0.0822 g, 0.15 mmol) and 4-bromo-9-N-4-bromophenyl-1,8-naphthalimide (2) (0.1508 g, 0.35 mmol) were used in this polymerization. ^{1}H NMR (600 MHz, $CDCl_3$) δ (ppm): 8.74 (br, 2H), 8.43 (br, 1H), 7.84 (br, 2H), 7.69 (br, 4H), 7.58 (br, 1H), 7.48 (br, 1H), 7.37 (br, 1H), 6.94 (br, 1H), 2.11 (br, 4H), 1.14 (br, 24H), 0.81 (br, 6H); ^{13}C NMR (150 MHz, $CDCl_3$) δ (ppm): 164.7, 151.8, 151.7, 139.9, 132.5, 131.6, 131.3, 130.3, 128.8, 128.7, 128.6, 128.2, 127.9, 127.1, 126.8, 126.7, 126.1, 121.3, 120.2, 119.8; FT-IR (KBr pellets, cm^{-1}): 2953, 2922, 2850, 1710, 1669, 1585, 1466, 1357, 1237, 810.

2.2.6. Poly[2,7-(9,9'-dioctylfluorene)-co-N-phenyl-1,8-naphthalimide] (PFONPN25)

9,9-Dioctylfluorene-2,7-diboronic acid bis(1,3-propanediol) ester (3) (0.2792 g, 0.50 mmol), 2,7-dibromo-9,9-dioctylfluorene (1) (0.1371 g, 0.25 mmol) and 4-bromo-9-N-4-bromophenyl-1,8-naphthalimide (2) (0.1077 g, 0.25 mmol) were used in this polymerization. ^{1}H NMR (600 MHz, $CDCl_3$) δ (ppm): 8.74 (br, 2H), 8.43 (br, 1H), 7.84 (br, 2H), 7.68 (br, 4H), 7.58 (br, 1H), 7.49 (br, 1H), 7.37 (br, 1H), 6.94 (br, 1H), 2.11 (br, 4H), 1.14 (br, 24H), 0.81 (br, 6H); ^{13}C NMR (150 MHz, $CDCl_3$) δ (ppm): 164.5, 152.0, 140.7, 140.2, 132.3, 131.5, 130.6, 129.6, 129.1, 128.7, 128.4, 128.2, 127.1, 126.3, 121.7, 120.5, 120.1, 111.5, 55.5, 40.5, 31.9, 30.2, 29.4, 24.1, 22.7, 14.2; FT-IR (KBr pellets, cm^{-1}): 2953, 2922, 2850, 1710, 1669, 1585, 1466, 1357, 1237, 810.

2.2.7. Poly[2,7-(9,9′-dioctylfluorene)-co-N-phenyl-1,8-naphthalimide] (PFONPN10)

9,9-Dioctylfluorene-2,7-diboronic acid bis(1,3-propanediol) ester (3) (0.2792 g, 0.50 mmol), 2,7-dibromo-9,9-dioctylfluorene (1) (0.2193 g, 0.40 mmol) and 4-bromo-9-N-4-bromophenyl-1,8-naphthalimide (2) (0.0431 g, 0.10 mmol) were used in this polymerization. ^{1}H NMR (600 MHz, $CDCl_3$) δ (ppm): 8.79, (br, 2H), 8.44 (br, 1H), 7.87 (br, 2H), 7.70 (br, 4H), 7.57 (br, 1H), 7.49 (br, 1H), 7.37 (br, 1H), 6.88 (br, 1H), 2.12 (br, 4H), 1.14 (br, 24H), 0.82 (br, 6H); ^{13}C NMR (150 MHz, $CDCl_3$): δ (ppm) 154.0, 140.7, 140.2, 126.3, 121.7, 120.1, 55.5, 40.6, 32.0, 30.2, 29.4, 24.1, 22.8, 14.2; FT-IR (KBr pellets, cm^{-1}): 2953, 2922, 2850, 1710, 1669, 1585, 1466, 1357, 1237, 810.

2.2.8. Poly[2,7-(9,9′-dioctylfluorene)-co-N-phenyl-1,8-naphthalimide] (PFONPN05)

9,9-Dioctylfluorene-2,7-diboronic acid bis(1,3-propanediol) ester (3) (0.2792 g, 0.50 mmol), 2,7-dibromo-9,9-dioctylfluorene (1) (0.2467 g, 0.45 mmol) and 4-bromo-9-N-4-bromophenyl- 1,8-naphthalimide (2) (0.0215 g, 0.05 mmol) were used in this polymerization. ^{1}H NMR (600 MHz, $CDCl_3$) δ (ppm): 8.75 (br, 2H), 8.44 (br, 1H), 7.85 (br, 2H), 7.70 (br, 4H), 7.56 (br, 1H), 7.49 (br, 1H), 7.37 (br, 1H), 6.83 (br, 1H), 2.1 (br, 4H), 1.14 (br, 24H), 0.80 (br, 6H); ^{13}C NMR (150 MHz, $CDCl_3$) δ (ppm): 152.0, 140.7, 140.2, 126.3, 121.7, 120.1, 55.5, 40.5, 32.0, 30.2, 29.4, 24.1, 22.8, 14.2; FT-IR (KBr pellets, cm^{-1}) 2953, 2922, 2850, 1669, 1468, 814.

2.2.9. Poly[2,7-(9,9′-dioctylfluorene)-co-N-phenyl-1,8-naphthalimide] (PFONPN01)

9,9-Dioctylfluorene-2,7-diboronic acid bis(1,3-propanediol) ester (3) (0.2792 g, 0.50 mmol), 2,7-dibromo-9,9-dioctylfluorene (1) (0.2687 g, 0.49 mmol) and 4-bromo-9-N-4-bromophenyl-1,8-naphthalimide (2) (0.0041 g, 0.01 mmol) were used in this polymerization. ^{1}H NMR (600 MHz, $CDCl_3$) δ (ppm): 7.85 (br, 2H), 7.71 (br, 4H), 2.1 (br, 4H), 1.14 (br, 24H), 0.73 (br, 6H); ^{13}C NMR (150 MHz, $CDCl_3$) δ (ppm): 152.0, 140.7, 140.2, 126.3, 121.7, 120.1, 55.5, 40.6, 32.0, 30.2, 29.4, 24.1, 22.8, 14.2; FT-IR (KBr pellets, cm^{-1}) 2953, 2922, 2850, 1468, 814.

2.2.10. PLED fabrication and characterization

In order to study the EL properties, PLEDs were fabricated using the as synthesized copolymers as active layers. The PLED device configuration is composed of a pre-cleaned and prepatterned indium tin oxide (ITO) as the transparent anode. The ITO surface was ultrasonically agitated and cleaned in 2% detergent, acetone and isopropanol,

each for five minutes at 60 °C. After cleaning, ~40 nm layer of poly(3,4-ethylendioxythiophene): poly(styrenesulfonate) (PEDOT:PSS) as a hole injecting layer was spin-coated at 3000 rpm for 60 seconds, baked for 15 minutes in an argon environment at 130 °C. The copolymers were dissolved in chlorobenzene (15 mg mL^{-1}) and spin-coated above the PEDOT:PSS layer under an ambient atmosphere and thermally treated at 150 °C for 15 minutes for the removal of residual solvent. The film thickness of the active layer was ~80 nm. Finally, calcium and aluminum was thermally evaporated at a rate of 2 Å s^{-1} and 10 Å s^{-1}, respectively at a base pressure of 10^{-6} mbar to form the cathode electrode. The active area of the diodes was 12 mm^2. The current density-voltage (J-V) characteristics of the fabricated PLEDs were measured using a Keithley 2400 source meter whereas the luminance and the EL spectra were recorded using an LCS-100 integrated sphere. All the devices were fabricated and characterized under an argon atmosphere inside a glove box.

2.3. Results and discussion

2.3.1. Synthesis and characterization of the polymers

The synthetic routes to the preparation of monomers and polymers are shown in Scheme 2.1. Monomer 2,7-dibromo-9,9'- dioctylfluorene (donor) (1) was prepared according to the reported procedure[36] and monomer 4-bromo-9-N-4-bromophenyl- 1,8-naphthalimide (acceptor) (2) was prepared from 4-bromo-1,8- napthalicanhydride and 4-bromo aniline. Donor-acceptor based random conjugated copolymers were synthesized from monomers 1, 2 and 3 using palladium(0) catalysed Suzuki coupling polymerization. The molar ratio of the 4-bromo-9-N-4-bromophenyl-1,8- naphthalimide moiety in the copolymers was controlled by adjusting the molar ratio of 1 and 2 while maintaining a 1 : 1 molar ratio between the dibromo monomers and 9,9'-dioctylfluorene- 2,7-diboronic acid bis(1,3-propanediol)ester. The colors of the PFONPN01, PFONPN05 and PFONPN10 polymer powders were light yellow and those of PFONPN35, PFONPN25 and PFONPN50 polymers were yellow. The ^1H and ^{13}C NMR spectra (Figure 2.1) of the polymers in chloroform-d, and FT-IR spectra (Figure 2.2) confirmed the expected polymer structures. In ^1H NMR spectra peaks were observed at 8.75 and 8.44 ppm due to the NPN moiety protons along with some other peaks merged with fluorene peaks. Similarly, in ^{13}C NMR spectra, peaks were observed at 164.7, 132.5, 131.3, 130.3, 128.8, 128.2, 127.9 and 127.1 ppm due to the NPN moiety carbons. The relative intensity of NPN peaks in both the ^1H and ^{13}C NMR spectra gradually increases as the NPN moiety increases in the polymer chain.

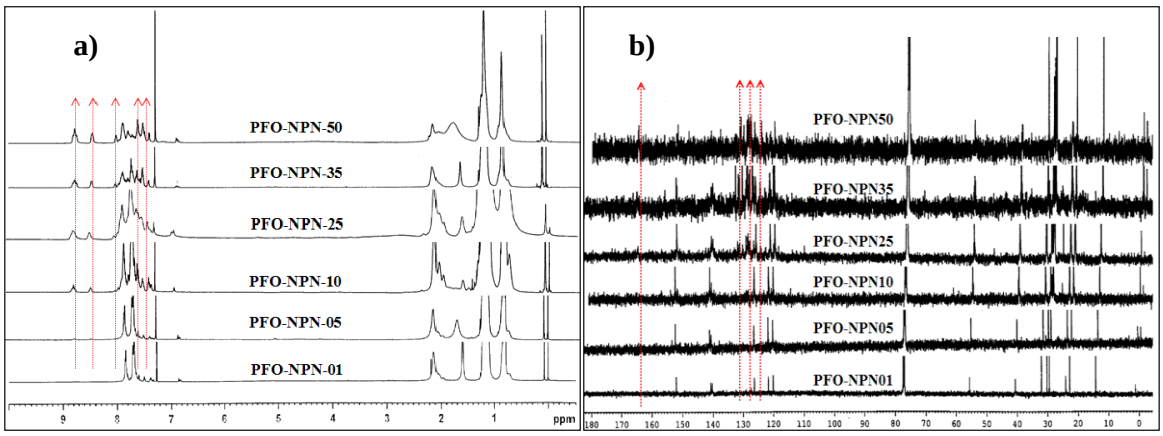

Figure 2.1: ^{1}H (a) and ^{13}C NMR (b) spectra of copolymers in $CDCl_3$

Table 2.1: NPN content in the copolymers

NPN content in the Polymers (mol %)		
Polymer	**Feed ratio**	**Actual content[a]**
PFONPN01	1	0.8
PFONPN05	5	5
PFONPN10	10	12
PFONPN25	25	28
PFONPN35	35	39
PFONPN50	50	48

[a] Calculated from the ^{1}H NMR spectra

The actual content of NPN in the polymers was estimated from their ^{1}H NMR spectra by comparing the integral values of the NPN unit with that of the fluorene monomer and are listed in Table 2.1. It was found that the actual content of NPN was very close to the feed ratio, suggesting that NPN has been fully incorporated into the main chain of the polymers during polymerization. In the FT-IR spectra of the PFONPN polymers the five peaks located at 1710, 1669, 1585, 1357 and 1237 cm^{-1} correspond to the NPN unit, and upon increasing the NPN moiety in the polymer chain, the relative intensity of these five peaks also shows an increase. The number-average molecular weights (M_n) of the copolymers, determined by GPC using a PMMA standard in THF, were found to be in the range of 11729-13389 with a polydispersity index (M_w/M_n) of 1.14 to 1.31 (Table 2.2). The polymerization results of copolymers are summarized in Table 2.2. Thermal properties of these copolymers were determined by TGA and DSC (Figure 2.3a and 2.3b) under nitrogen flow at a heating rate of 10 °C min^{-1}. The TGA curves of the copolymers are shown in Figure 2.3a. All the copolymers were found to exhibit very good thermal

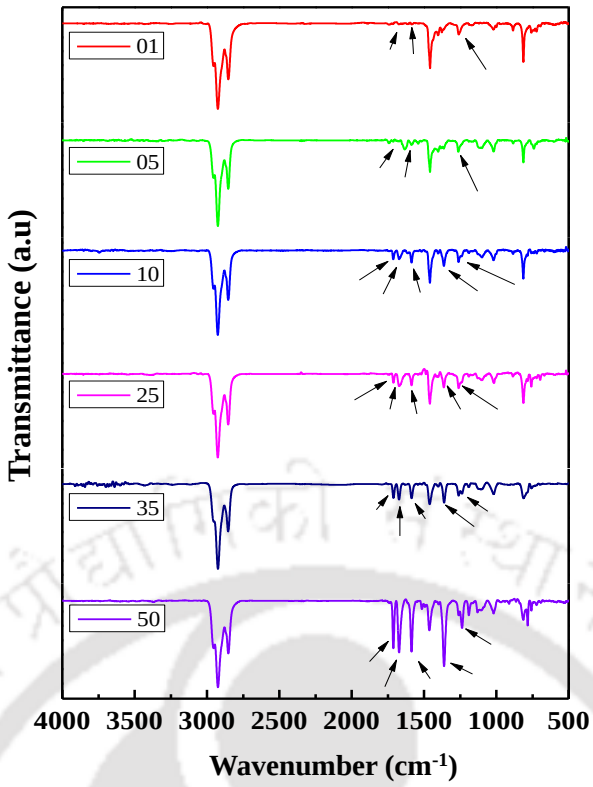

Figure 2.2: FT-IR spectra of copolymers

Table 2.2: Polymerization results and thermal data of copolymers

Polymer	M_n [a]	M_w [a]	PDI [a]	Yield (%)	T_d [b] (°C)	T_g [c] (°C)
PFONPN01	12463	14622	1.31	58	388	134.20
PFONPN05	13389	15213	1.17	67	405	123.48
PFONPN10	12057	14032	1.16	55	344	132.23
PFONPN25	12135	14146	1.26	62	380	133.33
PFONPN35	11729	13663	1.14	57	355	125.46
PFONPN50	12568	14747	1.17	61	342	132.85

[a] M_n, M_w and PDI of the polymers were determined by gel permeation chromatography using PMMA standards. [b] Onset decomposition temperature measured by TGA under nitrogen. [c] Glass transition temperature

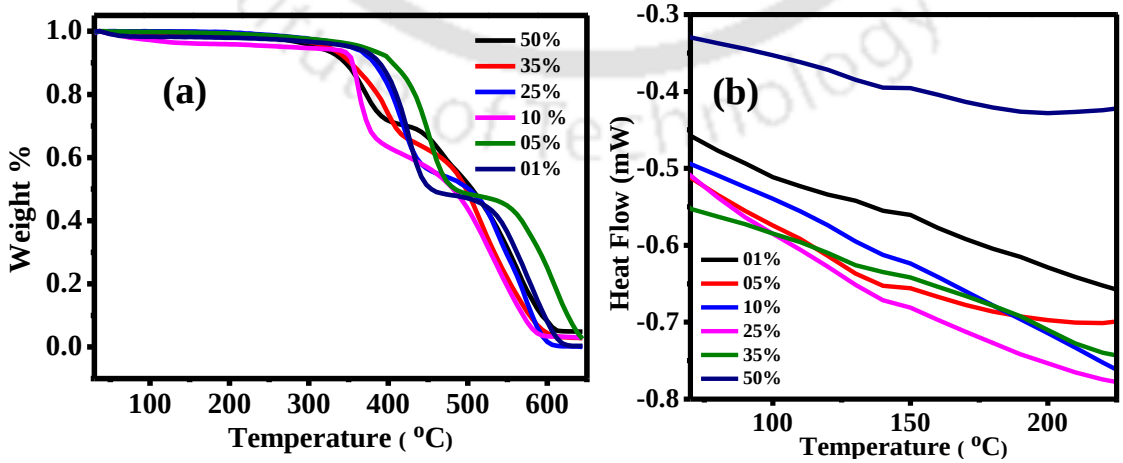

Figure 2.3: TGA (a) and DSC (b) curves of copolymers

stability with onset decomposition temperatures (T_d) in the range of 342-405 °C (Table 2.2) and no weight loss was observed at lower temperatures. Interestingly all copolymers showed two step degradation due to the presence of two different units in the polymer main chain. The glass transition temperature (T_g) of the copolymers was investigated by DSC (Table 2.2). The amorphous nature of all polymers was very useful in solution processing for PLED fabrication.

2.3.2. Optical and photoluminescence properties

The normalized UV-visible absorption properties of the PFONPN copolymers, both in solution (chloroform, 10^{-5} M) and solid states are shown in Figure 2.4a and 2.4b and the results are summarized in Table 2.3. In the solution state the PFONPN50 polymer shows two absorption peaks at 325 and 393 nm and all the remaining polymers showed single peaks viz. PFONPN35 at 365 nm, PFONPN25 at 370 nm, PFONPN10 at 363 nm and PFONPN05, PFONPN1 at 380 nm. For solid state measurements, the copolymer film with a thickness of approximately 80 nm was spin coated on a glass substrate from a chloroform solution. Also in the solid state PFONPN50 showed two peaks at 327 and 395 nm whereas the remaining polymers showed single peaks viz. PFONPN35 at 370 nm, PFONPN25 at 375 nm, PFONPN10 at 365 nm, PFONPN05 at 381 nm and PFONPN01

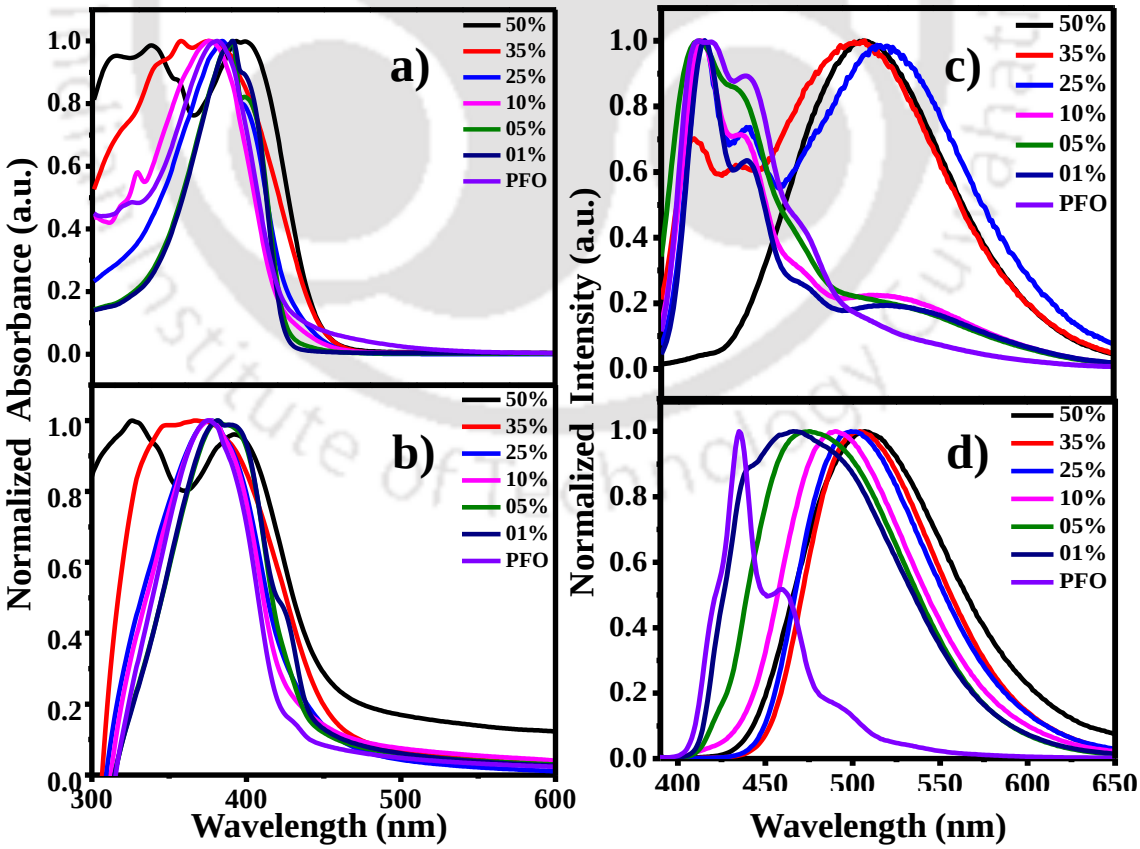

Figure 2.4: UV-Vis (a) & (b) and PL (c) & (d) spectra of copolymers in solution and solid state

at 380 nm. The optical band gaps (E_g) of all the polymers were estimated from the solid state UV-visible absorption edges. Both solution and solid state absorption maximum of all copolymers showed a slight blue shift with increase in fraction of NPN content because increase in the fraction of the NPN content in the polymer main chain induces a decrease in the effective conjugation length of fluorene units.[37,38] The normalized PL spectra of the PFONPN conjugated polymers, both in solution (chloroform 10^{-5} M) and solid states, are shown in Figure 2.4c and 2.4d and the results are summarized in Table 2.3. The solution state PL spectra of copolymers were taken at different excitations. The PL spectrum of PFONPN50 was taken at an excitation of 340 nm, and a single peak at 508 nm was obtained. The emission color of the PFO is completely quenched due to energy transfer from the PFO to NPN unit. All the remaining copolymers PFONPN35, PFONPN25, PFONPN10, PFONPN05 and PFONPN01 showed two peaks when excited at a wavelength of 380 nm. The peak in the blue region is due to the fluorene unit whereas the peak in the green region is because of the NPN unit. It was observed that the intensity of the green peak increases upon increasing the NPN content in the polymer chain. All these copolymers showed a single peak in the solid phase due to efficient charge transfer and strong energy transfer from PFO to NPN units. The solid state PL spectra of PFONPN50 was recorded at an excitation wavelength of 340 nm whereas for the remaining copolymers the solid state PL spectra were recorded at an excitation wavelength of 380 nm. The emission colors of the polymers are red shifted from 466 nm to 511 nm (blue to green) when the NPN content increases from 0.1 to 50 mol% in the polymer backbone. The PL quantum yields (Φ_{PL}) of the copolymers in the solid state

Table 2.3: Photophysical properties of the copolymers

	Chloroform solution		**Solid state**		
Polymer	**$\lambda_{max, abs}$ [nm]**	**$\lambda_{max, PL}$ [nm]**	**$\lambda_{max, abs}$ [nm]**	**$\lambda_{max, PL}$ [nm]**	**Φ_{PL}[a]**
PFONPN01	380	415, 519	380	466	0.74
PFONPN05	380	415, 520	381	477	0.69
PFONPN10	363	415, 520	365	490	0.42
PFONPN25	370	416, 517	375	500	0.34
PFONPN35	365	416, 504	370	505	0.27
PFONPN50	325, 393	508	327, 395	511	0.18

[a]Solid state PL quantum yields are estimated with polydioctylfluorene standard

were measured by excitation at 380 nm except PFONPN50 which was excited at 330 nm (Table 2.3). The solid state quantum yields of the polymers are estimated by comparing their fluorescence intensity to that of a thin film sample of the PFO polymer (Φ_F = 0.55).[39] The quantum yield values of copolymers decrease with increasing NPN unit, due to the concentration quenching effect of the NPN unit caused by aggregation of the chromophores.[22,40,41] A very good way to suppress this is by developing supramolecular compounds, such as rotaxanes, which suppress aggregation/quenching very effectively.[42]

2.3.3. Electrochemical and Electroluminescence properties

Cyclic voltammetry (CV) (Figure 2.5a) was performed to investigate the reduction and oxidation peaks of the copolymers and to estimate their highest occupied molecular orbital (HOMO) and lowest unoccupied molecular orbital (LUMO) energy levels. The copolymers were drop casted onto the carbon working electrode and silver and platinum wires were used as the reference electrode and counter electrode, respectively. The electrochemical properties of the copolymers were investigated in an electrolyte consisting of a solution of 0.1 M tetra butyl ammonium hexafluorophosphate (Bu_4NPF_6) in acetonitrile (CH_3CN) at room temperature under an argon atmosphere.

Table 2.4: Electrochemical potentials and energy levels of the PFONPN copolymers

Polymer	E_{ox}/ V	E_{red}/V	E_{HOMO}/eV	E_{LUMO}/eV	E_g/eV	Optical band gap/eV
PFONPN01	1.38	-0.69	-5.8	-2.9	2.9	2.95
PFONPN05	1.21	-1.2	-5.97	-3.5	2.47	2.71
PFONPN10	1.15	-1.3	-5.85	-3.4	2.45	2.70
PFONPN25	1.25	-1.16	-5.95	-3.52	2.41	2.69
PFONPN35	1.17	-1.2	-5.87	-3.5	2.37	2.67
PFONPN50	1.16	-1.18	-5.86	-3.5	2.34	2.62

The measurements were calibrated using ferrocene as standard. The PFONPN copolymers show two potential peaks (Figure 2.5a). The reduction potential, in the negative potential region (-1.18 to -1.23 V), is because of the NPN moiety as it has high electron affinity (because it possesses carbonyl groups). Similarly, the peak in the positive potential region (1.1 to 1.25 V) is oxidation potential for the fluorene unit. The HOMO and LUMO energies were calculated by submitting the onset reduction and onset oxidation peak values in E_{LUMO} = [(E_{red}-$E_{1/2}$(ferrocene)) + 4.8 eV], E_{HOMO} = [(E_{ox}-$E_{1/2}$(ferrocene)) + 4.8 eV]. The onset reduction and onset oxidation peak values, energy levels and band gaps of the copolymers are represented in Table 2.4.

In order to investigate the EL properties of the polymers, single-layer devices with a configuration of ITO/ PEDOT:PSS (40 nm)/polymer (80 nm)/Ca (10 nm)/Al (100 nm) were fabricated. The typical EL spectra and the current density-voltage (J-V) characteristics of all the PLEDs are shown in Figure 2.5b and 2.6b, respectively. The onset values for all the fabricated devices along with their emission maxima and CIE coordinates are listed in Table 2.5. From Figure 2.5b it is clear that the copolymer PFONPN01 shows three peaks at 434 nm, 464 nm and 486 nm, respectively. The first two peaks in the spectrum can be attributed to the PF main chain whereas the peak centered at 486 nm is due to the partial energy transfer from the PFO to NPN unit.[43-46] The PF emission, however, was completely quenched as the NPN content of the copolymer was increased. The EL spectra of all the other copolymers show only a single peak centered at 483 nm for PFONPN05, 493 nm for PFONPN10, 497 nm for PFONPN25, 504 nm for PFONPN35 and 506 nm for PFONPN50, respectively. The slight difference in the wavelength between the solid state fluorescence emission and the electroluminescence emission can be attributed to the different emission mechanism between PL and EL. Figure 2.6a shows the chromaticity diagram representing the CIE coordinates of the fabricated PLEDs. The chromaticity coordinates of the copolymers changed from x = 0.17, y = 0.22, for PFONPN01 to x = 0.24, y = 0.49 for PFONPN50. The PLED devices fabricated using these copolymers are found to exhibit very good results and the device performance is presented in Table 2.5. Figure 2.6c and 2.6d shows that the brightness and luminous efficiency of the devices are 5236 cd m^{-2} and 3.52 cd A^{-1} for PFONPN01, 3120 cd m^{-2} and 1.96 cd A^{-1} for PFONPN05, 2064 cd m^{-2} and 1.5 cd A-1 for PFONPN10, 1755 cd m^{-2} and 1.16 cd A^{-1} for PFONPN25, 1756 cd m^{-2} and 1.1 cd A^{-1} for PFONPN35 and 345 cd m^{-2} and 0.22 cd A^{-1} for PFONPN50.

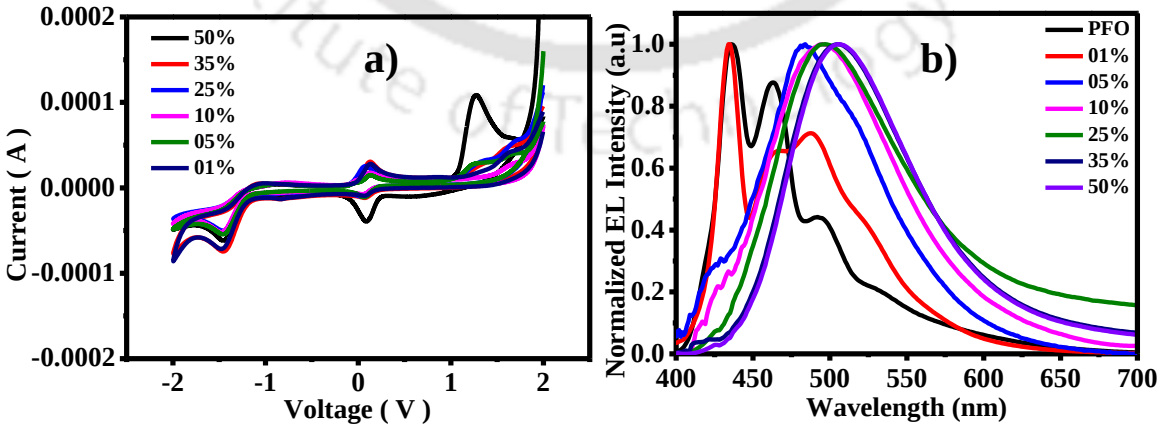

Figure 2.5: Cyclic voltammograms (a) and EL spectra (b) of copolymers.

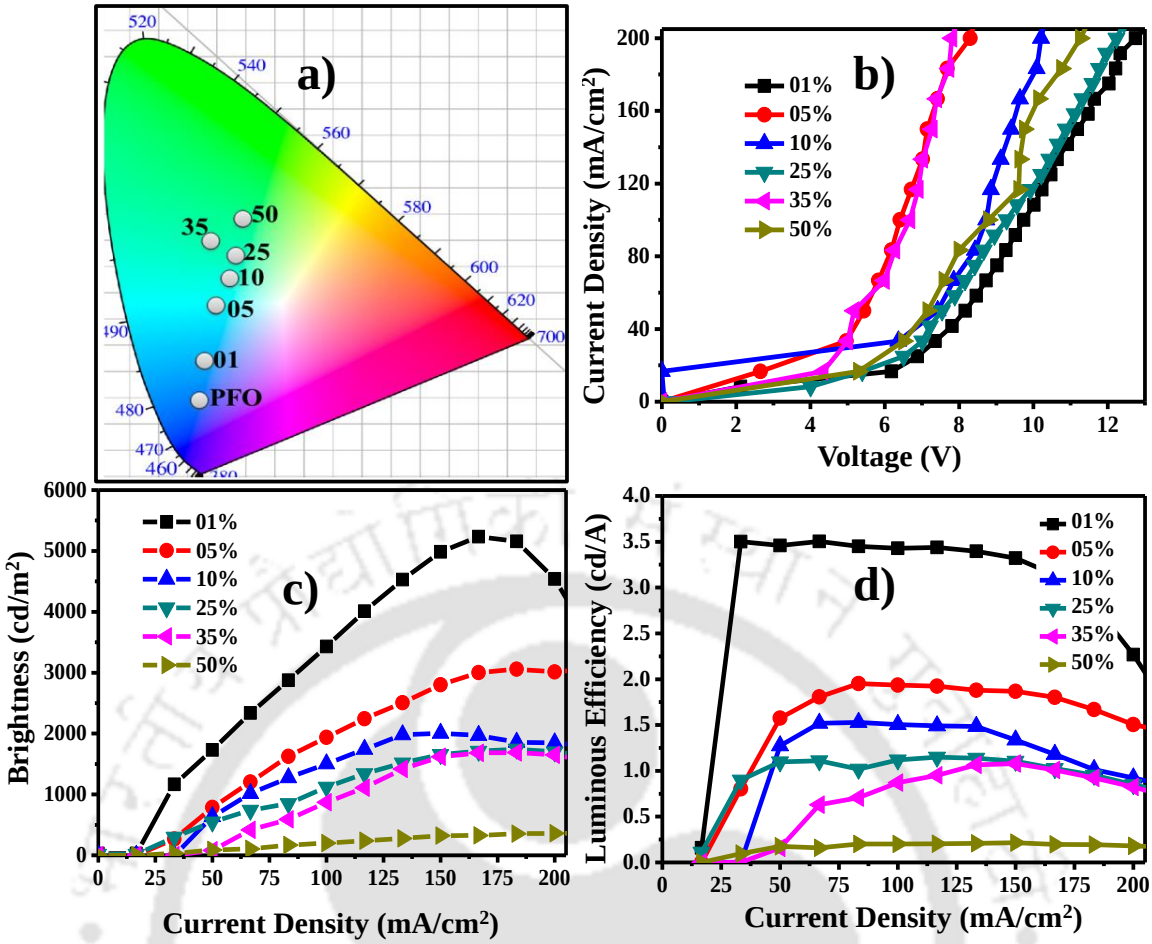

Figure 2.6: (a) Chromaticity diagram representing the CIE coordinates, (b) Current density-voltage (J-V), (c) Brightness vs. current density and (d) Luminous efficiency vs. current density characteristics of PLEDs

Table 2.5: Device characteristics of PLEDs based on copolymers

Polymer	Onset Voltage (V)	$\lambda_{max, EL}$ [nm]	Max. brightness (cd m^{-2})	Luminous efficiency (cd A^{-1})	CIE coordinate (x, y)[a]
PFO	6.5	436, 463, 493	1949	0.99	0.17, 0.15
PFONPN01	6.3	434, 464, 486	5236	3.52	0.17, 0.22
PFONPN05	5.4	483	3120	1.96	0.19, 0.32
PFONPN10	6.5	493	2064	1.5	0.22, 0.45
PFONPN25	5.7	497	1755	1.16	0.22, 0.37
PFONPN35	5.3	504	1756	1.1	0.23, 0.42
PFONPN50	5.5	506	345	0.22	0.24, 0.49

[a] Determined from the EL spectrum.

The enhanced device performance of PFONPN01 as compared to other polymer results was due to the well-balanced electron and holes in the polymer main chain. From these results, it is clear that upon increasing the NPN content the device brightness showed a decreasing trend. This was due to the high electron affinity of the NPN unit. As the concentration of the NPN unit increases, the electron accepting capacity of the polymer

also increases due to the excess electron attracting effect leading to decreasing device performance.

2.4. Summary

Six novel donor and acceptor based random conjugated copolymers (PFONPN) were synthesized by introducing the NPN unit as an acceptor into PF by the well-known palladium catalysed Suzuki coupling reaction. All copolymers were highly soluble in common organic solvents such as chlorobenzene, chloroform, dichloromethane and THF. The resulting copolymers exhibited excellent thermal stability and high glass transition temperature. The emission color of the PF (blue) could easily be tuned to green via efficient energy transfer to the acceptor (NPN) unit. In solid state PL, the PF fluorescence was totally quenched at NPN concentrations as low as 1% and the PFONPN copolymers exhibited maximum emission at 466-511 nm. The single layer PLED devices made using these PFONPN polymers with the configuration of ITO/PEDOT:PSS/ PFONPN/Ca:Al were found to be very bright with PFONPN01 giving the highest brightness of 5236 cd m^{-2} and a luminous efficiency of 3.52 cd A^{-1}. Like PL spectra, the EL spectra also showed the color tuning properties for the copolymers.

2.5. References

1. Burroughes, J. H.; Bradley, D. D. C.; Brown, A. R.; Marks, R. N.; Mackay, K.; Friend, R. H.; Burn, P. L.; Holmes, A. B. *Nature* **1990,** *347*, 539-541.
2. Kraft, A.; Grimsdale, A. C.; Holmes, A. B. *Angew. Chem. Int. Edit.* **1998,** *37*, 402-428.
3. Friend, R. H.; Gymer, R. W.; Holmes, A. B.; Burroughes, J. H.; Marks, R. N.; Taliani, C.; Bradley, D. D. C.; Dos Santos, D. A.; Bredas, J. L.; Logdlund, M.; Salaneck, W. R. *Nature* **1999,** *397*, 121-128.
4. Mitschke, U.; Bauerle, P. *J. Mater. Chem.* **2000,** *10*, 1471-1507.
5. Bernius, M. T.; Inbasekaran, M.; O'Brien, J.; Wu, W. S. *Adv. Mater.* **2000,** *12*, 1737-1750.
6. Klarner, G.; Lee, J. I.; Davey, M. H.; Miller, R. D. *Adv. Mater.* **1999,** *11*, 115-119.
7. Liao, L. S.; Fung, M. K.; Lee, C. S.; Lee, S. T.; Inbasekaran, M.; Woo, E. P.; Wu, W. W. *Appl. Phys. Lett.* **2000,** *76*, 3582-3584.
8. Bernius, M.; Inbasekaran, M.; Woo, E.; Wu, W. S.; Wujkowski, L. Fluorene-based Polymers-Preparation and Applications. *J. Mater. Sci-Mater. El.* **2000,** *11*, 111-116.
9. Muller, C. D.; Falcou, A.; Reckefuss, N.; Rojahn, M.; Wiederhirn, V.; Rudati, P.; Frohne, H.; Nuyken, O.; Becker, H.; Meerholz, K. *Nature* **2003,** *421* (6925), 829-833.
10. Liu, M. S.; Jiang, X. Z.; Liu, S.; Herguth, P.; Jen, A. K. Y. *Macromolecules* **2002,** *35* (9), 3532-3538.
11. Hou, Q.; Xu, Y. S.; Yang, W.; Yuan, M.; Peng, J. B.; Cao, Y. *J. Mater. Chem.* **2002,** *12*, 2887-2892.
12. Yang, J.; Jiang, C. Y.; Zhang, Y.; Yang, R. Q.; Yang, W.; Hou, Q.; Cao, Y. *Macromolecules* **2004,** *37*, 1211-1218.
13. Peng, Q.; Lu, Z. Y.; Huang, Y.; Xie, M. G.; Han, S. H.; Peng, J. B.; Cao, Y. *Macromolecules* **2004,** *37*, 260-266.
14. Pei, J.; Yu, W. L.; Huang, W.; Heeger, A. J. *Chem. Commun.* **2000,** 1631-1632.
15. Yang, R. Q.; Tian, R. Y.; Hou, Q.; Yang, W.; Cao, Y. *Macromolecules* **2003,** *36*, 7453-7460.
16. Beaupre, S.; Leclerc, M. *Adv. Funct. Mater.* **2002,** *12*, 192-196.
17. Liu, B.; Yu, W. L.; Lai, Y. H.; Huang, W. *Macromolecules* **2000,** *33*, 8945-8952.
18. Liu, M. S.; Luo, J. D.; Jen, A. K. Y. *Chem. Mater.* **2003,** *15*, 3496-3500.
19. Sonar, P.; Zhang, J. Y.; Grimsdale, A. C.; Mullen, K.; Surin, M.; Lazzaroni, R.; Leclere, P.; Tierney, S.; Heeney, M.; McCulloch, I. *Macromolecules* **2004,** *37*, 709-715.
20. Lim, E.; Jung, B. J.; Shim, H. K. *Macromolecules* **2003,** *36*, 4288-4293.
21. Islam, A.; Cheng, C. C.; Chi, S. H.; Lee, S. J.; Hela, P. G.; Chen, I. C.; Cheng, C. H. *J. Phys. Chem. B* **2005,** *109*, 5509-5517.
22. Liu, J.; Tu, G. L.; Zhou, Q. G.; Cheng, Y. X.; Geng, Y. H.; Wang, L. X.; Ma, D. G.; Jing, X. B.; Wang, F. S. *J. Mater. Chem.* **2006,** *16*, 1431-1438.
23. Mei, C. Y.; Tu, G. L.; Zhou, Q. G.; Cheng, Y. X.; Xie, Z. Y.; Ma, D. G.; Geng, Y. H.; Wang, L. X. *Polymer* **2006,** *47*, 4976-4984.

24. Coya, C.; Blanco, R.; Juarez, R.; Gomez, R.; Martinez, R.; de Andres, A.; Alvarez, A. L.; Zaldo, C.; Ramos, M. M.; de la Pena, A.; Seoane, C.; Segura, J. L. *Eur. Polym. J.* **2010,** *46*, 1778-1789.
25. Cacialli, F.; Friend, R. H.; Bouche, C. M.; Le Barny, P.; Facoetti, H.; Soyer, F.; Robin, P. *J. Appl. Phys.* **1998,** *83*, 2343-2356.
26. Dorlars, A.; Schellhammer, C. W.; Schroeder, J. *Angew.Chem., Int. Ed. Engl.* **1975,** *14*, 665-679.
27. Grabchev, I.; Chovelon, J. M.; Bojinov, V. *Polym. Advan. Technol.* **2004,** *15*, 382-386.
28. Adam, W.; Qian, X. H.; Sahamoller, C. R. *Tetrahedron* **1993,** *49*, 417-422.
29. Cacialli, F.; Bouche, C. M.; Le Barny, P.; Friend, R. H.; Facoetti, H.; Soyer, F.; Robin, P. *Opt. Mater* **1998,** *9*, 163-167.
30. Grabchev, I. *Dyes Pigments* **1998,** *38*, 219-226.
31. Hu, C.; Zhu, W. H.; Lin, W. Q.; Tian, H. *Synthetic. Met.* **1999,** *102*, 1129-1130.
32. Westerling, M.; Vijila, C.; Osterbacka, R.; Stubb, H. *Synthetic. Met.* **2003,** *135*, 321-322.
33. Tu, G. L.; Zhou, Q. G.; Cheng, Y. X.; Wang, L. X.; Ma, D. G.; Jing, X. B.; Wang, F. S. *Appl. Phys. Lett.* **2004,** *85*, 2172-2174.
34. Lee, J. F.; Hsu, S. L. C. *Polymer* **2009,** *50*, 5668-5674.
35. Lee, J. F.; Hsu, S. L. C. *Polymer* **2009,** *50*, 2558-2564.
36. Saikia, G.; Iyer, P. K. *J. Org. Chem.* **2010,** *75*, 2714-2717.
37. Klaerner, G.; Miller, R. D. *Macromolecules* **1998,** *31*, 2007-2009.
38. Asawapirom, U.; Scherf, U. *Macromol. Rapid. Comm.* **2001,** *22*, 746-749.
39. Grice, A. W.; Bradley, D. D. C.; Bernius, M. T.; Inbasekaran, M.; Wu, W. W.; Woo, E. P. *Appl. Phys. Lett.* **1998,** *73*, 629-631.
40. Morgado, J.; Cacialli, F.; Friend, R. H.; Iqbal, R.; Yahioglu, G.; Milgrom, L. R.; Moratti, S. C.; Holmes, A. B. *Chem. Phys. Lett.* **2000,** *325*, 552-558.
41. Tang, C. W.; Vanslyke, S. A.; Chen, C. H. *J. Appl. Phys.* **1989,** *65*, 3610-3616.
42. Petrozza, A.; Brovelli, S.; Michels, J. J.; Anderson, H. L.; Friend, R. H.; Silva, C.; Cacialli, F. *Adv. Mater.* **2008,** *20*, 3218-3223.
43. Scherf, U.; List, E. J. W. *Adv. Mater.* **2002,** *14*, 477-487.
44. Kulkarni, A. P.; Kong, X. X.; Jenekhe, S. A. *J. Phys. Chem. B* **2004,** *108*, 8689-8701.
45. Lemmer, U.; Heun, S.; Mahrt, R. F.; Scherf, U.; Hopmeier, M.; Siegner, U.; Gobel, E. O.; Mullen, K.; Bassler, H. *Chem. Phys. Lett.* **1995,** *240*, 373-378.
46. List, E. J. W.; Guentner, R.; de Freitas, P. S.; Scherf, U. *Adv. Mater.* **2002,** *14*, 374-378.

Appendix

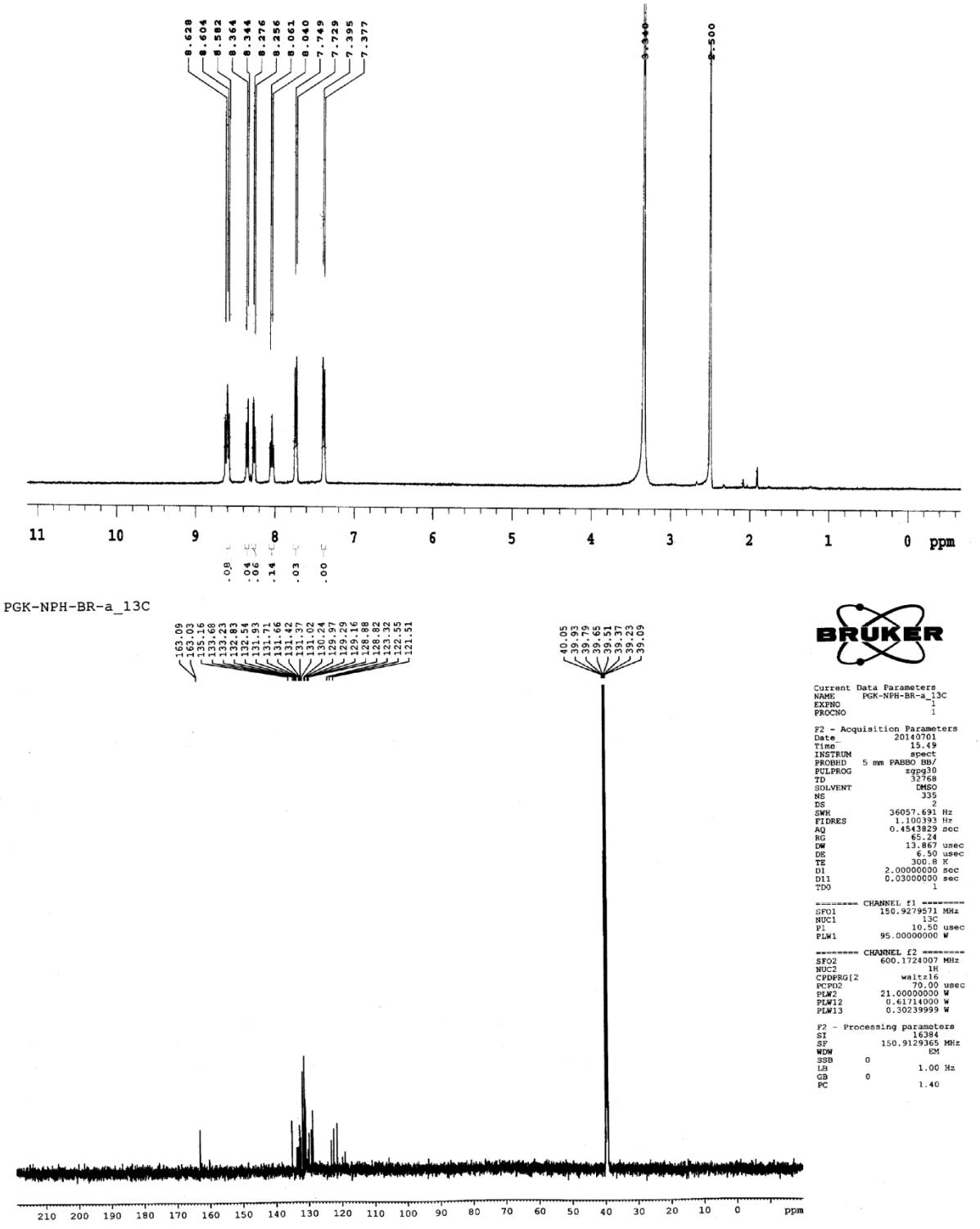

Figure 2.7: ^{1}H and ^{13}C NMR of the **4-bromo-9-*N*-4-bromophenyl-1,8-naphthalimide** in DMSO-d_6

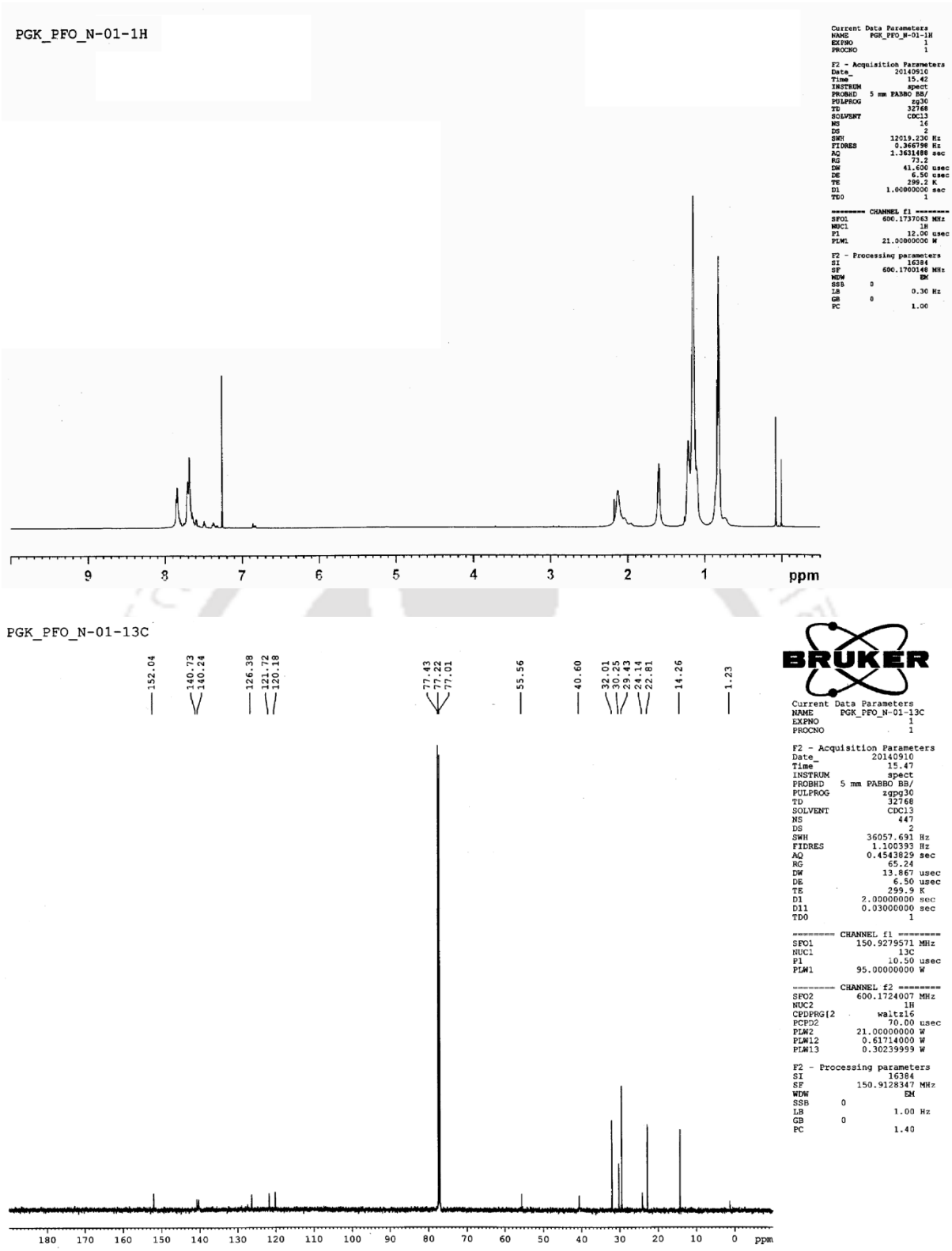

Figure 2.8: ^{1}H and ^{13}C NMR of the **PFONPN01** in $CDCl_3$

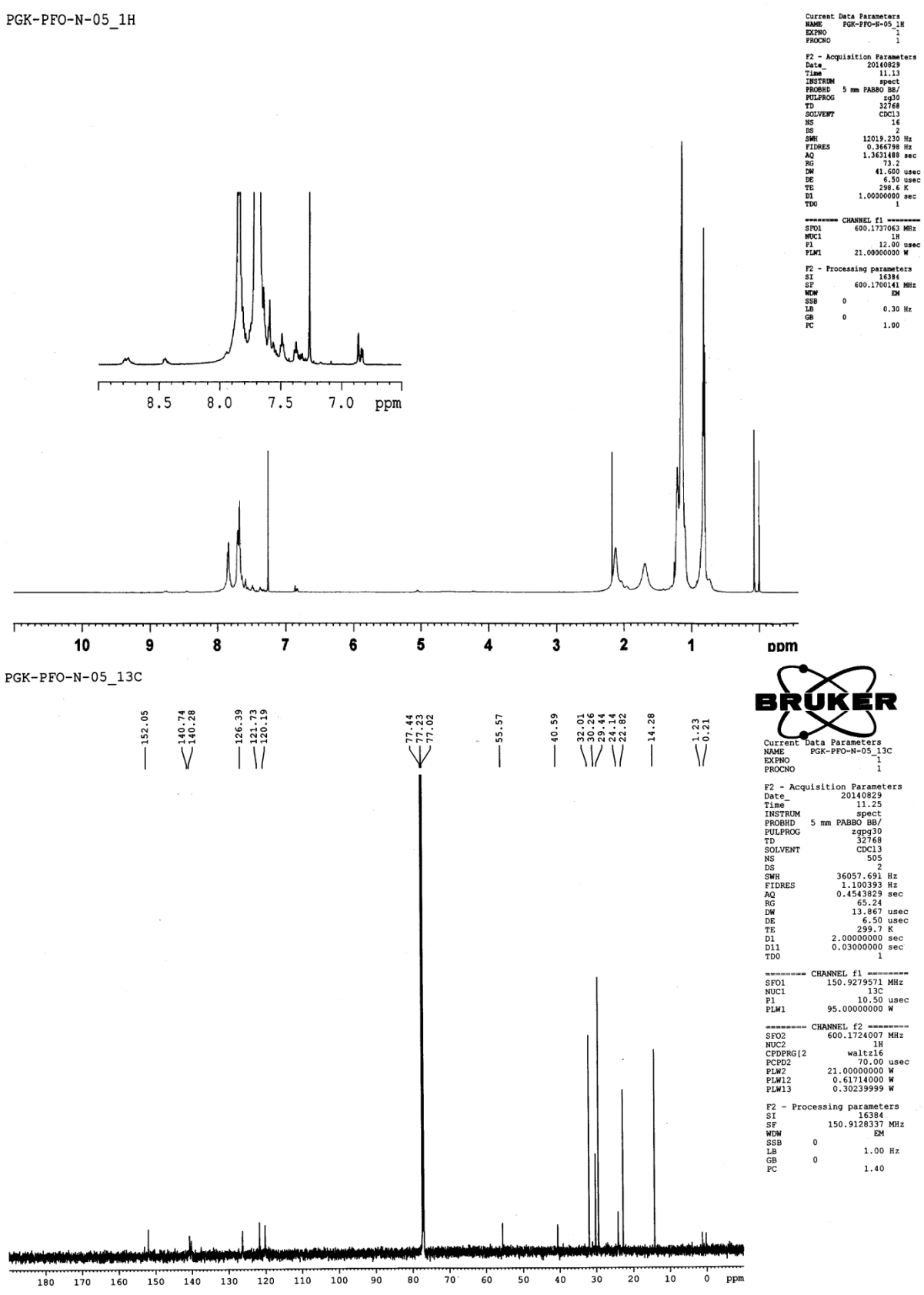

Figure 2.9: ^{1}H and ^{13}C NMR of the **PFONPN05** in $CDCl_3$

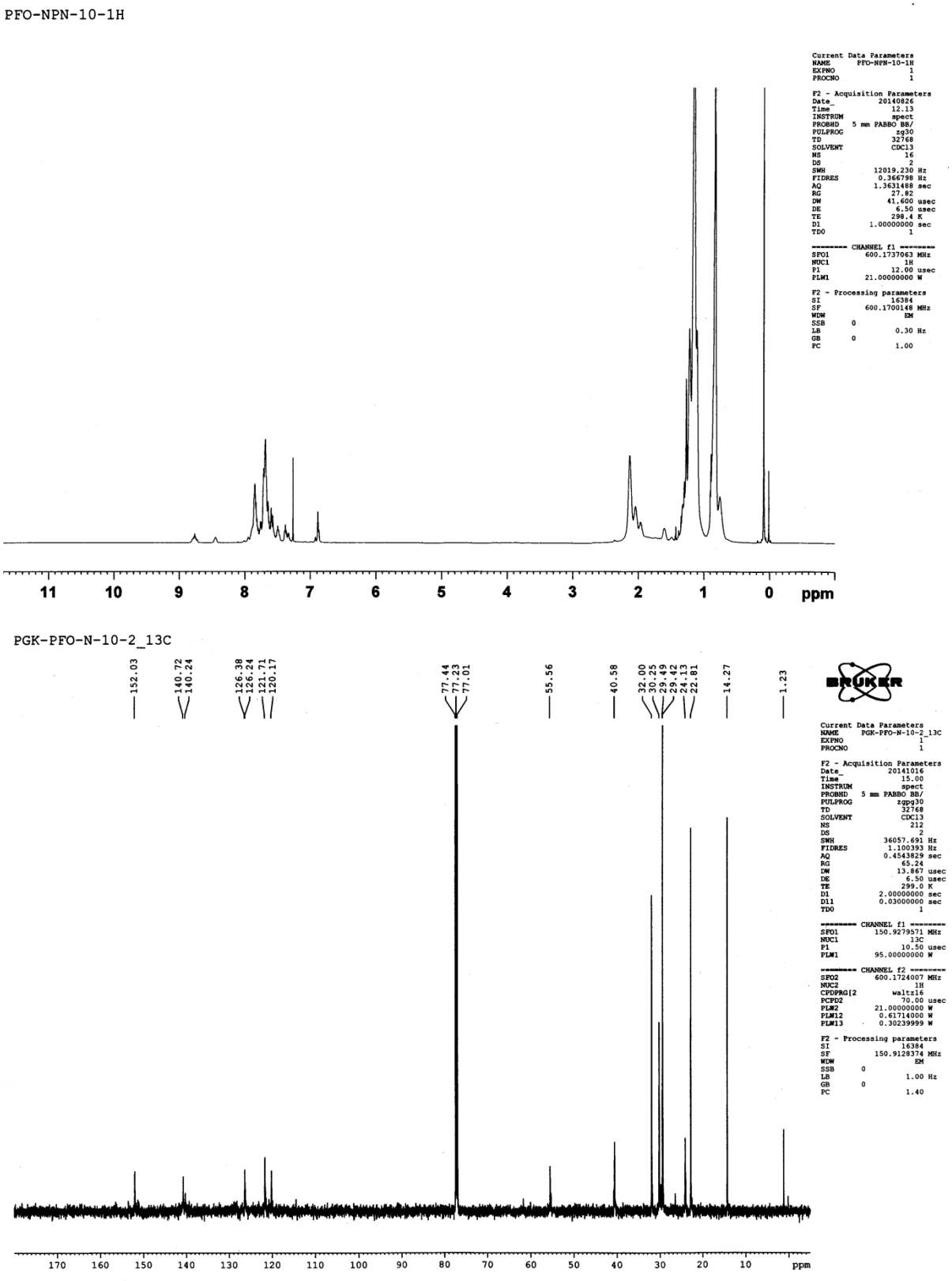

Figure 2.10: ^{1}H and ^{13}C NMR of the **PFONPN10** in $CDCl_3$

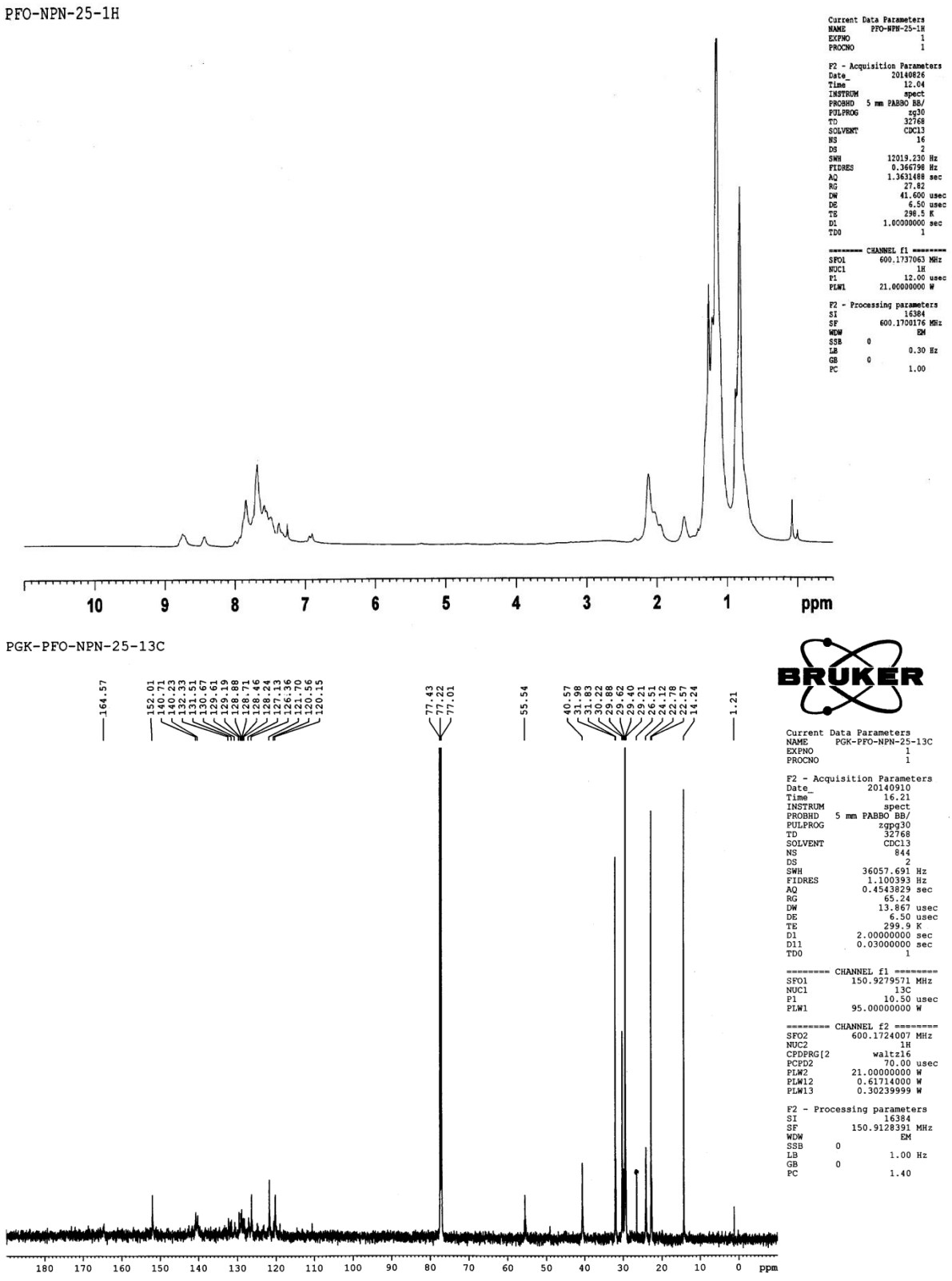

Figure 2.11: ^{1}H and ^{13}C NMR of the **PFONPN25** in $CDCl_3$

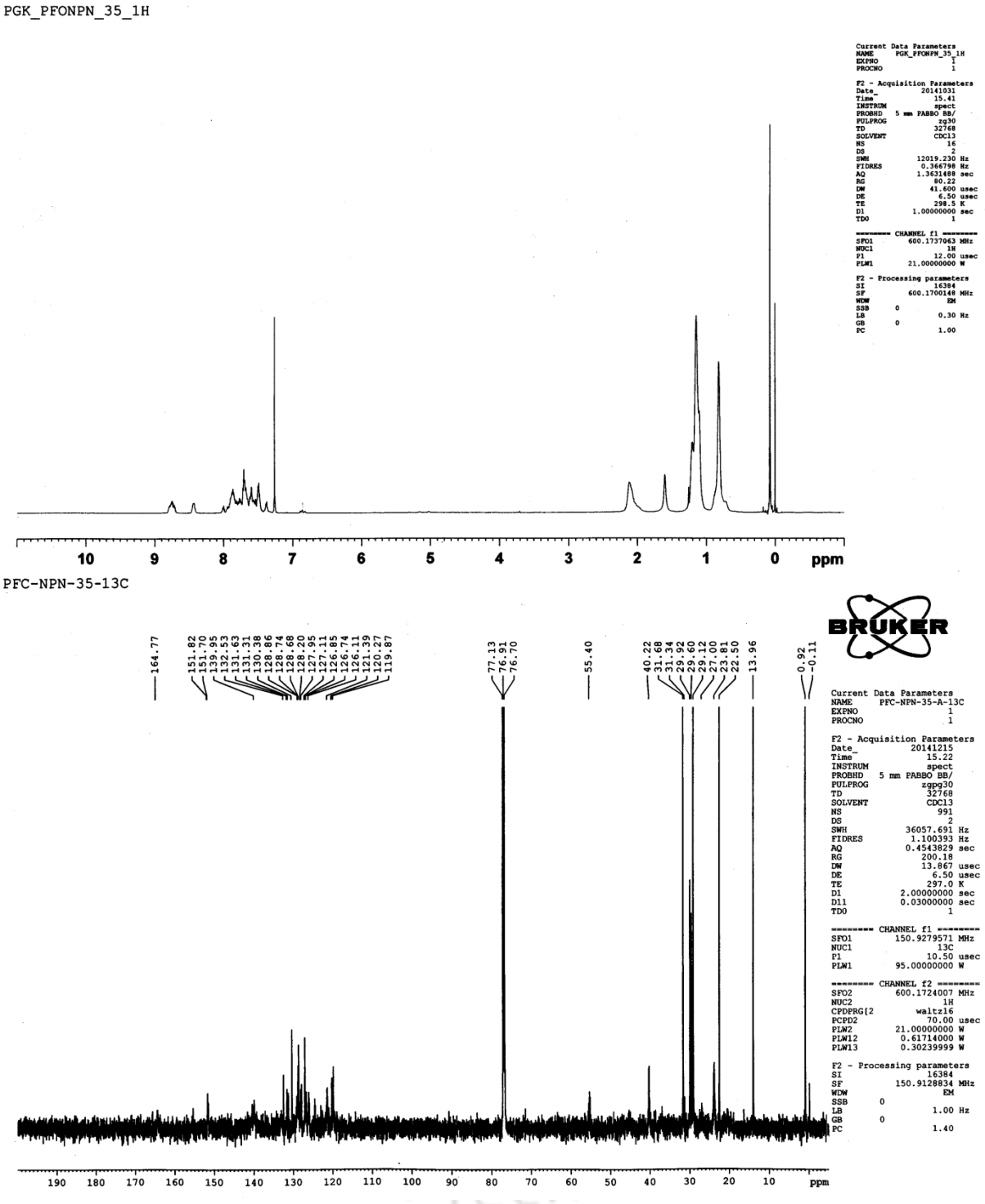

Figure 2.12: ^{1}H and ^{13}C NMR of the **PFONPN35** in $CDCl_3$

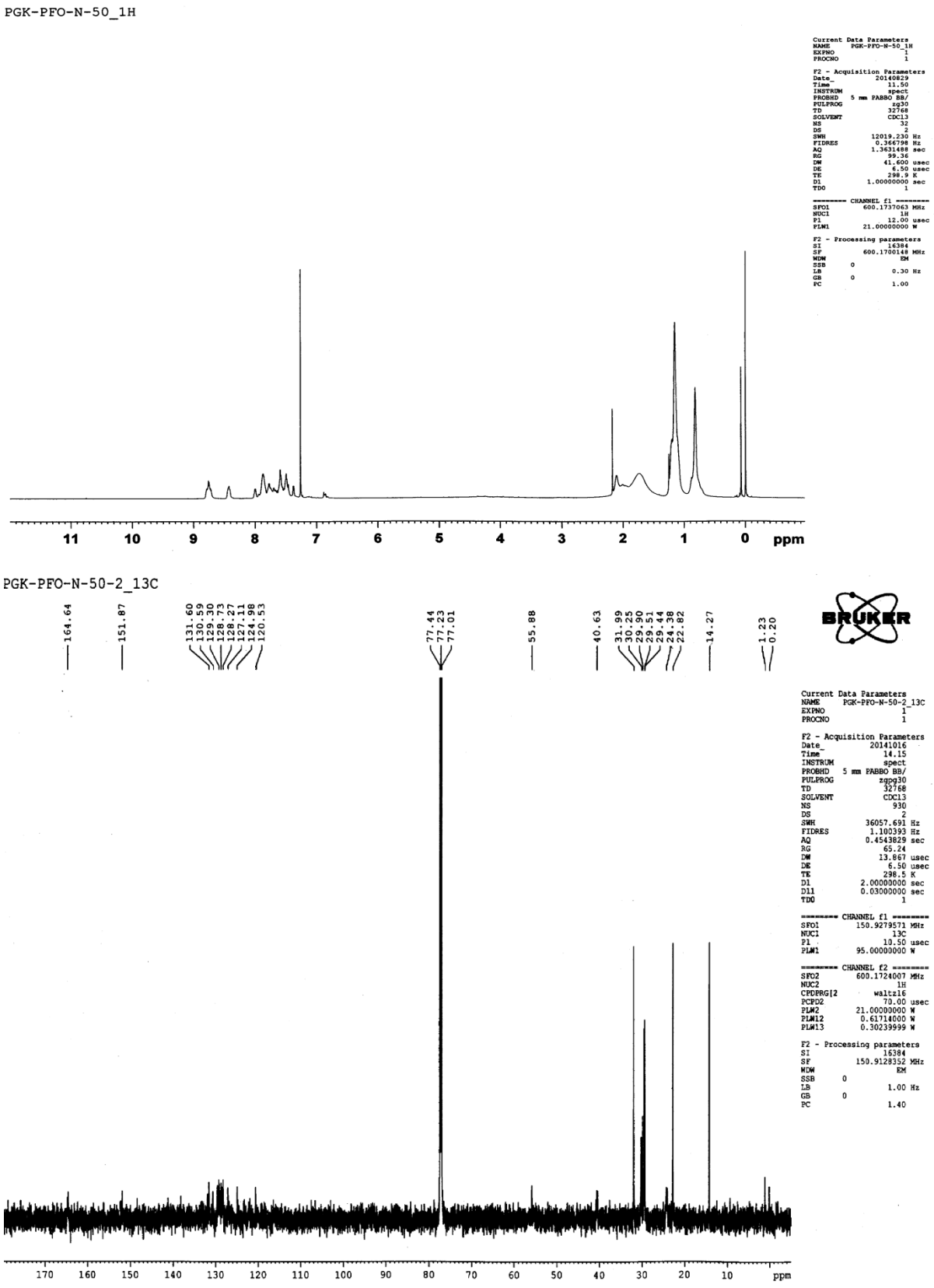

Figure 2.13: ^{1}H and ^{13}C NMR of the **PFONPN50** in $CDCl_3$

Chapter-3

Color Tunable Donor-Acceptor Electroluminescent Copolymers: Synthesis, Characterization, Photophysical Properties and PLED Fabrication

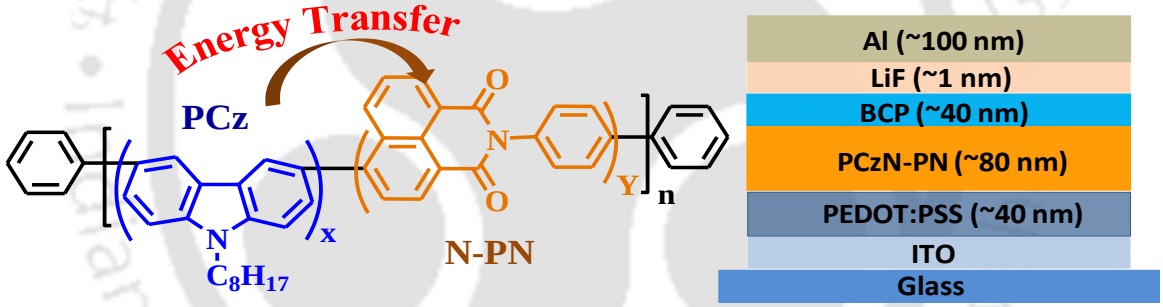

Gopikrishna, P.; Das, D.; Iyer, P. K. *ChemistrySelect,* 2017, *2,* 7044-7049.

Abstract

A series of novel color tunable donor-acceptor conjugated copolymers (CPs) were developed from N-octylcarbazole (Cz-O) and N-phenyl-1,8-naphthalimide (NPN) with a combination of feed ratios of Cz-O and NPN (50:50, 65:35, 75:25, 90:10, 95:05 and 99:01). The copolymers exhibited desirable solubility in organic solvents, color tunability from blue to orange and desired electrochemical properties and are utilized for PLED fabrication. The new CPs are well characterized using NMR, FT-IR, TGA, DSC, UV-Vis and photoluminescence (PL) spectroscopy and their structural and photophysical properties are well correlated. The PL emissions of the CPs are red shifted steadily with increase in the NPN content in the CP main chains. PLEDs were fabricated using these newly developed CPs as emissive layer (EML) in ITO/PEDOT:PSS/PCzNPN/BCP/LiF/Al configuration. Among all devices, PLEDs using PCzNPN05 copolymer as EML is found to give the best device performance with maximum brightness of 309 cd m^{-2} and 0.451 cd A^{-1} luminous efficiency.

3.1. Introduction

In the past few decades, CPs have attracted immense attention primarily due to their applications in large-area and flat-panel displays.[1-7] Ever since the first PLED based on poly(p-phenylenevinylene) (PPV) was reported in 1990,[8] a number of CPs have been developed, such as poly(p-phenylene)s,[9,10] poly(thiophene)s,[11] polyfluorenes (PFs),[12] polycarbazoles (PCzs)[13,14] etc. Among them, PFs and PCzs have been reported extensively for multi-color PLEDs as active materials[15] due to their exceptional optical, electrical and chemical properties. As PFs and PCzs are wide band gap materials,[16,17] their emission can be easily changed from blue to red region by inserting low band gap monomers into the polymer main chain. Although PFs are most widely used blue emitting CPs, their emission color changes from blue to greenish and to even yellow during device operation or thermal annealing in air due to the likely formation of fluorenone.[18-20] Therefore, PCzs possesses the ability to emerge as an alternate to PF derivatives. The carbazole derivatives have demonstrated strong hole-transporting ability and hence they are used as active material in optoelectronic devices. However, the lower electron injection and electron transport property of PCzs makes it difficult to balance the carriers inside EML during PLED operations and limits its performance as EML in OLEDs. An alternative method to improve the charge balance of PCzs is by introducing a suitable electron accepting moiety into the CP chain.[21-25] 1,8-naphthalimide (NI) derivatives (containing carbonyl functional groups) are reported as electron acceptors for OLEDs because of their good thermal, chemical and photostability and also high fluorescence quantum yields.[26,27] When NIs are substituted by an electron donating substituent at the 4th position, the fluorescent quantum yield is enhanced and the emission peak shifts to a longer range. The absorption, emission and electrochemical properties of the host polymer can also be varied by this process.[28-30] CPs incorporated with NI and its derivatives (monomers and polymers) can potentially be useful for optoelectronic applications because of the likely energy transfer from wide band gap to low band gap materials. In addition, there is a possibility for modifying the chemical structure of NI and its derivatives to improve its processability and electronic properties via imide moiety and carbocyclic core by chromophore substituents. However, limited reports based on the NI monomers and their polymers exist. Among these few reports, polymers emitting in the longer wavelength region are very less. Formation of donor-acceptor (D-A) combination represents an important approach for the preparation of luminescent materials with tunable properties. Introduction of such a D-A chain structure generally, leads to

significant changes in the electronic structure of the parent homo polymers. Polymer donor and polymer acceptor often results in shifts in the emission color which may or may not be desirable. Additionally, by acting as exciton or charge carrier traps, the donor or acceptor moieties can adversely affect the efficiency of energy and charge transfer processes and reduce the PL and EL efficiencies of the resultant copolymers. This makes it immensely challenging to design highly efficient copolymers with balanced hole or electron transport properties while retaining the high solid state PL quantum yields for efficient PLED performance. In this chapter, synthesis, characterization and study of EL properties of these copolymers with D-A systems by utilizing carbazole as donor and NPN as acceptor unit (see Scheme 3.1) has been reported. All the copolymers were prepared using the Suzuki coupling reaction using different feed ratios of the donor (PCz) and acceptor (NPN) in the CP main chain. By increasing the quantity of feed ratios of the NPN unit from 1 mol% to 50 mol% in the PCz back bone, the energy transfer from CP back bone to NPN moiety was controlled and consequently tuned to achieve the emission color of the copolymers from blue to orange. In thin film state, the PCz fluorescence was completely quenched even with PCzNPN01 copolymer indicating efficient energy transfer from the carbazole unit to NPN unit.

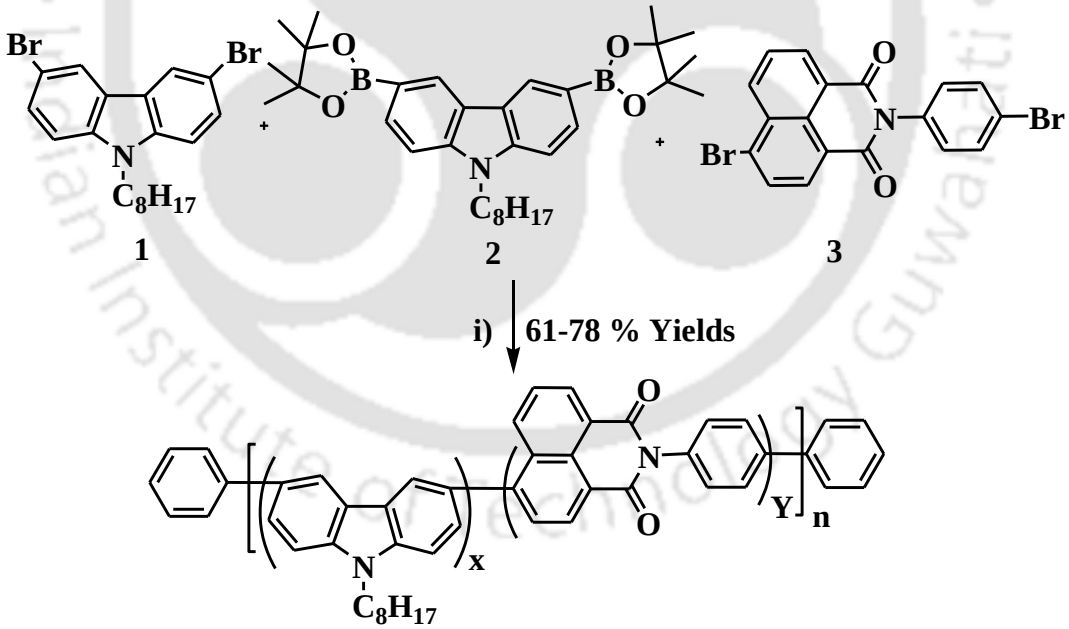

Scheme 3.1. Synthetic route for the copolymers. Feed ratio of Monomers: 99/01 (PCzNPN01), 95/05 (PCzNPN05), 90/10 (PCzNPN10), 75/25 (PCzNPN25), 65/35 (PCzNPN35), 50/50 (PCzNPN50). i) $Pd(PPh_3)_4$, Aliquat 336, 2M K_2CO_3, THF, 48 hrs, Benzene boronic acid and Iodobenzene.

PLEDs with as synthesized CP as emissive layer (EML) were fabricated in ITO/PEDOT:PSS/PCzNPN/BCP/LiF/Al configuration. Among all devices, PLEDs using PCzNPN05 (as shown in Scheme 3.1) copolymer as EML was observed to give the best

device performance with a maximum brightness of 309 cd m^{-2} and 0.451 cd A^{-1} luminous efficiency. The combination of carbazole and NPN units represents a significant approach for the preparation of luminescent materials with tunable properties and provided a novel molecular design for the PLEDs.

3.2. Experimental Section

3.2.1. Materials and Measurements

3,6-Dibromo-9H-carbazole, 1-bromooctane, 4-bromo 1,8-naphthalicanhydride, Bis(pinacolato)diboron, (1,1'-Bis (diphenyl phosphino))-ferrocene) dichloro palladium (II) complex with dichloromethane, Tetrakis(triphenylphosphine)palladium(0), Aliquat 336, glacial aceticacid (99.85%), 4-bromoaniline, tetrabutylammonium Iodide (TBAI), were purchased from Sigma-Aldrich. Chloroform, dichloromethane (DCM), 1,4 Dioxane and tetrahydrofuran (THF) was dried over sodium-benzophenone. N-octyl 3,6-Dibromo carbazole, 9-Octyl-3-(4,4,5,5-tetramethyl-[1,3,2]dioxaborolan-2-yl)-6-(4,4,5-trimethyl-[1,3,2] dioxaboro-lan-2-yl)-9H-carbazole and 4-bromo-9-N-4-bromophenyl-1,8-naphthalimide were prepared following published procedures.[31, 32]

^{1}H NMR spectra were recorded on Varian AS 400 MHz spectrometer. UV-visible and PL spectra were recorded with Varian Cary Eclipse spectrometer and PerkinElmer, Model Lambda-25 spectrometer, respectively. Cyclic voltagramms (CV) of the copolymers were measured using electrochemical workstation (CH instruments Model 700D series). Differential scanning calorimetry (DSC) was recorded on a Mettler Toledo, model DSC1, stare system. Thermo gravimetric analysis (TGA) was measured on Mettler Toledo, model TG/SDTA 851 e. The gel permeation chromatography (GPC) were recorded to calculate the molecular weight of the copolymers using waters 515 chromotograph (waters 2414 refractive index detectors) with THF as an eluent and calibration curve of polystyrene standards. FT-IR spectra of copolymers were recorded using a Perkin-Elmer-Spectrum. The current density-voltage (J-V) characteristics were measured using Keithley 2400 source meter whereas the EL spectra and the luminance were measured by CS 2000 spectroradiometer.

3.2.2. General Polymerization Procedure

9-Octyl-3-(4,4,5,5-tetramethyl-[1,3,2]dioxaborolan-2-yl)-6-(4,4,5-trimethyl-[1,3,2]dioxaborolan-2-yl)-9H-carbazole, dibromo compounds (4-bromo-9-N-4-bromophenyl-1,8-naphthalimide), **(3)** and N-octyl 3,6-Dibromo carbazole **(2)**, 12 mL of THF and $Pd(PPh_3)_4$ (0.015 mmol) were added into a two neck round bottom flask. Afterwards, 5 mL of 2 M aqueous K_2CO_3 and aliquat 336 (0.025 mmol) were added to the

flask. The reaction mixture was degassed thrice by freeze-thaw cycles to remove any trace amounts of oxygen completely and purge the argon gas to create inert atmosphere. The reaction mixture was stirred at 80 °C for 48 hours and iodo benzene was added as an end capper. Finally, after 4 hours the benzene boronic acid was added into the reaction mixture as another end capper and the reaction was continued further for 4 hours. The reaction mixture was then cooled to room temperature, poured into 100 mL of methanol and further stirred at room temperature for 3 hours. The copolymers were obtained by filtration and reprecipitated twice from methanol and acetone. Finally, the copolymers were further purified by soxhlet filtration with acetone to remove the catalyst residues, monomers and oligomers. The pure polymers were obtained with a yield of 61-78%.

3.2.3. Poly[3,6-(9,-octylcarbazole)-co-N-phenyl-1,8-naphthalimide](PCzNPN50)

9-Octyl-3-(4,4,5,5-tetramethyl-[1,3,2]dioxaborolan-2-yl)-6-(4,4,5-trimethyl-[1,3,2]dioxaborolan-2-yl)-9H-carbazole (3) (0.2792g, 0.50 mmol), and 4-bromo-9-N-4-bromophenyl-1,8-naphthalimide (2) (0.2155g, 0.50 mmol), were used in this polymerization. ^{1}H NMR (400 MHz, $CDCl_3$) δ (ppm): 8.69 (br, 2H), 8.48 (br, 1H), 8.32 (br, 1H), 7.88 (br, 2H), 7.69 (br, 6H), 7.54 (br, 2H), 7.22 (br, 1H), 4.49 (br, 2H), 2.30 (br, 2H), 2.02 (br, 2H), 1.25 (br, 8H), 0.85 (br, 3H); FT-IR (KBr pellets,cm^{-1}): 2955, 2925, 2850, 1709, 1670, 1586, 1489, 1362, 1234, 802.

3.2.4. Poly[3,6-(9,-octylcarbazole)-co-N-phenyl-1,8-naphthalimide] (PCzNPN35)

9-Octyl-3-(4,4,5,5-tetramethyl-[1,3,2]dioxaborolan-2-yl)-6-(4,4,5-trimethyl-[1,3,2]dioxaborolan-2-yl)-9H-carbazole (3) (0.2792g, 0.50 mmol), N-octyl 3,6-Dibromo carbazole (1) (0.1371g, 0.15 mmol) and 4-bromo-9-N-4-bromophenyl-1,8-naphthalimide (2) (0.1077g, 0.35 mmol), were used in this polymerization. ^{1}H NMR (400 MHz, $CDCl_3$) δ (ppm): 8.67 (br, 2H), 8.47 (br, 1H), 8.30 (br, 1H), 7.87 (br, 2H), 7.68 (br, 6H), 7.54 (br, 2H), 7.22 (br, 1H), 4.42 (br, 2H), 2.03 (br, 2H), 1.93 (br, 2H), 1.27 (br, 8H), 0.86 (br, 3H); FT-IR (KBr pellets,cm^{-1}): 2955, 2925, 2850, 1709, 1670, 1586, 1489, 1362, 1234, 802.

3.2.5. Poly[3,6-(9,-octylcarbazole)-co-N-phenyl-1,8-naphthalimide] (PCzNPN25)

9-Octyl-3-(4,4,5,5-tetramethyl-[1,3,2]dioxaborolan-2-yl)-6-(4,4,5-trimethyl-[1,3,2]dioxaborolan-2-yl)-9H-carbazole (3) (0.2792g, 0.50 mmol), N-octyl 3,6-Dibromo carbazole (1) (0.1371g, 0.25 mmol) and 4-bromo-9-N-4-bromophenyl-1,8-naphthalimide (2) (0.1077g, 0.25 mmol), were used in this polymerization. ^{1}H NMR (400 MHz, $CDCl_3$)

δ (ppm): 8.68 (br, 2H), 8.49 (br, 1H), 8.32 (br, 1H), 7.86 (br, 2H), 7.68 (br, 6H), 7.56 (br, 2H), 7.22 (br, 1H), 4.49 (br, 2H), 2.03 (br, 4H), 1.98 (br, 2H), 1.28 (br, 8H), 0.86 (br, 3H); FT-IR (KBr pellets,cm^{-1}): 2955, 2925, 2850, 1709, 1670, 1586, 1489, 1362, 1234, 802.

3.2.6. Poly[3,6-(9,-octylcarbazole)-co-N-phenyl-1,8-naphthalimide] (PCzNPN10)

9-Octyl-3-(4,4,5,5-tetramethyl-[1,3,2]dioxaborolan-2-yl)-6-(4,4,5-trimethyl-[1,3,2]dioxaborolan-2-yl)-9H-carbazole (3) (0.2792g, 0.50 mmol), N-octyl 3,6-Dibromo carbazole (1) (0.2193g, 0.40 mmol) and 4-bromo-9-N-4-bromophenyl-1,8-naphthalimide (2) (0.0431g, 0.10 mmol), were used in this polymerization. ^{1}H NMR (400 MHz, $CDCl_3$) δ (ppm): 8.69 (br, 2H), 8.49 (br, 1H), 8.30 (br, 1H), 7.90 (br, 2H), 7.71 (br, 6H), 7.54 (br, 2H), 7.49 (br, 1H), 4.37 (br, 2H), 1.92 (br, 2H), 1.73 (br, 2H), 1.26 (br, 8H), 0.86 (br, 3H); FT-IR (KBr pellets,cm^{-1}): 2955, 2925, 2850, 1709, 1670, 1586, 1489, 1362, 1234, 802.

3.2.7. Poly[3,6-(9,-octylcarbazole)-co-N-phenyl-1,8-naphthalimide] (PCzNPN05)

9-Octyl-3-(4,4,5,5-tetramethyl-[1,3,2]dioxaborolan-2-yl)-6-(4,4,5-trimethyl-[1,3,2]dioxaborolan-2-yl)-9H-carbazole (3) (0.2792g, 0.50 mmol), N-octyl 3,6-Dibromo carbazole (1) (0.2193g, 0.45 mmol) and 4-bromo-9-N-4-bromophenyl-1,8-naphthalimide (2) (0.0431g, 0.05 mmol), were used in this polymerization. ^{1}H NMR (400 MHz, $CDCl_3$) δ (ppm): 8.54 (br, 2H), 8.49 (br, 1H), 8.30 (br, 1H), 7.88 (br, 2H), 7.85 (br, 2H), 7.54 (br, 6H), 7.49 (br, 1H), 4.30 (br, 2H), 1.90 (br, 2H), 1.25 (br, 10H), 0.86 (br, 3H); FT-IR (KBr pellets,cm^{-1}): 2955, 2925, 2850, 1709, 1670, 1586, 1489, 1362, 1234, 802.

3.2.8. Poly[3,6-(9,-octylcarbazole)-co-N-phenyl-1,8-naphthalimide] (PCzNPN01)

9-Octyl-3-(4,4,5,5-tetramethyl-[1,3,2]dioxaborolan-2-yl)-6-(4,4,5-trimethyl-[1,3,2]dioxaborolan-2-yl)-9H-carbazole (3) (0.2792g, 0.50 mmol), N-octyl 3,6-Dibromo carbazole (1) (0.2193g, 0.49 mmol) and 4-bromo-9-N-4-bromophenyl-1,8-naphthalimide (2) (0.0431g, 0.01 mmol), were used in this polymerization. ^{1}H NMR (400 MHz, $CDCl_3$) δ (ppm): 8.58 (br, 2H), 8.49 (br, 1H), 7.90 (br, 2H), 7.51 (br, 2H), 4.31 (br, 2H), 1.88 (br, 2H), 1.25 (br, 10H), 0.86 (br, 3H); FT-IR (KBr pellets, cm^{-1}): 2955, 2925, 2850, 1480, 802.

3.2.9. PLEDs Fabrication and Characterization

To fabricate PLEDs using the as synthesized copolymers as active layer, indium tin oxide (ITO) was used as the transparent anode. On top of the ITO ~40 nm thin layer of poly (3,4-ethylendioxythiophene) : poly(styrenesulfonate) (PEDOT:PSS) was spin-coated

as a hole injecting layer and baked for 15 minute at 110 °C in argon environment. The emissive layer of ~75 nm was spin-coated above the PEDOT:PSS layer from the solutions of the copolymers in p-xylene (10 mg/mL) and thermally treated at 140 °C for 30 minute to remove the residual solvent. Finally, Bathocuproine (BCP) (10 nm), LiF (1 nm) and Al (100 nm) was thermally evaporated at a rate of 2 Å/s, 0.1 Å/s and 10 Å/s, respectively at a base pressure of 10^{-6} mbar as hole blocking layer and cathode, respectively. The emissive area of the PLEDs was 12 mm^2.

3.3. Results and discussion

3.3.1. Synthesis and Characterization of the Polymers

Scheme 3.1 shows the synthetic route for the preparation of different monomers. The monomers N-octyl 3,6-Dibromo carbazole (1),[31] 9-Octyl-3-(4,4,5,5-tetramethyl-[1,3,2]dioxaborolan-2-yl)-6-(4,4,5-trimethyl-[1,3,2] dioxaboro-lan-2-yl)-9H-carbazole (2)[31] and 4-bromo-9-N-4-bromophenyl-1,8-naphthalimide (3) were prepared according to the reported procedure.[32] The D-A based CPs were prepared from compounds 1, 2 and 3 using Suzuki polymerization. In all the copolymers, a 1:1 molar ratio was maintained between dibrominated compounds (1 and 3) and compound 2 and the feed ratio of the NPN moiety was altered by using suitable feed ratios of 1 and 3. Figure 3.1 and 3.2 shows the ^{1}H NMR spectra in $CDCl_3$, and FT-IR spectra of the copolymers which confirm the expected copolymer structures. In ^{1}H NMR spectra, apart from the peaks that merged with the carbazole peaks, four peaks at 8.69, 8.31, 7.69 and 7.22 ppm were observed suggesting the presence of NPN moiety. Similarly five peaks at 1709, 1670, 1586, 1362 and 1234 cm^{-1} that resemble the NPN moiety were observed in the FT-IR spectra. With an increase in the NPN feed ratio in the copolymer chain, the relative intensity of these five peaks was found to increase. These synthesized copolymers exhibited good solubility

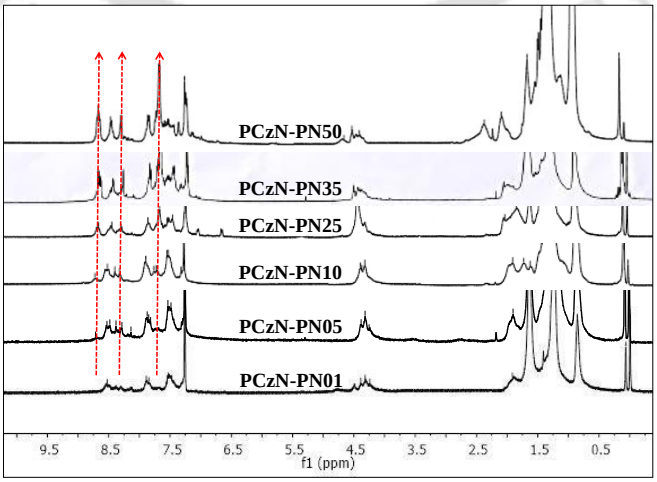

Figure 3.1: ^{1}H NMR spectra of copolymers in $CDCl_3$

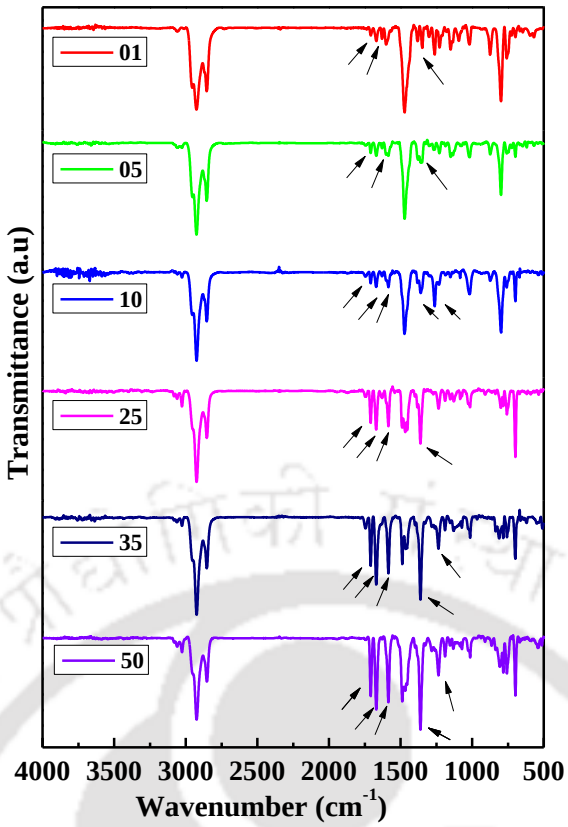

Figure 3.2: FT-IR spectra of copolymers

in common solvents such as $CHCl_3$, THF, chlorobenzene, p-xylene etc. The copolymers were found to show number-average molecular weights (M_n) in the range of 11519 to 18355 and a polydispersity index (M_w/M_n) of 1.12 to 1.42 as determined by GPC. Table 3.1 shows the results of polymerization of these newly synthesized carbazole based copolymers.

Table 3.1: Results of polymerization and thermal data of these newly synthesized carbazole based copolymers

Polymer	M_n[a]	M_w[a]	PDI[a]	Yield (%)	T_d[b] (°C)	T_g[c] (°C)
PCzNPN01	12365	16386	1.32	72	422	143
PCzNPN05	13256	17102	1.29	67	396	145
PCzNPN10	18355	26202	1.42	61	347	142
PCzNPN25	15332	18736	1.22	78	327	140
PCzNPN35	13472	16336	1.21	73	316	142
PCzNPN50	11519	15713	1.36	64	302	151

[a]M_n, M_w and polydispersity index of the copolymers as determined by GPC using polystyrene standards. [b]Onset decomposition temperature calculated from TGA. [c]Glass transition temperature

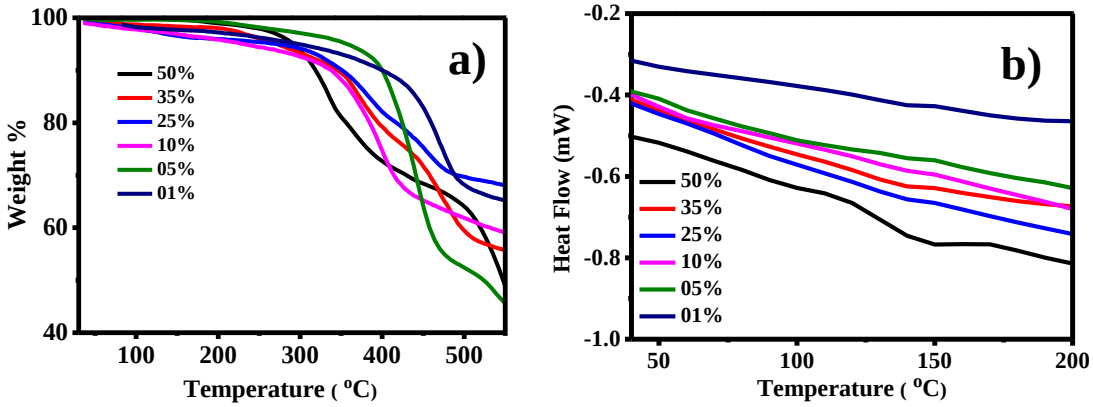

Figure 3.3: TGA (a) and DSC (b) curves of copolymers

Thermal properties of the copolymers were studied by TGA and DSC at a heating rate of 10 °C/min under nitrogen flow. The TGA curves and onset decomposition temperature (T_d) of the copolymers are presented in Figure 3.3a and Table 3.1. All the CPs exhibited satisfactory thermal stability with T_d in the range of 302-422 °C and no significant weight loss observed at lower temperature. The DSC curves and glass transition temperature (T_g) of the copolymers are shown in Figure 3.3b and Table 3.1. The DSC results indicate that all copolymers were amorphous and therefore could be solution processed for PLED fabrication.

3.3.2. Photophysical Properties

The normalized absorption spectra of copolymers in THF solution (10^{-5} M) and spin coated thin films (thickness of approximately 80 nm) are shown in Figure 3.4a and 3.4b and summarized in Table 3.2. All the copolymers showed similar absorption spectra in the solution and in the thin films. Three distinct absorption bands were observed in both the solution and thin films. In the solution state, three absorption bands were observed at 306 nm, 345 nm and 405 nm. Similarly, in thin films also three absorption bands were observed at 305 nm, 350 nm and 420 nm. The first absorption band at ~306 nm is due to π-π* transition of the carbazole segments as observed in the absorption spectrum of pure PCz and the long absorption bands at ~350 and ~420 nm, which increased linearly with increasing NPN units (from 1 to 50 mol% in the polymer chain), can be assigned to the NPN unit. The absorption wavelength of copolymers are somewhat blue shifted, in both solution and thin films, which is probably due to the increasing feed of the NPN unit in the CP backbone, which induces a decrease in the effective conjugation length of carbazole moieties. Figure 3.4c and 3.4d present the normalized PL spectra of the copolymers in THF solution and thin films, respectively (350 nm excitation), (Table 3.2). In solution state, PCzNPN25, PCzNPN35 and PCzNPN50

polymers showed single peak at 523 nm, due to efficient complete energy transfer from PCz to NPN moiety and the rest of the PCzN- PN10, PCzNPN05 and PCzNPN01 polymers exhibited three emission peaks at 402 nm, 421 nm and 523 nm due to incomplete energy transfer from PCz to NPN moiety. The peaks at blue region are due to the carbazole units, whereas, the peak at green region is due to the NPN unit. The intensity of the emission peak at green region (523 nm) was increased and the emission peaks at 402 nm and 421 nm decreases upon increasing the NPN unit in the CP chain.

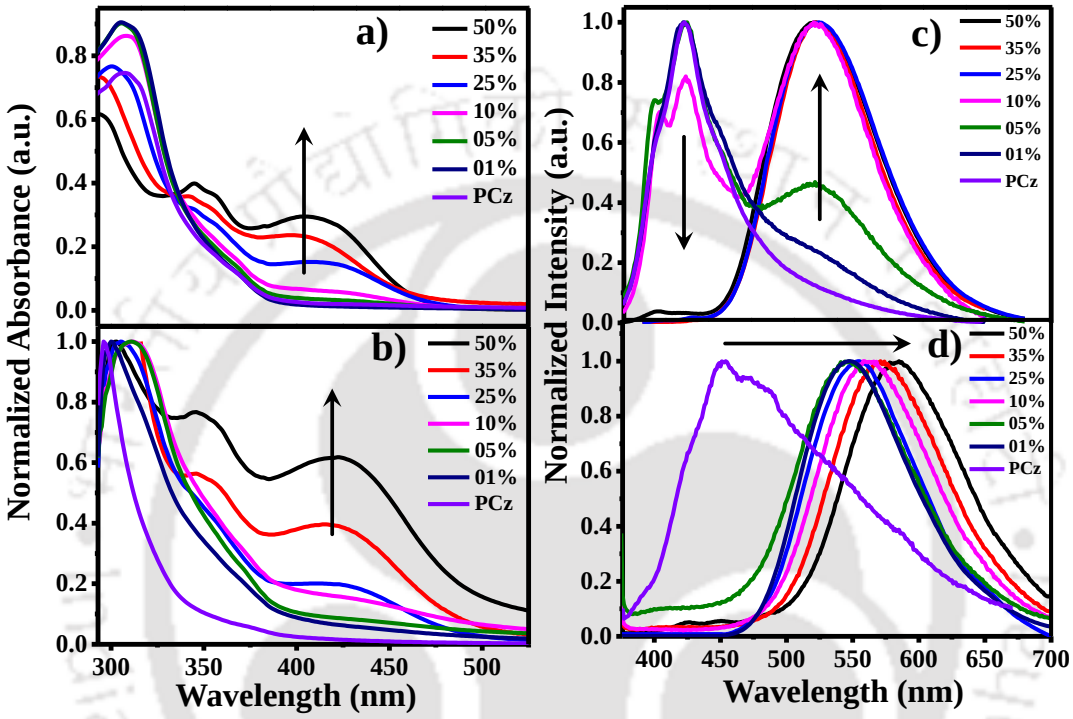

Figure 3.4: UV-Vis (a) & (b) and PL (c) & (d) spectra of copolymers in THF solution and thin film state

Table 3.2: Photophysical properties of the copolymers

	THF solution		Thin films		
Polymer	**$\lambda_{max, abs}$ [nm]**	**$\lambda_{max, PL}$ [nm]**	**$\lambda_{max, abs}$ [nm]**	**$\lambda_{max, PL}$ [nm]**	**Φ_{PL}[a]**
PCzNPN01	306	402, 421	300, 420	542	14.2
PCzNPN05	306	402, 421, 523	305, 420	544	14.5
PCzNPN10	306, 405	402, 421, 523	305, 420	552	11.6
PCzNPN25	300, 345, 405	523	304, 350, 420	560	12.5
PCzNPN35	292, 345, 405	523	304, 345, 420	571	8.3
PCzNPN50	292, 345, 405	523	304, 344, 420	583	2.4

[a]Solid state PL quantum yields are calculated with polydioctylfluorene standard

In thin films, all copolymers exhibited the single emission peak due to the efficient intra and intermolecular energy transfer from PCz to NPN moiety. The PCz emission was completely quenched even when the NPN concentration was as low as 1% due to efficient charge transfer and strong energy transfer from PCz to NPN moiety. The PL emission peaks are gradually red-shifted with the increase in NPN content in the CP chain from 542 nm for the copolymer PCzNPN01 to 583 nm for the alternating copolymer PCzNPN50. This red shift could be attributed to the increase of the effective conjugation length of the copolymers due to electron-withdrawing nature of NPN units. The PL quantum yields (Φ_F) of copolymers were measured in thin film state by comparison their fluorescence intensity to polyfluorene (Φ_F = 0.55)[33] relative intensity. The PL Φ_F values were tabulated in Table 3.2. The PL Φ_F values decreased on increasing the NPN mol% in the CP main chain due to the concentration quenching effect of the NPN moiety assigned to the aggregation of chromophores.[34,35]

3.3.3. Electrochemical Properties

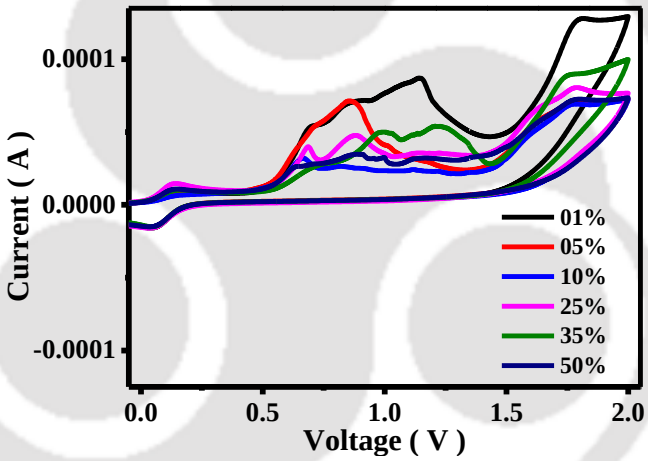

Figure 3.5: Cyclic Voltagramms of copolymers

To find the highest occupied molecular orbital (HOMO) and lowest unoccupied molecular orbital (LUMO) energy levels of the copolymers, Cyclic voltammetry (CV) (Figure 3.5) measurements were performed. The copolymers were dissolved in chloroform solution and drop casted onto the carbon working electrode whereas the platinum and silver wires were used as counter and reference electrodes, respectively. The electrochemical properties were studied in an electrolyte consisting of a solution of 0.1 M tetra butyl ammonium hexafluorophosphate (Bu_4NPF_6) in acetonitrile (CH_3CN) under Argon atmosphere. All CV curves of the copolymers were obtained using ferrocene as standard and all copolymers showed only oxidation potential peaks. The oxidation onset values, energy levels (HOMO and LUMO) and band gaps of the copolymers are summarized in Table 3.3. The HOMO energy levels were calculated by substituting onset

oxidation peak values in E_{HOMO} = -[(E_{ox} -$E_{1/2}$(ferrocene)) + 4.8 eV]. The LUMO energy levels were calculated from the optical band gap (E_{opt}) and the HOMO values using the empirical formula E_{LUMO} = [E_{opt}+ E_{HOMO}]eV. The optical band gaps were estimated from the onset absorption spectra of the CPs in the thin films state.

Table 3.3: Electrochemical potentials and energy levels of the PFONPN copolymers

Polymer	E_{ox}/V	E_{HOMO}/eV	E_{LUMO}/eV	Optical band gap/eV
PCzNPN01	0.54	-5.24	-1.88	3.36
PCzNPN05	0.52	-5.22	-1.91	3.31
PCzNPN10	0.52	-5.22	-1.93	3.29, 2.63
PCzNPN25	0.57	-5.27	-2.12	3.15, 2.58
PCzNPN35	0.53	-5.23	-2.27	2.96, 2.56
PCzNPN50	0.51	-5.21	-2.28	2.93, 2.54

3.3.4. Electroluminescence Properties

Polymer light emitting devices (PLEDs) in ITO/PEDOT:PSS/CP/BCP/LiF-Al configuration were fabricated using the newly synthesized carbazole based copolymers as emissive layer to explore their EL properties. Figure 3.6a, 3.6b and 3.6c displays the current density versus voltage (J-V), brightness versus voltage (B-V) and EL characteristics of these copolymers based PLEDs, respectively.

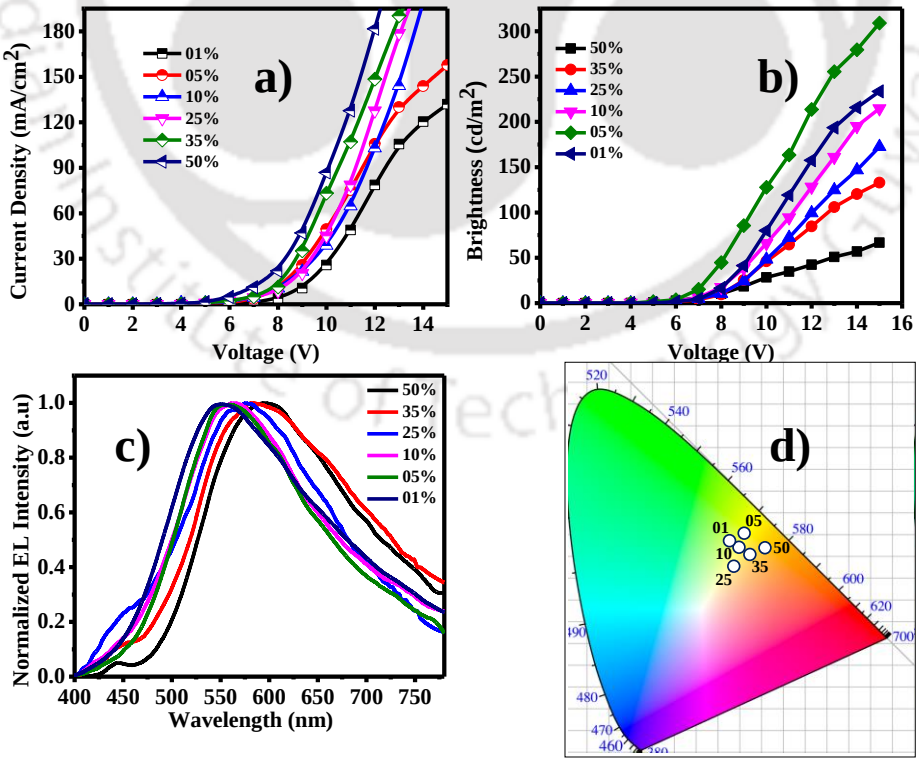

Figure 3.6: a) Current Density versus Voltage (J-V) b) Brightness versus Voltage (B-V) c) and d) Chromaticity diagram of the fabricated PLEDs.

Table 3.4: Different device parameters of the PLEDs based on these newly synthesized carbazole based copolymers

Polymer	Onset Voltage (V)	$\lambda_{max, EL}$ [nm]	Max. brightness (cd m^{-2})	Luminous efficiency (cd A^{-1})	CIE coordinate (x, y)[a]
PCzNPN01	4.8	547	234	0.422	0.40, 0.47
PCzNPN05	4.9	558	309	0.451	0.42, 0.48
PCzNPN10	5.4	561	215	0.178	0.41, 0.47
PCzNPN25	5.4	575	172	0.119	0.42, 0.44
PCzNPN35	5.6	586	133	0.084	0.46, 0.46
PCzNPN50	5.2	595	67	0.055	0.48, 0.47

[a] Determined from the EL spectrum

The key device parameters such as onset values, emission maxima and CIE coordinates for all the fabricated devices are listed in Table 3.4. As observed from Figure 3.6c, all CPs exhibited single emission peak in the range of 547-595 nm. No peaks were observed in the blue region suggesting efficient intra and intermolecular energy transfer from PCz to NPN moiety. The PCz emission (Blue emission) disappeared even at NPN concentration as low as 1%, suggesting strong and efficient charge / energy transfer from PCz to NPN moiety. Like PL, peaks in the EL emission were also gradually red-shifted as the NPN content increases in the polymer chain, from 547 nm for the copolymer PCzNPN01 to 595 nm for the alternating copolymer PCzNPN50. The slight red shift of the emission peak in EL as compared to that in PL originated because of the differences in their emission mechanism. As shown in the Figure 6d, the chromaticity coordinates of the fabricated PLEDs changed from (0.40, 0.47), for PCzNPN01 to (0.48, 0.47) for PCzNPN50. Figure 3.6a and 3.6b show that the brightness and current efficiency of the devices are 234 cd m^{-2} and 0.422 cd A^{-1} for PCzNPN01, 309 cd m^{-2} and 0.451 cd A^{-1} for PCzNPN05, 215 cd m^{-2} and 0.178 cd A^{-1} for PCzNPN10, 172 cd m^{-2} and 0.119 cd A^{-1} for PCzNPN25, 133 cd m^{-2} and 0.084 cd A^{-1} for PCzNPN35 and 67 cd m^{-2} and 0.055 cd A^{-1} for PCzNP-N50. It was also observed that due to its high electron affinity, the device brightness increased when NPN content increased from 1% to 5% in the PCz main chain and decreases thereafter. Upon increasing the NPN unit concentration from 1% to 5%, the charge balance improves in the device owing to the increased electron accepting property of the polymer resulting in increased brightness. On further increasing the NPN content,

the excess electron attracting effect lowers the PL quantum yields in the solid state leading to low device efficiency.

3.4. Summary

A series of new color tunable D-A based copolymers PCzNPN were successfully synthesized by Suzuki coupling reaction and well characterized to be used as emitting materials in PLEDs. These synthesized copolymers exhibited good solubility in common solvents like $CHCl_3$, THF, chlorobenzene, p-xylene etc. They also showed good thermal stability with high glass transition temperature. Efficient energy transfer from PCz to NPN unit was observed in solid state PL as well as in the EL spectra even when the NPN unit was as low as 1 mol% in PCz back bone. The PCz emission color could be tuned from blue to orange successfully. PLEDs were fabricated by using these copolymers as EML in the configuration ITO/PEDOT:PSS/PCzNPN/BCP/LiF/Al. Among all, PLEDs using PCzNPN05 copolymer as EML was found to give the best device performance with a maximum brightness of 309 cd m^{-2} and 0.451 cd A^{-1} luminous efficiency. The chromaticity coordinates for the PLEDs also varied from (0.40, 0.47) for PCzNPN01 to (0.48, 0.47) for PCzNPN50. Thus by introducing appropriate donor moiety such as carbazole and NPN based acceptor, efficient materials for PLED devices with color tunability and solution processability were achieved within the same polymer and not requiring additional materials.

3.5. References

1. Friend, R. H.; Gymer, R. W.; Holmes, A. B.; Burroughes, J. H.; Marks, R. N.; Taliani, C.; Bradley, D. D. C.; Dos Santos, D. A.; Bredas, J. L.; Logdlund, M.; Salaneck, W. R. *Nature* **1999,** *397*, 121-128.
2. Kraft, A.; Grimsdale, A. C.; Holmes, A. B. *Angew. Chem. Int. Edit.* **1998,** *37*, 402-428.
3. Bernius, M. T.; Inbasekaran, M.; O'Brien, J.; Wu, W. S. *Adv. Mater.* **2000,** *12*, 1737-1750.
4. Tarkka, R. M.; Zhang, X. J.; Jenekhe, S. A. *J. Am. Chem. Soc.* **1996,** *118*, 9438-9439.
5. Zhang, X. J.; Shetty, A. S.; Jenekhe, S. A. *Macromolecules* **1999,** *32*, 7422-7429.
6. Mitschke, U.; Bauerle, P. *J. Mater. Chem.* **2000,** *10*, 1471-1507.
7. Tonzola, C. J.; Alam, M. M.; Jenekhe, S. A. *Adv. Mater.* **2002,** *14*, 1086-1090.
8. Burroughes, J. H.; Bradley, D. D. C.; Brown, A. R.; Marks, R. N.; Mackay, K.; Friend, R. H.; Burn, P. L.; Holmes, A. B. *Nature* **1990,** *347*, 539-541.
9. Parker, I. D. *J. Appl. Phys.* **1994,** *75*, 1656-1666.
10. Lemmer, U.; Heun, S.; Mahrt, R. F.; Scherf, U.; Hopmeier, M.; Siegner, U.; Gobel, E. O.; Mullen, K.; Bassler, H. *Chem. Phys. Lett.* **1995,** *240*, 373-378.
11. Berggren, M.; Inganas, O.; Gustafsson, G.; Rasmusson, J.; Andersson, M. R.; Hjertberg, T.; Wennerstrom, O. *Nature* **1994,** *372*, 444-446.
12. Ohmori, Y.; Uchida, M.; Morishima, C.; Fujii, A.; Yoshino, K. *Jpn. J. Appl. Phys.* **1993,** *32*, L1663-L1666.
13. Romero, B.; Schaer, M.; Leclerc, M.; Ades, D.; Siove, A.; Zuppiroli, L. *Synthetic. Met.* **1996,** *80*, 271-277.
14. Mori, T.; Shinnai, T.; Kijima, M. *Polym. Chem.* **2011,** *2*, 2830-2834.
15. Wong, W. Y.; Liu, L.; Cui, D. M.; Leung, L. M.; Kwong, C. F.; Lee, T. H.; Ng, H. F. *Macromolecules* **2005,** *38*, 4970-4976.
16. Ranger, M.; Rondeau, D.; Leclerc, M. *Macromolecules* **1997,** *30*, 7686-7691.
17. Kido, J.; Hongawa, K.; Okuyama, K.; Nagai, K. *Appl. Phys. Lett.* **1993,** *63*, 2627-2629.
18. List, E. J. W.; Guentner, R.; de Freitas, P. S.; Scherf, U. *Adv. Mater.* **2002,** *14*, 374-378.
19. Romaner, L.; Pogantsch, A.; de Freitas, P. S.; Scherf, U.; Gaal, M.; Zojer, E.; List, E. J. W. *Adv. Funct. Mater.* **2003,** *13*, 597-601.
20. Peng, Q.; Peng, J. B.; Kang, E. T.; Neoh, K. G.; Cao, Y. *Macromolecules* **2005,** *38*, 7292-7298.
21. Morin, J. F.; Leclerc, M. *Macromolecules* **2002,** *35*, 8413-8417.
22. Huang, J.; Niu, Y. H.; Yang, W.; Mo, Y. Q.; Yuan, M.; Cao, Y. *Macromolecules* **2002,** *35*, 6080-6082.
23. Feng, G. L.; Ji, S. J.; Geng, L. J.; Bian, B.; Liu, Y. *J. Chem. Res-S.* **2008,** 137-140.

24. Gudeika, D.; Grazulevicius, J. V.; Volyniuk, D.; Butkute, R.; Juska, G.; Miasojedovas, A.; Gruodis, A.; Jursenas, S. *Dyes Pigments* **2015,** *114*, 239-252.
25. Zhang, Q. J.; Zhuang, H.; He, J. H.; Xia, S. G.; Li, H.; Li, N. J.; Xu, Q. F.; Lu, J. M. *J. Mater. Chem. C* **2015,** *3*, 6778-6785.
26. Cacialli, F.; Friend, R. H.; Bouche, C. M.; Le Barny, P.; Facoetti, H.; Soyer, F.; Robin, P. *J. Appl. Phys.* **1998,** *83*, 2343-2356.
27. Sun, H. H.; Tu, G. L.; Min, C. C.; Li, H. C.; Cheng, Y. X.; Wang, L. X.; Jing, X. B.; Wang, F. S.; Wu, H. B.; Peng, J. B.; Cao, Y. *Synthetic. Met.* **2003,** *135*, 231-233.
28. Dorlars, A.; Schellhammer, C. W.; Schroeder, J. *Angew. Chem. Int. Edit.* **1975,** *14*, 665-679.
29. Adam, W.; Qian, X. H.; Sahamoller, C. R. *Tetrahedron* **1993,** *49*, 417-422.
30. Lee, J. F.; Hsu, S. L. C. *Polymer* **2009,** *50*, 5668-5674.
31. Zhang, L.; Zeng, S. H.; Yin, L. X.; Ji, C. Y.; Li, K. C.; Li, Y. Q.; Wang, Y. *New. J. Chem.* **2013,** *37*, 632-639.
32. Gopikrishna, P.; Das, D.; Iyer, P. K. *J. Mater. Chem. C* **2015,** *3*, 9318-9326.
33. Grice, A. W.; Bradley, D. D. C.; Bernius, M. T.; Inbasekaran, M.; Wu, W. W.; Woo, E. P. *Appl. Phys. Lett.* **1998,** *73*, 629-631.
34. Liu, J.; Tu, G. L.; Zhou, Q. G.; Cheng, Y. X.; Geng, Y. H.; Wang, L. X.; Ma, D. G.; Jing, X. B.; Wang, F. S. *J. Mater. Chem.* **2006,** *16*, 1431-1438.
35. Petrozza, A.; Brovelli, S.; Michels, J. J.; Anderson, H. L.; Friend, R. H.; Silva, C.; Cacialli, F. *Adv. Mater.* **2008,** *20*, 3218-3223.

Appendix

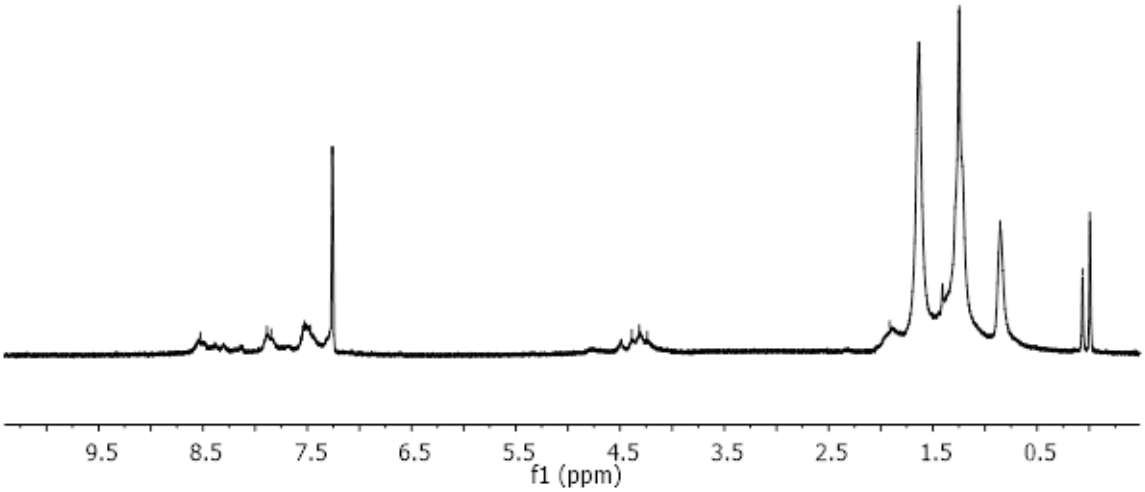

Figure 3.7: ^{1}H NMR of the **PCzNPN01** in $CDCl_3$

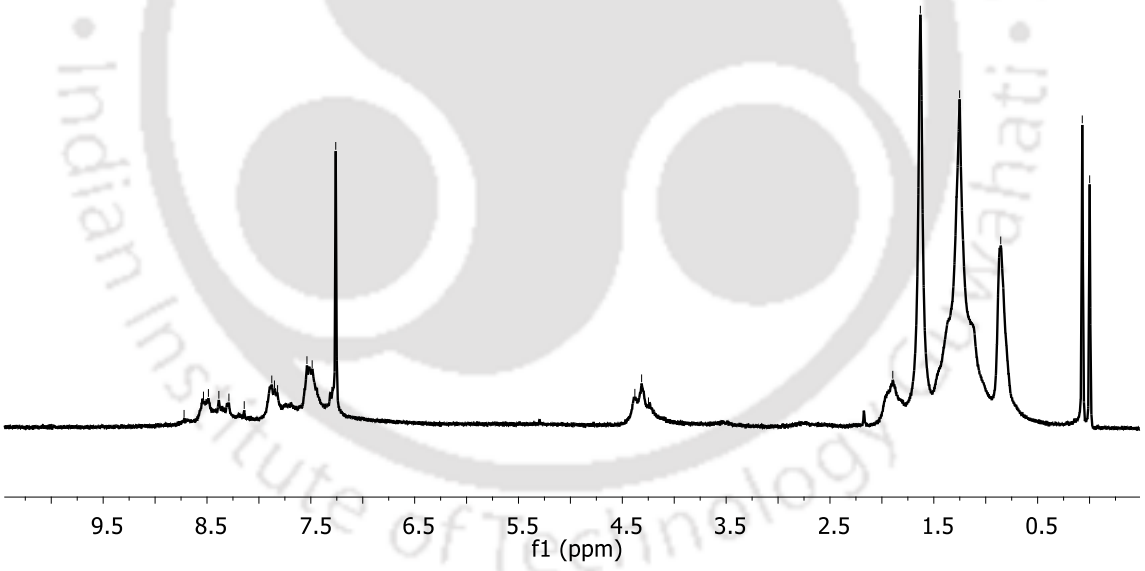

Figure 3.8: ^{1}H NMR of the **PCzNPN05** in $CDCl_3$

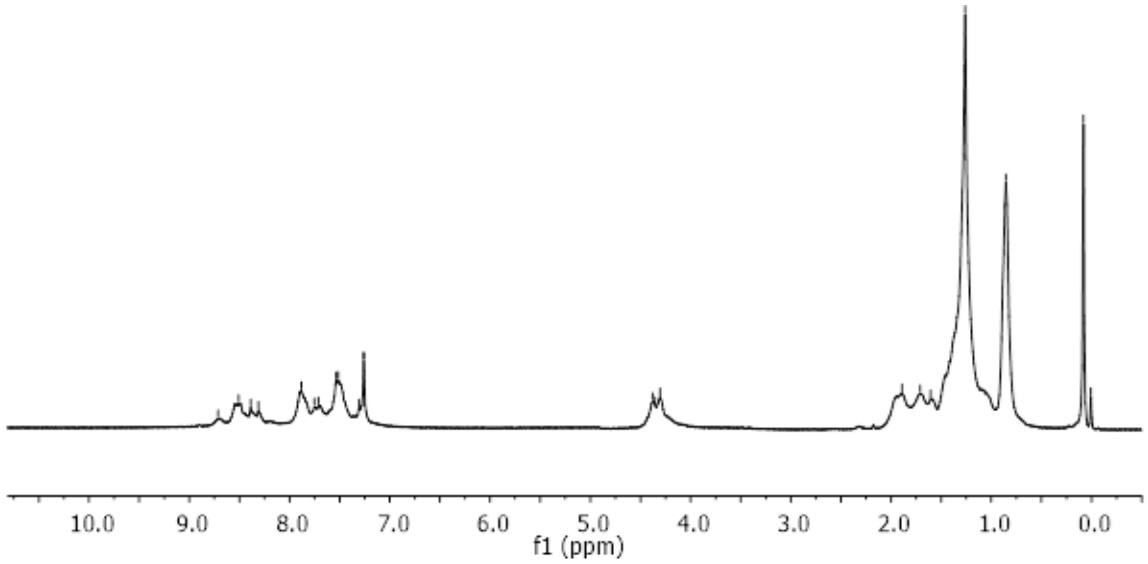

Figure 3.9: ^{1}H NMR of the **PCzNPN10** in $CDCl_3$

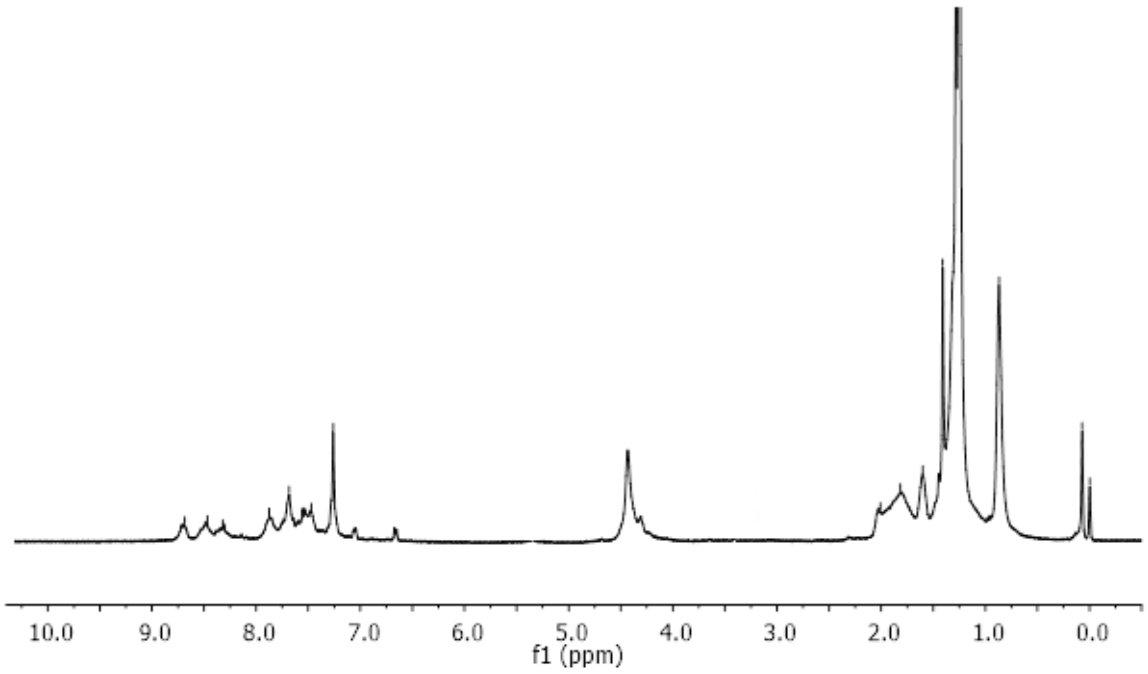

Figure 3.10: ^{1}H NMR of the **PCzNPN25** in $CDCl_3$

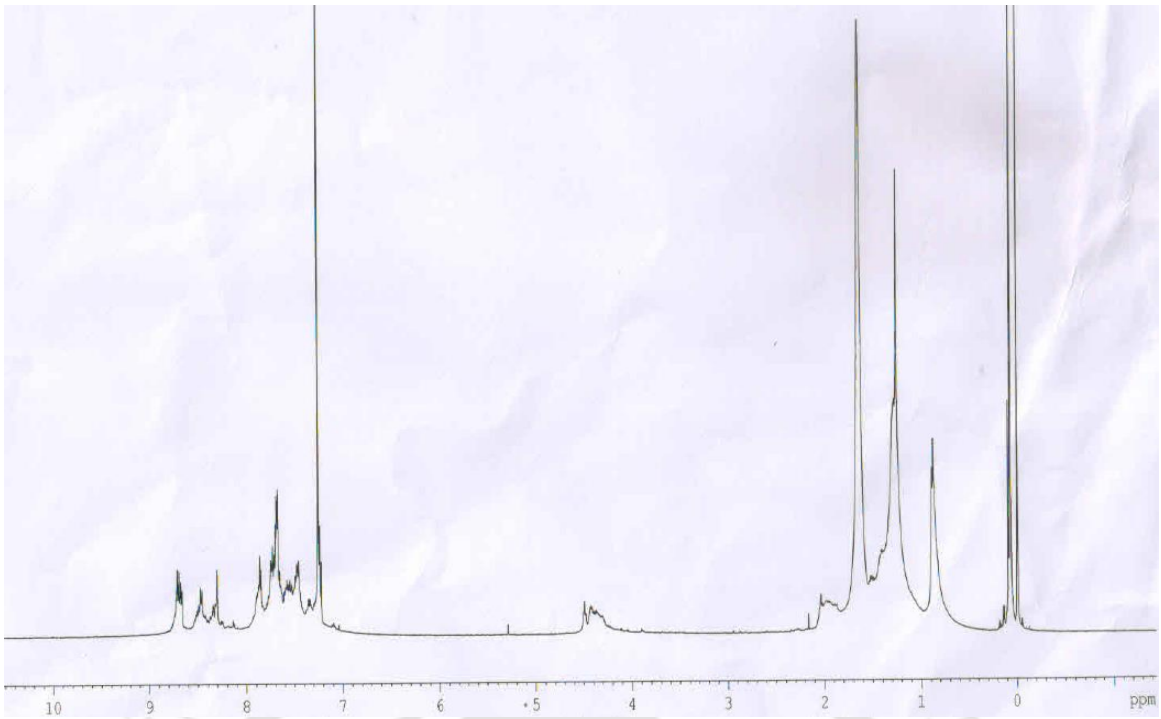

Figure 3.11: ^{1}H NMR of the **PCzNPN35** in $CDCl_3$

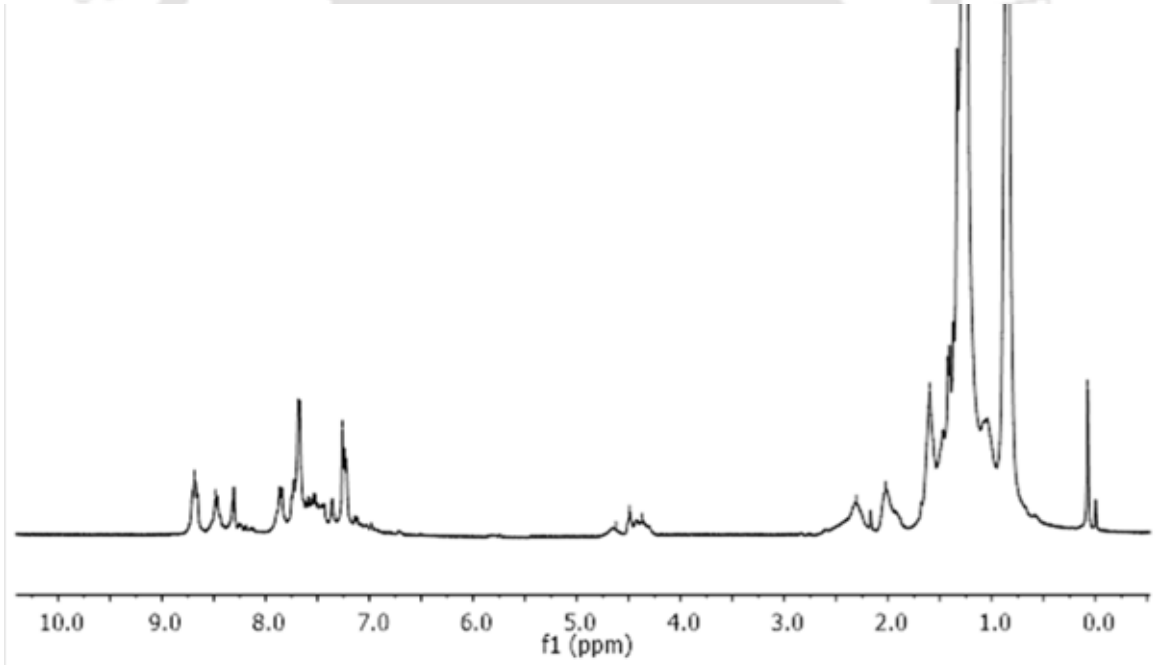

Figure 3.12: ^{1}H NMR of the **PCzNPN50** in $CDCl_3$

Chapter-4

Monosubstituted Dibenzofulvene-Based Luminogens: Aggregation-Induced Emission Enhancement and Dual-State Emission

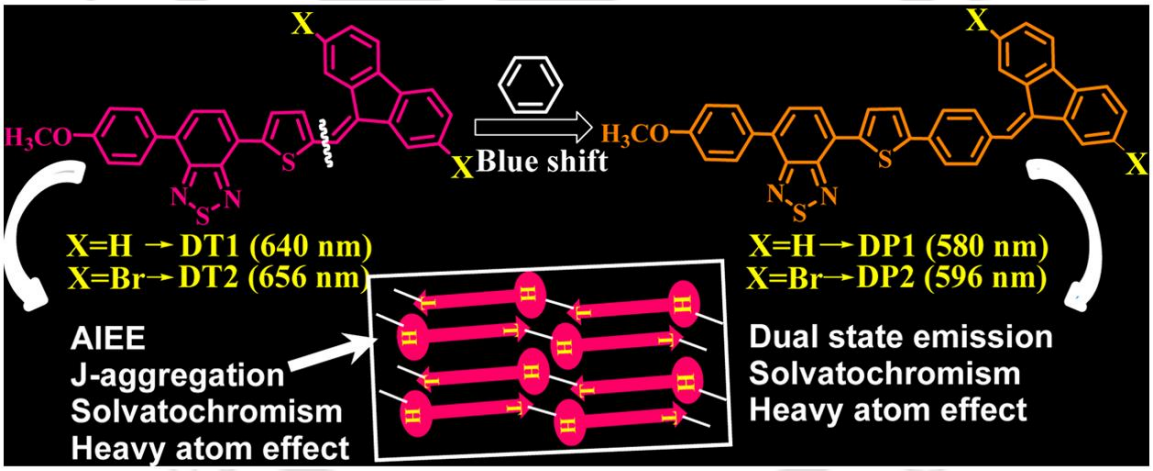

Gopikrishna, P.; Iyer, P. K. *J. Phys. Chem. C.* **2016**, *120,* 26556-26568.

Abstract

The observation of unusual aggregation-induced emission enhancement (AIEE) phenomenon in the deep red wavelength region, dual state emission, and intramolecular charge transfer of dibenzofulvene (DBF) derivatives are described. These consist of a series of newly synthesized donor-acceptor based M-DBF molecules (DT1, DT2, DP1, and DP2) with their cores comprising DBF molecules. Two luminogens with thiophene-substituted at the ninth position of DBF, viz. DT1 and DT2, displayed AIEE with predominant J-type aggregation due to the effect of intramolecular planarization and formation of nanoparticles in the aggregated state. In the DP1 and DP2 luminogens an extra phenyl ring was inserted at the ninth position of DBFs (between thiophene and DBF) that resulted in a blue-shift (~60 nm) as compared to the DT derivatives and exhibited a unique dual state emission with good quantum yields. This additional phenyl moiety reduces the effective conjugation length toward 2,1,3-benzothiadiazole from DBF and simultaneously interrupts the head to tail interaction and also prevents the J-type aggregation. All the four luminogens exhibited distinctive solvent-dependent photoluminescence (PL) behavior (solvatochromism) because of the efficient intramolecular charge transfer. The DT2 and DP2 luminogens showed heavy atom effect due to the presence of two bromine atoms. The HOMO and LUMO values of the luminogens were estimated by cyclic voltammetry (CV) and DFT calculations.

4.1. Introduction

The development of aggregation-induced emission (AIE) luminescent materials have attracted immense attention due to their potential applications in organic electronics,[1-4] bio-imaging, [5-8] and bio-sensors.[9-13] In many cases, the luminogens are highly emissive only in dilute solutions but remain non-emissive or less emissive in aggregated state. This is because the molecules in the aggregated state may experience strong π-π stacking interactions that lead to aggregation caused quenching (ACQ). This prompts the formation of detrimental species such as excimers or exciplexes, thus leading to poor solid state emission.[14,15] To resolve this ACQ effect in the aggregation phase, various chemical, physical, and engineering approaches have been attempted and established.[16-21] In contrast, the propeller-like small molecules show AIE phenomenon, reported first by Tang and co-workers in 2001, where the organic molecules are highly luminescent in the solid state due to aggregation. The AIE luminogens are non-emissive in certain solvents but become highly emissive in aggregated state. To date, several luminescent materials with AIE effect have been discovered, which mainly contain tetraphenylethylene (TPE)[22-24] and silole[25] derivatives. However, in solution state the phenyl rotors, contained in these structures, undergo dynamic intramolecular rotations that non-radiatively annihilate their excited state and become non-luminescent. Nevertheless, in the solid or aggregated state the molecules cannot pack through a π-π stacking process due to the restricted intramolecular rotation (RIR) mechanism. [22-25] Later in 2002, Park et al.[26] discovered an interesting AIEE phenomenon, which is caused by synergetic effect of intramolecular planarization and J-aggregation. Generally, AIEE luminogens show noteworthy emission in solution, which is significantly enhanced after aggregation. Few other AIEE active materials obtained via J-aggregation,[27,28] excimer formation,[29,30] activated phosphorescence,[31-33] and aurophilic interactions[34-36] have been reported. It is necessary to develop new AIEE materials with higher fluorescence intensity and quantum yields in solid state than in diluted solution because reports of AIEE materials are limited in literature compared to AIE materials. Polyfluorenes, oligofluorenes, and their substituted monomers have emerged as a very important class of optoelectronic materials due to their high luminescence efficiency, good charge-carrier mobility, and convenient color tunability.[37-40] However, very few reports are available based on disubstituted DBF, and most of these luminogens have DBFs that are diphenyl substituted (symmetric), presumably due to the assumption that bulky groups are indispensable to realize the RIR effect.[41-43] Consequently, no reports exist that are based

on mono-substituted DBF (M-DBF), where the AIE behavior has been observed and utilized practically. Recently, it has also been reported that propeller-shaped diphenyldibenzofulvene (DPDBF) molecules can be found either in ring-opened or ring-closed form (8-phenylbenzo[e]-acephenanthrylene). In the ring closed form of DPDBF, the phenyl group is locked and is found to be highly emissive in solution state. This suggests that the AIE effects of DPDBF are caused by the RIR phenomenon of their phenyl rings in the aggregated state.[44] Mono-phenyl substituted DBF, like 8-phenylbenzo[e]-acephenanthrylene, is also a good example for ACQ compounds.[44] However, most of these AIE compounds have shown emission in the blue-green region only. This suggests the need to develop red emitting materials that have enormous importance especially for applications in biological systems and organic optoelectronic devices. However, achieving red emission from a monomer based system is difficult in molecules that form aggregates. Such fluorescent molecules are generally prepared from fused planar rings with extended conjugation or π-conjugated electron-donating and accepting groups. Few examples of such luminogens include pyran containing dyes [e.g., 4-(dicyanomethylene)-2-methyl-6-{2-[(4-diethyl-amino)phenyl]ethyl}-4H-pyran(DCM)], [45,46] Nile red,[47] benzo-2,1,3-thiadiazole based chromophores,[48,49] BODIPYs,[50] and 4-amino-1,8-naphthalic anhydride derivatives.[51] However, as explained in literature most of them are highly red emissive in solution state and less fluorescent or non-fluorescent in water or solid state due to the emission quenching in aggregated state or strong dipole-dipole interactions and intermolecular π-π interactions. It is well documented that a small number of organic molecules have been found to exhibit AIEE properties in the red region.[52,53] Thus, the development of monomer based red emissive materials in solid state and in polar solvents will contribute in realizing applications primarily directed towards imaging and biology.

Recently, an interesting "dual state emission" phenomenon has also been discovered for organic luminescent materials, wherein the luminogens emit efficiently in solution as well as in the solid state. However, progress of dual state emitting materials is still at its preliminary stage.[54,55] Tang et al. reported dual state emitting luminogens by taking advantage of both ACQ (triphenylamine) and AIE (triphenylethylene) dyes that emit in both solution and solid states in the blue region.[56] These dual state luminogens have added advantages compared to ACQ, AIE, and AIEE luminogens. Hence, it is essential to develop new molecules that can emit efficiently in the solution and solid state and have emissions in the red region to realize broader applications such as cell imaging,

optoelectronic devices, and other light based applications. In this context, we report the development of four new D-A luminogens based on M-DBF. Among these four molecules, two are deep-red luminescent AIEE active with J-type aggregation and are substituted with thiophene, while the remaining two luminogens that interestingly possesses an additional phenyl moiety exhibit the rare dual state emission. These M-DBF luminogens are devoid of symmetry and are first examples of AIEE active luminogens with J-type aggregation having impressive and unique emission properties in the red spectral region. As represented in the Scheme 4.1, both the luminogens (DT1 and DT2) have similar structures; however, the DT2 molecule has two bromine atoms at second and seventh positions on the DBF. Still, this minor structural variation in DT1 and DT2 causes significant differences in their absorption and emission behavior that is assigned exclusively to the effect of substituted halogen (bromine) in DT2. Additionally, two structurally similar compounds (DP1 and DP2, Scheme 4.1) were also synthesized by inserting a phenyl ring between the thiophene and DBF to gain insight into the impressive emission behavior and the influence of heteroatom in comparison to the phenyl rings traditionally reported in literature.[32,57] Surprisingly, DP1 and DP2 monomers are highly emissive in both solution and solid state with dual state emission, which are likely to have very diverse applications. This is the first report of M-DBF luminogens with deep red AIEE active and dual state emission behavior. As mentioned earlier, M-DBF are ACQ compounds.[15] When the ninth position of DBF is free of substituent/partially substituted, there is less chance for RIR in the aggregated state.[41-43] However, the M-DBF reported here have a bulky substituent group "benzothiadiazole" at the para position of phenyl (DP1 and DP2) and fifth position of thiophene ring (DT1 and DT2). Since the donor and acceptor conjugated molecules are different in various D-A pairs, the density functional theory (DFT) and time-dependent density functional theory (TDDFT) methods have been very helpful in computing the optimization and excitation energies.[58,59]

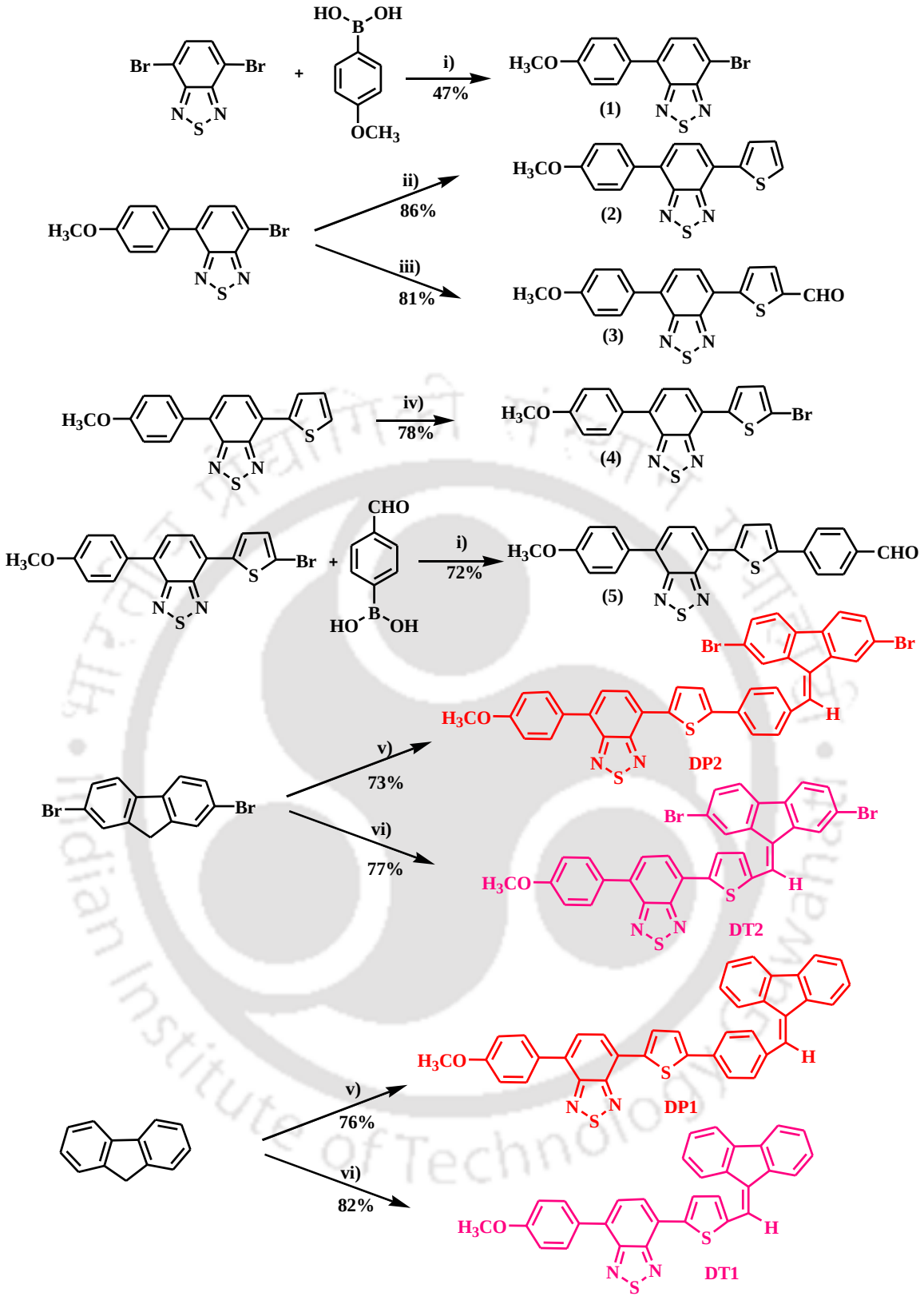

Scheme 4.1. Synthetic route for Monomers.

i) $Pd(PPh_3)_4$, 2M K_2CO_3, THF, 80 °C, 12 h. ii) Tributyl-thiophen-2-yl-stannane, $Pd(PPh_3)_4$, THF, 80 °C, 12 h, iii) 5-Formylthiophene-2-boronic acid, $Pd(PPh_3)_4$, 2M K_2CO_3, THF, 80 °C, 12 h. iv) NBS, THF: CH_3COOH (1:1), RT, 6 h. v) Compound (5) and EtOH, Potassium tert-butoxide, Reflux, 12 h. vi) Compound (3) and EtOH, Potassium tert-butoxide, Reflux, 12 h.

4.2. Experimental section

4.2.1. Materials and measurements

2,7-Dibromofluorene, 9H-fluorene, 4,7-dibromobenzo[c]-1,2,5- thiadiazole, 4-methoxy phenyl boronic acid, 2-(tributylstannyl)- thiophene, 4-formyl phenyl boronic acid, 5-formylthiophene-2 -boronicacid, tetrakis(triphenylphosphine)palladium(0), N-bromosuccinimide (NBS), and potassium tert-butoxide were purchased from Sigma-Aldrich and used without further purification. Absolute ethanol, chloroform, dichloromethane, and toluene were distilled over calcium chloride, and anhydrous tetrahydrofuran (THF) was obtained by drying over sodium/ benzophenone.

The ^{1}H and ^{13}C NMR spectra were recorded on Bruker 600 MHz NMR spectrometer. Mass spectra were recorded on Bruker MALDI-TOF. UV-visible spectra were measured by PerkinElmer, Model Lambda-25 spectrometer. Photoluminescence spectra were recorded with Varian Cary Eclipse spectrometer. Transmission electron microscopic (TEM) studies were done using a Tecnai G2 F20 S-twin JEOL 2100 transmission electron microscope. The dynamic light scattering (DLS) measurements were performed on Zetasizer Nano series Nano-ZS90 instrument.

4.2.2. Synthesis of 4-Bromo-7-(4-methoxy-phenyl)-benzo[1,2,5]thiadiazole (1)

The mixture of 4,7-dibromo-benzo[1,2,5]thiadiazole (1.eq), 4-methoxy phenyl boronic acid (0.7 eq), 12 mL THF and tetrakis(triphenyl phosphine)palladium(0) (0.015 eq) were added into a dry two neck round bottom flask. Subsequently, 4 mL 2M aqueous potassium carbonate was added to the flask. The reaction mixture was stirred at 80 °C for 12 h under argon atmosphere. The reaction mixture was then cooled to room temperature. After work up, the mixture was purified by column chromatography to give greenish yellow solid compound **1**. (yield: 47%); ^{1}H NMR (600 MHz, $CDCl_3$) δ (ppm): 7.89 (d, J=7.2 Hz, 1H), 7.86 (d, J=9 Hz, 2H), 7.52 (d, J=7.4 Hz, 1H), 7.05 (d, J=8.4 Hz, 2H), 3.89 (s, 3H). ^{13}C NMR (150 MHz, $CDCl_3$) δ (ppm): 160.33, 154.10, 153.49, 133.91, 132.54, 130.62, 129.28, 127.65, 114.42, 112.47, 55.63. HRMS (ESI): m/z $[M + H]^+$ Calcd: 320.9697, found 320.9690.

4.2.3. Synthesis of 4-(4-Methoxy-phenyl)-7-thiophen-2-yl-benzo[1,2,5]thiadiazole (2)

The mixture of 4-Bromo-7-(4-methoxy-phenyl)-benzo[1,2,5]thiadiazole (1) (1.eq), Tributyl-thiophen-2-yl-stannane (1.2 eq) 12 mL THF and tetrakis(triphenyl

phosphine)palladium(0) (0.015 eq) were added into a dry round bottom flask. The reaction mixture was stirred at 80 °C for 12 h under argon atmosphere. The resulting reaction mixture was cooled to room temperature and the crude product was purified by column chromatography to give yellow solid compound **2** (yield: 86%); ^{1}H NMR (600 MHz, $CDCl_3$) δ (ppm): 8.10 (d, *J*=3.6 Hz, 1H), 7.91 (dd, *J*=8.4 Hz, 6 Hz, 2H), 7.66 (d, *J*=7.2 Hz, 1H), 7.44 (d, *J*=4.8 Hz, 1H), 7.21 (t, 1H), 7.07 (d, *J*=8.4 Hz, 2H), 3.89 (s, 3H), ^{13}C NMR (150 MHz, $CDCl_3$) δ (ppm): 160.05, 154.22, 153.02, 139.70, 132.74, 130.58, 129.95, 128.15, 127.91, 127.52, 127.40, 126.73, 126.21, 125.98, 114.31, 55.59. HRMS (ESI): m/z $[M + H]^+$ Calcd: 325.0469, found 325.0468.

4.2.4. Synthesis of 5-[7-(4-Methoxy-phenyl)-benzo[1,2,5]thiadiazol-4-yl]-thiophene-2-carbaldehyde (3)

A mixture of compound 1 (1.eq), 5-formylthiophene-2-boronic acid (1.2 eq), 12 mL THF and tetrakis(triphenyl phosphine)palladium(0) (0.015 eq) were added into a dry two neck round bottom flask. Subsequently 4 mL 2M aqueous potassium carbonate were added to the flask. The reaction mixture was stirred at 80 °C for 12 hours under argon atmosphere. The reaction mixture was then cooled to room temperature. After work up, the mixture was purified by column chromatography to give yellow solid compound **3**. (yield: 81%); ^{1}H NMR (600 MHz, $CDCl_3$) δ (ppm): 9.98 (s, 1H), 8.21 (d, *J*=4.2 Hz, 1H), 8.04 (d, *J*=7.2 Hz, 1H), 7.94 (d, *J*=8.4 Hz, 2H), 7.85 (d, *J*=3.6 Hz, 1H), 7.72 (d, *J*=7.2 Hz, 1H), 7.08 (d, *J*=9 Hz, 2H), 3.90 (s, 3H). ^{13}C NMR (150 MHz, $CDCl_3$) δ (ppm): 183.2, 160.4, 154.1, 152.8, 149.1, 143.5, 137.0, 134.9, 130.7, 129.4, 128.0, 127.8, 127.0, 124.5, 114.4, 55.6. HRMS (ESI): m/z $[M + H]^+$ Calcd: 353.0418, found 353.0416.

4.2.5. Synthesis of 4-(5-Bromo-thiophen-2-yl)-7-(4-methoxy-phenyl)-benzo[1,2,5]thiadiazole (4)

4-(4-Methoxy-phenyl)-7-thiophen-2-yl-benzo[1,2,5]thiadiazole (2) (1.eq), was added into 12 mL THF and glacial acetic acid (1:1). After the solid dissolved completely, *N*-bromosuccinimide (1. eq) was added in one portion and stirred at room temperature for 6 h, under argon atmosphere. The reaction mixture was washed with brine and dried over anhydrous sodium sulfate. The solvent was removed at reduced pressure and the crude product was purified by column chromatography to give the product as a yellow solid compound **4** (yield: 78%); ^{1}H NMR (600 MHz, $CDCl_3$) δ (ppm): 7.915 (d, *J*=6 Hz, 2H), 7.84 (d, *J*=12 Hz, 1H), 7.795 (d, *J*=6 Hz, 1H), 7.665 (d, *J*=6 Hz, 1H), 7.155 (d, *J*=6 Hz, 1H), 7.075 (d, *J*=6 Hz, 2H), 3.90 (s, 3H). ^{13}C NMR (150 MHz, $CDCl_3$) δ (ppm):160.3,

153.8, 153.7, 133.4, 130.7, 130.5, 129.5, 127.2, 126.7, 125.5, 123.3, 114.3, 114.3, 109.2, 55.6. MALDI-TOF MS: $[M + H]^+$ Calcd. 404.53, Found: 404.08.

4.2.6. Synthesis of 4-{5-[7-(4-Methoxy-phenyl)-benzo[1,2,5]thiadiazol-4-yl]-thiophen-2-yl}-benzaldehyde (5)

4-(5-Bromo-thiophen-2-yl)-7-(4-methoxy-phenyl)-benzo[1,2,5]thiadiazole (3) (1.eq), 4-formyl phenyl boronic acid (1.2 eq), 12 mL of Tetrahydrofuran (THF) and tetrakis(triphenyl phosphine)palladium(0) (0.015 eq) were added into a dry two neck round bottom flask. Subsequently 4 mL 2M aqueous potassium carbonate were added to the flask. The reaction mixture was stirred at 80 °C for 12 h under argon atmosphere. The reaction mixture was then cooled to room temperature. The reaction mixture was washed with brine and dried over anhydrous sodium sulfate. The solvent was removed at a reduced pressure and the mixture purified by column chromatography to give light orange compound **5**. (yield: 72%); ^{1}H NMR (600 MHz, $CDCl_3$) δ (ppm): 9.96 (s, 1H), 7.92 (m, 3H), 7.85 (d, *J*=7.8 Hz, 2H), 7.77 (d, *J*=7.8 Hz, 2H), 7.54 (d, *J*=7.8 Hz, 1H), 7.49 (d, *J*=3.6 Hz, 2H), 7.05 (d, *J*=8.4 Hz, 2H), 3.88 (s, 3H).^{13}C NMR (150 MHz, $CDCl_3$) δ (ppm): 191.5, 160.3, 154.0, 153.8, 143.4, 142.8, 140.8, 139.4, 136.3, 135.7, 135.2, 134.2, 131.0, 130.7, 130.4, 130.2, 129.4, 126.1, 114.3, 55.5. HRMS (ESI): m/z $[M + H]^+$ Calcd: 429.0731, found 429.0737.

4.2.7. Synthesis of 4-{5-[4-(2,7-Dibromo-fluoren-9-ylidenemethyl)-phenyl]-thiophen-2-yl}-7-(4-methoxy-phenyl)-benzo[1,2,5]thiadiazole (6) (DP2)

A mixture of potassium tert-butoxide (1.2 eq) and 2,7-Dibromo-9H-fluorene (1.2 eq) was dissolved in 15 mL absolute ethanol. The resulting solution was refluxed for 1 h and compound 5 (1 eq) was added into reaction mixture and again refluxed for 18 h. The solvent was concentrated, and the residue was extracted with CH_2Cl_2 and evaporated. The residue was purified by column chromatography to give the product as an orange solid compound **DP2**. (yield: 73%); ^{1}H NMR (600 MHz, $CDCl_3$) δ (ppm): 8.14, (d, *J*=3.6 Hz, 1H), 7.97, (d, *J*=7.2 Hz, 1H), 7.95, (d, *J*=7.2 Hz, 2H), 7.90, (m, 3H), 7.84, (s, 1H), 7.82, (d, *J*=7.8 Hz, 2H), 7.70, (d, *J*=7.8 Hz, 2H), 7.67, (s, 1H), 7.64, (d, *J*=7.8 Hz, 1H), 7.54, (m, 2H), 7.50, (m, 2H), 7.46, (d, *J*=1.2 Hz, 1H), 7.08, (d, *J*=9 Hz, 2H), 3.90, (s, 3H). ^{13}C NMR (150 MHz, $CDCl_3$) δ (ppm): 160.1, 154.3, 154.0, 147.2, 144.5, 141.4, 141.3, 141.2, 139.4, 139.3, 138.1, 137.5, 137.1, 136.2, 135.3, 134.7, 134.1, 131.4, 130.9, 130.6, 130.3, 129.8, 129.7, 129.5, 129.3, 127.4, 126.6, 126.1, 124.6, 123.8, 121.1, 119.2, 114.3, 114.2, 55.6. MALDI-TOF MS: $[M + H]^+$ Calcd.734.95, Found: 734.10.

4.2.8. Synthesis of 4-[5-(2,7-Dibromo-fluoren-9-ylidenemethyl)-thiophen-2-yl]-7-(4-methoxy-phenyl)-benzo[1,2,5]thiadiazole (7) (DT2)

A mixture of potassium tert-butoxide (1.2 eq) and 2,7-Dibromo-9H-fluorene (1.2 eq) was dissolved in 15 mL absolute ethanol. The resulting solution was refluxed for 1 h and compound 3 (1 eq) was added into reaction mixture and again refluxed for 18 h. The solvent was cncentrated, and the residue was extracted with CH_2Cl_2 and evaporated. The residue was purified by column chromatography to give the product as a red solid compound **DT2**. (yield: 77%); ^{1}H NMR (600 MHz, $CDCl_3$) δ (ppm): 8.62, (s, 1H), 8.17, (d, *J*=6 Hz, 1H), 8.0, (d, *J*=7.2 Hz, 1H), 7.95, (d, *J*=8.4 Hz, 2H), 7.86, (s, 1H), 7.72, (d, *J*=7.2 Hz, 1H), 7.65, (s, 1H), 7.60, (d, *J*=3.6 Hz, 1H), 7.57, (d, *J*=7.8 Hz, 1H), 7.52, (d, *J*=8.4 Hz, 1H), 7.50, (d, *J*=7.8 Hz, 1H), 7.47, (d, *J*=6.6 Hz, 1H), 7.08, (d, *J*=9 Hz, 2H), 3.90, (s, 3H), ^{13}C NMR (150 MHz, $CDCl_3$) δ (ppm): 160.2, 154.1, 152.8, 142.9, 141.7, 139.4, 139.2, 137.7, 136.7, 133.5, 132.2, 131.7, 131.2, 130.6, 129.7, 127.9, 127.6, 127.3, 126.3, 123.6, 121.4, 121.3, 121.2, 121.1, 114.3, 55.6. MALDI-TOF MS: $[M + H]^+$ Calcd. 658.92, Found: 658.06.

4.2.9. Synthesis of 4-[5-(4-Fluoren-9-ylidenemethyl-phenyl)-thiophen-2-yl]-7-(4-methoxy-phenyl)-benzo[1,2,5]thiadiazole (8) (DP1)

A mixture of potassium tert-butoxide (1.2 eq) and 9H-fluorene (1.2 eq) was dissolved in 15 mL absolute ethanol. The resulting solution was refluxed for 1 h and compound 5 (1 eq) was added into the reaction mixture and again refluxed for 18 h. The solvent was concentrated and the residue was extracted with CH_2Cl_2 and evaporated. The residue was purified by column chromatography to give the product as a orange solid compound **DP1**. (yield: 76%); ^{1}H NMR (600 MHz, $CDCl_3$) δ (ppm): 7.94, (d, *J*=8.4 Hz, 1H), 7.84, (d, *J*=8.4 Hz, 1H), 7.80, (d, *J*=8.4 Hz, 1H), 7.73, (d, *J*=7.8 Hz, 2H), 7.69, (m, 2H), 7.65, (s, 1H), 7.62, (d, *J*=7.8 Hz, 1H), 7.57, (d, *J*=7.8 Hz, 1H), 7.52, (m, 2H), 7.46, (d, *J*=7.8 Hz, 1H), 7.36, (m, 4H), 7.12, (t, 1H), 7.07, (d, *J*=8.4 Hz, 2H), 7.03, (t, 1H), 3.89, (s, 3H), ^{13}C NMR (150 MHz, $CDCl_3$) δ (ppm): 160.1, 154.3, 154.0, 144.7, 141.5, 139.3, 139.3, 136.9, 136.8, 136.6, 133.8, 133.6, 130.9, 130.6, 130.3, 129.8, 129.0, 128.8, 128.8, 128.4, 127.2, 127.0, 126.9, 126.8, 126.3, 125.9, 125.8, 124.6, 124.4, 120.4, 120.4, 119.9, 119.8, 119.7, 114.3, 55.6. MALDI-TOF MS: $[M]^+$ calcd.576.13 Found: 576.29

4.2.10. Synthesis of 4-(5-Fluoren-9-ylidenemethyl-thiophen-2-yl)-7-(4-methoxy-phenyl)-benzo[1,2,5]thiadiazole (9) (DT1)

A mixture of potassium tert-butoxide (1.2 eq) and 9H-fluorene (1.2 eq) was dissolved in 15 mL absolute ethanol. The resulting solution was refluxed for 1 h and

compound 7 (1 eq.) was added into the reaction mixture and refluxed further for 18 h. The solvent was concentrated, and the residue was extracted with CH_2Cl_2 and evaporated. The residue was purified by column chromatography to give the product as a orange solid compound **DT1**. (yield: 82%); ^{1}H NMR (600 MHz, $CDCl_3$) δ (ppm): 8.35 (d, *J*=7.8 Hz, 1H), 8.19 (d, *J*=3.6 Hz, 1H), 7.97 (d, *J*=7.2 Hz, 1H), 7.94 (d, *J*=8.4 Hz, 2H), 7.75 (dd, *J*=7.2 Hz, 7.8 Hz, 2H), 7.71 (dd, *J*=3 Hz, 3 Hz, 2H), 7.76 (s, 1H), 7.59 (d, *J*=3.6 Hz, 1H), 7.37 (t, 2H), 7.33 (t, 1H), 7.24 (t, 1H), 7.08 (d, *J*=7.8 Hz, 2H), 3.90 (s, 3H). ^{13}C NMR (150 MHz, $CDCl_3$) δ (ppm): 160.1, 154.3, 152.9, 141.6, 141.5, 139.8, 139.1, 136.7, 136.3, 133.1, 131.0, 130.6, 129.8, 129.0, 128.5, 128.1, 127.4, 127.2, 127.1, 126.2, 124.7, 120.4, 120.0, 119.8, 118.9, 114.3, 55.6. MALDI-TOF MS: $[M + H]^+$ Calcd. 501.10, Found: 501.26.

4.2.11. Crystal Data

Table 4.1: Structure determination summary of **DT1** and **Compound-5**

Compound	DT1	Compound-5
Empirical formula	$C_{31}H_{20}N_2OS_2$	$C_{24}H_{16}N_2O_2S_2$
CCDC NO	1445372	1446140
Formula weight	500.61	428.51
Temperature/K	296 (2)	296 (2)
Crystal system	monoclinic	monoclinic
Space group	$P2_1/n$	$P2_1/c$
a/Å	10.1603(3)	9.4561(3)
b/Å	18.4764(5)	17.9251(6)
c/Å	12.9632(3)	12.1203(4)
α/°	90.00	90.00
β/°	92.126(2)	108.290(2)
γ/°	90.00	90.00
Volume/Å^3	2431.85(11)	1950.62(11)
Z	4	4
ρ_{calc}mg/mm^3	1.367	1.459
m/mm^{-1}	0.247	0.298
F(000)	1040.0	888.0
Crystal size/mm^3	0.32 × 0.24 × 0.12	0.28 × 0.24 × 0.21
2Θ range for data collection	3.84 to 50.5°	4.2 to 50.5°
Index ranges	$-11 \le h \le 12$, $-21 \le k \le 21$, $-15 \le l \le 14$	$-11 \le h \le 11$, $-21 \le k \le 21$, $-14 \le l \le 14$
Reflections collected	31332	17891
Independent reflections	4339[R(int) = 0.0369]	3492[R(int) = 0.0368]
Data/restraints/parameters	4339/0/326	3492/0/276
Goodness-of-fit on F^2	1.067	0.915
Final R indexes [I>=2σ (I)]	R_1 = 0.0401, wR_2 = 0.1158	R_1 = 0.0435, wR_2 = 0.1247
Final R indexes [all data]	R_1 = 0.0565, wR_2 = 0.1268	R_1 = 0.0714, wR_2 = 0.1431

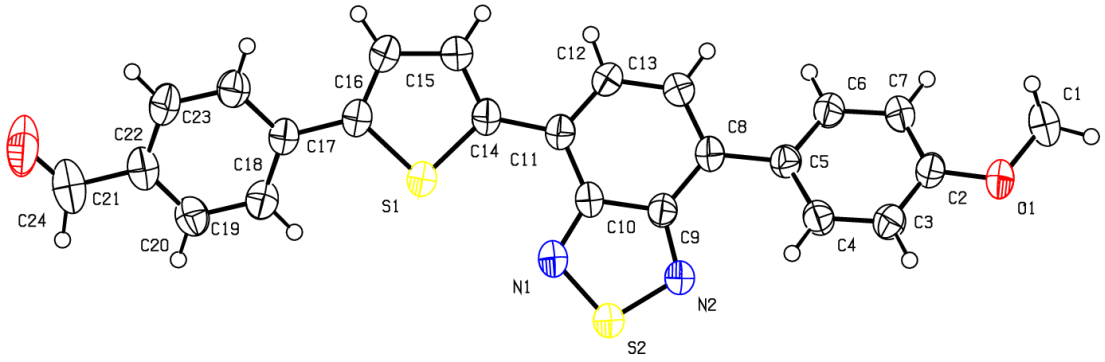

Figure 4.1: ORTEP diagram of **Compound-5**

4.3. Results and discussion

4.3.1. Optical and photoluminescence properties

The UV-vis spectrum of DT1 and DT2 showed two broad bands at 411, 486 nm and 420, 510 nm in solid state and 397, 468 nm and 421, 470 nm in THF solution (Figure 4.2a). The bands at longer wavelength region are due to the intramolecular charge transfer (ICT) process in the luminogens, while the shorter wavelength bands are π-π* transitions of the luminogens.

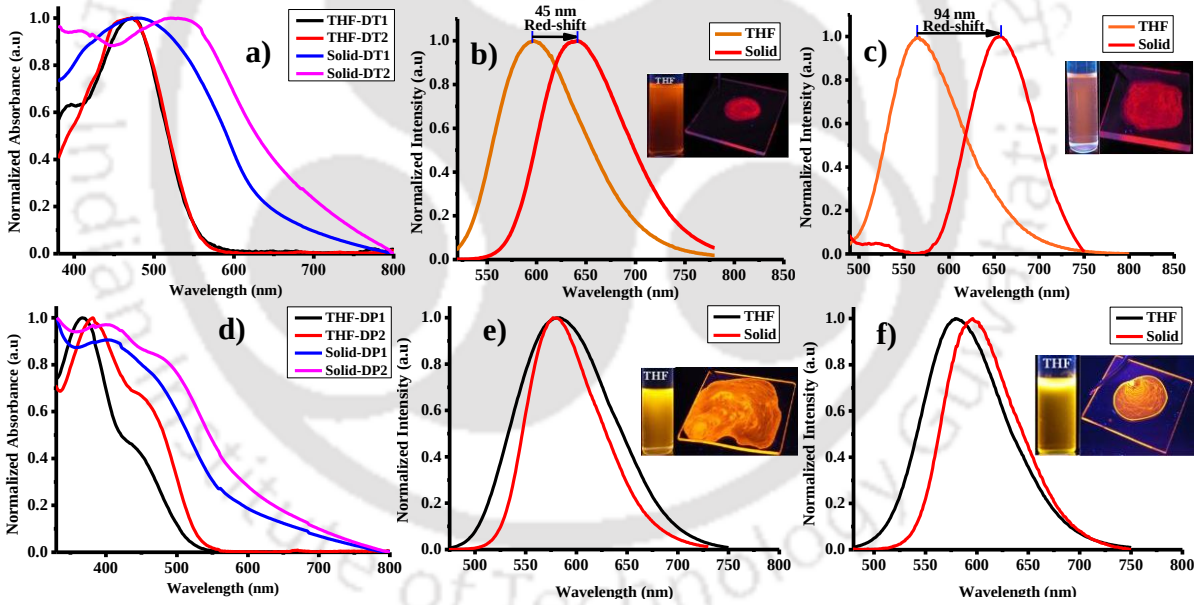

Figure 4.2: (a) Normalized UV-vis spectra of DT1 and DT2; PL spectra and photographs of (b) DT1 and (c) DT2 in THF solution and solid state. (d) Normalized UV-vis spectra of DP1 and DP2; PL spectra and photographs of (e) DP1 and (f) DP2 in THF solution and solid state. The photographs were taken under 365 nm UV lamp irradiation.

The thin films of DT1 and DT2 showed emission peaks at 640 and 656 nm (470 nm excitation), whereas their THF solution showed peaks at 595 and 562 nm (450 nm excitation) (Figure 4.2b,c, Table 4.2). It was interesting to note that the UV-vis and photoluminescence (PL) spectra of both DT1 and DT2 displayed a significant difference in the THF and solid state spectra, as mentioned in terms of Stokes shift. The optical

properties confirm that the solid state absorption and emission of DT1 were red-shifted by ~18 and ~45 nm. Similarly, the DT2 spectra were also red-shifted by ~40 and ~94 nm (deep red CIE coordinates, Figure 4.3a,b).

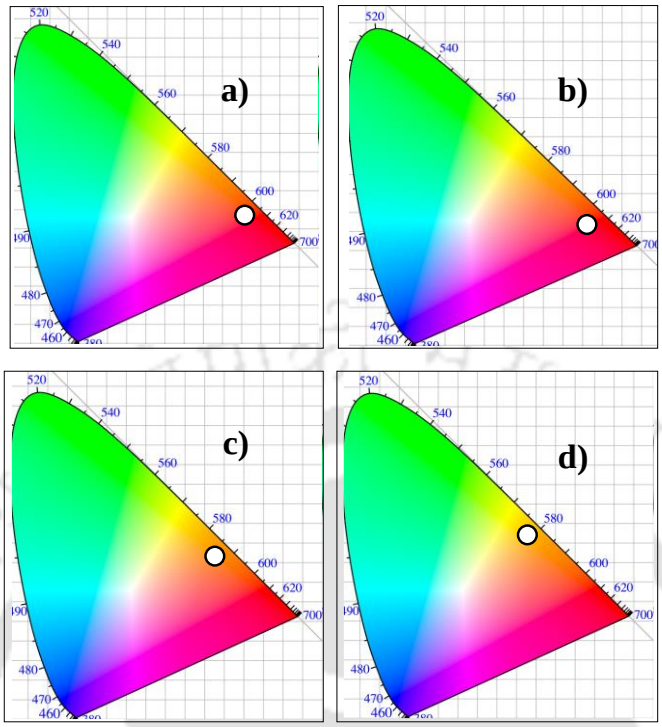

Figure 4.3: Chromaticity diagram representing the CIE coordinates of a**) DT1**, (0.65, 0.34), **b) DT2**, (0.66, 0.32), **c) DP1** (0.57, 0.42), and **d) DP2, (**0.51, 0.47).

The large redshift occurred due to the formation of J-type aggregation, (explained in more detail later). These results confirm that the DT2 showed more redshift than DT1 luminogen due to the heavy atom effect of the two substituted bromines.[57] The absorption spectra of DP1 and DP2 were also studied in both solution and solid state to explore the influence of introducing the phenyl ring. The DP1 exhibited two broad bands at 366, 445 nm in THF solution and 400, 478 nm in solid state. Similarly, DP2 exhibited two broad bands at 380, 445 nm in THF solution and 406, 486 nm in solid state (Figure 4.2d). The THF solutions of DP1 and DP2 showed emission peaks at 578 and 580 nm (430 nm excitation), whereas the thin films of DP1 and DP2 showed emission peaks at 580 and 596 nm (Figure 4.2e,f, Table 4.2) (450 nm excitation). Surprisingly, DP1 and DP2 molecules exhibited the unique dual state emission with a significant blue-shift (~60 nm) (orange-red CIE coordinates, Figure 4.3c,d). The additional phenyl ring greatly enhanced the PL quantum yield in both solutions (ranging from 0.9% in DT1 to 26.3% for DP1 and 0.6% in DT2 to 22.1% for DP2) and solid state (ranging from 2.6% in DT1 to 24.2% for DP1 and 2.0% in DT2 to 19.5% for DP2) (Table 4.2). These molecules exhibited bright orange emissions at 578 and 580 nm with high fluorescence quantum yields of 26.3% and

22.1% in THF solution, as well as in solid state at 580 and 596 nm with high fluorescence quantum yields of 24.2% and 19.5% (Table 4.2).

Table 4.2: Photophysical properties of **DT1**, **DT2**, **DP1** and **DP2** in THF and solid state.

Monomer	λ_{max}, abs [nm] THF	λ_{max}, abs [nm] Solid	λ_{max}, PL [nm] THF	λ_{max}, PL [nm] Solid	Φ_F [%][a]	Φ_F [%][b]	CIE coordinates (x, y)[c]
DT1	397, 468	411, 486	595	640	0.9	2.6	0.65, 0.34
DT2	421, 470	420, 510	562	656	0.6	2.0	0.66, 0.32
DP1	366, 445	400, 478	578	580	26.3	24.2	0.57, 0.42
DP2	380, 445	406, 486	580	596	22.1	19.5	0.51, 0.47

[a]The fluorescence quantum yield in THF related to Rhodamine 6G (Φ_F = 0.94 in DMF). [b]Solid state determined using an integrating sphere. [c]Determined from the solid state PL spectrum.

4.3.2. Intramolecular Charge Transfer (ICT)

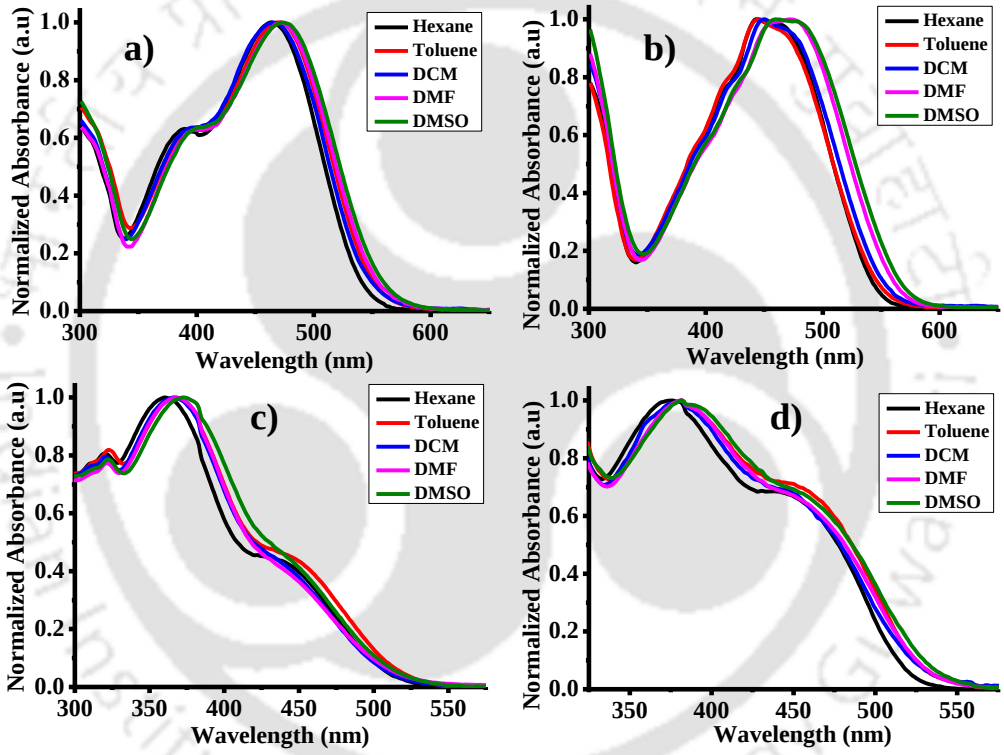

Figure 4.4: Normalized UV-vis of DT1 (a), DT2 (b), DP1 (c), and DP2 (d) in different solvents (5 μM).

The combination of electron-donating and electron-accepting groups readily offers the possibility for ICT excitations and solvatochromic effect due to its strong dependence on solvent polarity. The UV-vis and PL spectra of DT1, DT2, DP1, and DP2 luminogens were measured in different solvents to elucidate this solvatochromism effect. As shown in Figure 4.4 (summary in Table 4.3), the UV-vis spectra of the luminogens were modified, when the solvent polarity varied from nonpolar to polar. When the UV-vis spectra of these luminogens were recorded in diverse solvents (5 μM), viz. hexane, toluene,

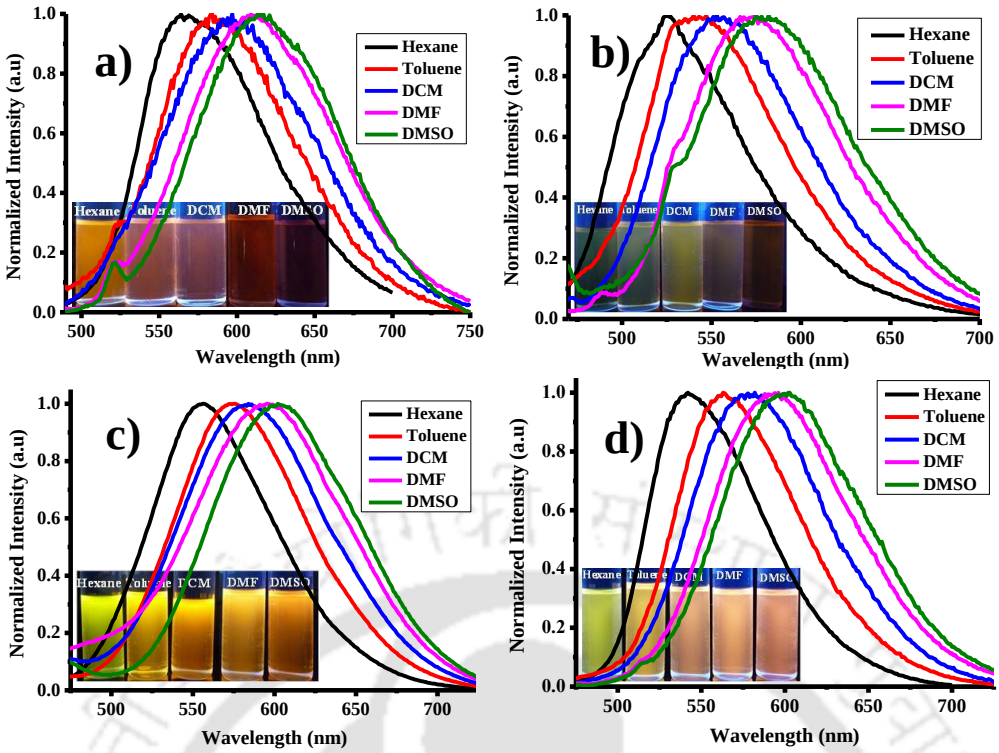

Figure 4.5: Normalized PL spectra of DT1 (a), DT2 (b), DP1 (c), and DP2 (d) in different solvents (5 μM). The photographs were taken under 365 nm hand-lamp irradiation.

Table 4.3: Photophysical properties of **DT1**, **DT2**, **DP1** and **DP2** in different solvents

Monomer	DT1		DT2		DP1		DP2	
	λ_{max}, abs [nm]	λ_{max}, PL [nm]	λ_{max}, abs [nm]	λ_{max}, PL [nm]	λ_{max}, abs [nm]	λ_{max}, PL [nm]	λ_{max}, abs [nm]	λ_{max}, PL [nm]
Hexane	387, 463	566	413, 454	524	360, 438	555	376, 434	540
Toluene	394, 469	583	415, 457	541	366, 445	574	381, 436	563
DCM	395, 465	598	420, 460	550	366, 442	580	380, 442	578
DMF	400, 473	608	423, 470	573	366, 448	595	382, 448	593
DMSO	403, 476	616	426, 474	582	374, 454	603	385, 453	602

dichloromethane (DCM), dimethylformamide (DMF), and dimethyl sulfoxide (DMSO), the absorption bands were slightly red-shifted. All luminogens exhibited two characteristic bands on varying the solvents; one is at shorter and the second at longer wavelength. The band at shorter wavelength is due to the π-π* transitions, whereas the longer wavelength band can be assigned to the ICT process between electron donor and electron acceptor in the luminogens. Figure 4.5 depicts the images of DT1, DT2, DP1, and DP2 luminogens under irradiation at 365 nm UV lamp after dissolving them in these different solvents. The fluorescence intensity and colors of the four luminogens were easily distinguishable by naked eyes in these solvents. The fluorescence emission spectra (Figure 4.5) of these luminogens were, however, strongly dependent on the solvent polarity. When the polarity of the solvent changes from hexane to DMSO, the emission

was remarkably red-shifted from 566 to 616 nm (~50 nm) for DT1, 524 to 582 nm (~58 nm) for DT2, 555 to 603 nm (~48 nm) for DP1, and 540 to 602 nm (~62 nm) for DP2 with a notable decrease in the fluorescence intensity in the four luminogens.

4.3.3. Aggregation Induced Emission Enhancement (AIEE) Properties

To investigate the possible AIEE characteristics of the luminogens, their spectral behaviors were studied in a binary solvent mixture system. For AIEE studies the good and poor solvents should be readily miscible as well as the luminogen should remain soluble in these binary mixtures; thus, THF and water were chosen as the solvent pair to evaluate the spectral properties. The UV-vis spectra were measured in various THF and water fraction (*fw*) ratio in which the luminogen concentrations were kept constant at 20 µM for DT1, DT2 and 40 µM for the DP1, DP2 luminogens. The *fw* (vol %) was changed from 0% to 100%. The UV-vis spectrum (Figure 4.6a,b) of DT1 and DT2 luminogens in pure THF (0% water) exhibited two strong absorption bands at 397, 468 nm and 421, 470 nm. On increasing the *fw* up to 60%, very negligible changes in the spectra of both the luminogens were observed; however, on reaching 70% *fw* the bands in both DT1 and DT2 were red-shifted to 475 nm (15 nm) and 490 nm (22 nm). From 80% to 100% such

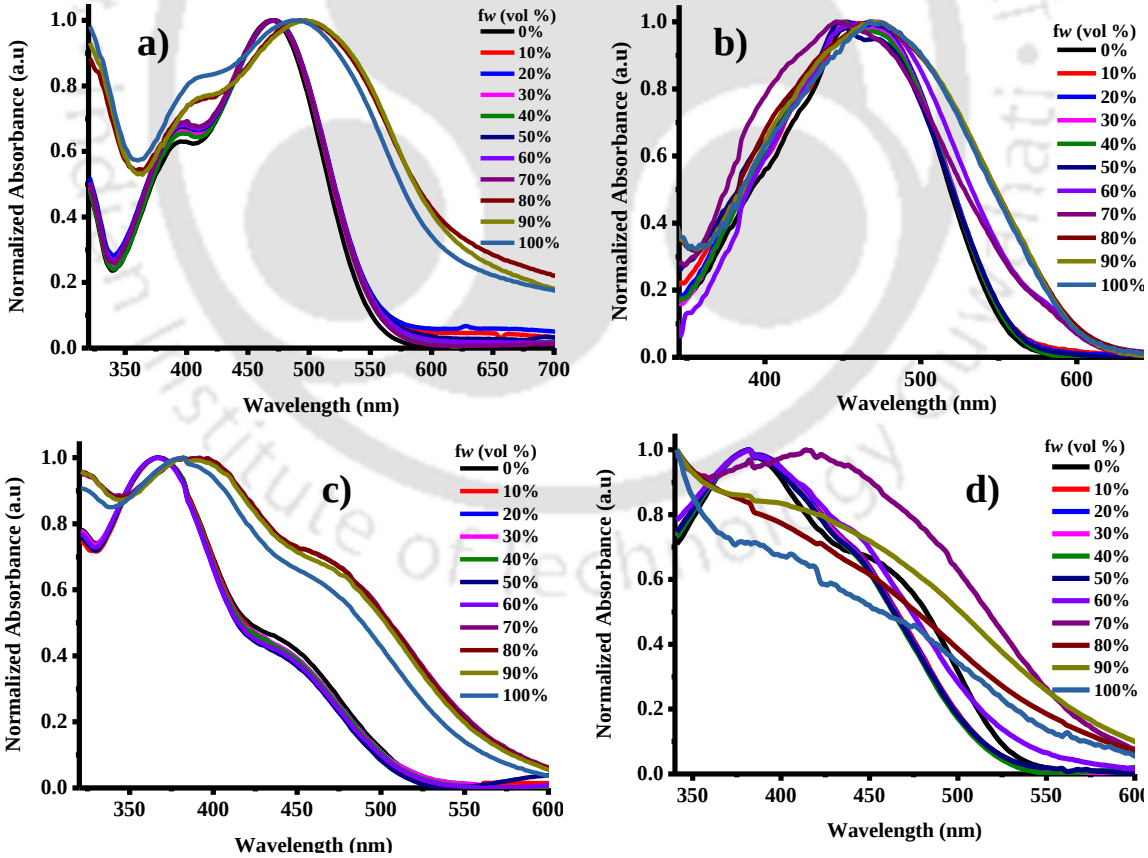

Figure 4.6: UV-vis spectra of (a) DT1 and (b) DT2, 20 µM, in THF and water mixtures and (c) DP1 and (d) DP2, 40 µM, in THF and water mixtures.

bathochromic shifts for the absorption bands were anticipated for J-type aggregation.[27,57,60] The above results confirm that the DT1 showed a bathochromic shift of 22 nm as compared to 15 nm of DT2 due to the two bromine atoms (heavy atom effect).[32,57] Similarly, the UV-vis absorption spectrum (Figure 4.6c,d) of DP1 and DP2 luminogens in pure THF (0% *fw*) exhibited two strong absorption bands at 366, 445 nm and 380, 445 nm. The UV-vis spectrum of DP1 showed no change in the band position up to 70% *fw*, above which the UV bands are red-shifted to 388 and 470 nm. However, in case of DP2 there was no significant change in the band position up to 60% *fw*. Beyond 60% the 380 nm band was red-shifted to 420 nm and gets merged with that of 445 nm resulting in a boarder band as compared to that in THF and appeared as a single band. Figure 4.7a-d shows the PL spectra, relative intensity, and actual changes in the solution color of DT1 and DT2 in water and THF mixtures (20 μM) with different *fw*. In pure THF solution both DT1 and DT2 luminogens exhibited orange color. However, when the *fw* was increased up to 60% the emission peak was red-shifted by ~12 nm for DT1 without any quenching in the PL intensity and ~17 nm for DT2 with quenching of fluorescence. This quenching of DT2 can be attributed to ICT process.[61] When the *fw* reached 70%, both the luminogens showed minor difference in their spectral behaviors. The DT1 luminogen showed an enhancement in PL intensity with redshifted (~7 nm) peak, which suggests the formation of J-aggregation. The PL intensity also enhanced on increasing the *fw* from 80% to 100%, and the peak was red-shifted from 595 to 640 nm (~45 nm), which can be attributed to the formation of nanoaggregates (confirmed by DLS and TEM, discussed in later sections). However, in the case of DT2, when the *fw* reached up to 70% (Figure 4.7c), the emission intensity decreased slightly with two shoulders at 575 and 656 nm. On increasing the *fw* above 70%, the intensity of the 575 nm peak was suppressed, whereas the 656 nm peak was enhanced significantly with a clear change in the color from orange-red to deep red. The large red-shifted (~94 nm) PL peak suggested the formation of J-aggregation, and with further increase of *fw* from 80% to 100%, nanoaggregate formation was observed. Increasing the *fw* (>70%) in mixed solvent system changed the form of both DT1 and DT2 luminogens from a dissolved or well dispersed state in pure THF to aggregated particles in the mixtures with higher *fw*. The emission of aggregates in both DT1 and DT2 luminogens revealed an impressive redshift of ~45 and ~94 nm, respectively, relative to that of the respective luminogens in THF solution, which is possibly due to the J-aggregate formation and RIR phenomenon in the aggregated state. As discussed above, both DT1 and DT2 luminogens are AIEE active

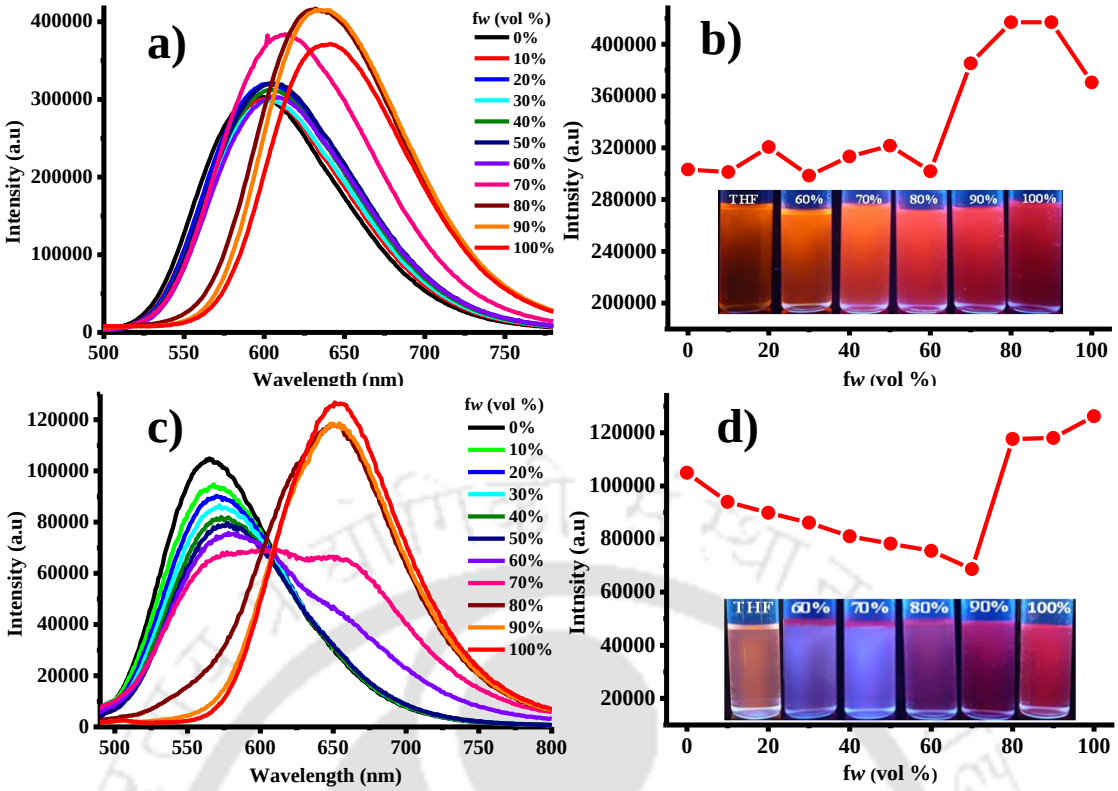

Figure 4.7: PL spectra and PL relative intensity of DT1 (a, b) and DT2 (c, d) (20 μM) in THF and water mixtures. The photographs were taken under 365 nm hand-UV lamp irradiation in THF-water mixtures.

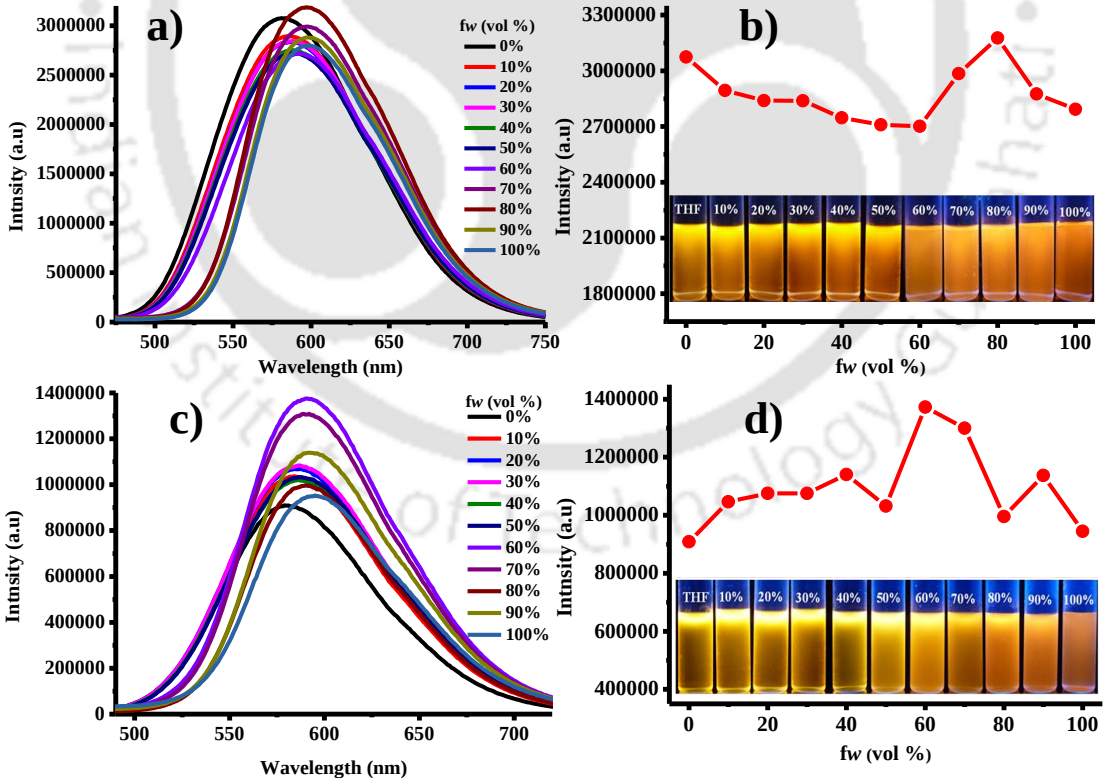

Figure 4.8: PL spectra and PL relative intensity of DP1 (a, b) and DP2 (c, d) (40 μM) in THF and water mixtures. The photographs were taken under 365 nm hand-UV lamp irradiation in THF-water mixtures.

and structurally similar, the only difference are the two bromines in DT2; however, there is a large solvatochromic effect on their emission behavior in both THF and water. Such red emitting AIEE luminogens have seldom been reported, despite having potential applications in diverse areas such as bio-imaging, therapy, optoelectronic devices, communication and security. Surprisingly, DT2 exhibits an emission maximum at 562 nm in THF, which is blue-shifted by ~33 nm as compared to that of DT1 in THF. As mentioned earlier, the only difference between the two molecules, DT1 and DT2 are the substituted bromine atoms. Since these bromine atoms act as weak electron-withdrawing groups and weakening the electron donating ability of DBF moiety, they may be responsible for the observed blue-shifts. Therefore, DT1 has a much larger Stokes shift in solution than DT2 because DT2 is a weaker donor-acceptor molecule as compared to DT1. Surprisingly, in 100% water, DT2 showed emission peak at 656 nm and DT1 showed emission peak at 640 nm, a redshift of 16 nm. These results validate the heavy atom effect in DT2 that considerably influences the emission blue-shift in THF and large redshift in the aggregated state. As discussed earlier, these DP1 and DP2 molecules exhibited bright orange emissions at 578 and 580 nm in THF solution and at 580 and 596 nm in solid state (Figure 4.2) confirming their dual state emission behavior. Further, Figure 4.8a-d shows the PL spectra, relative intensity, and actual changes in the solution color of DP1 and DP2 in water and THF mixtures (40 μM) with different *fw*. Very interestingly, DP1 and DP2 luminogens exhibited dual state emission, confirming that both these luminogens are highly emissive in THF as well as in the aggregated state. When *fw* is changed from 0 to 100% there is no large change in the PL intensity; nevertheless, the peak was red-shifted from 578 to 594 nm (~16 nm) for DP1. On the contrary, DP2 showed very little difference in the emission spectrum; yet, when the *fw* reached up to 50%, the peak showed a slight redshift (~7 nm) with a minor increase in the peak intensity. On increasing the *fw* up to 60%, the peak intensity was further enhanced, and when the *fw* reached up to 100%, the peak again showed a minor redshift with decreased peak intensity. Overall, the PL was red-shifted from 580 to 597 nm (~17 nm). The DP1 and DP2 luminogens almost showed the same behavior, when the *fw* changed from 0 to 100%. However, the solid state emission of DP2 is ~16 nm red-shifted compared to DP1, due to the heavy atom effect of the two bromines in DP2. Such unique dual state emission properties extending up to the red spectral region have not been reported previously and render them not only fundamentally significant but also provide avenues for diverse interdisciplinary applications.

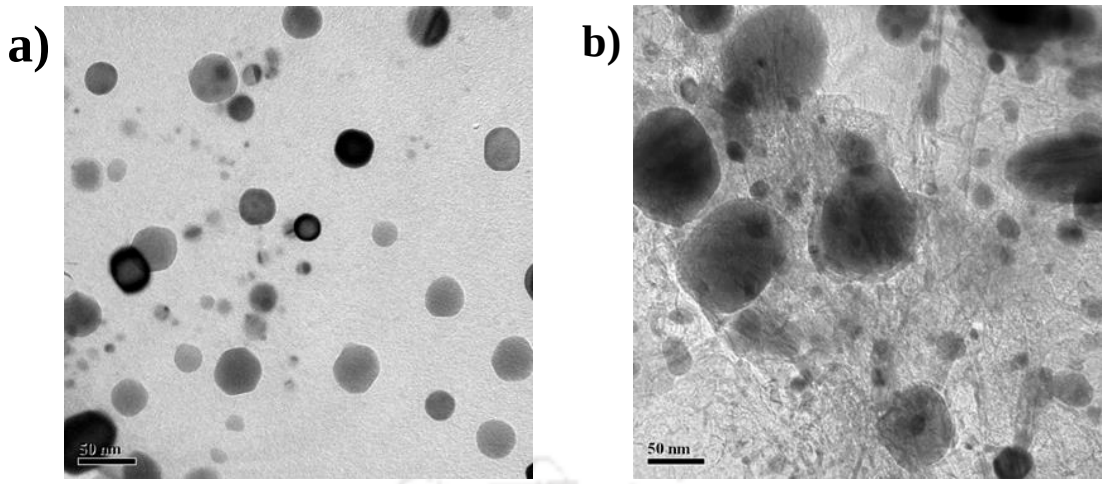

Figure 4.9: TEM images of a) DT1 and b) DT2.

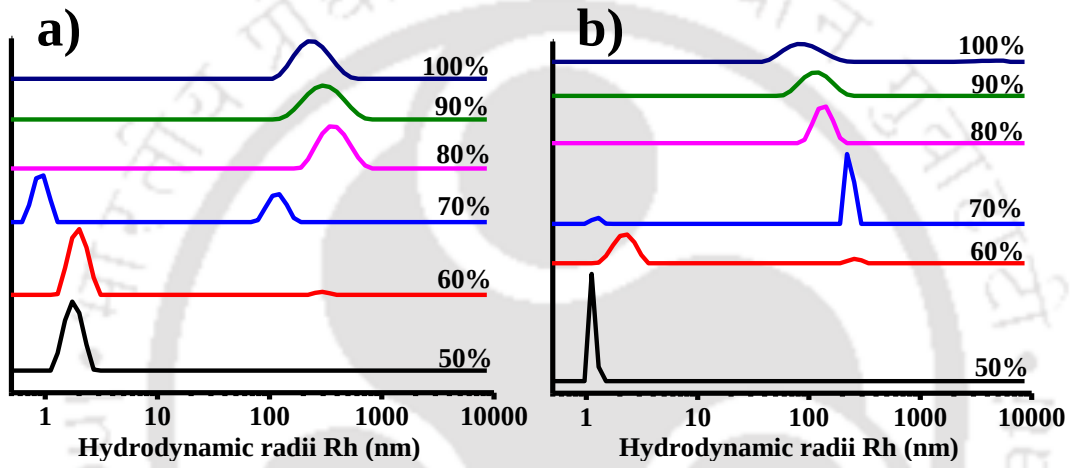

Figure 4.10: DLS curves of a) DT1 and b) DT2 in THF (50%) and H_2O (100%) mixtures.

Further, to confirm the formation of nanoaggregates on varying the solvent, transmission electron microscopy (TEM) and dynamic light scattering (DLS) experiments were carried out for both DT1 and DT2 luminogens. Figure 4.9 shows the TEM images of molecular nanoaggregates of DT1 and DT2 luminogens. The THF/H_2O (1:9) solution of DT1 and DT2 luminogens were drop-casted onto TEM grids and the images clearly indicated that the average size of nanoparticles were 20-50 nm. To further investigate the formation of aggregated nanoparticles these luminogens were characterized by DLS. By changing the *fw* from 50 to 100% the aggregated nanoparticles were well dispersed with increasing *fw* (Figure 4.10). When the *fw* reached up to 70%, both DT1 and DT2 luminogens began to aggregate into nanoparticles, giving a size distribution of ~150 nm that increased from 70% to 100% *fw* with the nanoparticles showing higher stability at higher *fw*. When the *fw* was above 70% the polarity of the system is enhanced, hence bringing about the redshift in emission and thus validating these results with the PL intensity changes. When the *fw* was more in this system, the aggregated nanoparticles experienced RIR effect of

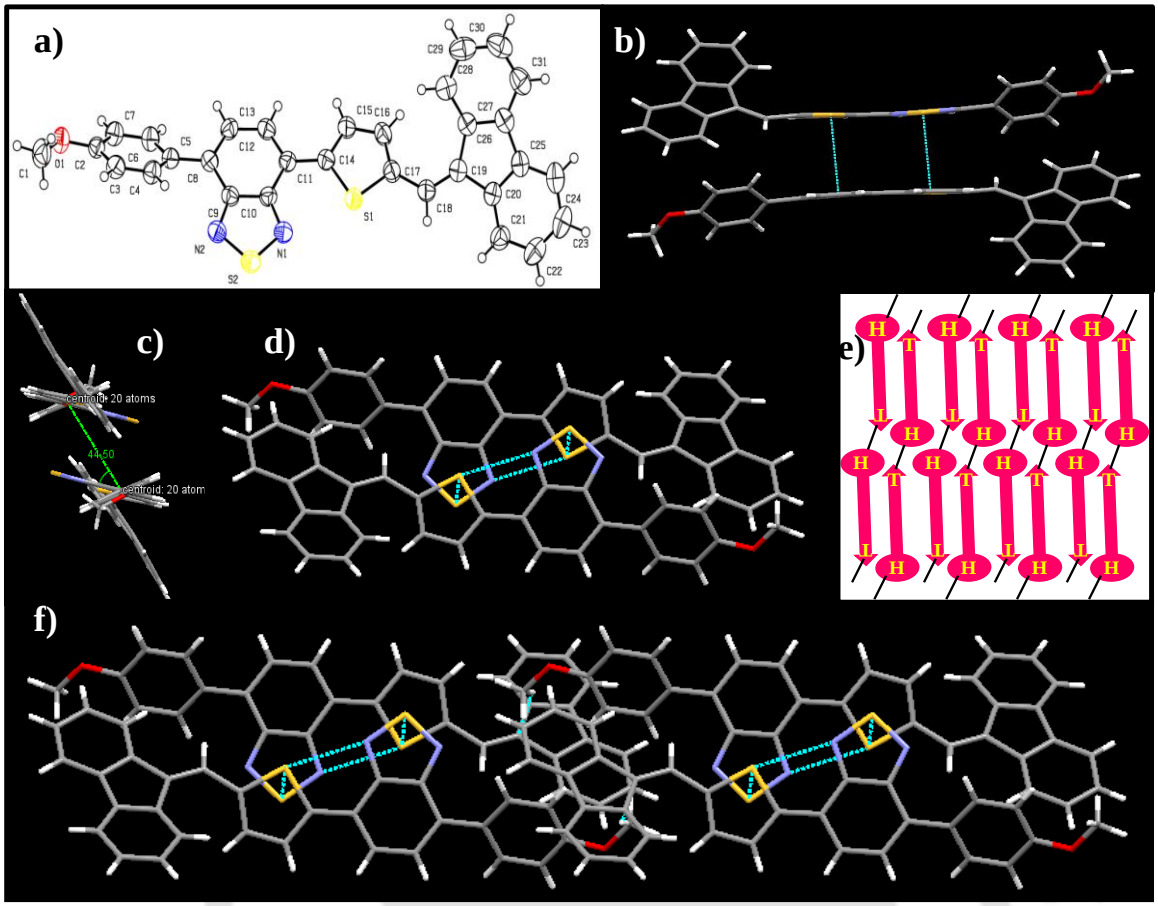

Figure 4.11: (a) ORTEP drawing of DT1. (b) Length side view of the two adjacent molecules linked by intermolecular S···S interactions (3.596 Å). (c) Width side view with a slip angle of 44.5° (d) Top view. (e) Schematic representation of head-to-tail packing of DT1. (f) Top view of the extended dimers via C–H···π (2.836 Å) intermolecular interactions in single crystals.

the thiophene moiety with respect to the DBF moiety in both DT1 and DT2 luminogens, which results in likely micellization. To supplement the mechanism of this AIEE behavior, the geometry and packing arrangements of DT1 were checked in the crystal state. The single crystal of DT1 was obtained by the slow evaporation of the dichloromethane solution. The ORTEP view of DT1 (Figure 4.11a) showed twisted molecular structure nevertheless, both the thiophene and benzothiadiazole are in the same plane with interaction of intramolecular S···N (2.893 Å). The dihedral angles between paramethoxy phenyl and benzothiadiazole groups are twist-linked with a dihedral angle of 122.04°; the thiophene and DBF moiety are twist-linked with a dihedral angle of 120.31°. According to the molecular exciton model,[62,63] head to tail alignment of the transition dipoles of the monomeric dyes align in a coplanar inclined fashion with a slip angle of $\theta<54.7°$. As shown in the structure of DT1 (Figure 4.9b-d), two adjacent molecules are packed with highly tilted and end to end arrangement as dimers by intermolecular S···S interactions (3.596 Å) between the thiophene 'S' from one molecule

and benzothiadiazole 'S' from the other via head-to-tail fashion with a slip angle of 44.5° (Figure 4.11c). These tilted dimers are further extended (Figure 4.11f) via the C-H···π (2.836 Å) interactions to form uniform rows. This highly tilted end-to-end with head to tail arrangement is favorable for J-type aggregation and can induce the PL intensity changes with bathochromic shift in UV-vis absorption spectrum. When compared with DT1, the DT2 luminogen was more red-shifted due to the heavy atom effect of the two bromines on the DBF.

4.3.4. Density Functional Theory (DFT) Calculations

To further understand the ground state geometry of the luminogens, DFT calculations by Gaussian09 A.02 software package[64] were carried out for optimization using the B3LYP functional with 6-31G basis set.[65] The optimized structures and the orbital distributions of HOMO and LUMO energy levels of luminogens are shown in Figures 3.12 and 3.13 and Table 4.4. These structures reveal that all the four luminogens exhibited nonplanar configurations. Furthermore, in both the DT luminogens, the thiophene and benzothiadiazole units are in one plane, whereas the DBF paramethoxy phenyl groups are out of plane (in a boat configuration at a dihedral angle of 118.05° and 121.68°). However, in DP luminogens the thiophene, benzothiadiazole, and phenyl units are nearly in one plane, but the remaining two DBF and paramethoxy phenyl groups are

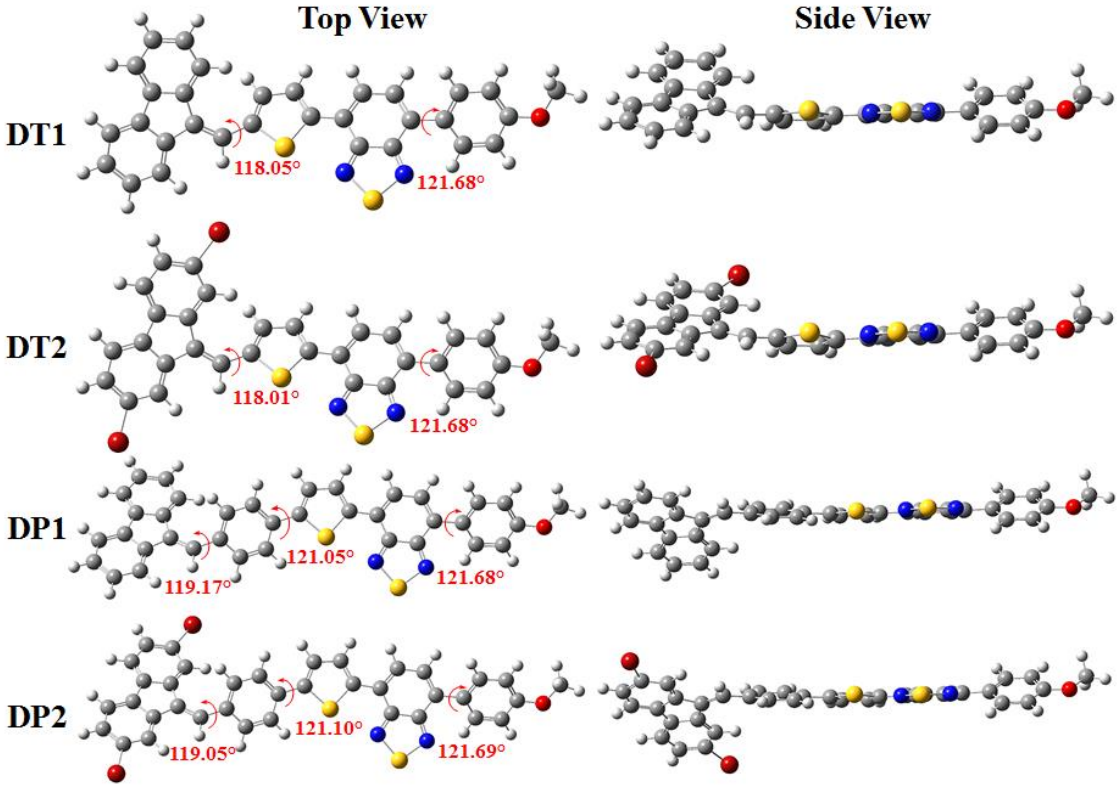

Figure 4.12: Optimized molecular structures of DT1, DT2, DP1, and DP2.

out of plane (DBF is inclined downward at a dihedral angle of 119.17°, and paramethoxy phenyl groups is above the plane at a dihedral angle of 121.68° giving a chair configuration). The dihedral angles ($\theta_{D\text{-}A}$) are represented in Figure 4.12. Fortunately, we could obtain the single crystal X-ray structure of DT1, and on comparison of the dihedral angles ($\theta_{D\text{-}A}$) with this crystal structure, it was observed that the optimized structures are almost similar to this experimental structure.

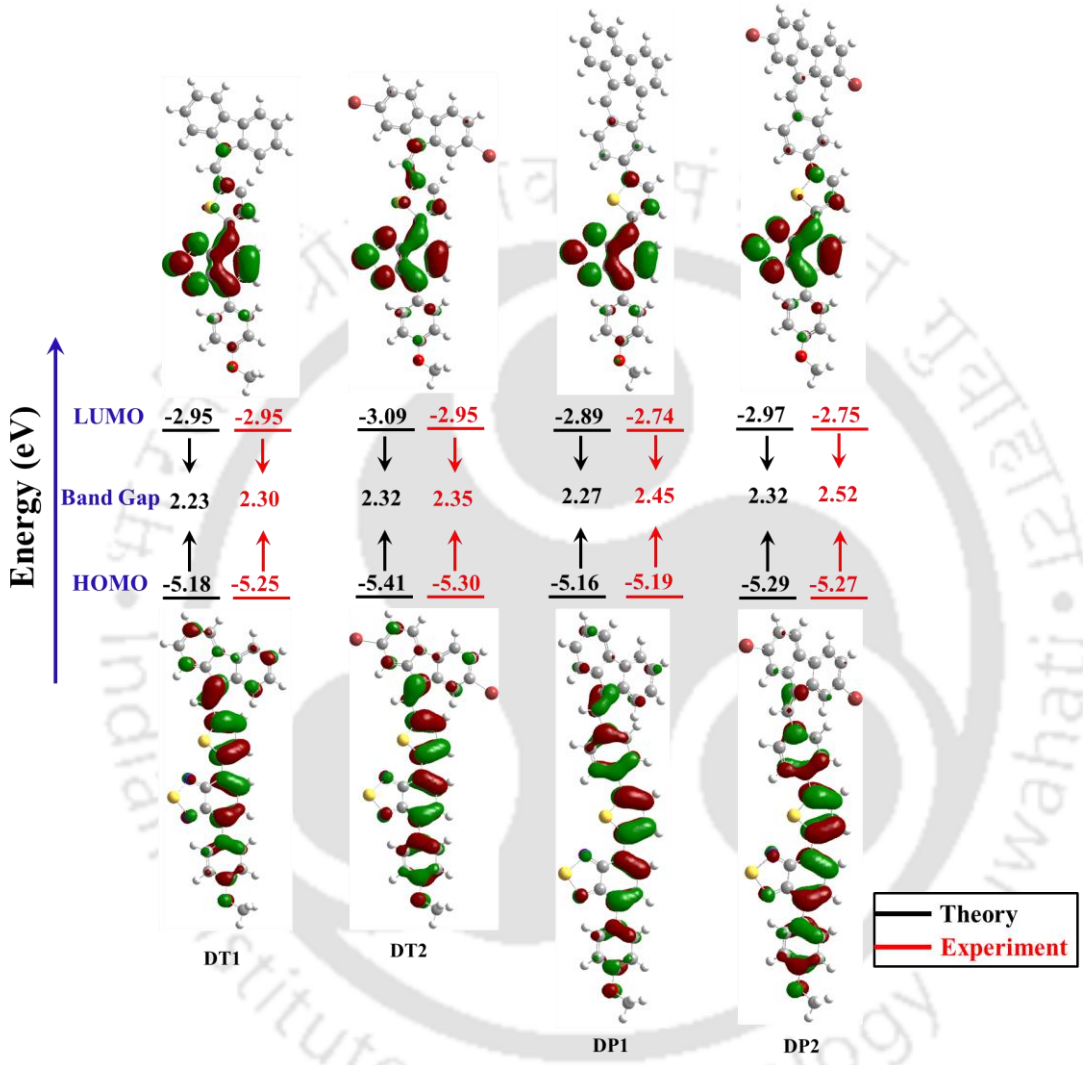

Figure 4.13: Molecular orbital (isovalue = 0.03) amplitude plots of HOMO and LUMO levels and the comparison of energy levels estimated from electrochemical data and theoretical data of the four luminogens.

As shown in Figure 4.11, in DT1 luminogens, the two adjacent molecules are packed with highly tilted and end to end arrangement as dimers by intermolecular S···S interactions (3.596 Å) between the thiophene 'S' from one molecule and benzothiadiazole 'S' of the other via head to tail fashion. This can be beneficial for the formation of J-aggregation, as well as it can enhance the emission intensity in the aggregated state. The DP1 and DP2 molecules exhibited dual state emission. When compared to the DT molecules, these

luminogens showed blue-shift in both the absorption and emission spectra. The extra phenyl unit thus reduces the effective conjugation length toward the 2,1,3-benzothiadiazole from DBF. Figure 4.13 depicts the HOMO and LUMO orbitals of DT and DP luminogens, where the thiophene units in DT molecules are directly attached to DBF and the HOMO is majorly localized on thiophene as well as on DBF and paramethoxy phenyl unit. It is interesting to note that in DP molecules the HOMO is mainly localized on thiophene, phenyl, and paramethoxy phenyl unit and partially localized on DBF unit. These results confirm that when DBF is directly attached with thiophene, it acts as a strong electron donor as compared to the phenyl, indicating that the phenyl unit between thiophene and DBF reduces the donating capacity of DBF moiety. Also, no red shift in the emission spectra of DP luminogens from solution to solid state was observed, thereby indicating that the phenyl unit might have interrupted the end-to-end arrangement as dimers by intermolecular S···S interactions. As observed, the phenyl unit, thiophene, and benzothiazole are nearly in the same plane, whereas the DBF is inclined downward and the paramethoxy phenyl groups is inclined upward (Figure 4.12). Owing to this arrangement, the DP molecules are not able to form a dimer unlike the DT molecules. Thus, steric crowding plays a crucial role in this phenomenon. Similarly, the LUMO is mainly localized on the benzothidiazole group for the four luminogens.

A comparison of the DT and DP electron distribution indicates that the electron density of DP luminogens is lower than that of DT. Moreover, the results of the theoretical calculation strongly supported the experimental observations that better conjugation in DT luminogens is the main reason for the red-shift of the emission compared to DP luminogens.

Table 4.4: TD-DFT calculations of the luminogens

	TD-DFT		
Monomer	λ_{theory} **(nm)**	**f**	**Composition**
DT1	370 ($S_0 \rightarrow S_8$)	0.47,	H→ L+1 (64.6%) = π-π* H-2 →L (26.0%) = π-π*,
	500 ($S_0 \rightarrow S_3$)	0.89	H→ L (91.2%) = π-π* (ICT)),
DT2	368, ($S_0 \rightarrow S_8$)	0.45,	H→ L+1 (73.2%) = π-π* H-2 →L(17.0%) = π-π*,
	512 ($S_0 \rightarrow S_3$)	0.96	H→L (92.8%) = π−π* (ICT)
DP1	352 ($S_0 \rightarrow S_8$)	0.89	H→ L+1 (49.7%) = π-π* H-1 →L (27.3%) = π-π*
	495 ($S_0 \rightarrow S_4$)	0.87	H→L (92.8%) = π-π* (ICT)
DP2	370 ($S_0 \rightarrow S_8$)	0.97	H→ L+1 (59.4%) = π-π* H-1 →L (16.8%) = π-π*
	499 ($S_0 \rightarrow S_4$)	0.91	H→ L (91.0%) = π-π* (ICT)

The theoretical calculations also suggest efficient ICT between the donor and acceptor. The UV absorption transitions were obtained using TD-DFT/ CAM-B3LYP/6-31G(d,p)[66]

level studies. These results suggested that two major transitions transpired at the regions 352-370 nm and 495-512 nm (see Figure 4.14 to 3.17 and Table 4.4) for the four luminogens. The transitions at longer wavelength are due to the ICT processes from the major contribution of HOMO orbitals to the LUMO orbitals, while the former transitions are π-π* transitions with the major contribution from the HOMO orbitals to the LUMO+1 orbitals of the luminogens. The simulated absorption spectra of luminogens showed good agreement with only a minor deviation as compared to experimental results (Figure 4.2).

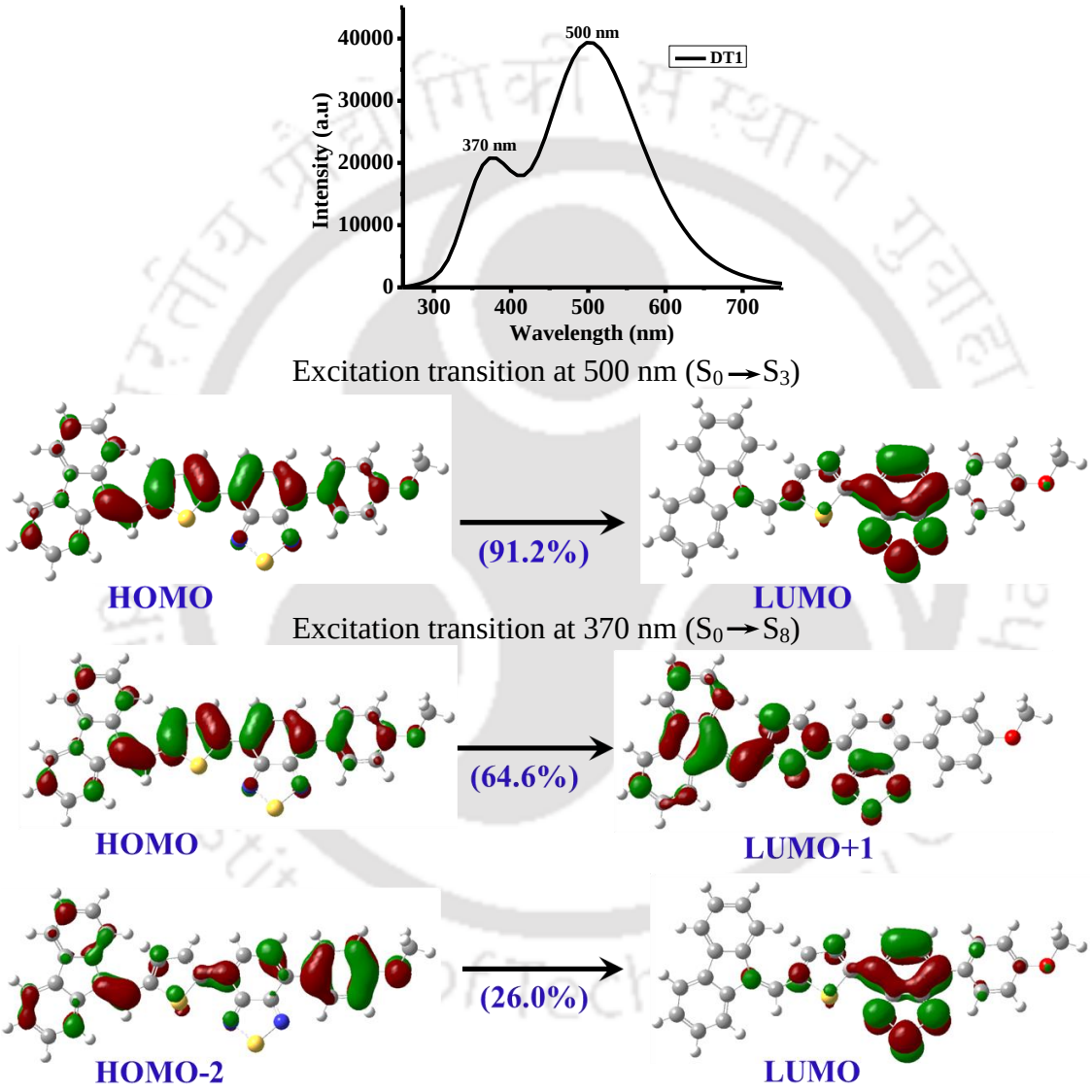

Figure 4.14: TD-DFT simulated absorption spectra and contributing orbitals at each excitation of **DT1** luminogen (isovalue = 0.03).

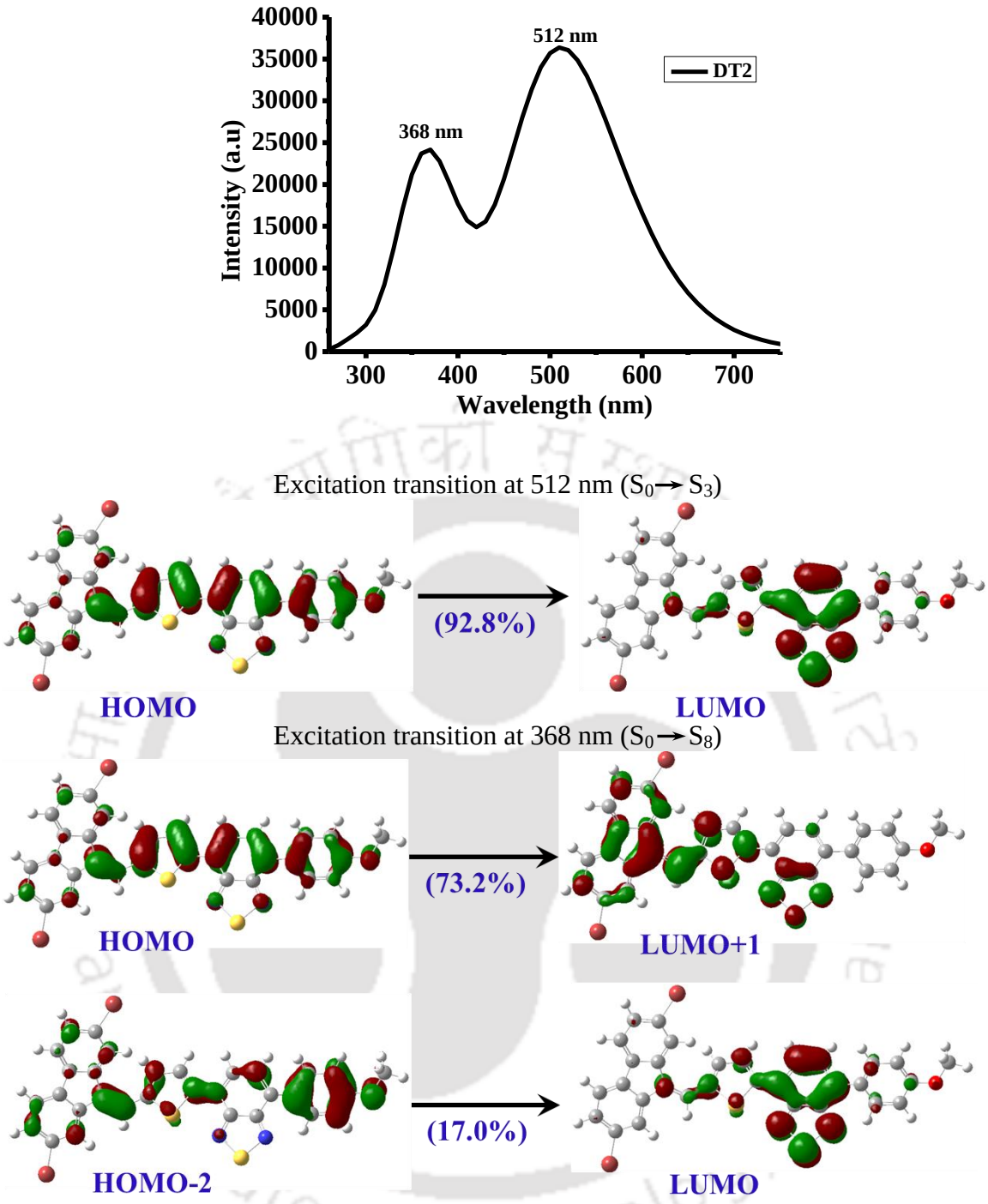

Figure 4.15: TD-DFT simulated absorption spectra and contributing orbitals at each excitation of **DT2** luminogen (isovalue = 0.03).

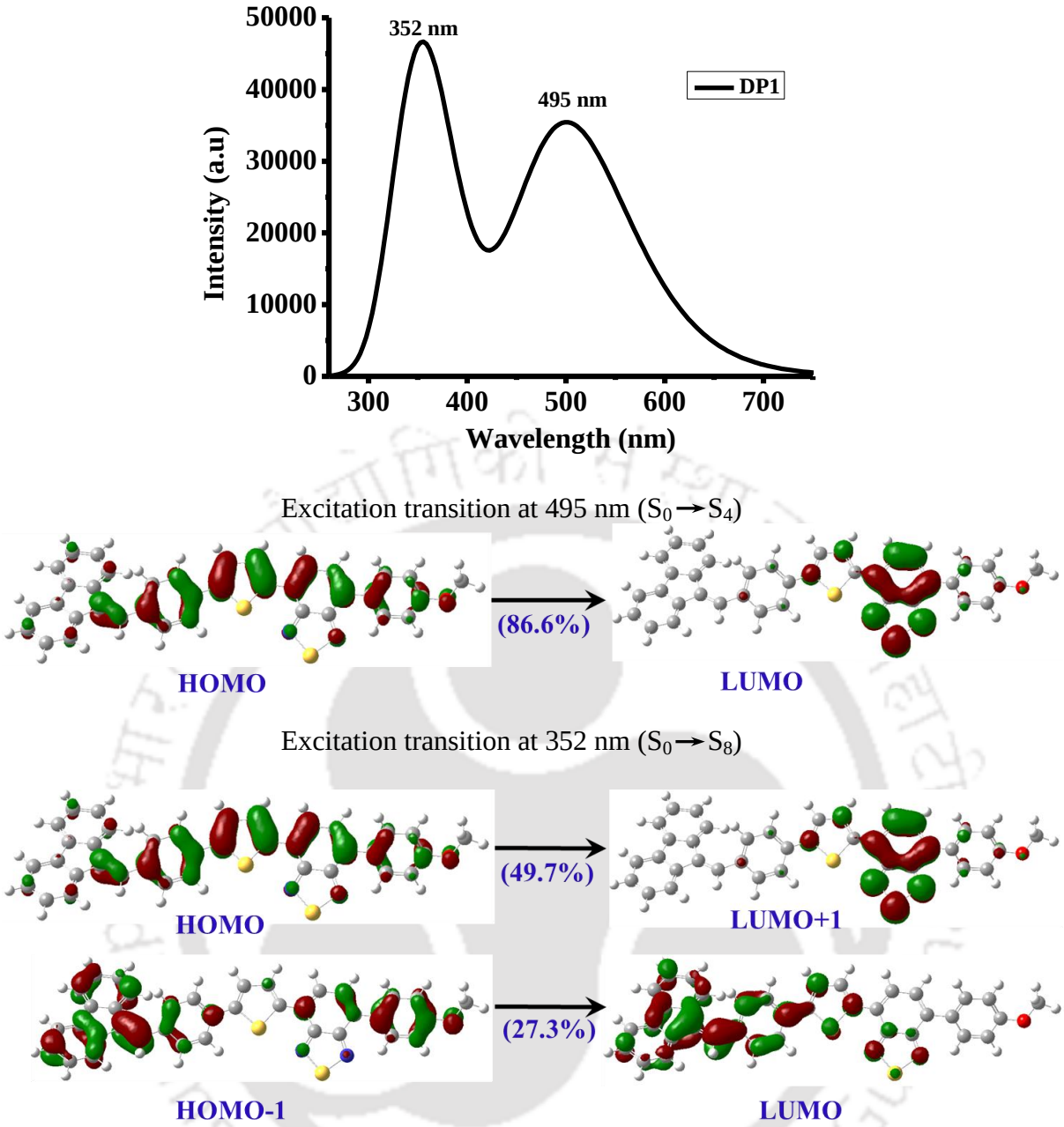

Figure 4.16: TD-DFT simulated absorption spectra and contributing orbitals at each excitation of **DP1** luminogen (isovalue = 0.03).

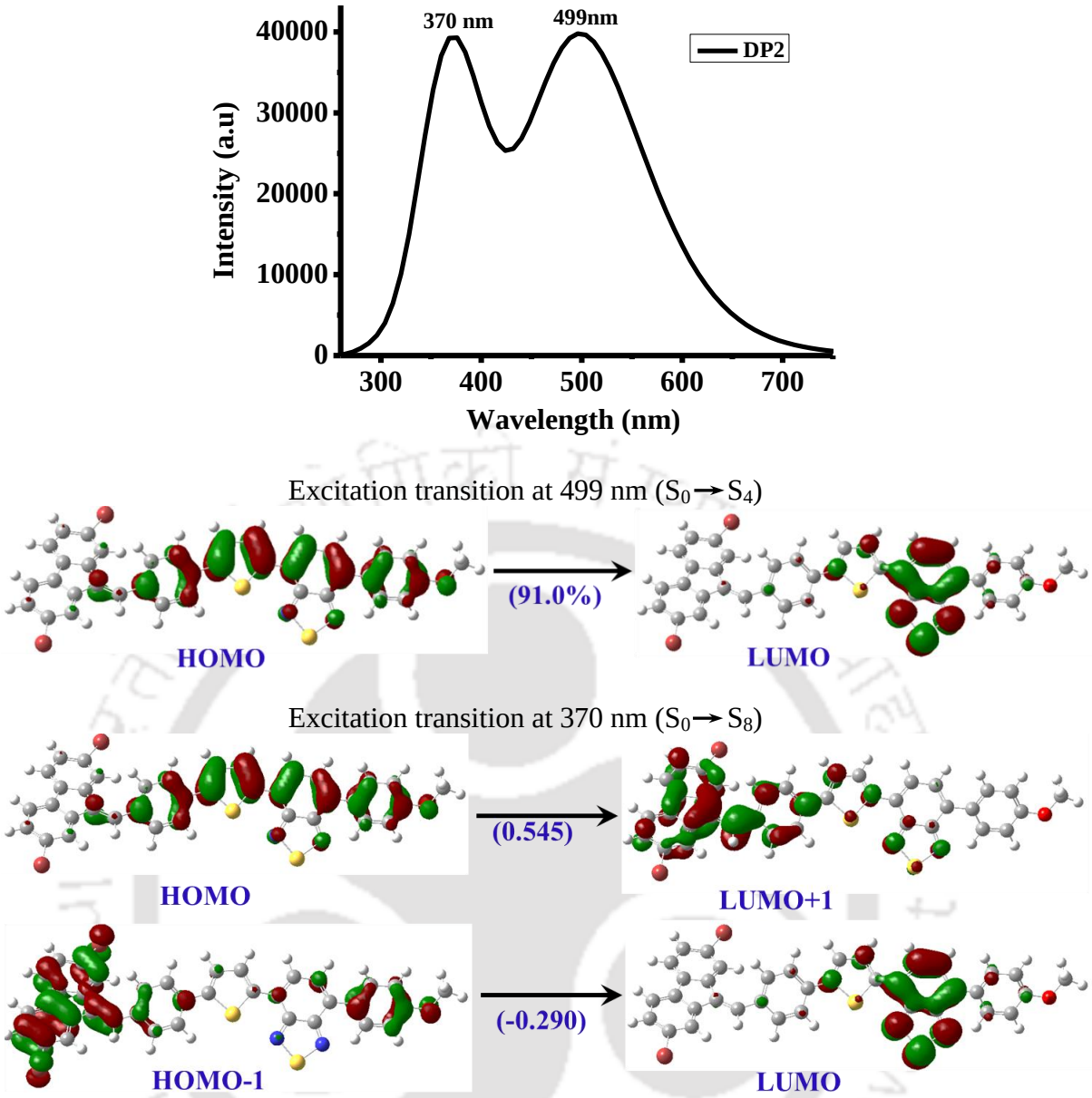

Figure 4.17: TD-DFT simulated absorption spectra and contributing orbitals at each excitation of **DP2** luminogen (isovalue = 0.03).

Table 4.5: Comparison of Energy Levels Estimated from Electrochemical Studies with Theoretical DFT

Monomer	Electrochemical Potentials and Energy Levels					DFT data (eV)		
	E_{ox}/V	E_{red}/V	E_{HOMO}/eV	E_{LUMO}/eV	E_g/eV	HOMO	LUMO	H-L Gap
DT1	0.85	-1.45	-5.25	-2.95	2.30	-5.18	-2.95	2.23
DT2	0.90	-1.45	-5.30	-2.95	2.35	-5.41	-3.09	2.32
DP1	0.79	-1.66	-5.19	-2.74	2.45	-5.16	-2.89	2.27
DP2	0.87	-1.65	-5.27	-2.75	2.52	-5.29	-2.97	2.32

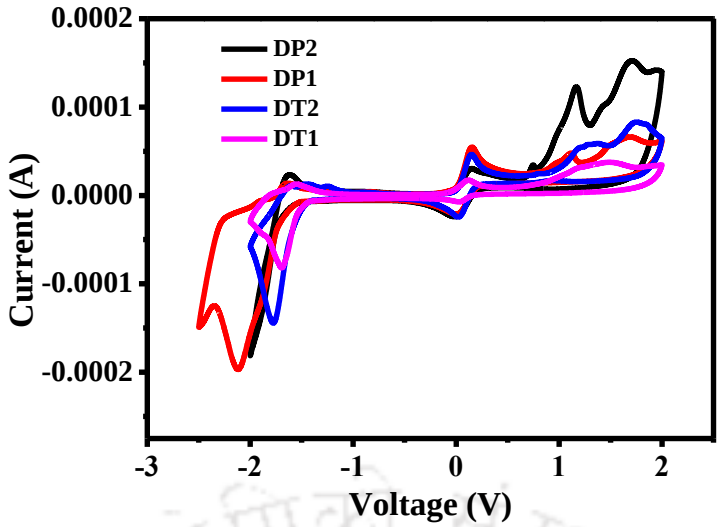

Figure 4.18: Cyclic voltammograms of Luminogens

4.3.5. Electrochemical Properties

The highest occupied molecular orbital (HOMO) and lowest unoccupied molecular orbital (LUMO) energy levels of luminogens were estimated by Cyclic voltammetry (CV) (Figure 4.18). These luminogens were coated on carbon electrode, whereas silver electrode select as the reference electrode and platinum wire was used as counter electrode. The 0.1 M tetrabutylammonium hexafluorophosphate (Bu_4NPF_6) solution in acetonitrile (CH_3CN) was used as electrolyte solution to investigate the electrochemical properties of the luminogens under argon atmosphere at room temperature and calibrated by using ferrocene as standard. As shown in Figure 4.18, all four luminogens displayed both oxidation and reduction peaks. The electrochemical properties of luminogens are represented in Table 4.5. The HOMO and LUMO energies were estimated by substituting the both onset (reduction and oxidation) peak values in E_{LUMO} = -[(E_{red} - $E_{1/2}$(ferrocene)) + 4.8 eV], E_{HOMO} = -[(E_{ox} - $E_{1/2}$(ferrocene)) + 4.8 eV]. As shown in Figure 10, the experimental and theoretical studies reveal that the HOMO energy levels of the brominated luminogens (DT2 and DP2) are deeper, and it leads to blue-shifts of their emission. This is due to effect of bromine atoms, which are present on the donor (DBF) unit in both DT2 and DP2 molecules. If the bromine atoms had been on the acceptor, they would have brought down the LUMO energy levels instead, causing a redshift.[67]

4.4. Summary

In summary, four novel M-DBFs were successfully synthesized and their photophysical properties exhibited (a) AIEE phenomenon in the red wavelength region,

(b) dual state emission, and (c) solvatochromism behavior. It was interesting to note that the thiophene-substituted luminogens exhibited AIEE with huge red-shifted emission in aggregated state, ~45 nm red-shifted for DT1 (640 nm) and ~94 nm red-shifted for DT2 (656 nm). The UV-vis, PL (both solution and solid state) spectra, solvatochromic effect, TEM, and DLS provided strong proof for the AIEE phenomenon. However, the phenyl substituted (DP1 and DP2) DBFs exhibited efficient dual state emission phenomenon. To confirm the dual state property of DP1 and DP2, the AIEE studies were also performed. These results demonstrated that DP1 and DP2 luminogens possessed exceptional optical properties with dual state emitting behavior. Incorporation of phenyl ring between the thiophene and DBF led to the twisted conformations in the aggregated state and more rigid conformations in solution due to the extended conjugation. In contrast, the thiophene moiety attached directly to the DBF in DT1 and DT2 are AIEE-active with a weakly luminescent behavior in THF due to the free rotation of thiophene moiety with respect to the DBF moiety. Thus, the direct linkage of either thiophene ring or phenyl ring to DBF moiety significantly influenced the morphology and electronic properties of these luminogens. Based on these results we concluded that M-DBF acts as an intermediate between ACQ and AIE materials, and this strategy provided a new class of AIE as well as dual state active materials. The present results offer a new strategy for the development of red emitting materials in aggregated state as well as solution state based on the simple M-DBFs. These new luminogens are likely to stimulate interest in academic research as well as industry with applications in organic light emitting diodes, bio-imaging, therapeutics, security, photovoltaics, and other optical applications due to their high quantum yields even in aggregated form.

4.5. References

1. Shih, P. I.; Chuang, C. Y.; Chien, C. H.; Diau, E. W. G.; Shu, C. F. *Adv. Funct. Mater.* **2007,** *17*, 3141-3146.
2. Lee, Y. T.; Chiang, C. L.; Chen, C. T. *Chem. Commun.* **2008**, 217-219.
3. Li, H. Y.; Chi, Z. G.; Zhang, X. Q.; Xu, B. J.; Liu, S. W.; Zhang, Y.; Xu, J. R. *Chem. Commun.* **2011,** *47*, 11273-11275.
4. Chang, Z. F.; Jiang, Y. B.; He, B. R.; Chen, J.; Yang, Z. Y.; Lu, P.; Kwok, H. S.; Zhao, Z. J.; Qiu, H. Y.; Tang, B. Z. *Chem. Commun.* **2013,** *49*, 594-596.
5. Hong, Y. N.; Lam, J. W. Y.; Tang, B. Z. *Chem. Soc. Rev.* **2011**, *40*, 5361-5388.
6. Hong, Y. N.; Meng, L. M.; Chen, S. J.; Leung, C. W. T.; Da, L. T.; Faisal, M.; Silva, D. A.; Liu, J. Z.; Lam, J. W. Y.; Huang, X. H.; Tang, B. Z. *J. Am. Chem. Soc.* **2012,** *134*, 1680-1689.
7. Yu, Y.; Feng, C.; Hong, Y. N.; Liu, J. Z.; Chen, S. J.; Ng, K. M.; Luo, K. Q.; Tang, B. Z. *Adv. Mater.* **2011,** *23*, 3298-3302.
8. Geng, J. L.; Li, K.; Ding, D.; Zhang, X. H.; Qin, W.; Liu, J. Z.; Tang, B. Z.; Liu, B. *Small* **2012,** *8*, 3655-3663.
9. Toal, S. J.; Magde, D.; Trogler, W. C. *Chem. Commun.* **2005,** 5465-5467.
10. Hong, Y. N.; Lam, J. W. Y.; Tang, B. Z. Aggregation-Induced Emission: Phenomenon, Mechanism and Applications. *Chem. Commun.* **2009,** 4332-4353.
11. Peng, L. H.; Wang, M.; Zhang, G. X.; Zhang, D. Q.; Zhu, D. B. *Org. Lett.* **2009,** *11*, 1943-1946.
12. Liu, Y.; Tang, Y. H.; Barashkov, N. N.; Irgibaeva, I. S.; Lam, J. W. Y.; Hu, R. R.; Birimzhanova, D.; Yu, Y.; Tang, B. Z. *J. Am. Chem. Soc.* **2010,** *132*, 13951-13953.
13. Chi, Z. G.; Zhang, X. Q.; Xu, B. J.; Zhou, X.; Ma, C. P.; Zhang, Y.; Liu, S. W.; Xu, J. R. *Chem. Soc. Rev.* **2012,** *41*, 3878-3896.
14. Grabowski, Z. R.; Rotkiewicz, K.; Rettig, W. *Chem. Rev.* **2003,** *103*, 3899-4031.
15. Jenekhe, S. A.; Osaheni, J. A. *Science* **1994,** *265*, 765-768.
16. Hecht, S.; Frechet, J. M. J. *Angew. Chem. Int. Edit.* **2001,** *40*, 74-91.
17. Setayesh, S.; Grimsdale, A. C.; Weil, T.; Enkelmann, V.; Mullen, K.; Meghdadi, F.; List, E. J. W.; Leising, G. *J. Am. Chem. Soc.* **2001,** *123*, 946-953.
18. Marsitzky, D.; Vestberg, R.; Blainey, P.; Tang, B. T.; Hawker, C. J.; Carter, K. R. *J. Am. Chem. Soc.* **2001,** *123*, 6965-6972.
19. Lee, S. H.; Jang, B. B.; Kafafi, Z. H. *J. Am. Chem. Soc.* **2005,** *127*, 9071-9078.
20. Swager, T. M. *Acc. Chem. Res.* **2008,** *41*, 1181-1189;
21. Grimsdale, A. C.; Chan, K. L.; Martin, R. E.; Jokisz, P. G.; Holmes, A. B. *Chem. Rev.* **2009,** *109*, 897-1091.
22. Wang, M.; Zhang, G. X.; Zhang, D. Q.; Zhu, D. B.; Tang, B. Z. *J. Mater. Chem.* **2010,** *20*, 1858-1867.
23. Lee, M. J.; Moon, J. H.; Jun, E. J.; Kim, G. G.; Kwon, Y. U.; Lee, J. Y.; Yoon, J. Y. *Chem. Commum.* **2014,** *50*, 5851-5853.
24. Gu, X. G.; Yao, J. J.; Zhang, G. X.; Zhang, C. Y.; Yan, L.; Zhao, Y. S.; Zhang, D. Q. *Chem. Asian. J.* **2013,** *8*, 2362-2369.

25. Luo, J. D.; Xie, Z. L.; Lam, J. W. Y.; Cheng, L.; Chen, H. Y.; Qiu, C. F.; Kwok, H. S.; Zhan, X. W.; Liu, Y. Q.; Zhu, D. B.; et al. *Chem. Commun.* **2001,** 1740-1741.
26. An, B. K.; Kwon, S. K.; Jung, S. D.; Park, S. Y. *J. Am. Chem. Soc.* **2002,** *124*, 14410-14415.
27. Qian, Y.; Li, S. Y.; Zhang, G. Q.; Wang, Q.; Wang, S. Q.; Xu, H. J.; Li, C. Z.; Li, Y.; Yang, G. Q. *J. Phys. Chem. B* **2007,** *111*, 5861-5868.
28. Zhang, Y.; Wang, J. H.; Zheng, W. J.; Chen, T. F.; Tong, Q. X.; Li, D. *J. Mater. Chem. B* **2014,** *2*, 4159-4166.
29. Zhao, Q.; Li, L.; Li, F. Y.; Yu, M. X.; Liu, Z. P.; Yi, T.; Huang, C. H. *Chem. Commun.* **2008,** 685-687.
30. Huang, K. W.; Wu, H. Z.; Shi, M.; Li, F. Y.; Yi, T.; Huang, C. H. *Chem. Commun.* **2009,** 1243-1245.
31. Yuan, W. Z.; Shen, X. Y.; Zhao, H.; Lam, J. W. Y.; Tang, L.; Lu, P.; Wang, C. L.; Liu, Y.; Wang, Z. M.; Zheng, Q.; et al. *J. Phys. Chem. C* **2010,** *114*, 6090-6099.
32. Bolton, O.; Lee, K.; Kim, H. J.; Lin, K. Y.; Kim, J. *Nat. Chem.* **2011,** *3*, 205-210.
33. Zhang, Z.; Xu, B.; Su, J.; Shen, L.; Xie, Y.; Tian, H. *Angew. Chem. Int. Ed*. **2011,** *50*, 11654-11657.
34. Luo, Z. T.; Yuan, X.; Yu, Y.; Zhang, Q. B.; Leong, D. T.; Lee, J. Y.; Xie, J. P. *J. Am. Chem. Soc.* **2012,** *134*, 16662-16670.
35. Ni, W. X.; Li, M.; Zheng, J.; Zhan, S. Z.; Qiu, Y. M.; Ng, S. W.; Li, D. *Angew. Chem. Int. Ed*. **2013,** *52*, 13472-13476.
36. Ni, W. X.; Qiu, Y. M.; Li, M.; Zheng, J.; Sun, R. W. Y.; Zhan, S. Z.; Ng, S. W.; Li, D. *J. Am. Chem. Soc.* **2014,** *136*, 9532-9535.
37. Kraft, A.; Grimsdale, A. C.; Holmes, A. B. *Angew. Chem. Int. Ed.* **1998,** *37*, 402-408.
38. Bao, Z. A.; Lovinger, A. J.; Brown, J. *J. Am. Chem. Soc.* **1998,** *120*, 207-208.
39. Muller, C. D.; Falcou, A.; Reckefuss, N.; Rojahn, M.; Wiederhirn, V.; Rudati, P.; Frohne, H.; Nuyken, O.; Becker, H.; Meerholz, K. *Nature* **2003,** *421*, 829-833.
40. Gopikrishna, P.; Das, D.; Iyer, P. K. *J. Mater. Chem*. C **2015,** *3*, 9318-9326.
41. Tong, H.; Dong, Y. Q.; Haussler, M.; Lam, J. W. Y.; Sung, H. H. Y.; Williams, I. D.; Sun, J. Z.; Tang, B. Z. *Chem. Commun.* **2006,** 1133-1135.
42. Dong, Y. Q.; Lam, J. W. Y.; Qin, A. J.; Li, Z.; Sun, J. Z.; Sung, H. H. Y.; Williams, I. D.; Tang, B. Z. *Chem. Commun.* **2007,** 40-42.
43. Zeng, Q.; Li, Z.; Dong, Y. Q.; Di, C. A.; Qin, A. J.; Hong, Y. N.; Ji, L.; Zhu, Z. C.; Jim, C. K. W.; Yu, G.; et al. *Chem. Commun.* **2007,** 70-72.
44. Tong, H.; Dong, Y. Q.; Hong, Y. N.; Haussler, M.; Lam, J. W. Y.; Sung, H. H. Y.; Yu, X. M.; Sun, J. X.; Williams, I. D.; Kwok, H. S.; et al. *J. Phys. Chem. C* **2007,** *111*, 2287-2294.
45. Nuesch, F.; Berner, D.; Tutis, E.; Schaer, M.; Ma, C.; Wang, X.; Zhang, B.; Zuppiroli, L. *Adv. Funct. Mater.* **2005,** *15*, 323-330.
46. Chang, Y. J.; Chow, T. J. *J. Mater. Chem.* **2011,** *21*, 3091-3099.
47. Du, H.; Fuh, R. C. A.; Li, J. Z.; Corkan, L. A.; Lindsey, J. S. *Photochem. Photobiol.* **1998,** *68*, 141-142.
48. Thomas, K. R. J.; Lin, J. T.; Velusamy, M.; Tao, Y. T. C.; Chuen, H. *Adv. Funct. Mater.* **2004,** *14*, 83-90.

49. Li, Z. H.; Wong, M. S.; Fukutani, H.; Tao, Y. *Chem. Mater.* **2005,** *17,* 5032-5040.
50. Ulrich, G.; Ziessel, R.; Harriman, A. *Angew. Chem. Int. Ed.* **2008,** *47*, 1184-1201.
51. slam, A.; Cheng, C. C.; Chi, S. H.; Lee, S. J.; Hela, P. G.; Chen, I. C.; Cheng, C. H. *J. Phys. Chem. B* **2005,** *109*, 5509-5517.
52. Zhao, Z. J.; He, B. R.; Tang, B. *Chem. Sci.* **2015,** *6*, 5347-5365.
53. Dai, Q.; Liu, W. M.; Zeng, L. T.; Lee, C. S.; Wu, J. S.; Wang, P. F. *Cryst. Eng. Comm.* **2011,** *13*, 4617-4624.
54. Li, W. J.; Liu, D. D.; Shen, F. Z.; Ma, D. G.; Wang, Z. M.; Feng, T.; Xu, Y. X.; Yang, B.; Ma, Y. G. *Adv. Funct. Mater.* **2012,** *22*, 2797-2803.
55. Liu, Y. W.; Zhang, Y.; Wu, X. H.; Lan, Q.; Chen, C. S.; Liu, S. W.; Chi, Z. G.; Jiang. L.; Chen, X. D.; Xu, J. R. *J. Mater. Chem. C.*, **2014,** *2*, 1068-1075.
56. Chen, G.; Li, W.; Zhou, T.; Peng, Q.; Zhai, D.; Li, H.; Yuan, W. Z.; Zhang, Y.; Tang, B. Z. *Adv. Mater.* **2015,** *27*, 4496–4501.
57. Zhang, Y.; Wang, J. H.; Zheng, J.; Li, D. *Chem. Commun.* **2015,** *51*, 6350-6353.
58. Hedstrom, S.; Henriksson, P.; Wang, E.; Andersson, M. R.; Persson, P. *Phys. Chem. Chem. Phys.*, **2014,** *16*, 24853-24865.
59. Pastore, M.; Mosconi, E.; De Angelis, F.; Gratzel, M. *J. Phys. Chem. C* **2010,** *114* (15), 7205-7212.
60. Qian, Y.; Li, S. Y.; Wang, Q.; Sheng, X. H.; Wu, S. K.; Wang, S. Q.; Li, J.; Yang, G. Q. *Soft Matter* **2012,** *8*, 757-764.
61. Zhang, G. F.; Aldred, M. P.; Gong, W. L.; Li, C.; Zhu, M. Q. *Chem. Commun.* **2012,** *48*, 7711-7713.
62. Jelley, E. E. *Nature* **1936,** *138*, 1009-1010.
63. Würthner, F.; Kaiser, T. E.; Saha-Möller, C. R. *Angew. Chem. Int. Ed.* **2011,** *50*, 3376-3410.
64. Frisch, M. J.; Trucks, G. W.; Schlegel, H. B.; Scuseria, G. E.; Robb, M. A.; Cheeseman, J. R.; Scalmani, G.; Barone, V.; Mennucci, B.; Petersson, G. A.; et al. *Gaussian 09*, revision D.01; Gaussian, Inc.: Wallingford, CT, 2013.
65. Becke, A. D. *J. Chem. Phys.* **1993,** *98*, 1372-1377.
66. Yanai, T.; Tew, D. P.; Handy, N. C. *Chem. Phys. Lett.* **2004,** *393*, 51-57.
67. Hedstrom, S.; Tao, Q.; Wang, E. G.; Persson, P. *Phys. Chem. Chem. Phys.* **2015,** *17*, 26677-26689.

Appendix

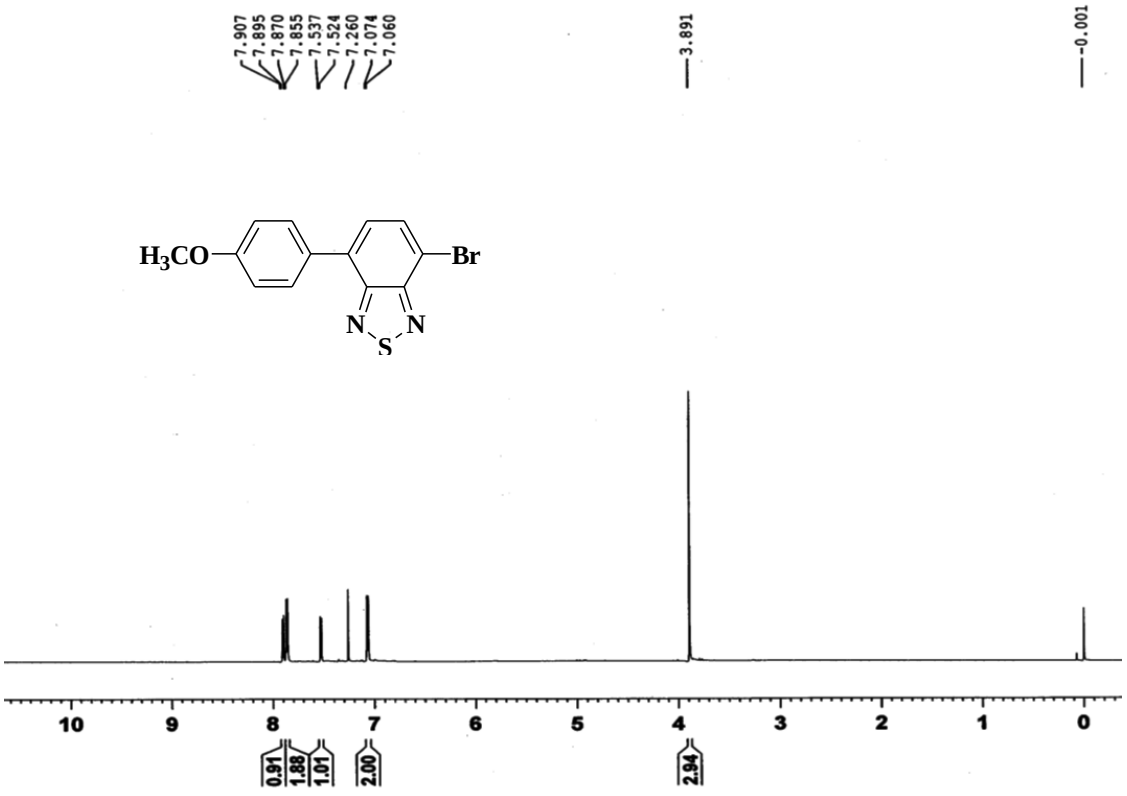

Figure 4.19: The ^{1}H NMR of the **Compound-1** in $CDCl_3$

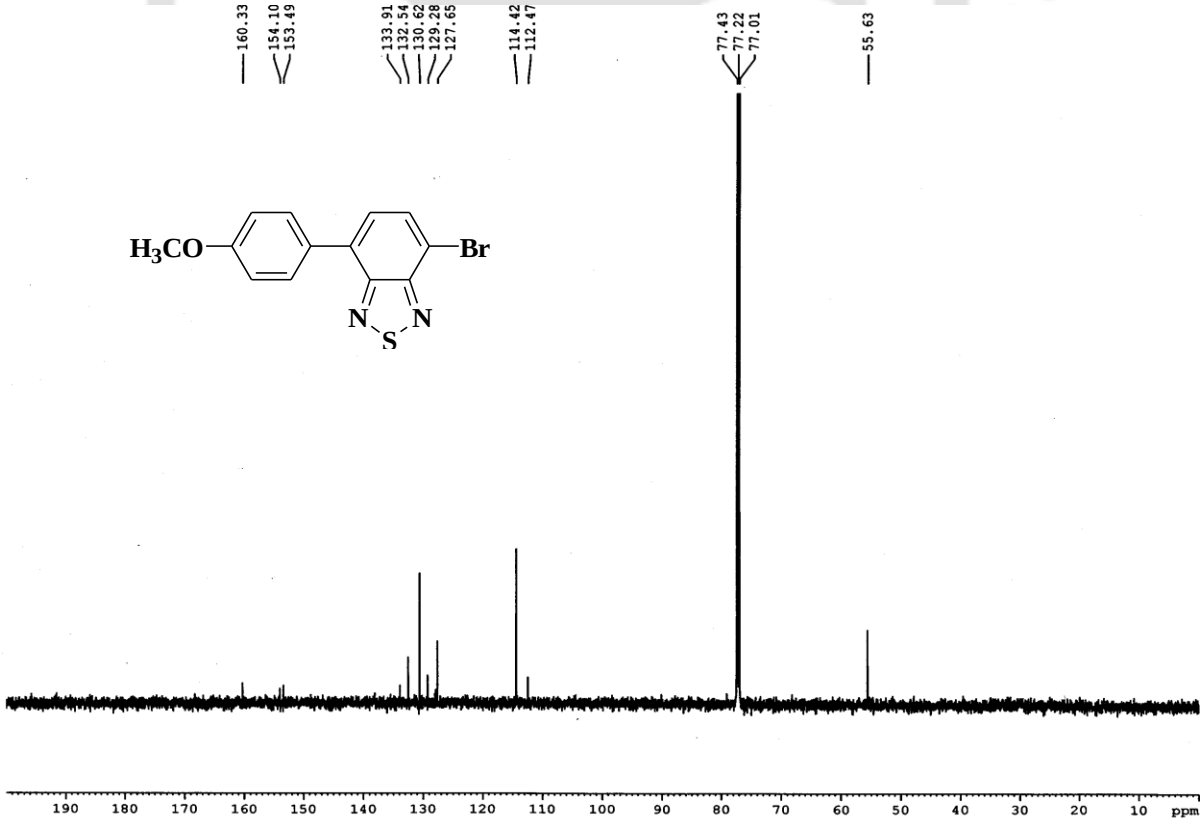

Figure 4.20: The ^{13}C NMR of the **Compound-1** in $CDCl_3$

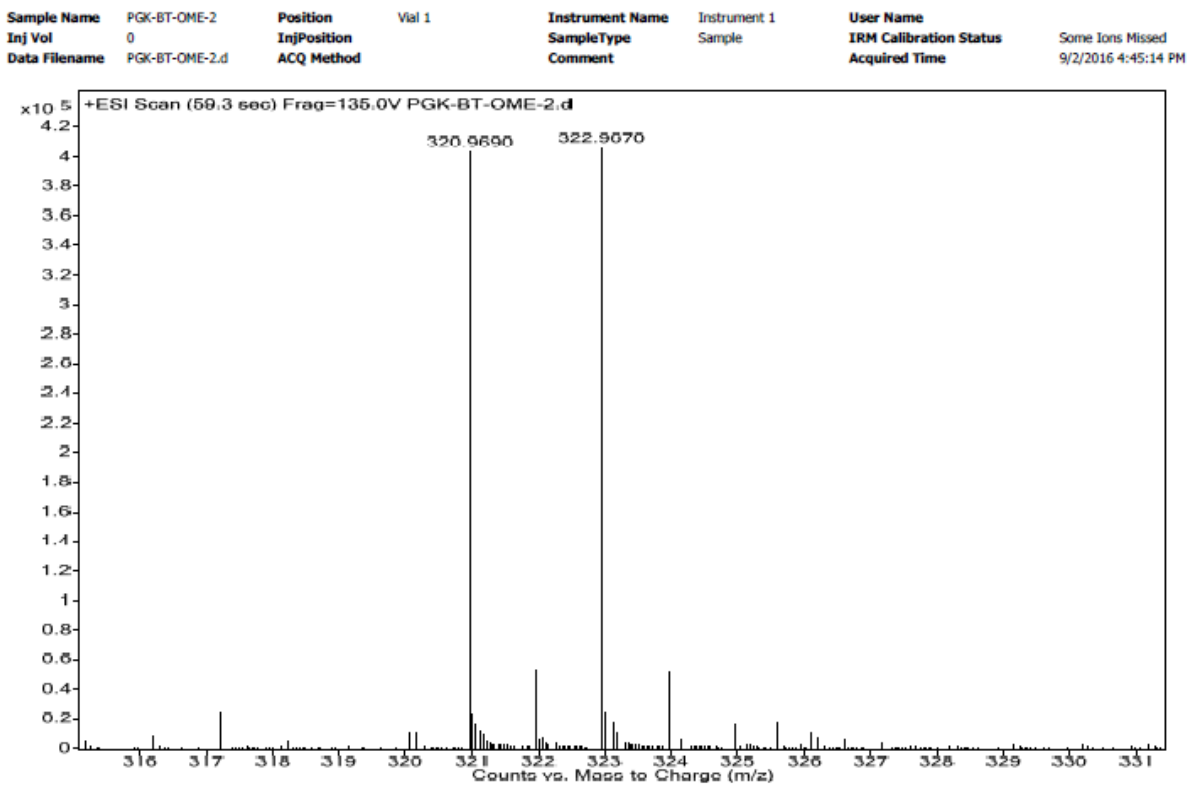

Figure 4.21: HRMS of the **Compound-1**

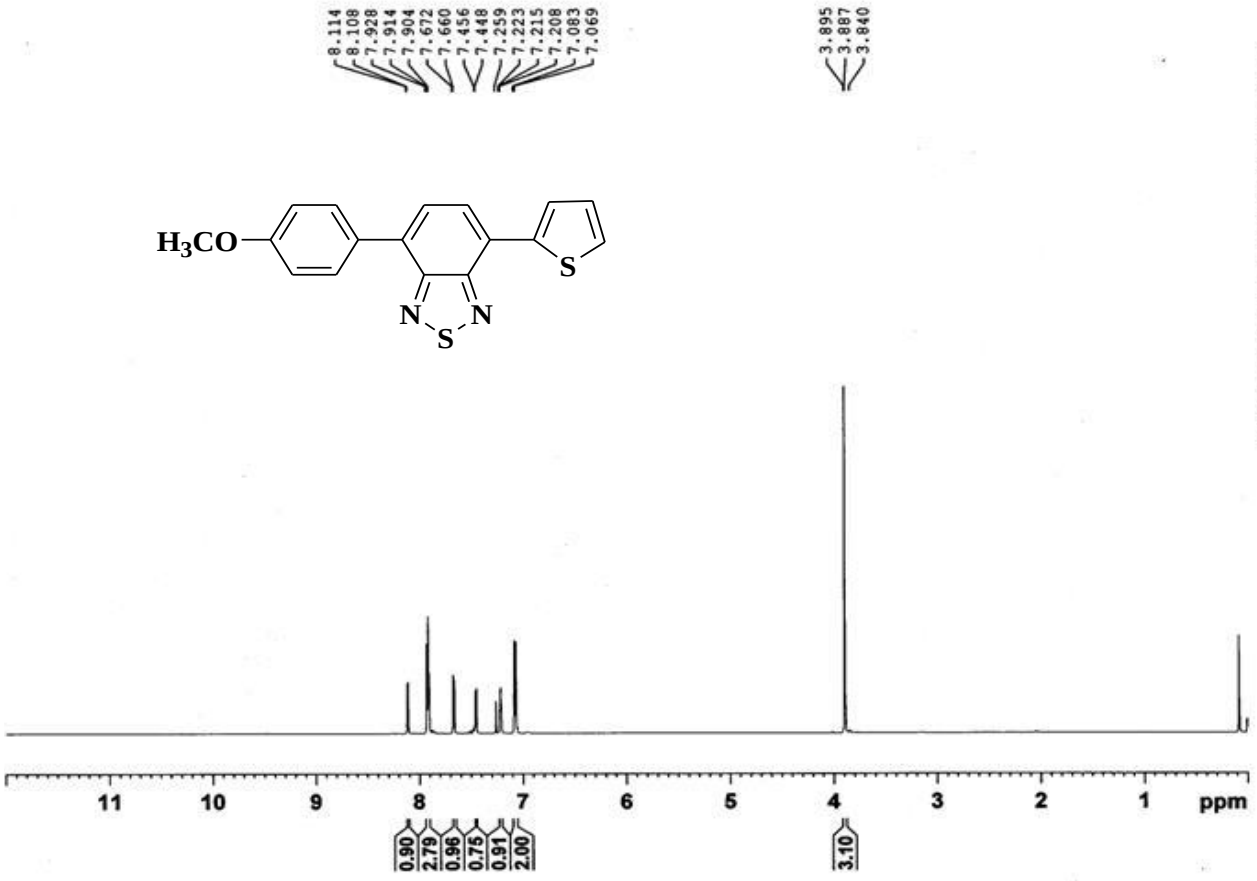

Figure 4.22: The ^{1}H NMR of the **Compound-2** in $CDCl_3$

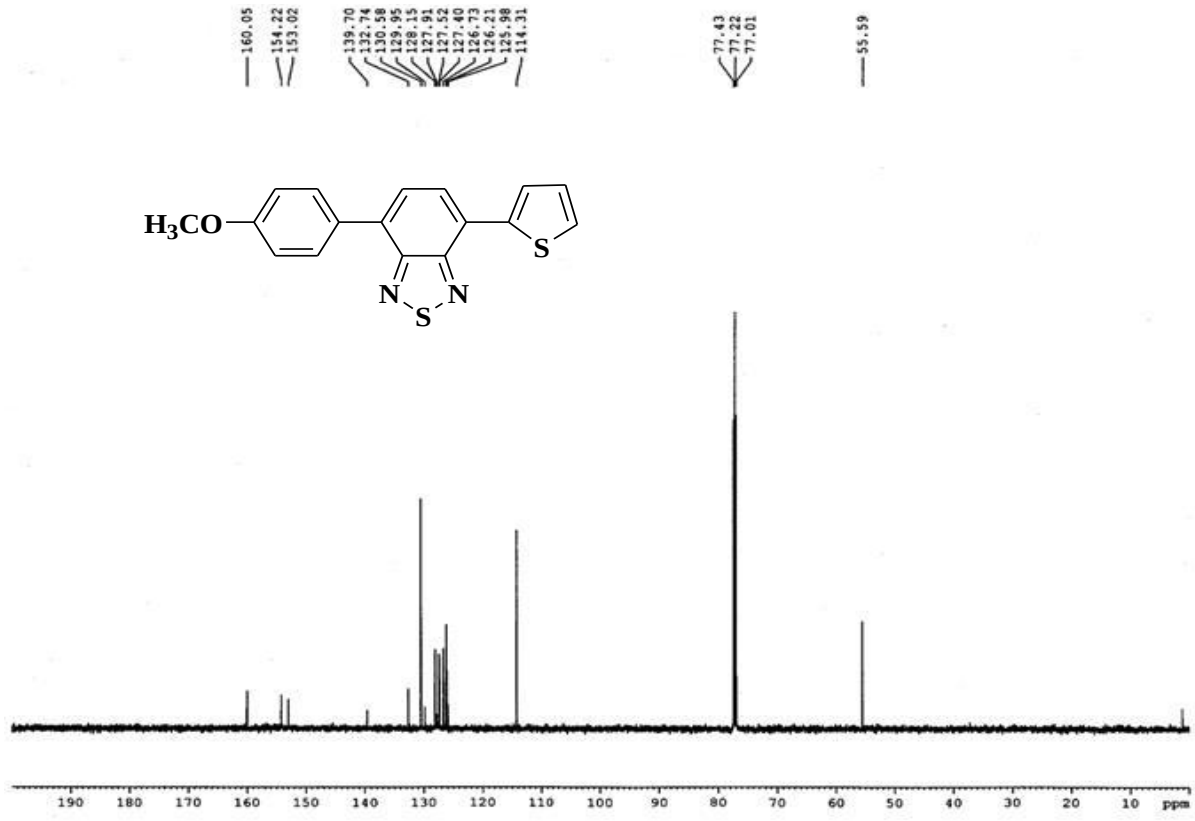

Figure 4.23: The ^{13}C NMR of the **Compound-2** in $CDCl_3$

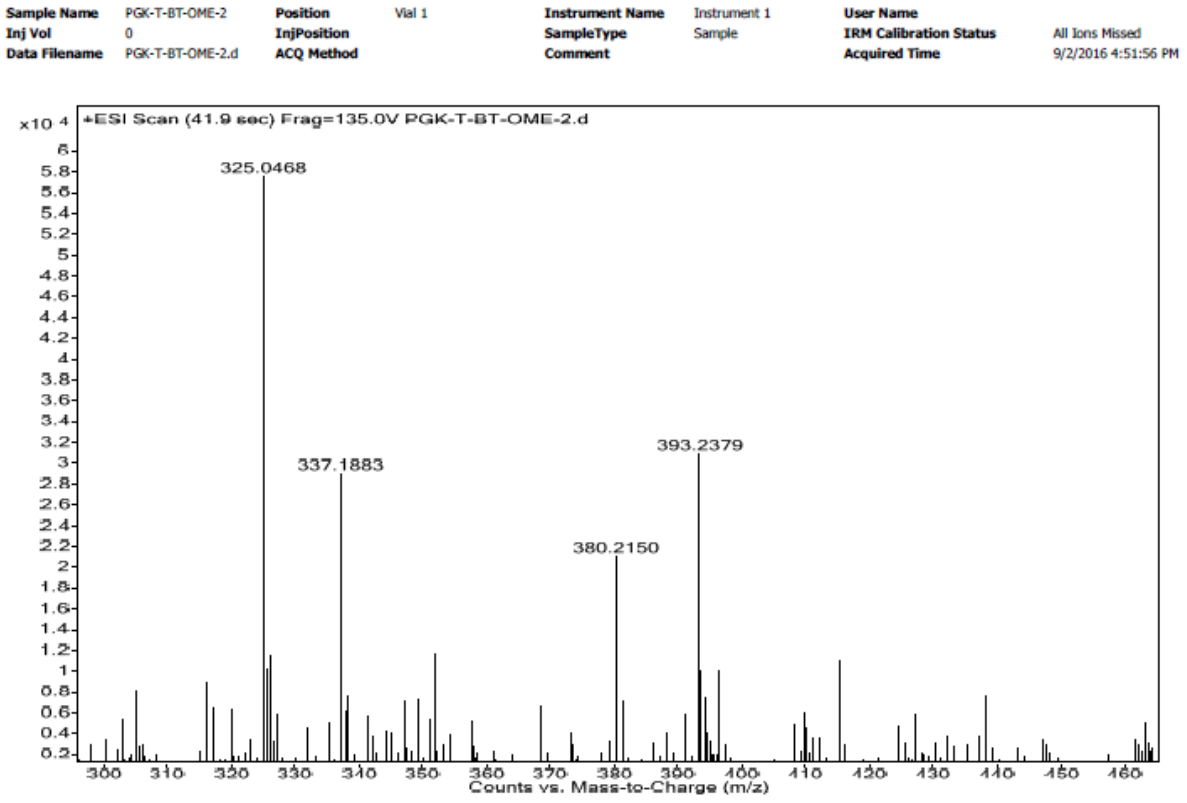

Figure 4.24: HRMS of the **Compound-2**

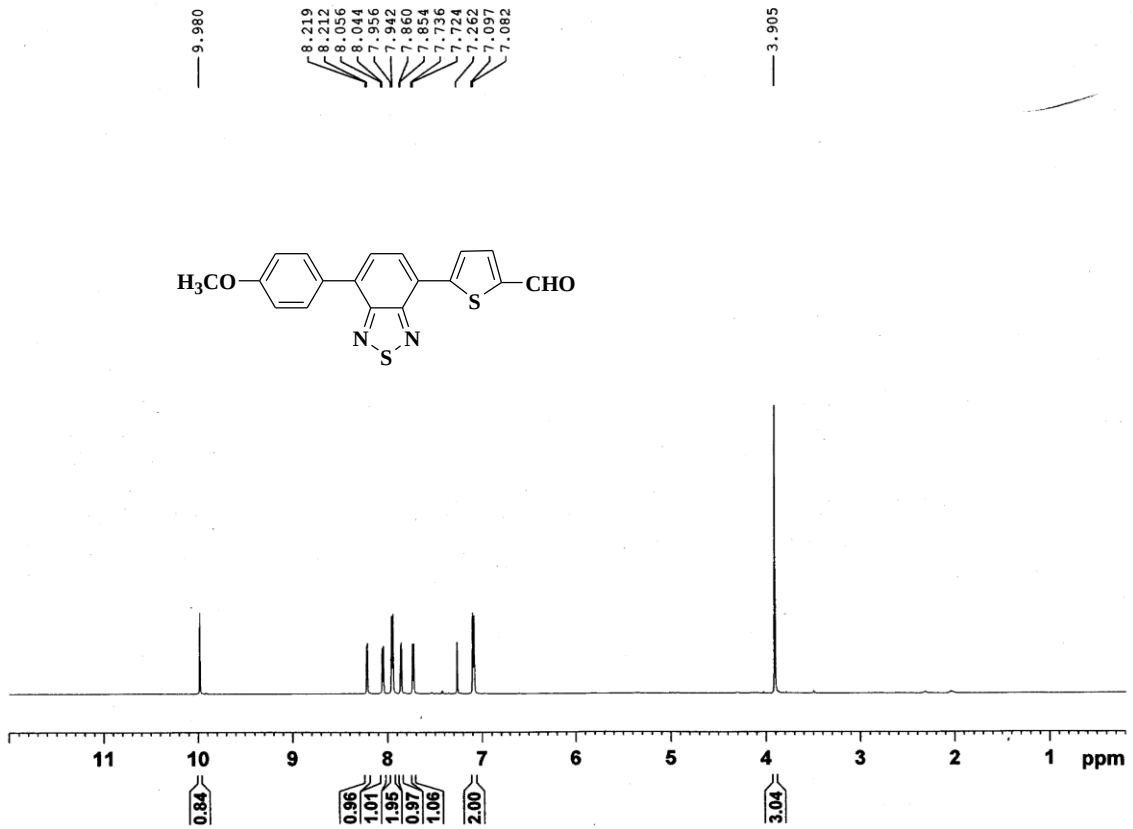

Figure 4.25: The ^{1}H NMR of the **Compound-3** in $CDCl_3$

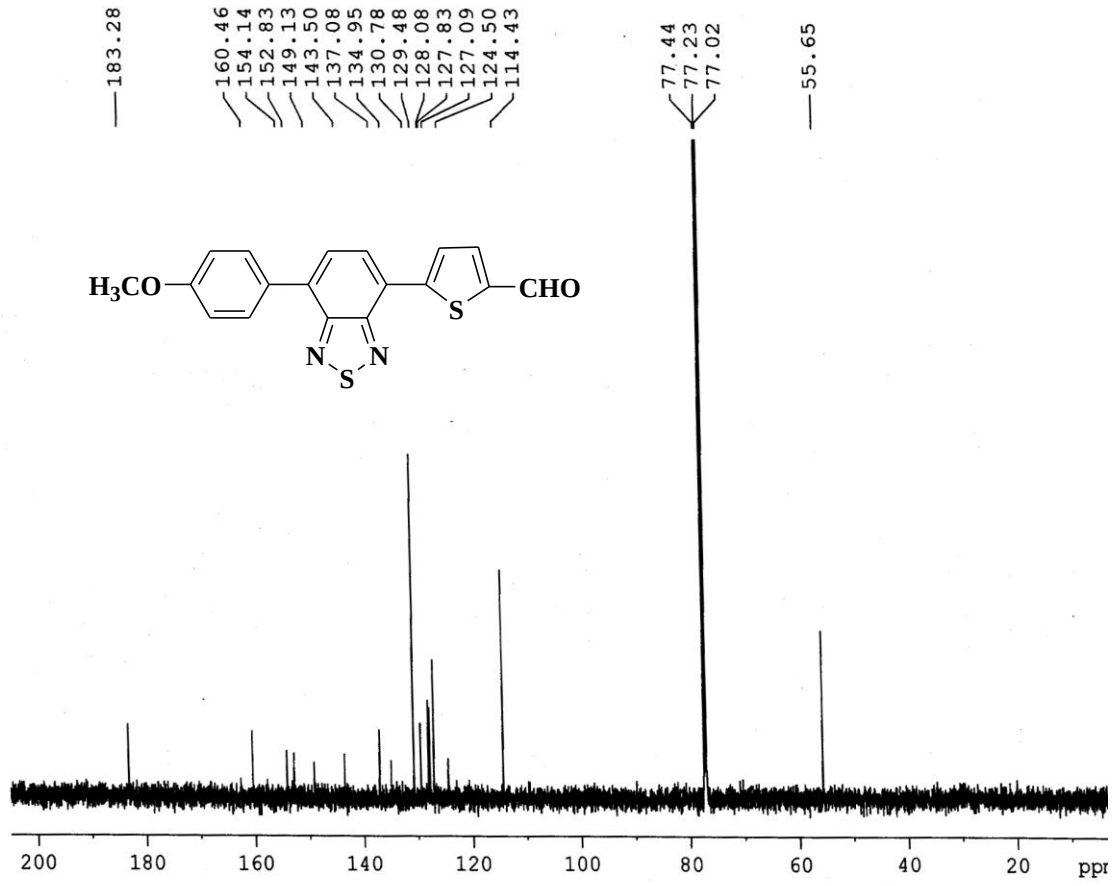

Figure 4.26: The ^{13}C NMR of the **Compound-3** in $CDCl_3$

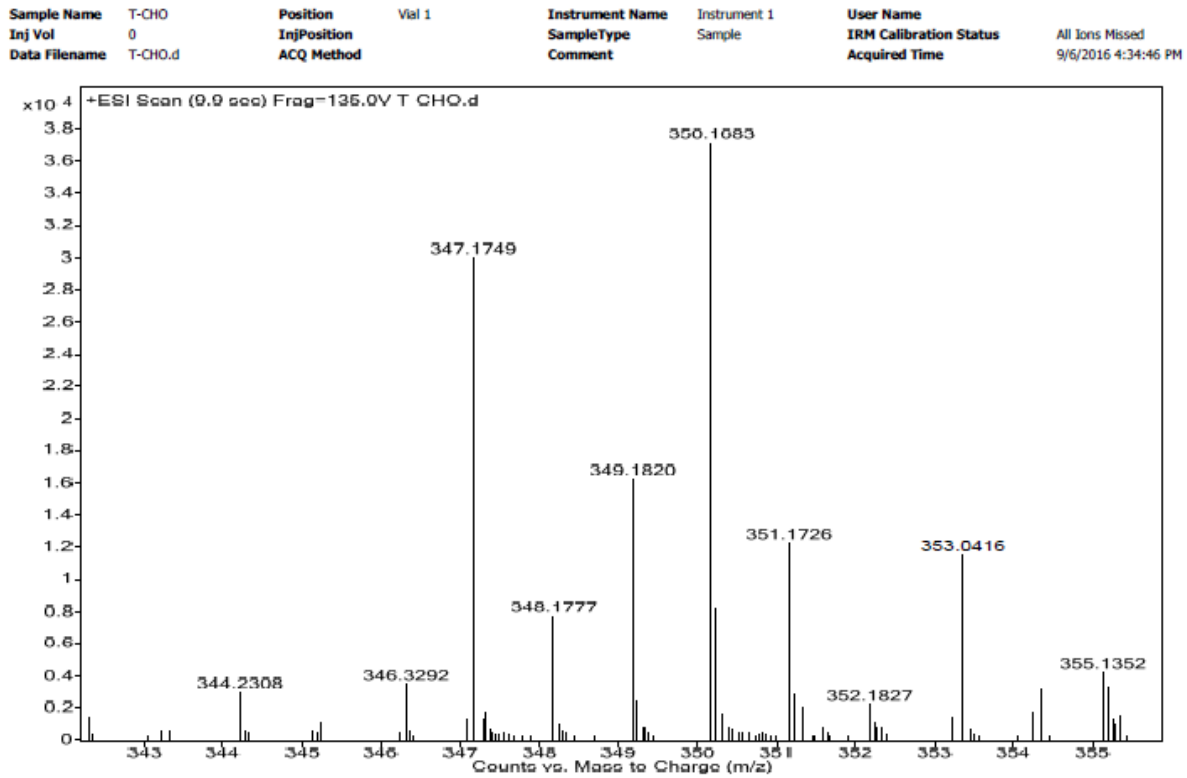

Figure 4.27: HRMS of the **Compound-3**

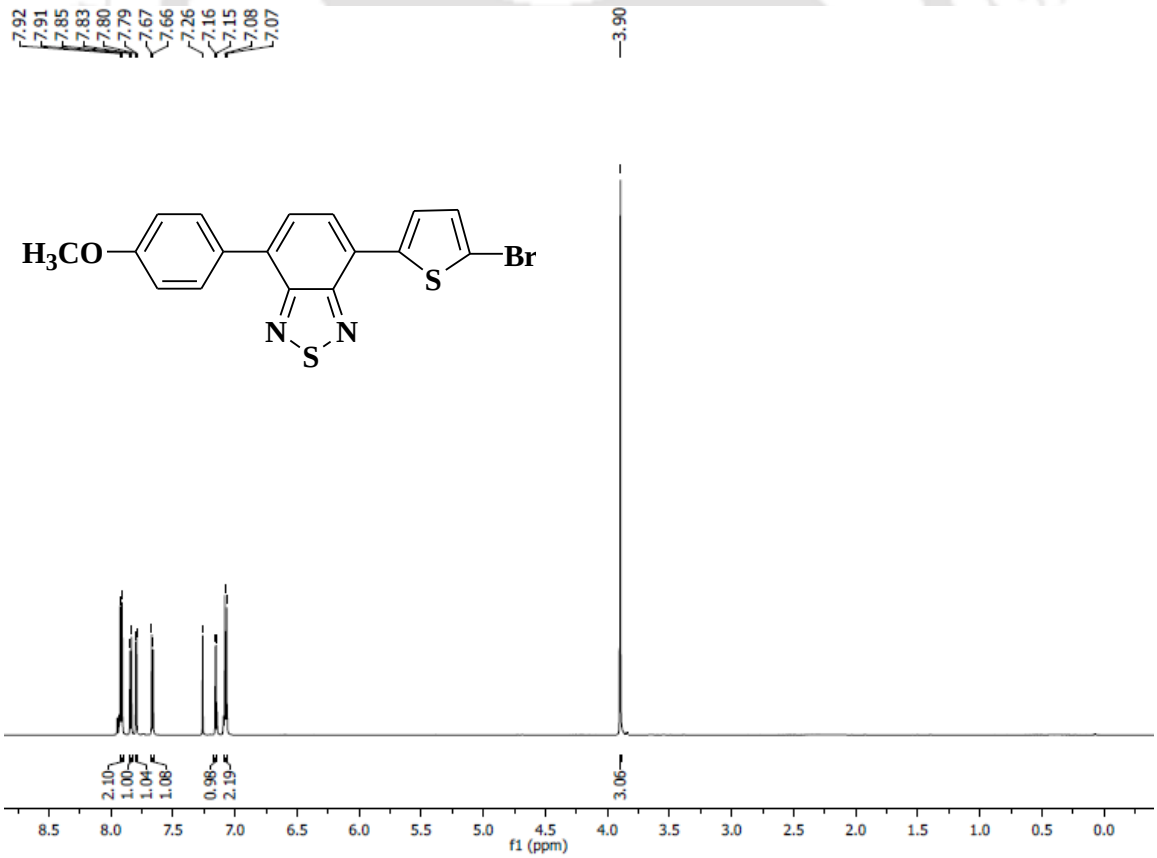

Figure 4.28: The ^{1}H NMR of the **Compound-4** in $CDCl_3$

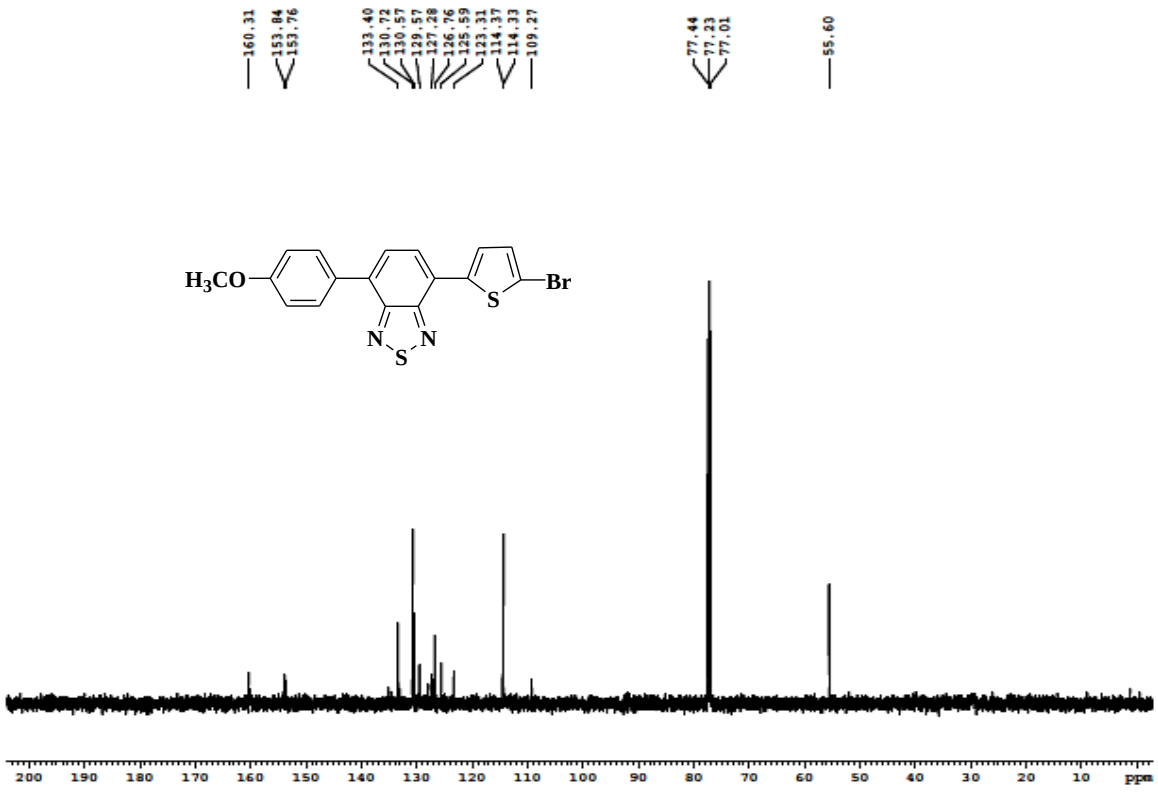

Figure 4.29: The ^{13}C NMR of the **Compound-4** in $CDCl_3$

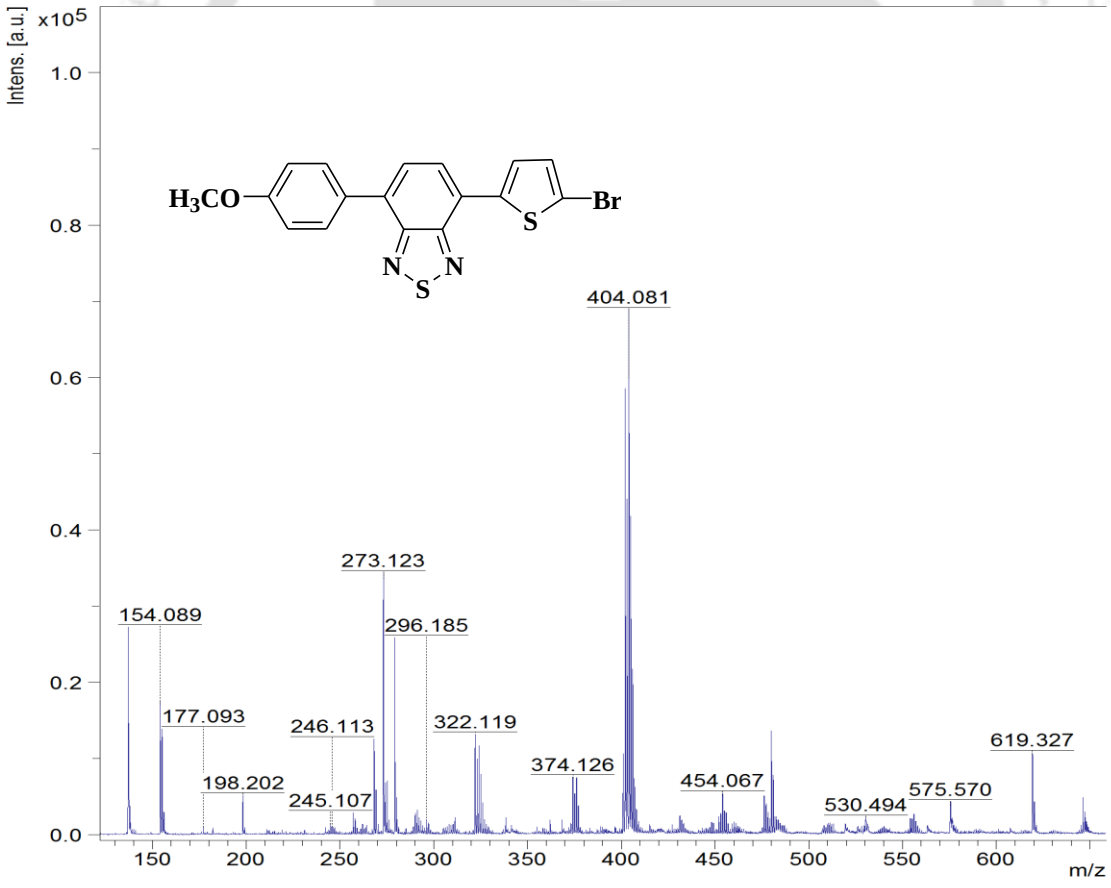

Figure 4.30: The time-of-flight mass spectrum of the **Compound-4**

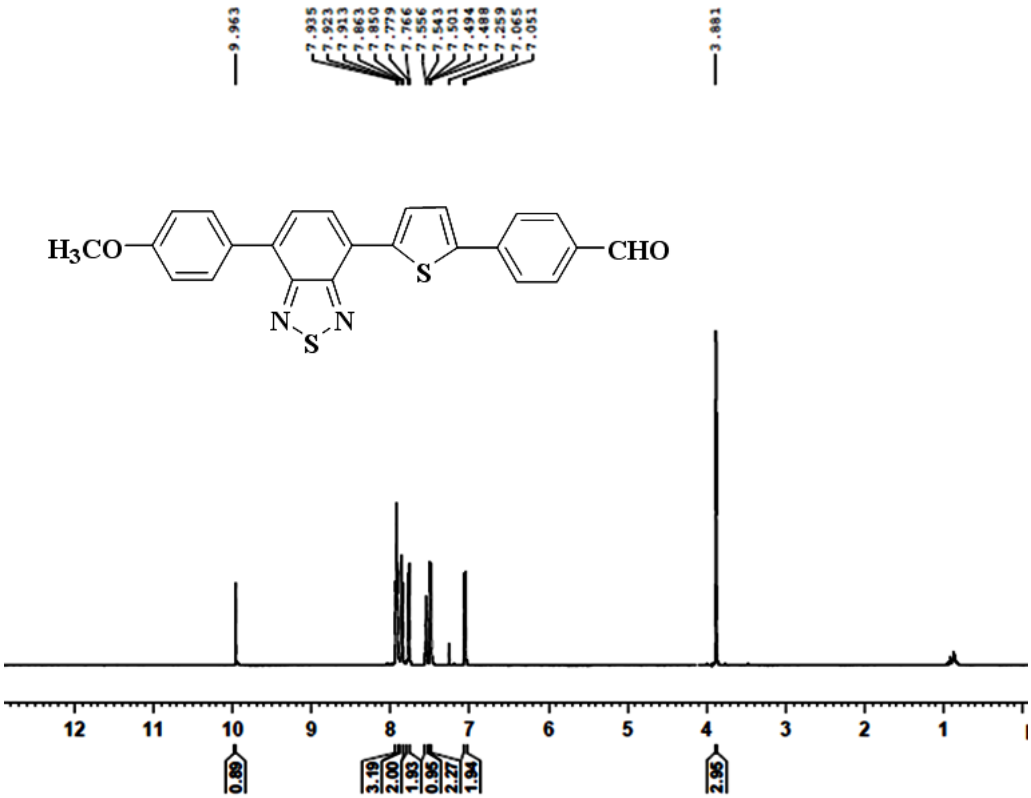

Figure 4.31: The ^{1}H NMR of the **Compound-5** in $CDCl_3$

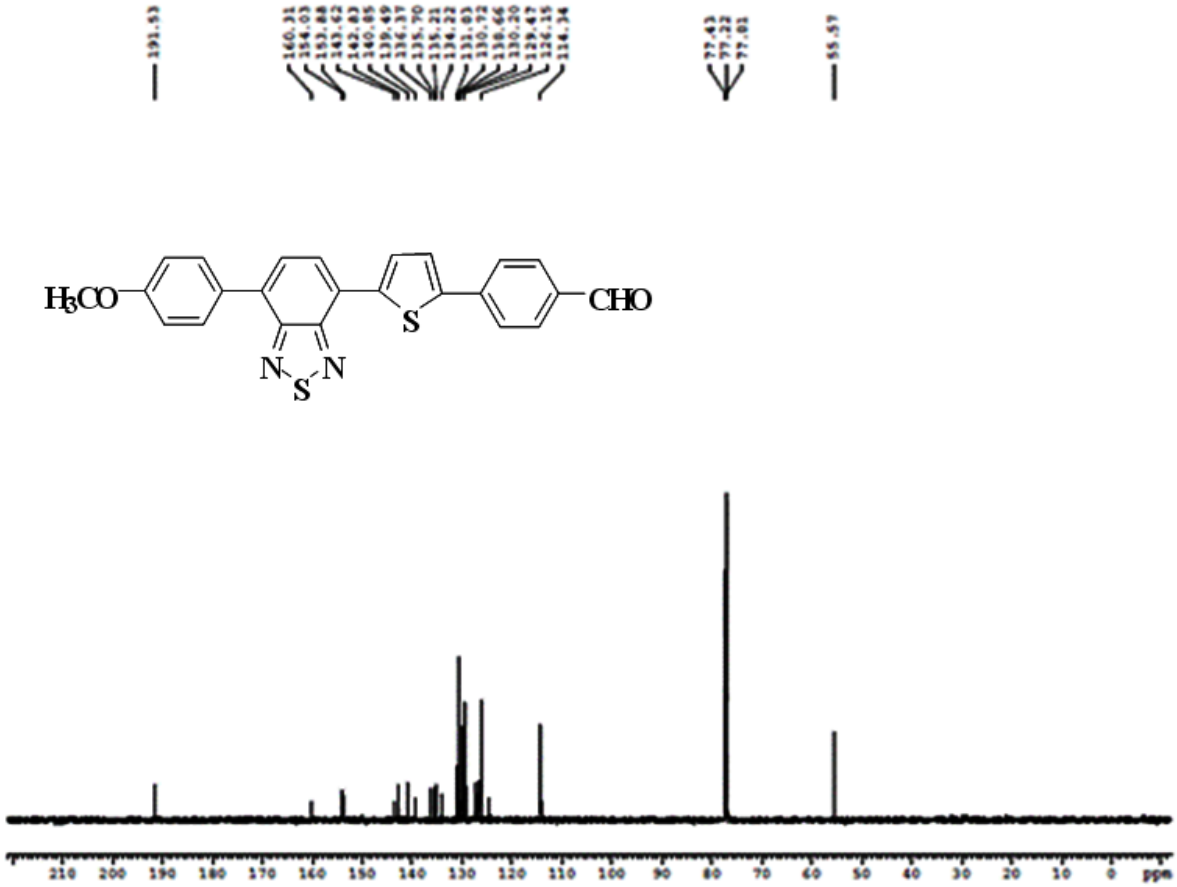

Figure 4.32: The ^{13}C NMR of the **Compound-5** in $CDCl_3$

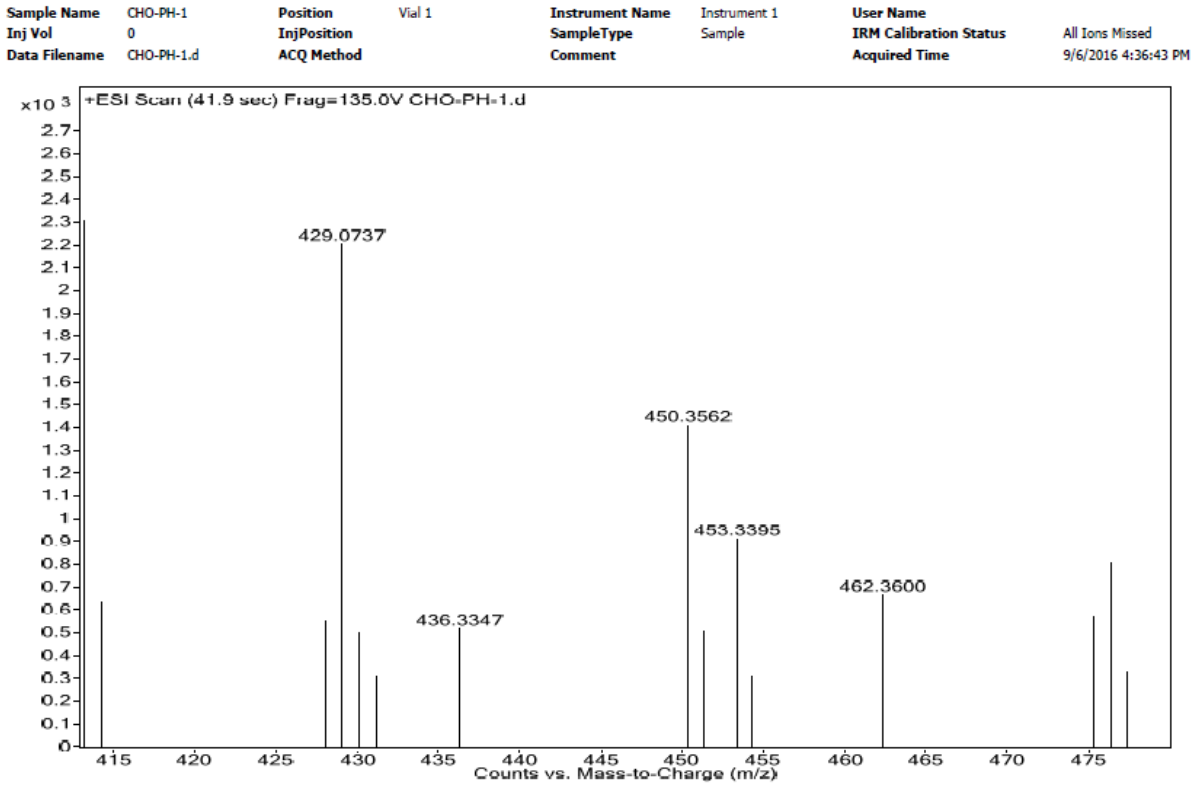

Figure 4.33: HRMS of the **Compound-5**

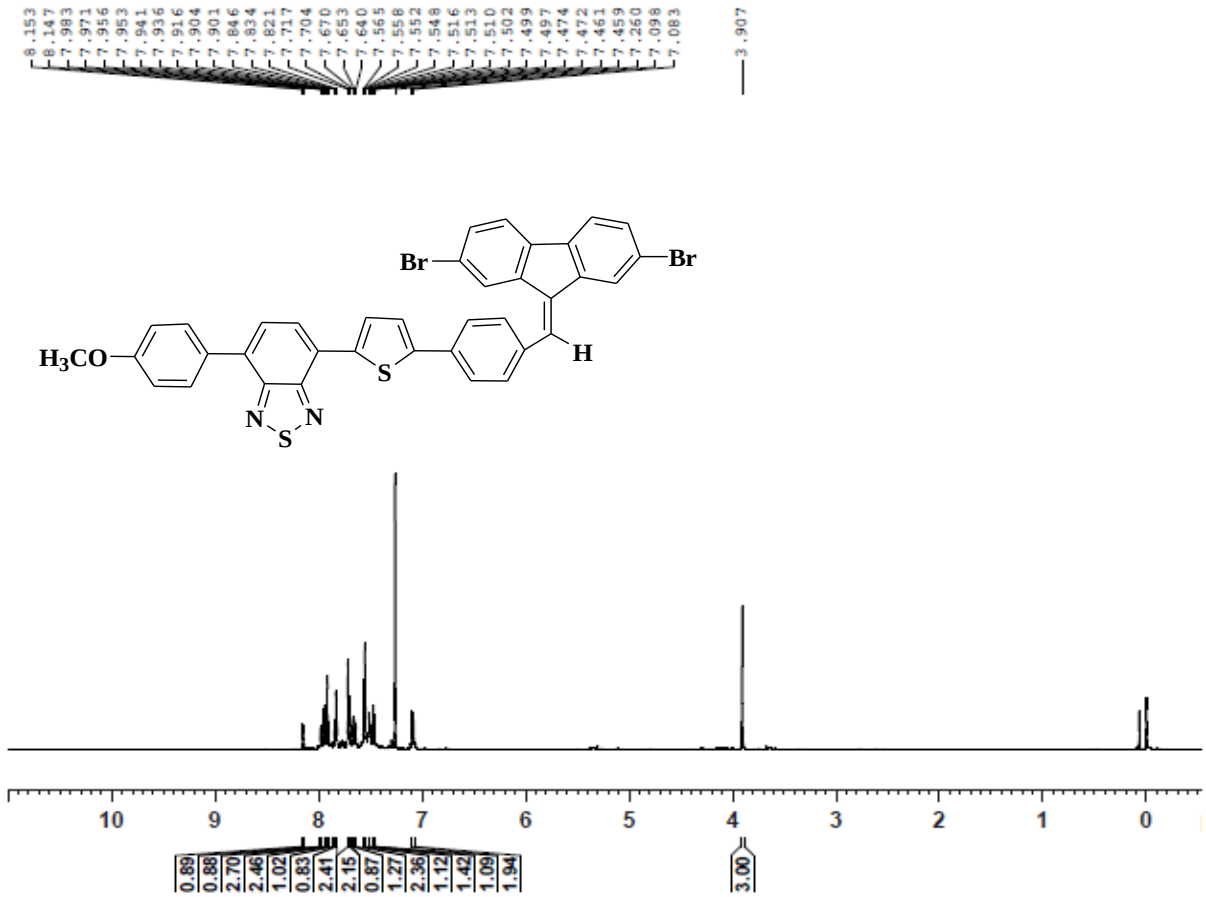

Figure 4.34: The ^{1}H NMR of the **DP2** in $CDCl_3$

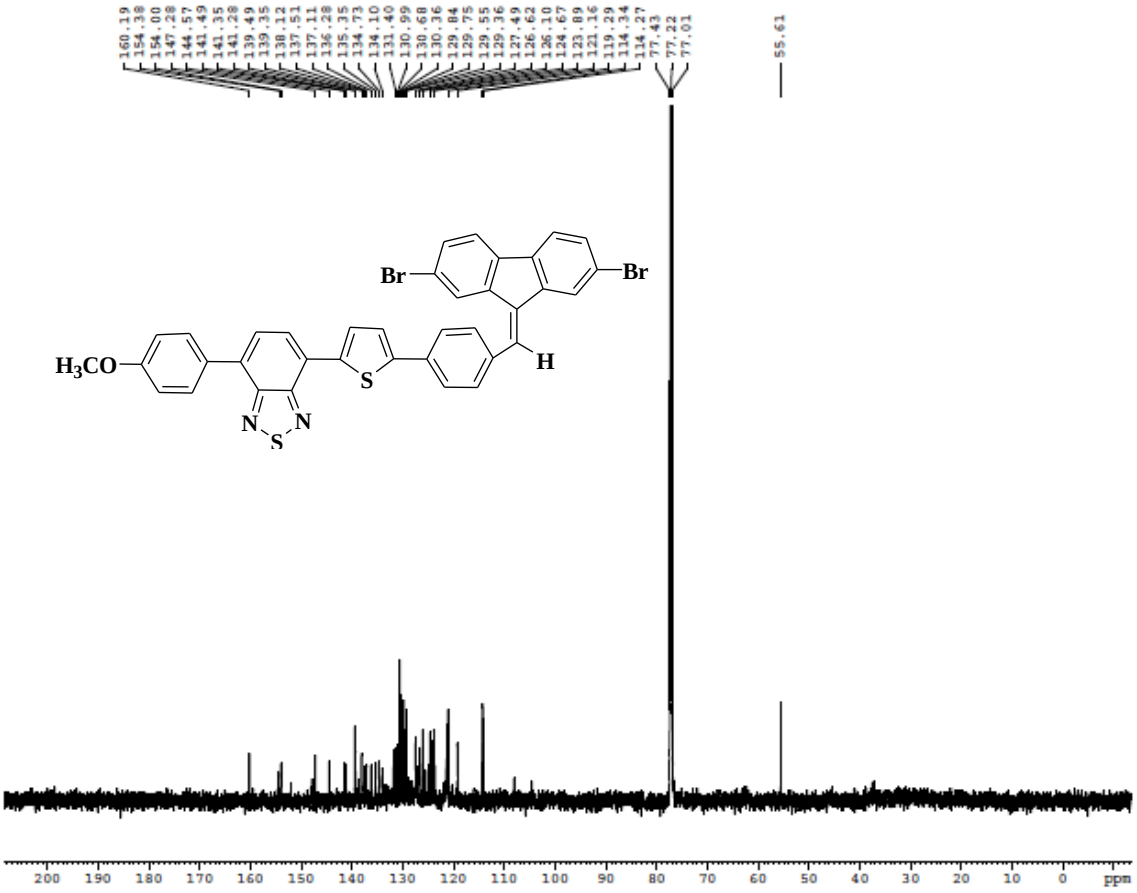

Figure 4.35: The ^{13}C NMR of the **DP2** in $CDCl_3$

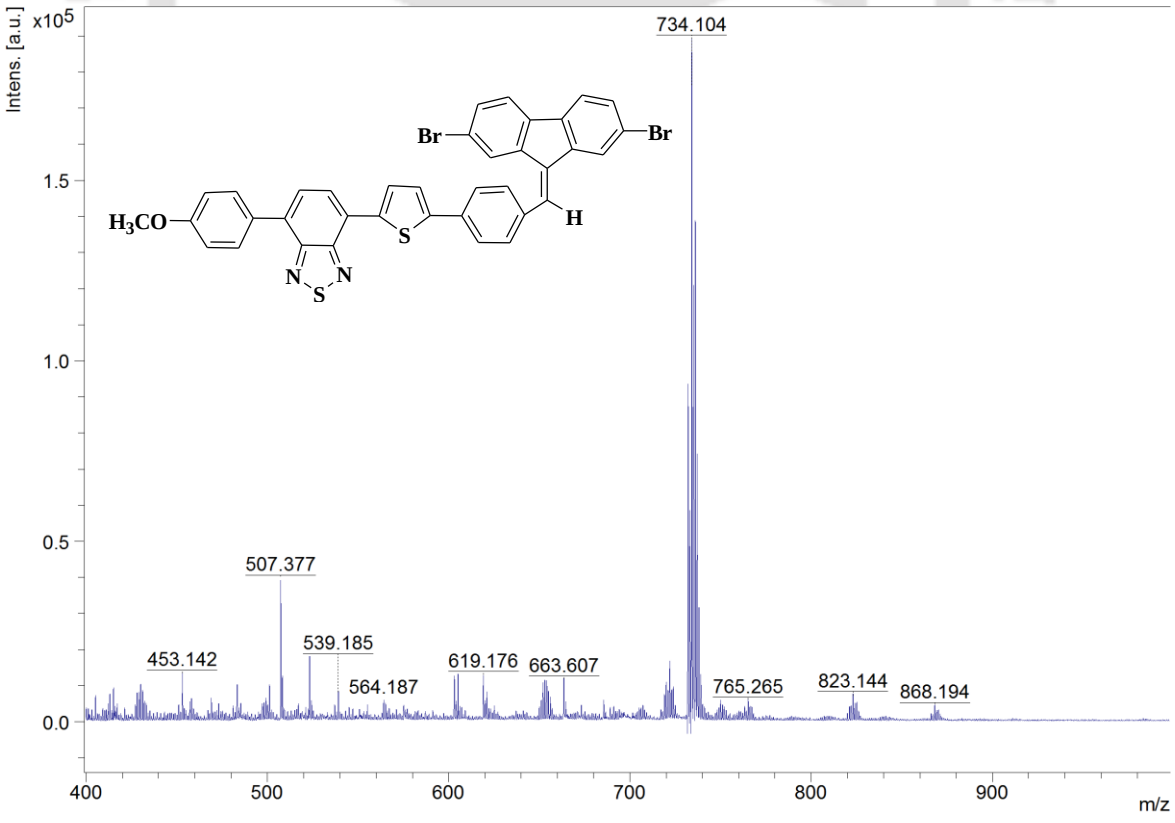

Figure 4.36: The time-of-flight mass spectrum of the **DP2**

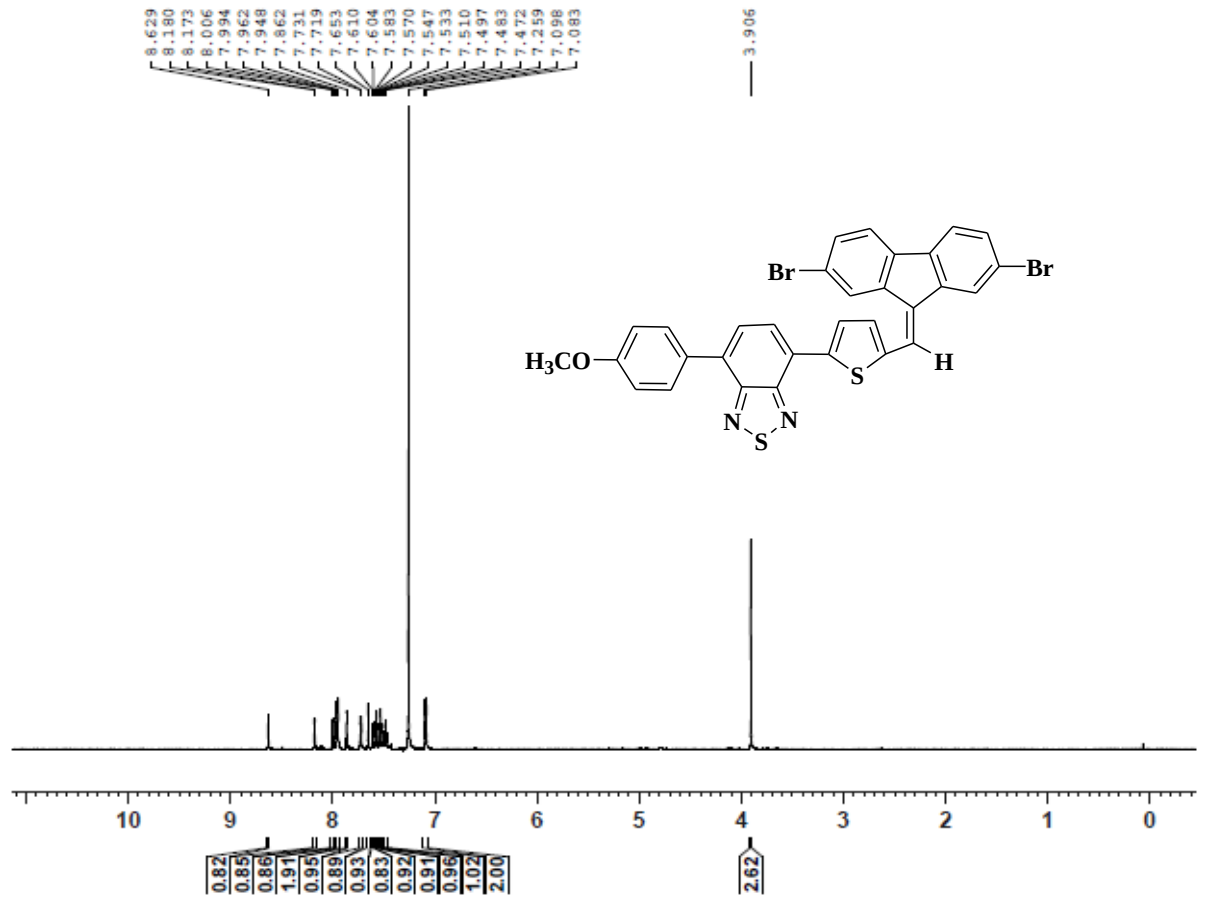

Figure 4.37: The ^{1}H NMR of the **DT2** in $CDCl_3$

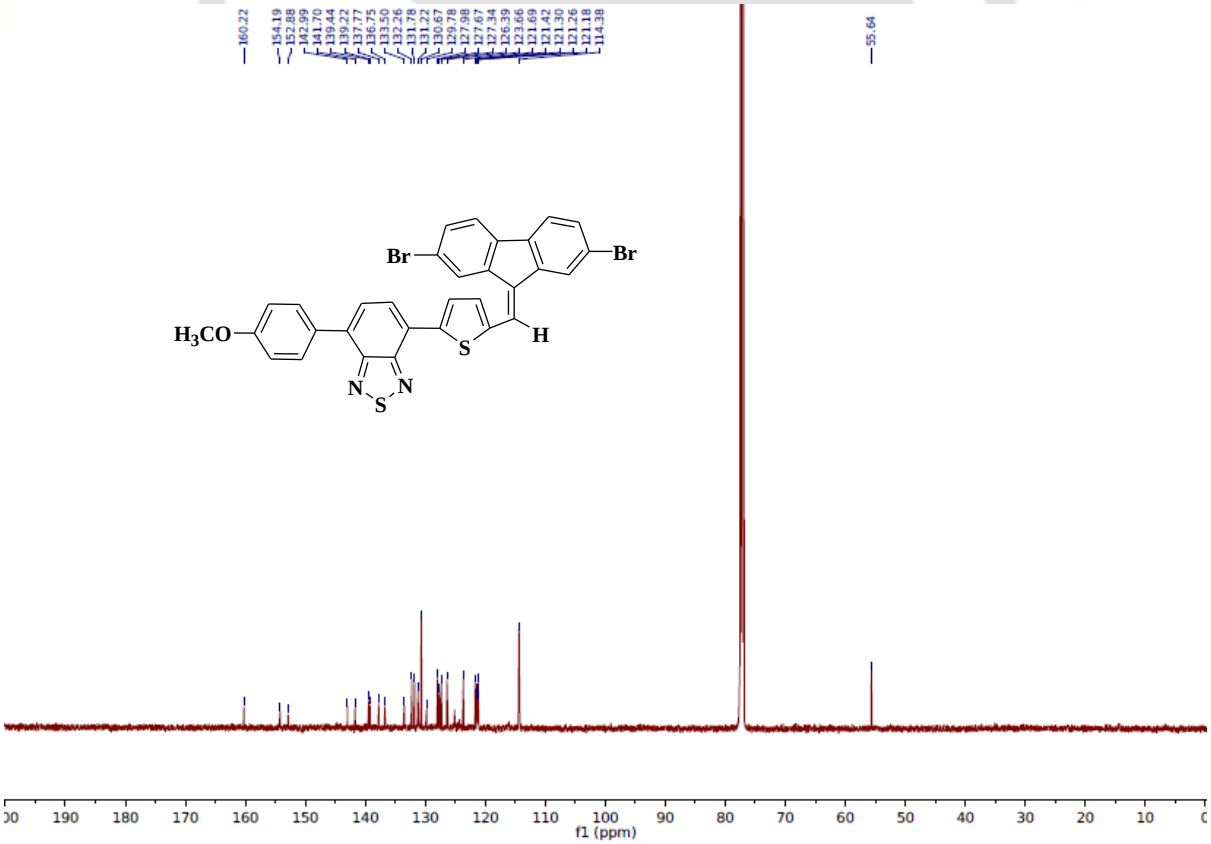

Figure 4.38: The ^{13} NMR of the **DT2** in $CDCl_3$

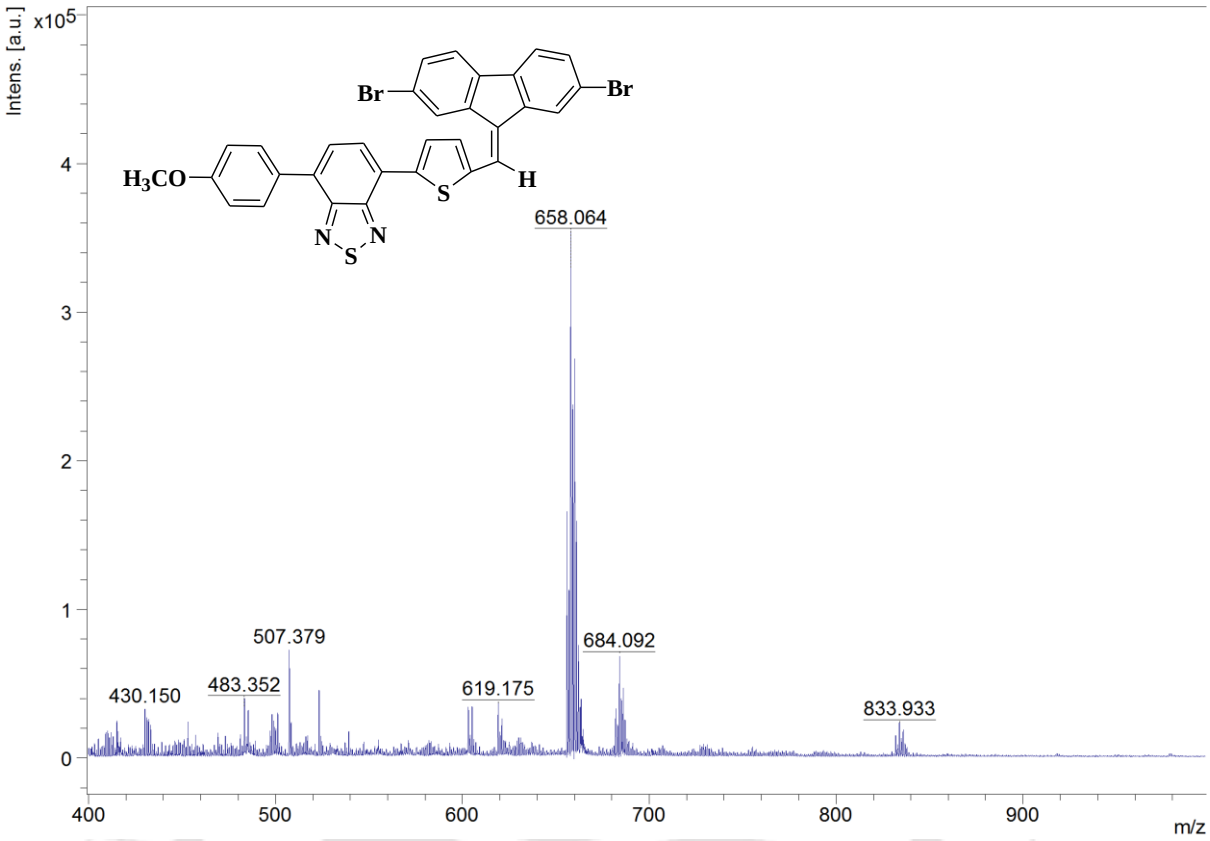

Figure 4.39: The time-of-flight mass spectrum of the **DT2**

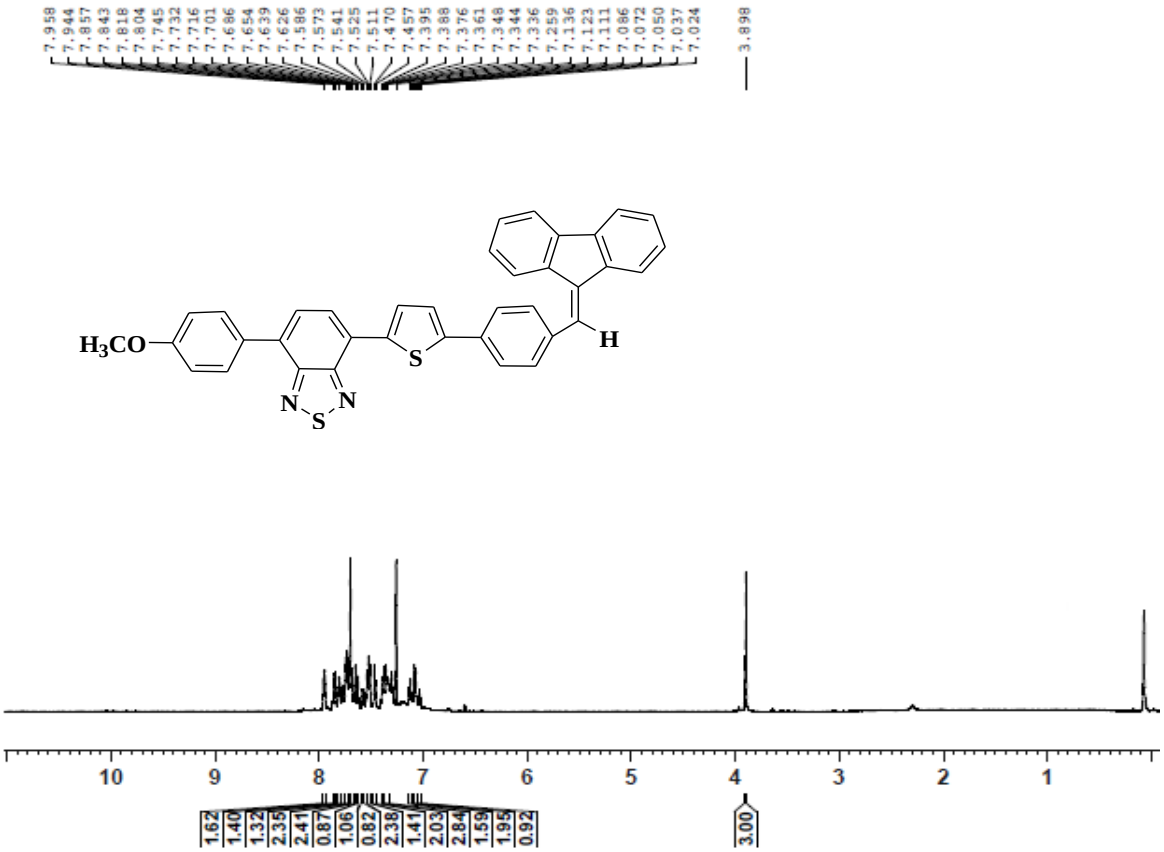

Figure 4.40: The ^{1}H NMR of the **DP1** in $CDCl_3$

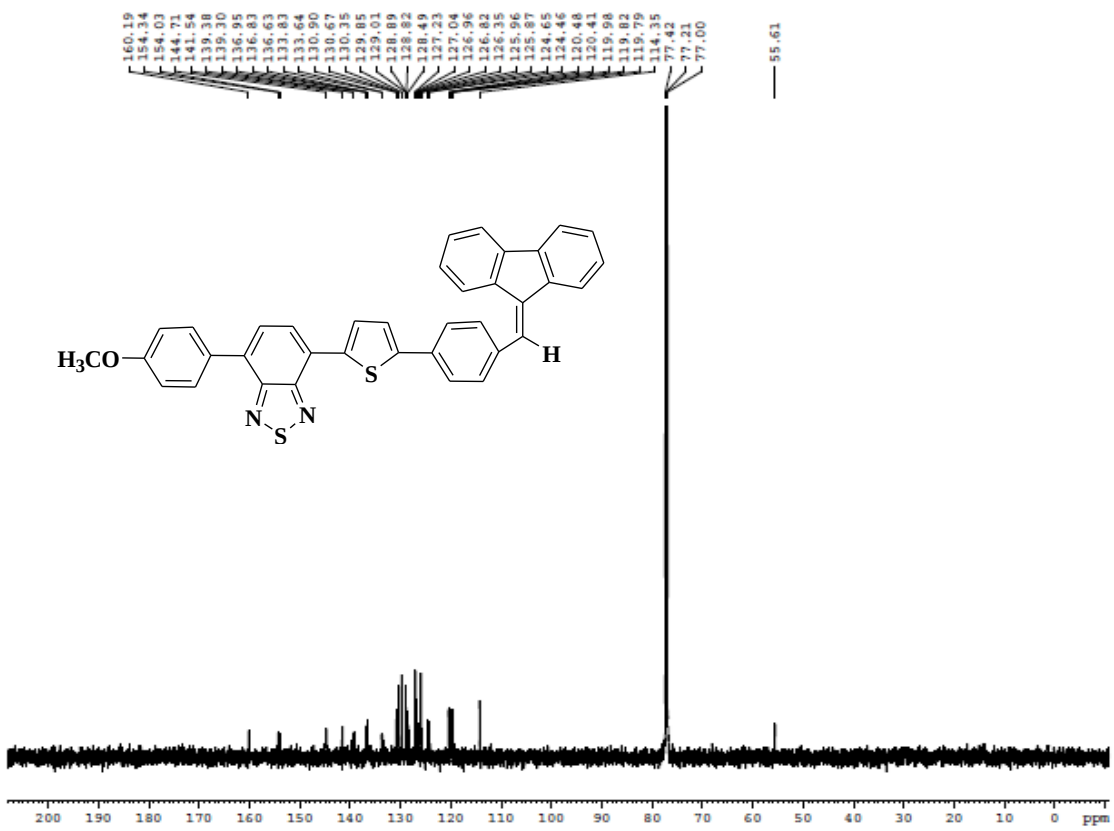

Figure 4.41: The ^{13}C NMR of the **DP1** in $CDCl_3$

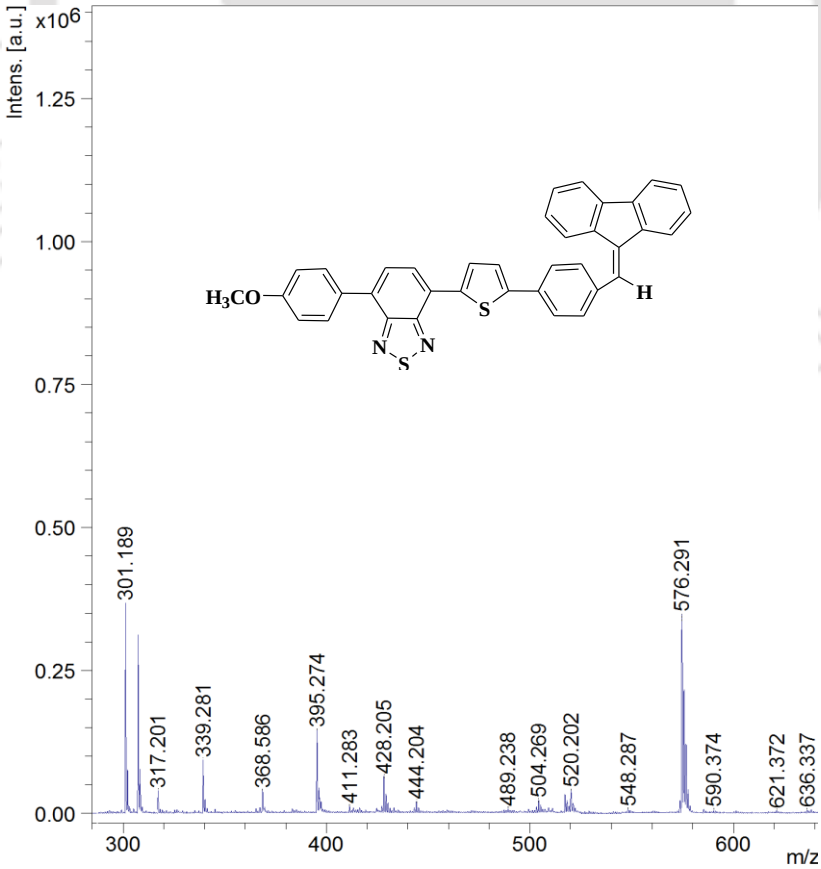

Figure 4.42: The time-of-flight mass spectrum of the **DT2**

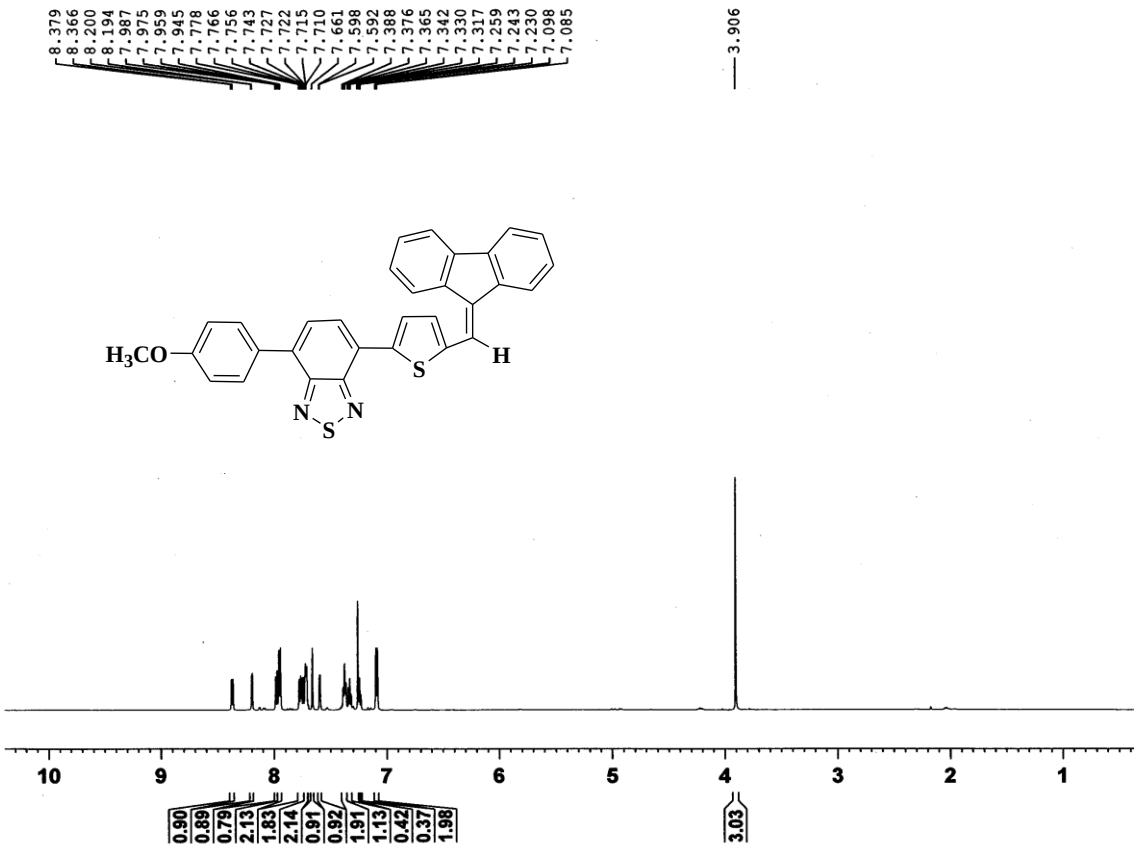

Figure 4.43: The ^{1}H NMR of the **DT1** in $CDCl_3$

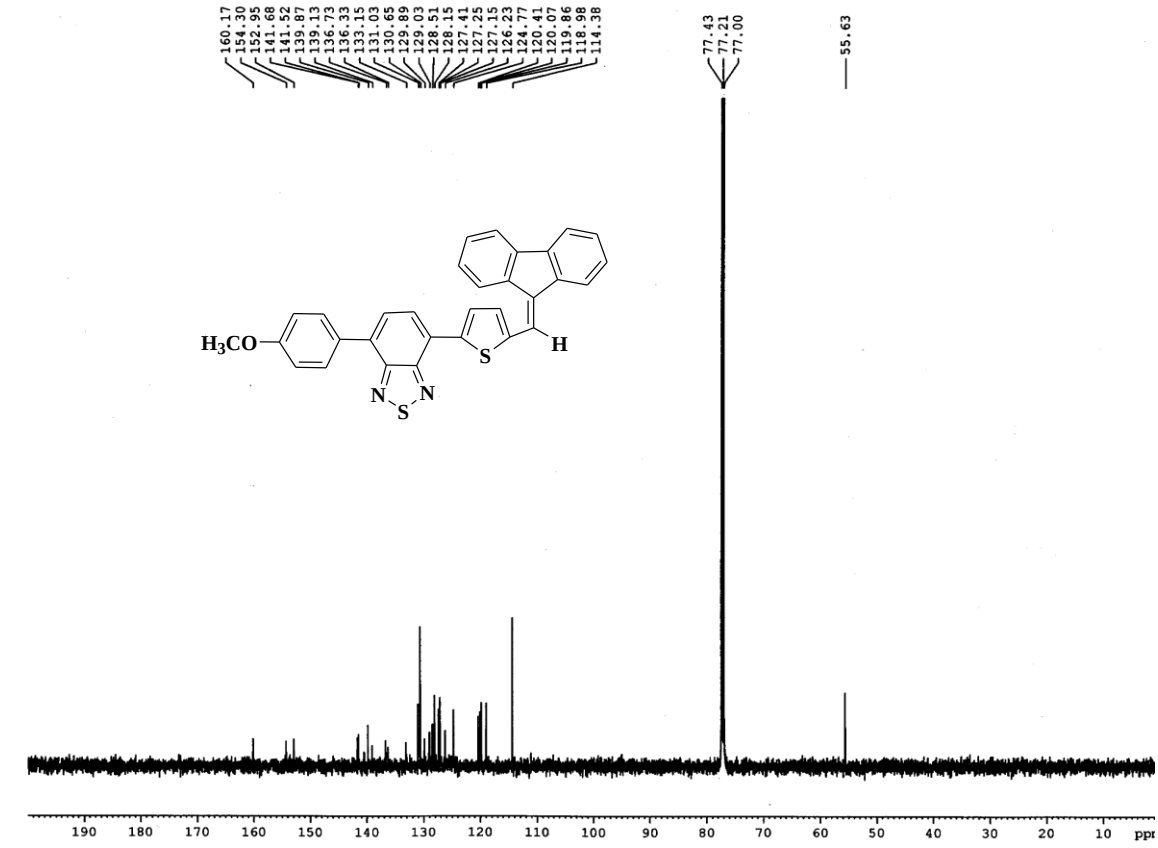

Figure 4.44: The ^{13}C NMR of the **DT1** in $CDCl_3$

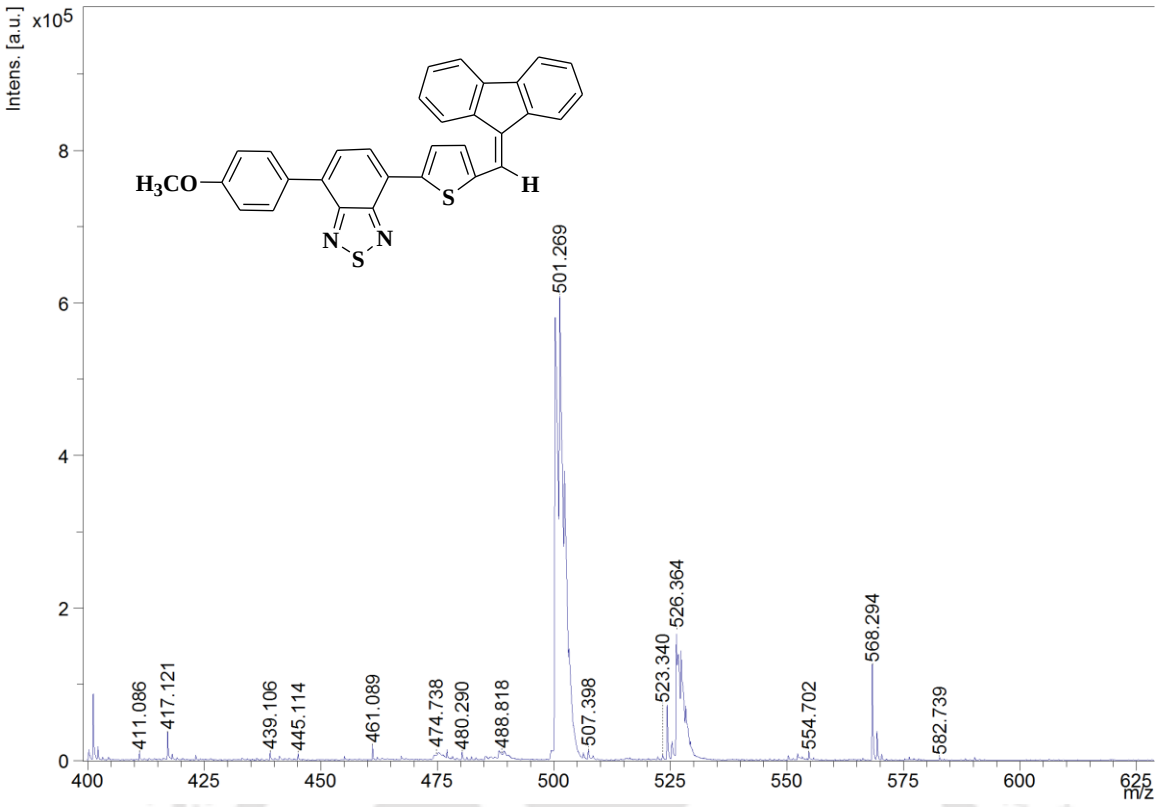

Figure 4.45: The time-of-flight mass spectrum of the **DT1**

Chapter-5

Saturated and Stable White Electroluminescence from Linear Single Polymer Systems based on Polyfluorene and Mono-Substituted Dibenzofulvene Derivatives

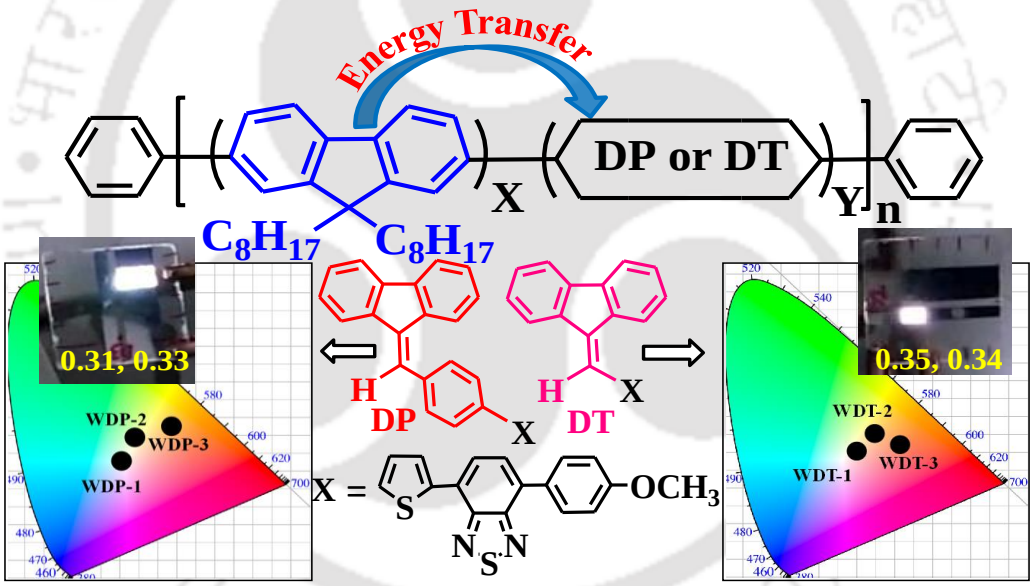

Gopikrishna, P.; Das, D.; Adil, L. R.; Iyer, P. K. *J. Phys. Chem. C.* **2017**, *121,* 18137-18143.

Abstract

The development of new electroluminescent copolymer based materials for white polymer light emitting diodes (WPLED) with special emphasis on novelty of utilizing aggregation-induced emission enhancement (AIEE) active or dual state emitting, mono-substituted dibenzofulvene (M-DBF) derivatives, i.e. 4-(5-fluoren-9-ylidenemethyl-thiophen-2-yl)-7-(4-methoxy-phenyl)-benzo[1,2,5]- thiadiazole (DT) or 4-[5-(4-fluoren-9-ylidenemethyl-phenyl)-thiophen-2-yl]-7-(4-methoxy-phenyl)-benzo[1,2,5]thiadiazole (DP), as orange/red fluorophores into polyfluorene (PF) main chain is demonstrated. The mol % of these M-DBF monomer based small π-system has been optimized to as low as 0.0003, 0.0006, and 0.001% in the poly[2,7-(9,9'-dioctylfluorene)- co-4-(5-fluoren-9-ylidenemethyl-thiophen-2-yl)-7-(4-methoxy-phenyl) benzo[1,2,5]thiadiazole (WDT) and poly[2,7-(9,9'- dioctylfluorene)-co-4-[5-(4-fluoren-9-ylidenemethyl-phenyl)-thiophen-2-yl]-7-(4-methoxy-phenyl)-benzo[1,2,5] thiadiazole (WDP) copolymers, respectively. Here, the utilization of "dual emission" peaks from PFO and M-DBFs in the blue and orange region that enabled the fabrication of bias-independent WPLEDs which is fundamentally very important and highly challenging in the case of linear polymers has been reported. These copolymers showed excellent solubility in organic solvents viz. $CHCl_3$, THF, toluene, p-xylene, etc. The synthesized copolymers were characterized by UV−vis and photoluminescence (PL) spectroscopy, and WPLEDs with ITO/PEDOT:PSS /WDP or WDT/TPBi/LiF/Al configurations were also fabricated to study their electroluminescence (EL) properties. Partial energy transfer has been achieved by adjusting the PFO and DT or DP concentrations in the single polymer main chain leading to the white emission in a facile manner. The copolymers WDP-1 and WDT-1 gave saturated white emission with CIE coordinates of (0.31, 0.33) and (0.35, 0.34) between 8-14 voltages and exhibiting excellent voltage independent emission. The highest luminous efficiencies of 7.82 cd A^{-1} and 4.57 cd A^{-1} were achieved for WDP and WDT polymers with the highest brightness values of 9753 cd m^{-2} and 7436 cd m^{-2}, respectively.

5.1. Introduction

Recently, WPLEDs have gained significant attention in the research community owing to their potential utilization in next generation display technology and solid state lighting sources.[1-8] To realize pure white emission, the EL spectra of WPLEDs should cover the whole visible wavelength range from 400 to 800 nm for any voltage.[9] In this regard, different approaches have been established to achieve WPLEDs, such as multiple emissive layer systems,[10,11] small molecule doped polymer,[12-16] polymer-polymer blends,[17-22] single polymer systems, etc.[23-27] The WPLEDs using the blends (small molecule-polymer or polymer-polymer) as the emissive layers have challenging fabrication issues and often lead to phase separation that results in voltage dependent emission characteristics. Moreover, it is established that stable and saturated white light with required CIE coordinates are practically unfeasible. The single polymer systems offer a facile way to realize pure white emission, and they offer a few vital advantages such as a simple fabrication process, no phase separation, and no dependence of EL on the driving voltage. Single polymers containing either primary or complementary color emitting units in the polyfluorene (PF) main chain have been successfully synthesized and reported by numerous groups.[23-27] PFs are highly promising candidates for light emitting applications as they possess high solid state PL and EL efficiencies as well as excellent thermal stabilities. In addition, PFs and their copolymers have good solubility in organic solvents and form good films.[28,29] Generally, PFs are electron donors with high band gaps and they emit in the blue region which can be easily manipulated.[30] Single polymer white emission with high EL performance and good CIE coordinates can be achieved by introducing orange chromophores into the PF main chain but remains highly challenging. However, good quality WPLEDs require high EL performance and CIE coordinates, along with saturated emission color with good stability.[31-33] In the solid state, linear single polymer systems may show unsaturated emission due to the strong intermolecular interactions between polymer chains. The strong π-π interactions, in the case of linear rigid polymer chains, make it difficult to precisely control the energy transfer and therefore obtain pure white emission with good color stability. To overcome this problem, single polymers with star-shaped structures have been designed and synthesized.[34-37] When compared with their linear counterparts, these star-shaped systems exhibit significantly less concentration quenching in the solid state due to reduced intermolecular interactions and show improved device efficiency.[38] Recently, white electroluminescent copolymers have been reported by introducing the orange or red AIEE active luminogens

into the PF main chain.[39,40] Generally, aggregation induced emission (AIE) or AIEE molecules that become highly emissive in the aggregate state are nonplanar, propeller shaped structures, and due to the non-planarity they can effectively reduce the π-π interactions in the solid state. However, research on AIEE active molecules containing polymers and their application in PLEDs is still at a preliminary level and opens up an immense scope of improvement due to the unique photophysical properties they offer in the solid/ aggregated state. In this chapter, taking advantage of the above properties and the necessity to develop bright and efficient WPLEDs, the stable linear single layer white emitting copolymers synthesized using the Suzuki coupling reaction by incorporating orange emitting, i.e., dual state emitting (DP), and red emitting, AIEE active (DT) small π-system M-DBF into the PFO main chain.

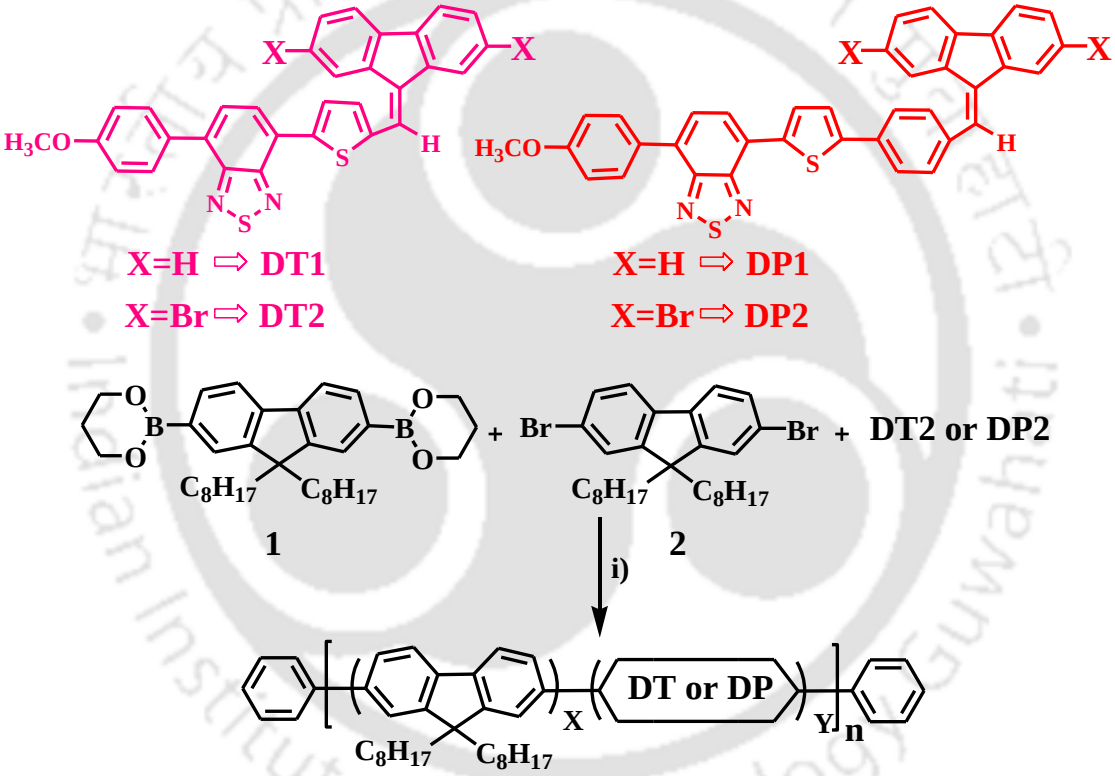

Scheme 5.1. Chemical structures of DT1, DT2, DP1 and DP2. Synthetic route for Polymers Feed ratio of Monomers: 99.9997/0.0003 (WDT-1 or WDP-1), 99.9994/0.0006 (WDT-2 or WDP-2), 99.999/0.001 (WDT-3 or WDP-3). i) $Pd(pph_3)_4$, aliquat 336, 2M K_2CO_3, THF, 48 hrs, Benzene boronicacid, Iodobenzene, 80 °C.

To realize white emission, three different comonomer concentrations (0.0003, 0.0006, and 0.001 mol %) were used, and the PFO emission color was successfully tuned from blue to white by controlling the M-DBFs feed ratios. The white light emissions were achieved from the single copolymers (WDP-1 and WDT-1) by incorporation of a minute amount of DP (0.0003 mol %) or DT (0.0003 mol %) in the polymerization mixture. The devices fabricated using WDP-1 or WDT-1 copolymers were found to emit white

emission with CIE coordinates of (0.31, 0.33) and (0.35, 0.34) that are very close to standard CIE coordinates (0.33, 0.33) with maximum luminous efficiencies of 7.82 cd A^{-1} and 4.57 cd A^{-1} exhibiting highest brightness values of 9753 cd m^{-2} and 7436 cd m^{-2}. Carefully choosing the fluorophore ratio and understanding the molecular mechanisms for generated white light via this study would provide vital leads to design new polymers for stable white light independent of applied voltage. This work reports the utilization of both dual state as well as AIEE active fluorophores as a special small π-system for the first time in a copolymer for stable and efficient WPLED devices.

5.2. Experimental section

5.2.1. Materials and measurements

2,7-Dibromofluorene, 9H-fluorene, 1-bromooctane, 4,7-Dibromobenzo[c]-1,2,5-thiadiazole, 4-methoxy phenyl boronic acid, 2-(Tributylstannyl)thiophene, 4- formyl phenyl boronic acid, 5-formylthiophene-2-boronicacid, NBromosuccinimide (NBS), and potassium tertbutoxide, 9,9'-dioctylfluorene- 2,7-diboronic acid bis(1,3-propanediol)-ester, tetrakis-(triphenylphosphine) palladium(0), aliquat 336 and PEDOT:PSS were purchased from Sigma-Aldrich and 2,2′,2"-(1,3,5-Benzinetriyl)-tris(1-phenyl-1-H-benzimidazole) (TPBi) was purchased from Ossila and used without further purification. Absolute ethanol, chloroform, dichloromethane and toluene were distilled over calcium chloride and anhydrous tetrahydrofuran was dried over sodium benzophenone.

^{1}H and ^{13}C NMR spectra were recorded on Varian AS 400 MHz and Bruker 600 MHz NMR spectrometers. UV-visible spectra were recorded using a Perkin Elmer, Model Lambda-25 spectrometer. Photoluminescence (PL) spectra were recorded using a Varian Cary Eclipse spectrometer. Electrochemical measurements were carried out under argon atmosphere on a deoxygenated solution of 0.1 M tetra butyl ammonium perchlorate (TBAP) in acetonitrile by using a CH instrument (Model 700D series). Glassy carbon was used as a working electrode, platinum as a counter electrode, and Ag/Ag^{+} as a reference electrode. The gel permeation chromatography (GPC) measurements were recorded on a Waters 515 chromatograph connected to Waters 2414 refractive index detectors by using THF as an eluent and the calibration curve of PMMA standards. The current density-voltage (J-V) characteristics of the fabricated WPLEDs were measured using Keithley 2400 source meter whereas the luminance and the EL spectra were measured using CS 2000 spectroradiometer.

5.2.2. General polymerization procedure

9,9-dioctylfluorene-2,7-diboronic acid bis(1,3-propanediol) ester, dibromo compounds (2,7-dibromo-9,9-dioctylfluorene, DP2 and DT2), 12 mL Tetrahydrofuran (THF) and tetrakis(triphenyl phosphine)palladium(0) $(Pdpph_3)_4$ (0.015 mmol) were added into a dry two neck round bottom flask. Subsequently 5 mL 2M aqueous K_2CO_3 and aliquat 336 (0.025 mmol) were added to the flask. The reaction mixture was degassed thrice by freeze-thaw cycles to remove trace amounts of oxygen completely. The reaction mixture was stirred at 80 °C for 2 days, and iodobenzene was added as an end capper. After 4 hours, benzene boronic acid was dissolved in 1 mL THF and added into the reaction mixture as another end capper and stirring continued further for 4 hours. The reaction mixture was then cooled to room temperature, poured into 100 mL methanol and further stirred at room temperature for 4 hours. The desired polymer was collected by filtration and reprecipitated twice from methanol and acetone. The polymers were further purified by soxhlet filtration with acetone to remove oligomers and catalyst residues. After drying the polymers yield of 53-65% were obtained. The resulted polymers were soluble in common organic solvents.

5.2.3. Poly[2,7-(9,9'-dioctylfluorene)] (PFO)

9,9-Dioctylfluorene-2,7-diboronic acid bis(1,3-propanediol) ester (1) (0.2792 g, 0.5000 mmol) and 2,7-dibromo- 9,9-dioctylfluorene (2) (0.2741 g, 0.5000 mmol) ^{1}H NMR (600 MHz, $CDCl_3$) δ (ppm): ^{13}C NMR (150 MHz, $CDCl_3$) δ (ppm): 7.85 (br, 2H), 7.71 (br, 4H), 2.1 (br, 4H), 1.14 (br, 24H), 0.73 (br, 6H); 152.04, 140.73, 140.24, 126.38, 121.72, 120.18, 55.56, 40.60, 32.01, 30.25, 29.43, 24.14, 22.81, 14.26.

5.2.4. Poly[2,7-(9,9'-dioctylfluorene)-co-4-[5-(4-Fluoren-9-ylidenemethyl-phenyl)-thiophen-2-yl]-7-(4-methoxy-phenyl)-benzo[1,2,5]thiadiazole] (WDP-1)

9,9-Dioctylfluorene-2,7-diboronic acid bis(1,3-propanediol) ester (1) (0.2792 g, 0.5000 mmol), 2,7-dibromo-9,9-dioctylfluorene (2) (0.2740 g, 0.4997 mmol) and 4-{5-[4-(2,7-Dibromo-fluoren-9-ylidenemethyl)-phenyl]-thiophen-2-yl}-7- (4-methoxy-phenyl) ben-zo[1,2,5]thiadiazole (DP2) ($2.2x10^{-4}$ g, 0.0003 mmol) were used in this polymerization. Gel-permeation chromatography GPC: M_n = 16433, PDI = 1.40 (PMMA standards).

5.2.5. Poly[2,7-(9,9'-dioctylfluorene)-co-4-[5-(4-Fluoren-9-ylidenemethyl-phenyl)-thiophen-2-yl]-7-(4-methoxy-phenyl)-benzo[1,2,5]thiadiazole] (WDP-2)

9,9-Dioctylfluorene-2,7-diboronic acid bis(1,3-propanediol) ester (1) (0.2792 g, 0.5000 mmol) 2,7-dibromo-9,9-dioctylfluorene (2) (0.2738 g, 0.4994 mmol) and 4-{5-[4-(2,7-Dibromo-fluoren-9-ylidenemethyl)-phenyl]-thiophen-2-yl}-7- (4-methoxy-phenyl) ben-zo[1,2,5]thiadiazole (DP2) ($4.4x10^{-4}$ g, 0.0006 mmol) were used in this polymerization. GPC: M_n = 16624, PDI = 1.56 (PMMA standards).

5.2.6. Poly[2,7-(9,9'-dioctylfluorene)-co-4-[5-(4-Fluoren-9-ylidenemethyl-phenyl)-thiophen-2-yl]-7-(4-methoxy-phenyl)-benzo[1,2,5]thiadiazole] (WDP-3)

9,9-Dioctylfluorene-2,7-diboronic acid bis(1,3-propanediol) ester (1) (0.2792 g, 0.5000 mmol), 2,7-dibromo-9,9-dioctylfluorene (2) (0.2736 g, 0.499 mmol) and 4-{5-[4-(2,7-Dibromo-fluoren-9-ylidenemethyl)-phenyl]-thiophen-2-yl}-7-(4- methoxy-phenyl) ben-zo[1,2,5]thiadiazole (DP2) ($7.34x10^{-4}$ g, 0.001 mmol) were used in this polymerization. (GPC): M_n = 15733, polydispersity index PDI = 1.34 (PMMA standards).

5.2.7. Poly[2,7-(9,9'-dioctylfluorene)-co-4-(5-Fluoren-9-ylidenemethyl-thiophen-2-yl)-7-(4-methoxy-phenyl)-benzo[1,2,5]thiadiazole] (WDT-1)

9,9-Dioctylfluorene-2,7-diboronic acid bis(1,3-propanediol) ester (1) (0.2792 g, 0.5000 mmol), 2,7-dibromo-9,9-dioctylfluorene (2) (0.2740 g, 0.4997 mmol) and 4-[5-(2,7-Dibromo-fluoren-9-ylidenemethyl)-thiophen-2-yl]-7-(4-methoxyphenyl)-benzo[1,2,5]thiadiazole (DT2) ($1.97x10^{-4}$ g, 0.0003 mmol), were used in this polymerization. GPC: M_n = 17338, PDI = 1.64 (PMMA standards).

5.2.8. Poly[2,7-(9,9'-dioctylfluorene)-co-4-(5-Fluoren-9-ylidenemethyl-thiophen-2-yl)-7-(4-methoxy-phenyl)-benzo[1,2,5]thiadiazole] (WDT-2)

9,9-Dioctylfluorene-2,7-diboronic acid bis(1,3-propanediol) ester (1) (0.2792 g, 0.5000 mmol), 2,7-dibromo-9,9-dioctylfluorene (2) (0.2738 g, 0.4994 mmol) and 4-[5-(2,7-Dibromo-fluoren-9-ylidenemethyl)-thiophen-2-yl]-7-(4-methoxyphenyl)-benzo[1,2,5]thiadiazole (DT2) ($3.95x10^{-4}$ g, 0.0006 mmol), were used in this polymerization. GPC: M_n = 14342, PDI = 1.82 (PMMA standards).

5.2.9. Poly[2,7-(9,9′-dioctylfluorene)-co-4-(5-Fluoren-9-ylidenemethyl-thiophen-2-yl)-7-(4-methoxy-phenyl)-benzo[1,2,5]thiadiazole] (WDT-3)

9,9-Dioctylfluorene-2,7-diboronic acid bis(1,3-propanediol) ester (1) (0.2792 g, 0.5000 mmol) 2,7-dibromo-9,9-dioctylfluorene (2) (0.2736 g, 0.499 mmol) and 4-[5-(2,7-Dibromo-fluoren-9-ylidenemethyl)-thiophen-2-yl]-7-(4-methoxyphenyl)-benzo[1,2,5]thiadiazole (DT2) ($6.58x10^{-4}$ g, 0.001 mmol) were used in this polymerization. GPC: M_n = 16143, PDI = 1.48 (PMMA standards). The all copolymers were showed the same ^{1}H and ^{13}C NMR to the PFO. This is due to the M-DBFs concentrations were too low in the polymer main chain.

5.2.10. WPLEDs Fabrication and characterization

WPLEDs were fabricated using the as synthesized copolymers (WDT & WDP) as active layer. The WPLED device configuration is composed of a pre-cleaned and pre-patterned indium tin oxide (ITO) as the transparent anode. The ITO surface was ultrasonically agitated and cleaned in 2% detergent, acetone and isopropanol, each for five minutes. After cleaning, ~40 nm thin layer of poly (3,4-ethylendioxythiophene) : poly(styrenesulfonate) (PEDOT:PSS) as a hole injecting layer was spin-coated at 3000 rpm for 60 seconds, then baked for 15 minute in argon environment at 130 °C. The copolymers were dissolved in chloro benzene (10 mg/mL) and spin-coated above the PEDOT:PSS layer under ambient atmosphere and thermally treated at 140 °C for 30 minute for the removal of residual solvent. The film thickness of the active layer was ~70 nm. Finally, ~30 nm of TPBi, ~1 nm of LiF and ~100 nm of aluminium (Al) were thermally evaporated at a rate of 2 Å/s, 0.1 Å/s and 10 Å/s, respectively at a base pressure of 10^{-6} mbar as electron transporting as well as hole blocking layer and cathode, respectively. The active area of the diodes was 12 mm^2. The current density versus voltage (J-V) characteristics of the fabricated WPLEDs were measured using Keithley 2400 source meter whereas the luminance and the EL spectra were measured using CS 2000 spectroradiometer. All the devices were fabricated and characterized under Argon atmosphere inside a glove box.

5.3. Results and discussion

5.3.1. Synthesis and Characterization of the Polymers

The model compounds and synthetic route of the copolymers is presented in Scheme 5.1. The monomers DT1, DT2, DP1, DP2, and 2,7-dibromo-9,9′-dioctylfluorene were prepared according to reported procedures.[41,42] The random conjugated copolymers

were synthesized from monomers 1, 2 and DT2 or DP2 using Suzuki coupling polymerization. The copolymer powders were light yellow in color.

5.3.2. Optical Properties

The solid state UV-visible (UV-vis) and photoluminescence (PL) spectra of DT1 and DP1 are shown in Figure 5.1. The DT1 and DP1 showed two absorption bands at 411, 486 and 400, 478 nm, respectively. The bands at shorter wavelength regions result from the π-π* transitions of the monomers, whereas the later bands were due to intramolecular charge transfer (ICT) process.[41] The absorption spectra of monomers had good overlap with the solid state emission spectra of PFO, clearly indicating possible Förster energy transfer from PFO to DT1 and DP1 monomers in the copolymers (Figure 5.1). The DT1 and DP1 monomers exhibited red and orange emissions at 640 and 580 nm with solid state PL quantum yields of 2.6% and 24.2%, respectively.

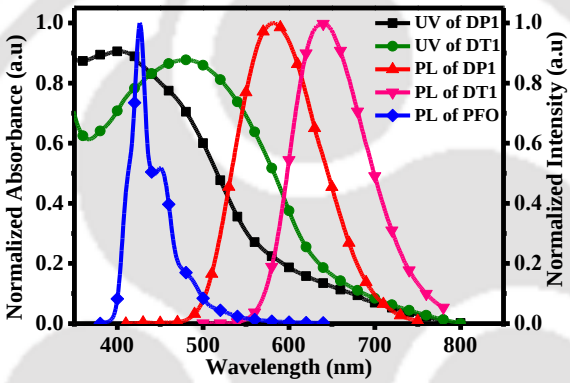

Figure 5.1: UV-vis absorption spectra of DP1 and DT1 and the PL spectra of DP1, DT1, and PFO

The solution and solid state UV-vis spectra of the six copolymers (Figure 5.2a, b) exhibited a single absorption band at ~380 nm which can be attributed to the π-π* transitions of the conjugated PFs main chain. There is no band observed for the monomers (DT1 or DP1) in absorption spectra due to their small feed ratios. The small peak observed in the solid state absorption spectra at ~430 nm was due to the beta phase formation of PFO, assigned to heating of spin coated copolymer thin films.

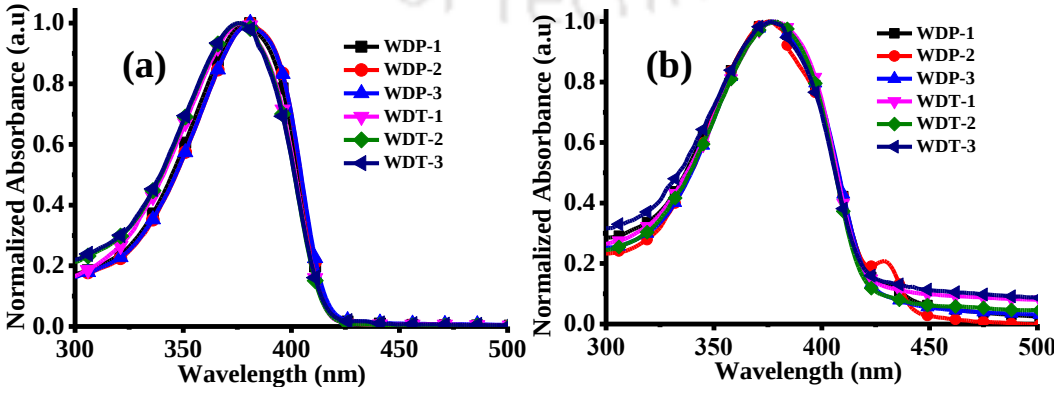

Figure 5.2: UV-vis spectra of copolymers (a) in THF solution and (b) in solid state

PL spectra (Figure 5.3a,b) of the copolymers were recorded in solution as well as solid state at an excitation wavelength of 380 nm. All copolymers show blue emission in the solution state similar to that of PFO due to the fluorene unit. In contrast, the solid state of copolymers shows dominant blue emission from the PFO main chain along with an additional peak in the orange region. The additional peaks observed in solid state PL at 588 nm for DT1 and 567 nm for DP1 are due to the Förster energy transfer from the PFO main chain to DT1 or DP1 monomers. The concentrations of the monomers (DT1 or DP1) were carefully adjusted in the PFO main chain to generate the partial energy transfer from PFO to monomers, thereby achieving the desired white light. As seen in Figure 5.3b, the PL intensity of the copolymers depended on the monomer concentrations in the polymer main chain, and the PL intensity was directly proportional to the monomer concentration. It has been observed that in the copolymer the monomer emission values were blue-shifted (~52 nm for DT1 and ~13 nm for DP1) from their characteristic emission values (Figure 5.3b; ~640 nm for DT1 and ~580 nm for DP1) due to the lower concentration of the monomer ratios in the copolymers. Compared to DP1, the DT1 monomer emission was blue-shifted from 640 to 578 nm. The DT1 monomer exhibited AIEE with predominant J-type aggregation (head to tail interaction) due to the effect of intramolecular planarization and formation of nanoparticles in the aggregated state.[41] When the DT1 monomer was inserted into the polymer main chain, there was no possibility of the head to tail interaction between two DT1 monomers, and hence no J-type arrangement is likely to be formed in the polymer thereby resulting in the blue shift.

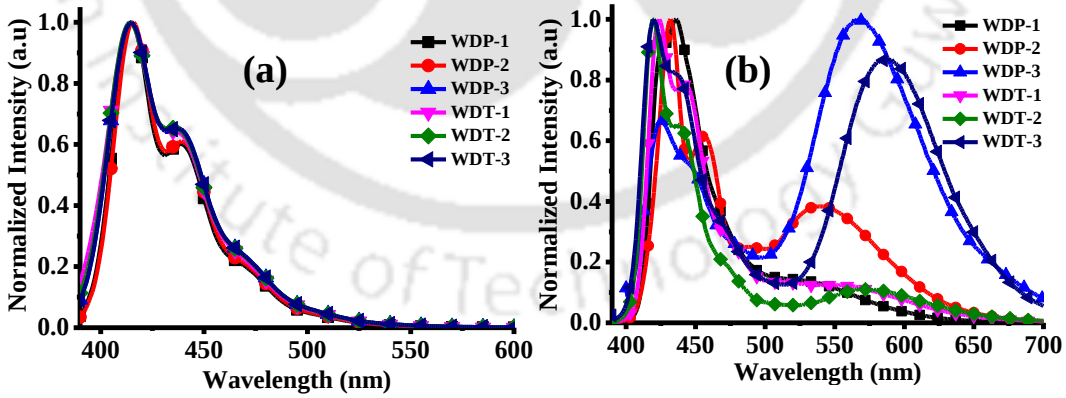

Figure 5.3: PL spectra of copolymers (a) in THF solution and (b) in solid state

5.3.3. Electrochemical Properties

To find out the energy levels of DT1, DP1, and copolymers, CV measurements were done. The CV curves are shown in Figure 5.4, and their reduction and oxidation onset values, energy levels, and band gaps are listed in Table 5.1. The energy levels of the

DT1, DP1, and PFO are presented in Figure 5.5, and energy levels and band gaps are listed in Table 5.2. The HOMO and LUMO values were estimated by submitting the reduction and oxidation onset values in E_{LUMO} = -[(E_{red} - $E_{1/2}$(ferrocene)) + 4.8 eV] and E_{HOMO} = -[(E_{ox} - $E_{1/2}$(ferrocene)) + 4.8 eV].

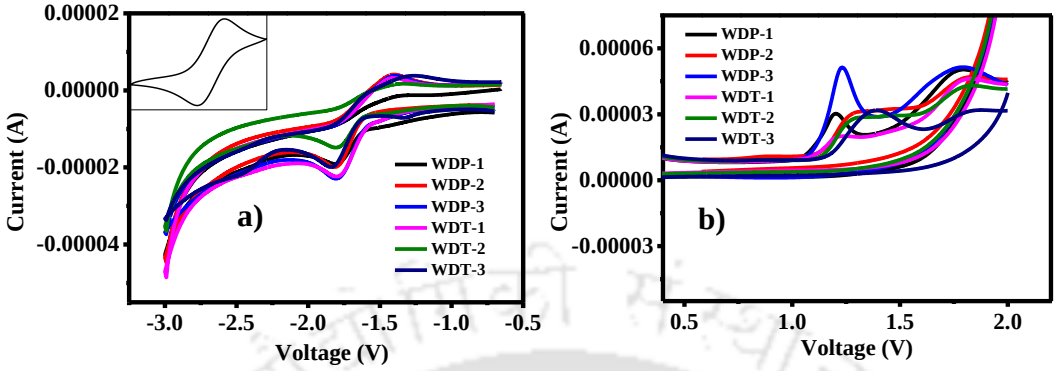

Figure 5.4: (a) Reduction and (b) Oxidation cyclic voltammograms of copolymers. Inset ferrocene standard

Table 5.1: Electrochemical potentials and energy levels of the copolymers

Polymer	E_{ox}/V	E_{red}/V	E_{HOMO}/eV	E_{LUMO}/eV	E_g/eV
WDP-1	1.20	-1.65	-5.60	-2.75	2.85
WDP-2	1.26	-1.67	-5.66	-2.73	2.93
WDP-3	1.22	-1.64	-5.62	-2.76	2.86
WDT-1	1.23	-1.62	-5.63	-2.78	2.85
WDT-2	1.27	-1.70	-5.67	-2.70	2.97
WDT-3	1.29	-1.68	-5.69	-2.72	2.97

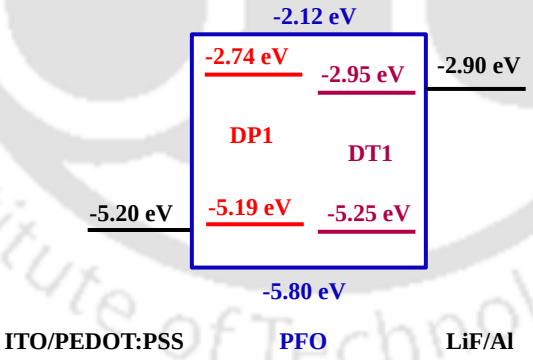

Figure 5.5: Energy levels of DP1, DT1 and PFO

Table 5.2: Photophysical properties and energy levels of the DT1 and DP1 monomers

Monomer	λ max, abs [nm][a]	λ max, PL [nm][a]	Φ_{PL}[%][b]	HOMO [eV]	LUMO [eV]	E_g/eV
DT1	411, 486	640	2.6	-5.25	-2.95	2.30
DP1	400, 478	580	24.2	-5.19	-2.74	2.45

[a]Measured in thin film form. [b]Solid state PL quantum yields are determined using an integrating sphere.

5.3.4. Electroluminescence properties

To explore the EL properties of these copolymers, PLEDs were fabricated with ITO/PEDOT:PSS (40 nm)/WDP or WDT (~70 nm)/TPBi (30 nm) /LiF (1 nm)/Al (100 nm) configuration. Figure 5.6 shows the EL characteristics of the as fabricated WPLEDs. The copolymers exhibited dual emission peaks at blue region from the PFO (432 nm & 462 nm) and orange region from the M-DBFs (554-574 nm for WDP or 578-604 nm for WDT), respectively. The EL spectra exhibited a slight difference in blue region as compared with PL, and much higher intensity of the M-DBFs was observed in the orange region, probably due to the charge trapping effect of M-DBF derivatives.[43] The emission from the copolymers was found to vary from blue to orange and the 2nd peak at orange region was also slightly red shifted, when the M-DBFs content increased from 0.0003-0.001 mol%. Figure 5.7 shows the CIE coordinates of the fabricated WPLEDs in the chromaticity diagram. The EL emission maxima along with their CIE coordinates of the different WPLEDs are listed in Table 5.3. Among all devices, WPLEDs with WDT-1 and WDP-1 copolymers were found to give white emission with CIE coordinates of

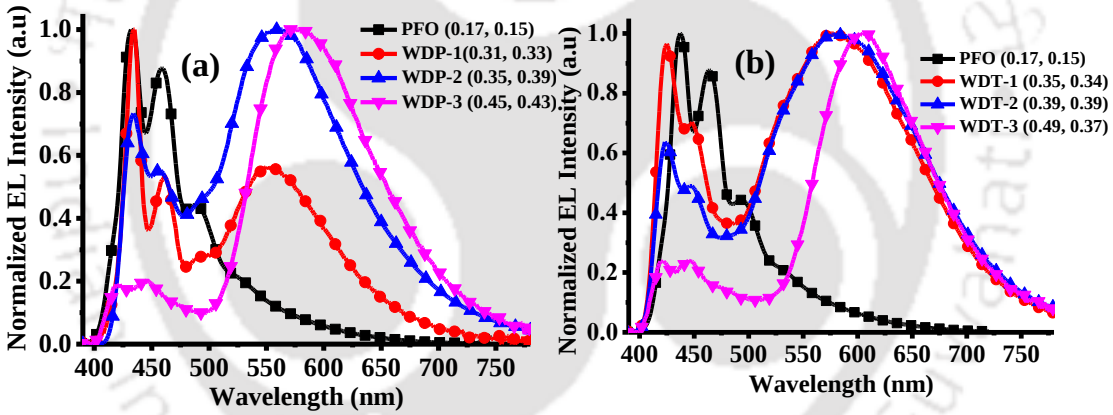

Figure 5.6: EL spectra of a) WDP and b) WDT WPLEDs

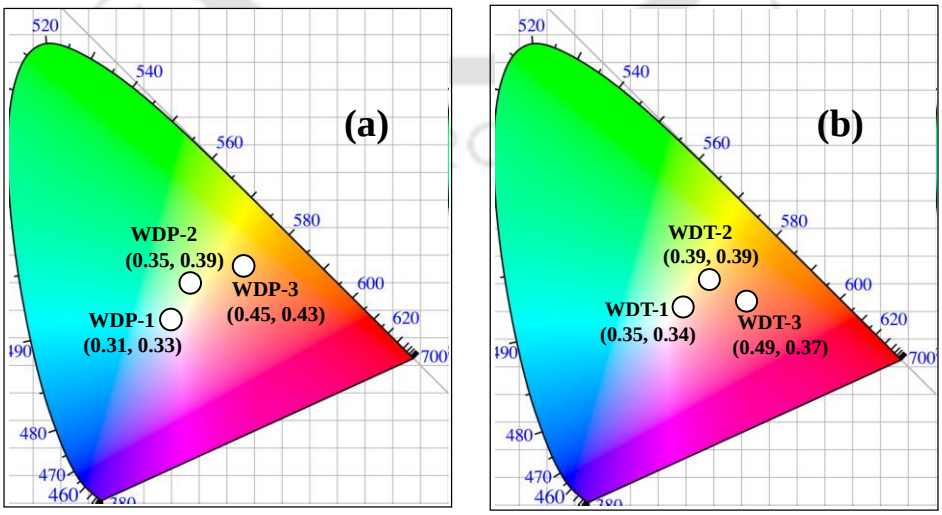

Figure 5.7: CIE Coordinates Diagrams of a) WDP and b) WDT WPLEDs

(0.35, 0.34) and (0.31, 0.33), respectively nearly matching to that of the standard white light (0.33, 0.33). Furthermore, the EL spectra of both WDT-1 and WDP-1 (Figure 5.8a and 5.8b) were very stable and bias-independent when the bias voltage increases from 8 V to 14 V, which is precisely necessary for display applications and fundamentally important. Generally, linear single layer systems have strong π-π interactions, which result in unsaturated EL spectra whereas the above copolymers showed high stability and bias-independent EL, since the copolymer chains did not experience π-π interactions due to the dual state as well as AIEE active fluorophores.

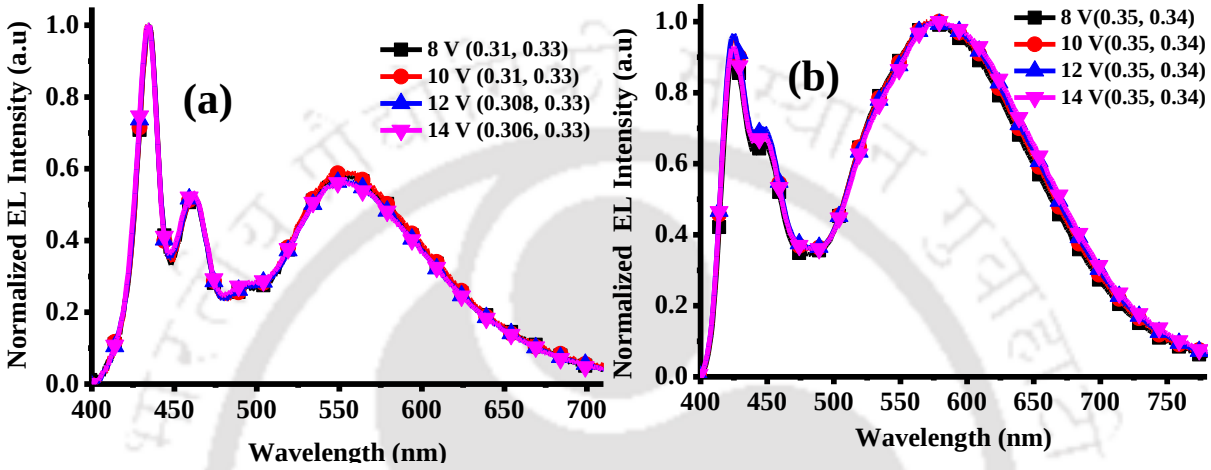

Figure 5.8: Normalized EL of a) WDP-1 and b) WDT-1 WPLEDs at different voltages

Table 5.3: Device characteristics of WPLEDs

Polymer	Onset voltage (V)	EL emission λ_{max} (nm)	Max. Brightness (cd/m^2)	Luminous efficiency (cd/A)	CIEcoordinate (x,y)[a]
WDP-1	4.47	432, 462, 554	9753	7.82	0.31, 0.33
WDP-2	4.68	432, 460, 558	9127	6.63	0.35, 0.39
WDP-3	5.06	421, 445, 574	6654	4.41	0.45, 0.43
WDT-1	4.14	424, 446, 578	7436	4.57	0.35, 0.34
WDT-2	5.01	424, 446, 583	5997	3.84	0.39, 0.39
WDT-3	5.29	420, 445, 604	4559	3.06	0.49, 0.37

[a]Determined from the EL spectrum.

Figure 5.9 shows the Current density v/s Voltage (J-V), Brightness v/s Voltage (B-V) and Luminous Efficiency v/s Brightness (L-B) characteristics of the WPLEDs and their key device parameters are listed in Table 5.3. The brightness and luminous efficiency of the devices are 9753 cd m^{-2} and 7.82cd A^{-1} for WDP-1, 9127 cd m^{-2} and 6.63 cd A^{-1} for WDP-2, 6654 cd m^{-2} and 4.41cd A^{-1} for WDP-3, 7436 cd m^{-2} and 4.5 7cd A^{-1} for WDT-1, 5997 cd m^{-2} and 3.84 cd A^{-1} for WDT-2 and 4559 cd m^{-2} and 3.06 cd A^{-1} for WDT-3. Compared to WDT, WDP copolymers exhibited high brightness and luminous efficiency,

which may be due to the high PL quantum yield of DP1 (Φ_F = 24.2 %) monomer as compared to that of DT1 (Φ_F = 2.6 %) in the solid state.

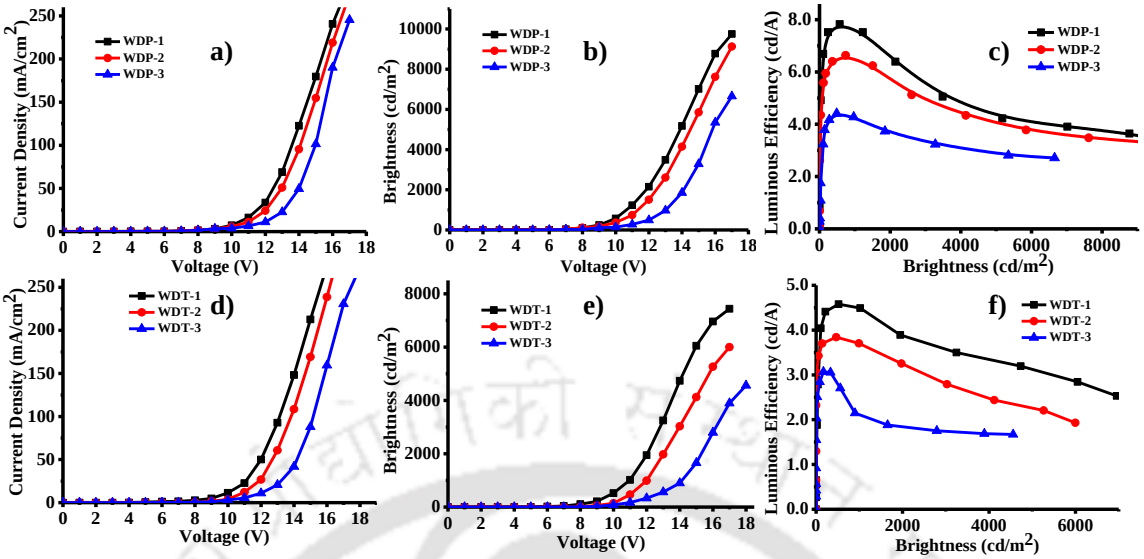

Figure 5.9: Current density v/s Voltage (J-V), Brightness v/s Voltage (B-V) and Luminous Efficiency v/s Brightness (L-B) characteristics of WDP a), b) & c) and WDT d), e) & f) WPLEDs.

5.4. Summary

Bias-independent WPLEDs comprising of two series of stable linear single layer white light emitting copolymers incorporating orange or red emitting special small π-system derivatives of M-DBF (0.0003-0.001 mol%.) into PFO main chain were developed. White light emission was achieved from the single copolymers (WDP-1 & WDT-1) by incorporation of very small amount of DP (0.0003) and DT (0.0003) comonomer ratios in the polymerization mixture. Single layer PLEDs were fabricated using these copolymers, with the configuration ITO/PEDOT:PSS (40 nm)/WDP or WDT (~70 nm)/TPBi (30 nm) /LiF (1 nm)/Al (100 nm). The devices fabricated using WDP-1 and WDT-1 copolymers were found to emit white emission with CIE coordinates of (0.31, 0.33) and (0.35, 0.34) and exhibited highest brightness values of 9753 cd m^{-2} and 7436 cd m^{-2} with a maximum luminous efficiency of 7.82 cd A^{-1} and 4.57 cd A^{-1}, respectively. Importantly, the EL spectra of both WDP-1 and WDT-1 were found to be very stable and bias-independent when the bias voltage increases from 8 V to 14 V. This unique approach to generate stable white emitting from linear single layer copolymers by incorporating AIE active and dual state emitting small π-system luminogen materials in polymer main chain provides a favorable path to fabricate highly efficient WPLEDs using solution processed technique for the first time.

5.5. References

1. Strukelj, M.; Jordan, R. H.; Dodabalapur, A. *J. Am. Chem. Soc.* **1996,** *118*, 1213-1214.
2. Holmes, R. J.; Forrest, S. R.; Tung, Y. J.; Kwong, R. C.; Brown, J. J.; Garon, S.; Thompson, M. E. *Appl. Phys. Lett.* **2003,** *82*, 2422-2424.
3. D'Andrade, B. W.; Forrest, S. R. *Adv. Mater.* **2004,** *16*, 1585-1595.
4. Furuta, P. T.; Deng, L.; Garon, S.; Thompson, M. E.; Frechet, J. M. J. *J. Am. Chem. Soc.* **2004,** *126*, 15388-15389.
5. Wu, H. B.; Ying, L.; Yang, W.; Cao, Y. *Chem. Soc. Rev.* **2009,** *38*, 3391-3400.
6. Furuta, P.; Brooks, J.; Thompson, M. E.; Frechet, J. M. J. *J. Am. Chem. Soc.* **2003,** *125*, 13165-13172.
7. Coppo, P.; Duati, M.; Kozhevnikov, V. N.; Hofstraat, J. W.; De Cola, L. *Angew. Chem. Int. Ed.* **2005,** *44*, 1806-1810.
8. Das, D.; Gopikrishna, P.; Narasimhan, R.; Singh, A.; Dey, A.; Iyer, P. K. *Phys. Chem. Chem. Phys.* **2016,** 18, 33077-33084.
9. Kido, J.; Kimura, M.; Nagai, K. *Science* **1995,** *267*, 1332-1334.
10. Jordan, R. H.; Dodabalapur, A.; Strukelj, M.; Miller, T. M. *Appl. Phys. Lett.* **1996,** *68*, 1192-1194.
11. D'Andrade, B. W.; Brooks, J.; Adamovich, V.; Thompson, M. E.; Forrest, S. R. *Adv. Mater.* **2002,** *14*, 1032-1036.
12. Kido, J.; Hongawa, K.; Okuyama, K.; Nagai, K. *Appl. Phys. Lett.* **1994,** *64*, 815-817.
13. Das, D.; Gopikrishna, P.; Singh, A.; Dey, A.; Iyer, P. K. *ChemistrySelect* **2017,** *2*, 3184-3190.
14. Zhu, M. R.; Zou, J. H.; Hu, S. J.; Li, C. G.; Yang, C. L.; Wu, H. B.; Qin, J. G.; Cao, Y. *J. Mater. Chem.* **2012,** *22*, 361-366.
15. Xu, Q. F.; Duong, H. M.; Wudl, F.; Yang, Y. *Appl. Phys. Lett.* **2004,** *85*, 3357-3359.
16. Das, D.; Gopikrishna, P.; Singh, A.; Dey, A.; Iyer, P. K. *Phys. Chem. Chem. Phys.* **2016,** *18*, 7389-7394.
17. Granstrom, M.; Inganas, O. *Appl. Phys. Lett.* **1996,** *68*, 147-149.
18. Huang, J. S.; Li, G.; Wu, E.; Xu, Q. F.; Yang, Y. *Adv. Mater.* **2006,** *18*, 114-117.
19. Shih, P. I.; Tseng, Y. H.; Wu, F. I.; Dixit, A. K.; Shu, C. F. Stable and Efficient White Electroluminescent Devices Based on a Single Emitting Layer of Polymer Blends. *Adv. Funct. Mater.* **2006,** *16*, 1582-1589.
20. Tasch, S.; List, E. J. W.; Ekstrom, O.; Graupner, W.; Leising, G.; Schlichting, P.; Rohr, U.; Geerts, Y.; Scherf, U.; Mullen, K. *Appl. Phys. Lett.* **1997,** *71*, 2883-2885.
21. Yu, L.; Liu, J.; Hu, S. J.; He, R. F.; Yang, W.; Wu, H. B.; Peng, J. B.; Xia, R. D.; Bradley, D. D. C. *Adv. Funct. Mater.* **2013,** *23*, 4366-4376.
22. Liang, J. F.; Zhao, S.; Jiang, X. F.; Guo, T.; Yip, H. L.; Ying, L.; Huang, F.; Yang, W.; Cao, Y. *ACS Appl. Mater. Interfaces* **2016,** *8*, 6164-6173.
23. Lee, S. K.; Hwang, D. H.; Jung, B. J.; Cho, N. S.; Lee, J.; Lee, J. D.; Shim, H. K. *Adv. Funct. Mater.* **2005,** *15*, 1647-1655.
24. Liu, J.; Zhou, Q. G.; Cheng, Y. X.; Geng, Y. H.; Wang, L. X.; Ma, D. G.; Jing, X. B.; Wang, F. S. *Adv. Mater.* **2005,** *17*, 2974-2978.

25. Luo, J.; Li, X. Z.; Hou, Q.; Peng, J. B.; Yang, W.; Cao, Y. *Adv. Mater.* **2007,** *19*, 1113-1117.
26. Tu, G. L.; Mei, C. Y.; Zhou, Q. G.; Cheng, Y. X.; Geng, Y. H.; Wang, L. X.; Ma, D. G.; Jing, X. B.; Wang, F. S. *Adv. Funct. Mater.* **2006,** *16*, 101-106.
27. Liu, J.; Shao, S. Y.; Chen, L.; Xie, Z. Y.; Cheng, Y. X.; Geng, Y. H.; Wang, L. X.; Jing, X. B.; Wang, F. S. *Adv. Mater.* **2007,** *19*, 1859-1863.
28. Scherf, U.; List, E. J. W. *Adv. Mater.* **2002,** *14*, 477-487.
29. Miteva, T.; Meisel, A.; Knoll, W.; Nothofer, H. G.; Scherf, U.; Muller, D. C.; Meerholz, K.; Yasuda, A.; Neher, D. *Adv. Mater.* **2001,** *13*, 565-570.
30. Liao, L. S.; Fung, M. K.; Lee, C. S.; Lee, S. T.; Inbasekaran, M.; Woo, E. P.; Wu, W. W. *Appl. Phys. Lett.* **2000,** *76*, 3582-3584.
31. Li, B. S.; Li, J.; Fu, Y. Q.; Bo, Z. S. *J. Am. Chem. Soc.* **2004,** *126*, 3430-3431.
32. Lin, W. J.; Chen, W. C.; Wu, W. C.; Niu, Y. H.; Jen, A. K. Y. *Macromolecules* **2004,** *37*, 2335-2341.
33. Li, B. S.; Xu, X. J.; Sun, M. H.; Fu, Y. Q.; Yu, G.; Liu, Y. Q.; Bo, Z. S. *Macromolecules* **2006,** *39*, 456-461.
34. Lai, W. Y.; He, Q. Y.; Zhu, R.; Chen, Q. Q.; Huang, W. *Adv. Funct. Mater.* **2008,** *18*, 265-276.
35. Xia, R. D.; Lai, W. Y.; Levermore, P. A.; Huang, W.; Bradley, D. D. C. *Adv. Funct. Mater.* **2009,** *19*, 2844-2850.
36. Lai, W. Y.; Zhu, R.; Fan, Q. L.; Hou, L. T.; Cao, Y.; Huang, W. *Macromolecules* **2006,** *39*, 3707-3709.
37. Jiu, Y. D.; Liu, C. F.; Wang, J. Y.; Lai, W. Y.; Jiang, Y.; Xu, W. D.; Zhang, X. W.; Huang, W. *Polym. Chem.* **2015,** *6*, 8019-8028.
38. He, R. F.; Xu, J.; Xue, Y.; Chen, D. C.; Ying, L.; Yang, W.; Cao, Y. *J. Mater. Chem. C.* **2014,** *2*, 7881-7890.
39. Ananthakrishnan, S. J.; Varathan, E.; Subramanian, V.; Somanathan, N.; Mandal, A. B. *J. Phys. Chem. C* **2014,** *118*, 28084-28094.
40. Ravindran, E.; Varathan, E.; Subramanian, V.; Somanathan, N. *J. Mater. Chem. C* **2016,** *4*, 8027-8040.
41. Gopikrishna, P.; Iyer, P. K. *J. Phys. Chem. C* **2016,** *120*, 26556-26568.
42. Saikia, G.; Iyer, P. K. *J. Org. Chem.* **2010,** *75*, 2714-2717.
43. Shaheen, S. E.; Kippelen, B.; Peyghambarian, N.; Wang, J. F.; Anderson, J. D.; Mash, E. A.; Lee, P. A.; Armstrong, N. R.; Kawabe, Y. *J. Appl. Phys.* **1999,** *85*, 7939-7945.

Chapter-6

Bridge-Driven Aggregation control in Dibenzofulvene-Naphthalimide Based Donor-Bridge-Acceptor Systems: Enabling Fluorescence Enhancement, Blue to Red Emission and Solvatochromism

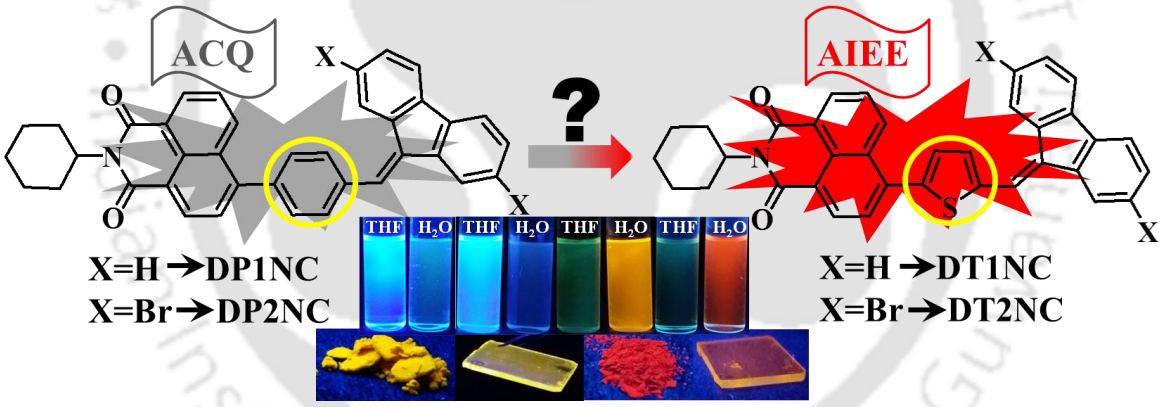

Gopikrishna, P.; Adil, L. R.; Iyer, P. K. *Mater. Chem. Front.* **2017,** DOI: 10.1039/C7QM00357A.

Abstract

Four novel 1,8-naphthalimide (NC) and mono-substituted dibenzofulvene based derivatives have been designed and successfully synthesized. Two luminogens were substituted by thiophene bridge (DT1NC and DT2NC), while the two other luminogens were substituted by phenyl bridge (DP1NC and DP2NC) between NC and dibenzofulvene (DBF) units. This minor structural modification crafts striking changes in the photophysical behavior. DT1NC and DT2NC displayed aggregation induced emission enhancement (AIEE) behavior. They also showed orange and red emission (575 nm and 602 nm), respectively, with large bathochromic shifts (35 nm and 112 nm) and high quantum yields (84.10% and 65.65%) in the aggregated state because of ladder type J-aggregation. DP1NC exhibited weak AIEE behavior in the blue region, while DP2NC showed an AIE inactive nature because of the strong C-H···π intermolecular interactions. All the luminogens showed positive solvatochromism caused by intramolecular charge transfer (ICT). The DT2NC and DP2NC luminogens were substituted with two bromine atoms at the 2,7 positions of the DBF moiety, but unexpectedly only DT2NC showed a strong heavy atom effect. Theoretical and experimental HOMO and LUMO energy levels were estimated by density functional theory and cyclic voltammetry, respectively. All luminogens displayed excellent thermal stabilities and good morphological behavior.

6.1. Introduction

Strong solid state or aggregated state emissive organic luminescent materials have attracted great attention in the field of organic light emitting diodes (OLEDs),[1-4] bio-imaging[5-8] and chemo-sensors.[9-12] Many conventional organic materials have been synthesized and utilized in various fields. Nevertheless, the major problem with these materials are their high emission in dilute solutions, and also they become less or non-emissive in solid or aggregated state due to the occurrence of typical π-π intermolecular interactions, which leads to aggregation caused quenching (ACQ).[13-15] To overcome this problem a new class of organic materials have been developed by Tang et al. (2001) that displayed exactly opposite property to that of ACQ materials.[16] These materials exhibited unique properties i.e., less or non-fluorescent in the solution state but highly emissive in the solid state or aggregated state. In solution state free intramolecular rotations are highly probable when molecules go to excited state by absorbing energy. Thus, the absorbed energy was consumed for intermolecular rotations leading to non-radiative relaxation pathways while coming back to the ground state.[17] These materials possess non-planar or propeller shaped structures. In solid state or aggregated state free intramolecular rotations are restricted by the phenomena called restriction of intramolecular rotation (RIR). Because of the non-planarity they cannot come close to each other which leads to high emission in the solid state or aggregated state. Another interesting aggregation induced emission enhancement (AIEE) phenomena has been reported by Park et al. (2002).[18] These luminescent materials have an advantage of emitting in both solution as well as in solid state, but compared to solution state the fluorescence emission or quantum yields are higher in the solid state or aggregated state. Many of the AIEE active materials have been prepared by different mechanisms such as J-type aggregation, activated phosphorescence and excimer formation. To date, several AIE and AIEE active materials have been reported, but those are mainly based on tetraphenylethelene (TPE),[19-21] silole[16,22-25] and phenothiazine derivatives.[26,27] However, very few reports are available in literature on DBF derivatives. DBFs are of two types based on the substituents at the 9th position i.e., di-substituted and mono-substituted DBFs. Most of them are based on di-substituted DBFs and their optical properties are limited to blue to green wavelength region. Mono-substituted DBF derivatives possess unique optical characteristics that are rather unusual and

overlooked.[28] Previous results divulged that depending on the substituent on the DBF, the luminogens exhibited diverse and exceptional photophysical properties. In addition, 1,8-naphthalimide and its derivatives have great advantages in the field of OLEDs[29-31] and bio-imaging,[32,33] because of their good thermal stability, photostability and high fluorescence quantum yields. Recently, AIEE active luminogens based on 1,8-naphthalimide derivatives have also been reported.[34-37] The photophysical, electrochemical and thermal properties of the 1,8-naphthalimide can be varied depending on the substituents. It is a well-known that introduction of an electron donating group at the 4th position of the 1,8-naphthalimde molecule bestows it with high fluorescence.[38] In the past decades, few donor molecules with triphenyl amine, carbazole, TPE etc. have been developed.[29,36,39,40] Therefore, it is necessary to design and develop new materials possessing strong electron donors as well as exhibiting high fluorescence in solid state. In this chapter, four novel organic molecules, designed and synthesised via simple condensation and Suzuki coupling reactions based on mono-substituted DBFs and 1,8-naphthalimide derivatives. These luminogens exhibit AIEE active phenomena, heavy atom effect and solvatochromism. The emission colors were successfully tuned from blue to red region because of the electron donating ability of the donor at the 4th positon of 1,8-nathpthalimide moiety. Two thiophene substituted DBFs (DT1NC and DT2NC) and two phenyl substituted DBFs (DP1NC and DP2NC) as donor substituents were chosen in this study. The thiophene substituted DBFs exhibit unique AIEE phenomena with large bathochromic shift and high florescence quantum yields in the aggregated state. On the other hand, the phenyl substituted DBFs showed high fluorescence quantum yields in solution state and less or no emission in the aggregated state. The bromine substituted luminogens greatly influenced the photophysical, thermal and electrochemical properties and also exhibited solvatochromism. Density functional theory (DFT) was used to compute the ground state optimization. Time-dependent density functional theory (TD-DFT) method was utilized to estimate the absorption spectra and excitation energies for all the luminogens.[41,42]

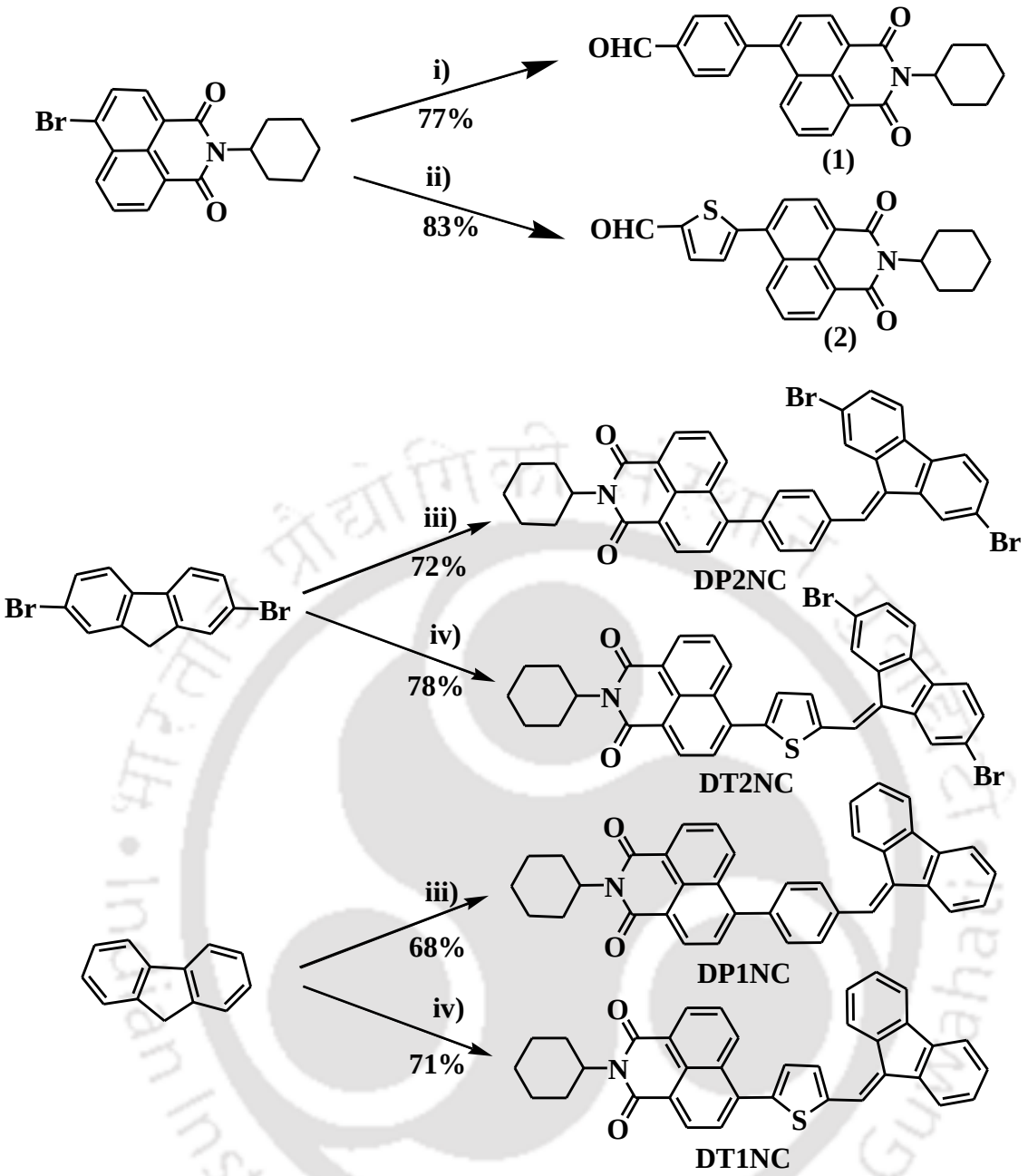

Scheme 6.1: Synthetic route for Monomers. i) 4-Formylphenylboronic acid, $Pd(PPh_3)_4$, 2M K_2CO_3, THF, 12 h, 80 °C ii) 5-Formylthiophene-2-boronic acid, $Pd(PPh_3)_4$, 2M K_2CO_3, THF, 12 h. 80 °C iii) Compound (1) and EtOH, Potassium tert-butoxide, Reflux, 12 h. iv) Compound (2) and EtOH, Potassium tert-butoxide, Reflux, 12 h.

6.2. Experimental section

6.2.1. Materials and Instrumentation

4-bromo-1,8-naphthalicanhydride, cyclohexyl amine, 9H-fluorene, 2,7-Dibromofluorene, 5-formylthiophene-2 -boronicacid, 4-formyl phenyl boronic acid, tetrakis(triphenylphosphine)palladium(0) and potassium tert-butoxide were purchased from Sigma-Aldrich India and used without further purification. Anhydrous tetrahydrofuran (THF) was obtained by drying over sodium/ benzophenone and all

solvents were used after distilled. The ^{1}H and ^{13}C NMR spectra were recorded on Bruker 600 MHz NMR spectrometer. HRMS spectra were recorded on a waters (Micro mass MSTechnologies) Q-Tof MS Analyzer Spectrometer. UV-visible spectra were measured by PerkinElmer, Model Lambda-25 spectrometer. Photoluminescence (PL) spectra were recorded with Varian Cary Eclipse spectrometer. Field emission scanning electron microscopy (FE-SEM) experiments were carried out on a Carl Zeiss, SIGMA VP instrument. The dynamic light scattering (DLS) studies were done using Zetasizer Nano series Nano-ZS90 instrument.

6.2.2. Synthesis of 4-(2-Cyclohexyl-1,3-dioxo-2,3-dihydro-1H-benzo[de]isoquinolin-6-yl)-benzaldehyde (1)

A mixture of N-cyclohexy6-Bromo-2-cyclohexyl-benzo[de]isoquinoline-1,3-dione (1.eq), 4-Formylphenylboronic acid (1.2 eq), 12 mL of THF and tetrakis(triphenyl phosphine)palladium(0) (0.015 eq) were added into a dry two neck round bottom flask. Subsequently 4 mL 2M aqueous potassium carbonate was added to the flask. The reaction mixture was stirred at 80 °C for 12 hours under argon atmosphere. The reaction mixture was then cooled to room temperature. After work up, the mixture was purified by column chromatography to give white color **compound 1**. (Yield: 77%); ^{1}H NMR (600 MHz, $CDCl_3$) δ (ppm): 10.15 (s, 1H), 8.62 (dd, *J*=6 Hz, 6 Hz 2H), 8.14 (d, *J*=6 Hz, 1H), 8.07 (d, *J*=12 Hz, 2H), 7.70 (m, 4H), 5.04 (m, 1H), 2.56 (m, 2H), 1.89 (m, 2H), 1.75 (m, 2H), 1.45 (m, 2H), 1.33 (m, 2H), ^{13}C NMR (150 MHz, $CDCl_3$) δ (ppm): 191.8, 164.7, 164.5, 145.2, 144.9, 136.3, 131.7, 130.8, 130.7, 130.1, 129.7, 128.8, 128.0, 127.4, 123.8, 123.39, 54.1, 29.3, 26.7, 25.6. HRMS (ESI): m/z $[M + H]^+$ calcd: 384.1600; found: 384.1606.

6.2.3. Synthesis of 5-(2-Cyclohexyl-1,3-dioxo-2,3-dihydro-1H-benzo[de]isoquinolin-6-yl)-thiophene-2-carbaldehyde (2)

A mixture of 6-Bromo-2-cyclohexyl-benzo[de]isoquinoline-1,3-dione (1 eq), 5-formylthiophene-2-boronic acid (1.2 eq), 12 mL of THF and tetrakis(triphenyl phosphine)palladium(0) (0.015 eq) were added into a dry two neck round bottom flask. Subsequently 4 mL 2M aqueous potassium carbonate was added to the flask. The reaction mixture was stirred at 80 °C for 12 hours under argon atmosphere. The reaction mixture was then cooled to room temperature. After work up, the mixture was purified by column chromatography to give light green color solid **compound 2**. (Yield: 83%); ^{1}H NMR (600 MHz, $CDCl_3$) δ (ppm): 10.01 (s, 1H), 8.64 (d, *J*=6 Hz, 1H), 8.60 (d, *J*=6 Hz, 1H), 8.49 (d, *J*=6 Hz, 1H), 7.89 (d, *J*=6 Hz, 1H), 7.84 (d, *J*=6 Hz, 1H), 7.79 (t, 1H), 7.43 (d, *J*= 6 Hz, 1H), 5.03 (m, 1H), 2.55 (m, 2H), 1.90 (m, 2H), 1.75 (m, 2H), 1.44 (m, 2H), 1.34 (m,

2H),^{13}C NMR (150 MHz, $CDCl_3$) δ (ppm): 182.8, 164.5, 164.2, 149.5, 145.2, 137.1, 136.3, 131.6, 131.2, 130.4, 129.7, 129.0, 128.9, 127.9, 126.6, 124.1, 124.0, 54.2, 29.3, 26.7, 25.6. HRMS (ESI): m/z $[M + H]^+$: calcd: 390.1164; found: 390.1153.

6.2.4. Synthesis of 2-Cyclohexyl-6-[4-(2,7-dibromo-fluoren-9-ylidenemethyl)-phenyl]-benzo[de]isoquinoline-1,3-dione (DP2NC)

A mixture of potassium tert-butoxide (1.2 eq) and 2,7-Dibromo-9H-fluorene (1.2 eq) was dissolved in 15 mL absolute ethanol. The resulting solution was refluxed for 1 hour than compound 1 (1 eq) was added into reaction mixture and again refluxed for 24 hours. The solvent was removed, and the residue was extracted with Chloroform. The solvent was evaporated. The residue was purified by column chromatography to give product as a yellow color solid compound **DP2NC**. (Yield: 72%); ^{1}H NMR (600 MHz, $CDCl_3$) δ (ppm): 8.66 (d, *J*=6 Hz, 1H), 8.63 (d, *J*=6 Hz, 1H), 8.34 (d, *J*=6 Hz, 1H), 7.94 (s, 1H), 7.79 (m, 2H), 7.74 (m, 4H), 7.64 (d, 2H), 7.57 (d, *J*=6 Hz, 2H), 7.53 (d, *J*=6 Hz, 1H), 7.47 (d, *J*=6 Hz, 1H), 5.07 (m, 1H), 2.59 (m, 2H), 2.04 (m, 2H), 1.93 (m, 2H), 1.49 (m, 4H), ^{13}C NMR (150 MHz, $CDCl_3$) δ (ppm): 164.8, 164.7, 139.5, 139.4, 138.1, 137.3, 136.2, 132.2, 131.6, 131.3, 130.8, 130.5, 129.6, 129.0, 128.0, 127.7, 127.3, 124.0, 121.58, 121.3, 121.2, 121.0, 114.2, 54.0, 29.3, 26.7, 25.6. HRMS (ESI): m/z $[M + H]^+$: calcd: 690.0466; found: 690.0455.

6.2.5. Synthesis of 2-Cyclohexyl-6-[5-(2,7-dibromo-fluoren-9-ylidenemethyl)-thiophen-2-yl]-benzo[de]isoquinoline-1,3-dione (DT2NC)

A mixture of potassium tert-butoxide (1.2 eq) and 2,7-Dibromo-9H-fluorene (1.2 eq) was dissolved in 15 mL absolute ethanol. The resulting solution was refluxed for 1 hour than compound 2 (1 eq) was added into reaction mixture and again refluxed for 18 hours. The solvent was removed, and the residue was extracted with Chloroform. The solvent was evaporated. The residue was purified by column chromatography to give product as a orange color solid compound **DT2NC.** (Yield: 78%); ^{1}H NMR (600 MHz, $CDCl_3$) δ (ppm): 8.71 (d, *J*= 12 Hz, 1H), 8.65 (d, *J*= 12 Hz, 1H), 8.61 (d, *J*= 12 Hz, 1H), 8.43 (s, 1H), 7.89 (m, 2H), 7.82 (t, 1H), 7.64 (s, 1H), 7.54 (m, 4H), 7.43 (d, *J*= 6 Hz, 1H), 5.05 (m, 1H), 2.57 (m, 2H), 1.90 (m, 2H), 1.75 (m, 2H), 1.43 (m, 4H), ^{13}C NMR (150 MHz, $CDCl_3$) δ (ppm): 164.7, 164.4, 143.0, 140.4, 139.4, 137.8, 137.0, 135.1, 132.1, 131.8, 131.6, 131.5, 131.2, 130.7, 129.8, 129.6, 129.1, 128.8, 127.7, 127.6, 123.8, 121.5, 121.4, 121.3, 121.2, 120.7, 54.1, 29.3, 26.7, 25.6. HRMS (ESI): m/z $[M + H]^+$: calcd: 696.0030; found: 696.0033.

6.2.6. Synthesis of 2-Cyclohexyl-6-(4-fluoren-9-ylidenemethyl-phenyl)-benzo[de]isoquinoline-1,3-dione (DP1NC)

A mixture of potassium tert-butoxide (1.2 eq) and 9H-fluorene (1.2 eq) was dissolved in 15 mL absolute ethanol. The resulting solution was refluxed for 1 hour than compound 1 (1 eq) was added into reaction mixture and again refluxed for 18 hours. The solvent was removed, and the residue was extracted with Chloroform. The solvent was evaporated. The residue was purified by column chromatography to give product as a yellow color solid compound **DP1NC**. (Yield: 68%); ^{1}H NMR (600 MHz, $CDCl_3$) δ (ppm): 8.66-8.63 (dd, *J*= 6 Hz, *J*= 6 Hz, 2H), 8.34 (d, *J*= 12 Hz, 1H), 7.83 (d, 1H), 7.77 (m, 3H), 7.75 (m, 5H), 7.60 (d, *J*= 6 Hz, 2H), 7.40 (t, 1H), 7.36 (m, 2H), 7.13 (t, 1H), 5.07 (m, 1H), 2.59 (m, 2H), 1.91 (m, 2H), 1.77 (m, 2H), 1.45 (m, 4H), ^{13}C NMR (150 MHz, $CDCl_3$) δ (ppm): 164.9, 164.7, 146.1, 139.6, 139.4, 138.7, 137.3, 136.5, 134.8, 132.2, 131.3, 130.9, 130.2, 130.0, 129.9, 129.2, 129.0, 128.6, 128.1, 127.3, 127.1, 126.9, 126.3, 124.5, 120.5, 120.1, 119.8, 54.0, 29.3, 26.7, 25.7. HRMS (ESI): m/z $[M + H]^+$: calcd: 532.2277; found: 532.2301.

6.2.7. Synthesis of 2-Cyclohexyl-6-(5-fluoren-9-ylidenemethyl-thiophen-2-yl)-benzo[de]isoquinoline-1,3-dione (DT1NC)

A mixture of potassium tert-butoxide (1.2 eq) and 9H-fluorene (1.2 eq) was dissolved in 15 mL absolute ethanol. The resulting solution was refluxed for 1 hour than compound 2 (1 eq) was added into reaction mixture and again refluxed for 18 hours. The solvent was removed, and the residue was extracted with Chloroform. The solvent was evaporated. The residue was purified by column chromatography to give product as a orange solid compound **DT1NC.** (Yield: 71%);^{1}H NMR (600 MHz, $CDCl_3$) δ (ppm): 8.72 (d, *J*= 12 Hz, 1H), 8.63 (d, *J*= 12 Hz, 1H), 8.61 (d, *J*= 12 Hz, 1H), 8.30 (d, *J*= 12 Hz, 1H), 7.89 (d, *J*= 12 Hz, 1H), 7.75 (m, 4H), 7.64 (s, 1H), 7.59 (d, *J*= 6 Hz, 1H), 7.37 (m, 4H), 7.25 (m, 1H), 5.05 (m, 1H), 2.58 (m, 2H), 1.88 (m, 2H), 1.77 (m, 2H), 1.42 (m, 4H), ^{13}C NMR (150 MHz, $CDCl_3$) δ (ppm): 164.7, 164.5, 141.8, 141.7, 139.6, 138.2, 136.2, 131.9, 131.5, 131.4, 130.7, 130.7, 130.5, 130.4, 129.4, 129.3, 129.1, 128.7, 128.7, 127.5, 127.3, 127.1, 124.6, 120.4, 120.1, 119.1, 118.1, 118.0, 54.1, 29.3, 26.7, 25.6. HRMS (ESI): m/z calcd: 538.1841; found: 538.1844.

6.2.8. Crystal Data

Table 6.1: Structure determination summary of **DP1NC** and **DP2NC**

Compound	DP1NC	DP2NC
Empirical formula	$C_{38}H_{29}NO_2$	$C_{38}H_{27}Br_2NO_2$
CCDC NO	1525968	1525969
Formula weight	531.62	689.41
Temperature/K	296 (2)	296 (2)
Crystal system	monoclinic	monoclinic
Space group	P 2_1/c	C 2/c
a/Å	11.2762(6)	19.610(2)
b/Å	13.9376(8)	15.469(2)
c/Å	17.8045(11)	20.516(2)
α/°	90.00	90.00
β/°	101.143(4)	107.135(11)
γ/°	90.00	90.00
Volume/Å^3	2745.5(3)	5947.2(12)
Z	4	8
ρ_{calc}mg/mm^3	1.286	1.540
m/mm^{-1}	0.079	2.763
F(000)	1120.0	2784.0
Crystal size/mm^3	0.28 × 0.24 × 0.21	0.28 × 0.24 × 0.21
2Θ range for data collection	3.74 to 50°	3.42 to 50°
Index ranges	$-13 \le h \le 12$, $-16 \le k \le 16$, $-21 \le l \le 20$	$-17 \le h \le 23$, $-18 \le k \le 18$, $-24 \le l \le 24$
Reflections collected	26930	32449
Independent reflections	4837[R(int) = 0.0712]	5249[R(int) = 0.0866]
Data/restraints/parameters	4837/0/370	5249/0/388
Goodness-of-fit on F^2	0.978	0.985
Final R indexes [I>=2σ (I)]	R1 = 0.0545, wR2 = 0.1472	R1 = 0.0436, wR2 = 0.1186
Final R indexes [all data]	R1 = 0.1213, wR2 = 0.1844	R1 = 0.1421, wR2 = 0.1870

6.3. Results and discussion

6.3.1. Synthesis and characterization

The model structures of DT1NC, DT2NC, DP1NC and DP2NC are shown in Scheme 6.1 and synthesized using the Suzuki coupling reaction followed by condensation reactions in good yields. All the synthesized compounds were characterized well by ^{1}H, ^{13}C NMR, high resolution mass spectrometry (HRMS) and single crystal X-ray analysis (DP1NC and DP2NC).

6.3.2. Solvatochromism

It is well accepted that the donor-acceptor organic systems readily offer solvatochromic phenomenon. The UV-visible and photoluminescence (PL) spectra

of luminogens were studied in various organic solvents such as hexane, toluene, DCM, acetonitrile, DMF and DMSO. The solvatochromic study was performed by changing solvents from non-polar (hexane) to polar (DMSO) with a constant concentration (10 μM) for all luminogens. Figure 6.1 shows the absorption spectra of all luminogens. The absorption values summarized in Table 6.2 depict that among all the luminogens, DTNC (DT1NC and DT2NC) exhibited two absorption bands, the former band (343 to 350 nm and 355 to 361 nm for DT1NC and DT2NC, respectively) was attributed to the π-π* transition and the latter band (392 to 425 nm and 392 to 419 nm for DT1NC and DT2NC, respectively) indicated the intramolecular charge transfer (ICT). DPNC (DP1NC and DP2NC) luminogens showed a single broad absorption band (350 to 362 nm for DP1NC and 352 to 362 nm for DP2NC).

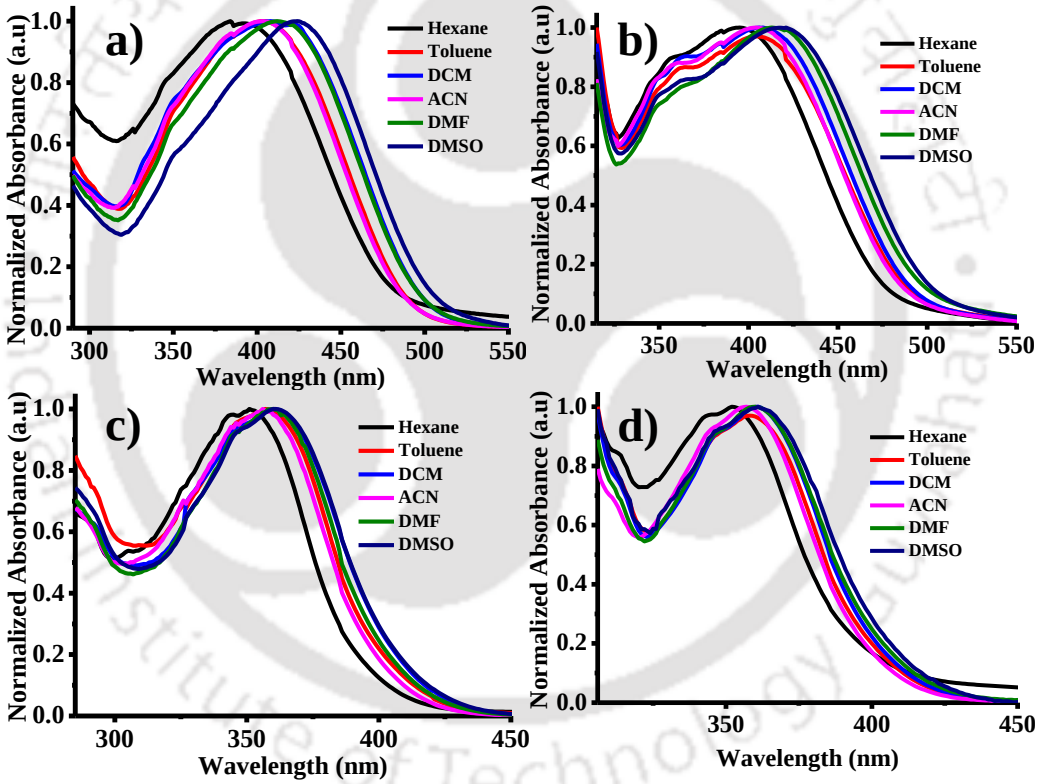

Figure 6.1: UV-visible spectra of the (a) DT1NC, (b) DT2NC, (c) DP1NC and (d) DP2NC in different solvents.

The absorption bands were gradually red-shifted for all the luminogens on changing the solvent polarity from non-polar to polar. The PL spectra of all luminogens are displayed in Figure 6.2 and the emission values are presented in Table 6.2 in different solvents. Interestingly, for all the luminogens, with an increase in polarity from hexane to DMSO, the emission peaks red-shifted remarkably from 522 to 572 nm (50 nm) for DT1NC, from 426 to 500 nm (74 nm)

for DT2NC, from 402 to 435 nm (33 nm) for DP1NC and from 397 to 432 nm (35 nm) for DP2NC. The DT1NC and DT2NC luminogens showed two peaks for almost all the solvents. The peak at the lower wavelength region is due to the locally excited state of the NC moiety and that at the higher wavelength region is due to the ICT between mono-substituted DBF and NC. As shown in Figure 6.2, the DT2NC luminogen does not exhibit the ICT band in hexane, toluene and DCM solvents, but in DT1NC, the intensity of the locally excited emission band is reduced. This significant change is observed because of bromine atoms on the DBF moiety. The bromine atoms act as weak withdrawing groups because of which the donating capacity of the DBF is reduced.

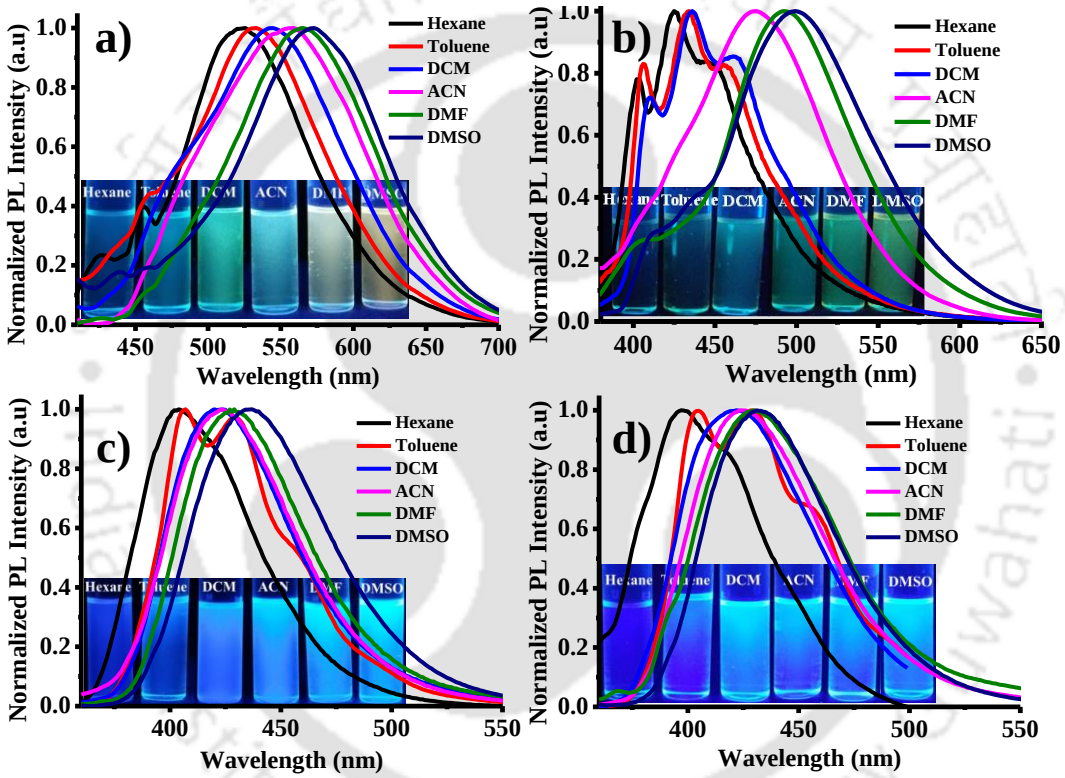

Figure 6.2: PL spectra of the (a) DT1NC, (b) DT2NC, (c) DP1NC and (d) DP2NC in different solvents. The photographs were taken under 365 nm UV lamp.

Surprisingly, the emission intensity is enhanced by changing the solvent polarity from hexane to DMSO, particularly in brominated (DT2NC and DP2NC) luminogens. Normally, in a solvatochromic phenomenon, when the solvent polarity is increased, the emission intensity decreases. It is well known that for 1,8-naphthalimide derivatives, the triplet and singlet states can be arranged according to the polarity of the solvent.[43,44] In non-polar solvents, the triplet state T2 becomes lower than the singlet state S1, facilitating an efficient intersystem crossing (ISC) process. Therefore, in the presence of heavy (bromine) atoms, the fluorescence

intensity gets completely quenched, promoting efficient ISC. As the polarity of the solvent is changed from non-polar to polar, the T2 state shifts to higher energies, and then the ISC process decreases, resulting in an increase in the fluorescence intensity. For better visibility of the emission colors and intensity, the luminogens were dissolved in different solvents and the images were captured using 365 nm UV lamp irradiation (Figure 6.2). Surprisingly, both absorption and PL peaks were blue-shift as observed in DT2NC compared to DT1NC for all the solvents. In particular, a greater blue-shift was observed in PL spectra, for example 96 nm for hexane, 101 nm for toluene, 108 nm for DCM, 82 nm for acetonitrile, 73 nm for DMF and 72 nm DMSO. When closely examined, both luminogens (Scheme 6.1) i.e. DT1NC and DT2NC are structurally identical but the DT2NC luminogen possesses two extra bromine atoms. Since the bromine atom acts as weak withdrawing group, on introducing the two bromine atoms on the DBF moiety (DT2NC), the donating capacity of the DBF decreases. However, in DPNC luminogens i.e., from DP1NC to DP2NC a great difference was not observed in both absorption and PL spectra.

Table 6.2: Photophysical properties of all luminogens in different solvents.

Monomer	**DT1NC**		**DT2NC**		**DP1NC**		**DP2NC**	
	λ_{max}, abs [nm]	λ_{max}, PL [nm]	λ_{max}, abs [nm]	λ_{max}, PL [nm]	λ_{max}, abs [nm]	λ_{max}, PL [nm]	λ_{max}, abs [nm]	λ_{max}, PL [nm]
Hexane	343, 392	522	355, 392	426	350	402	352	397
Toluene	347, 403	532	356, 403	431	356	406	357	405
DCM	347, 408	543	360, 407	435	358	422	359	421
ACN	347, 404	554	360, 403	472	358	424	357	423
DMF	348, 416	565	361, 414	492	360	428	359	429
DMSO	350, 425	571	361, 419	500	362	435	362	432

Thus, the bromine atoms do not affect DP2NC as much as affect DT2NC. This is because in DPNC luminogens, the DBF moiety does not acting as a strong donor unit. This majorly due to the fact that the phenyl bridge unit is present almost orthogonally between 1,8-naphthalimide (NC) and the DBF moiety, which reduces the effective conjugation length towards the NC from DBF.[45]

6.3.3. Aggregation Induced Emission Enhancement (AIEE) Properties

To realize the AIEE active or inactive behavior of all the luminogens, a good solvent (THF) and a poor solvent (water) were selected. The concentration of

all the luminogens were kept constant (i.e. 50 μM). Thereafter, UV-visible and PL spectra were recorded by varying the water fraction (*fw*) in THF.

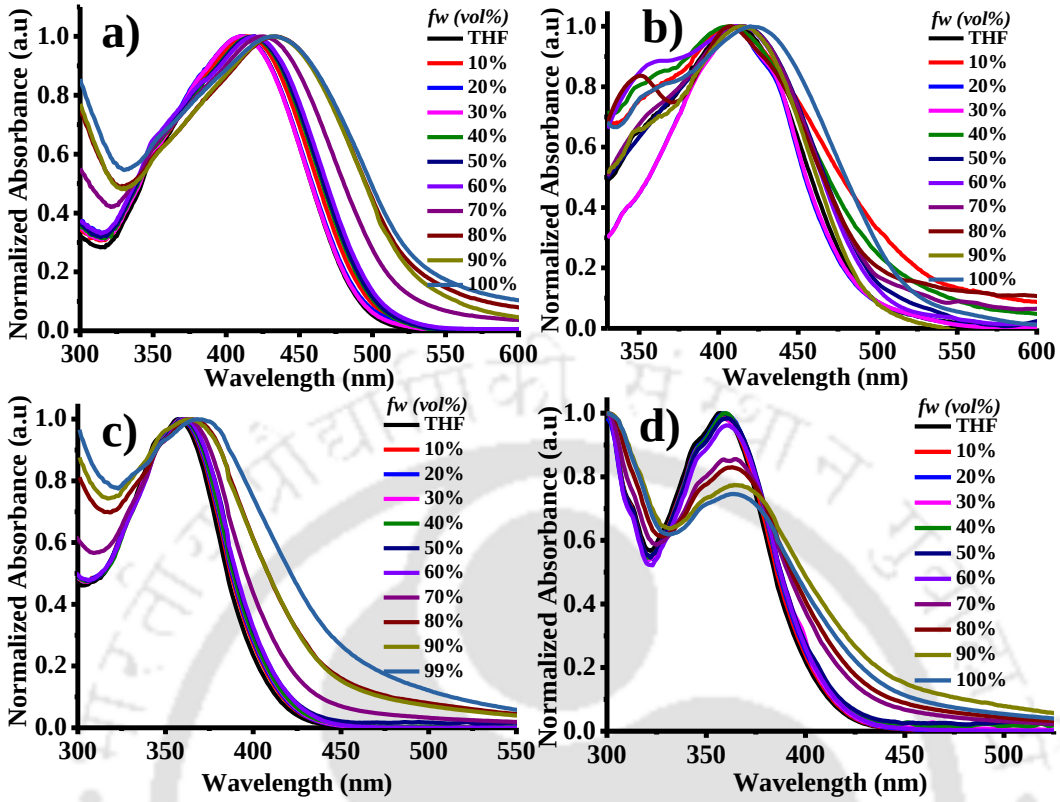

Figure 6.3: UV-visible spectra of the (a) DT1NC, (b) DT2NC, (c) DP1NC and (d) DP2NC in THF and water mixtures.

The UV-visible spectra were studied by increasing the *fw* in the THF solution from 0% to 99%. As mentioned earlier, the DTNC luminogens showed two bands, one at the shorter wavelength region for π-π* transition and the second for ICT. On the contrary, the two DPNC luminogens showed single band only for π-π* transition. Figure 6.3 explains that when *fw* is varied from 0% to 99% the absorption peak gradually shifted towards longer wavelength region (22 nm for DT1NC, 14 nm DT2NC, 11 nm for DP1NC and 8 nm for DP2NC). This might be due to the increasing solvent polarity or formation of J-type aggregation. Similarly, the PL spectra were studied for all luminogens by increasing *fw* in THF solution (Figure 6.4). Surprisingly, it was noticed that both DTNC luminogens exhibited the strong AIEE active behavior and the remaining two DPNC luminogens displayed the ACQ behavior. It is to be noted that both DT1NC and DT2NC luminogens exhibited weak emission with less quantum yields of 9.35 % for DT1NC and 5.46 % for DT2NC in THF. This might be due to the intermolecular rotation of DBF moiety and thiophene. On increasing *fw* from 0% to 99% the emission intensity

gradually increases and the peaks were red-shifted. In 99% *fw* the luminogens exhibited strong fluorescence with high quantum yields of 84.10% for DT1NC and 65.65% for DT2NC. These results clearly reveal that on increasing the *fw* in the THF solution, the formation of nanoparticles was initiated (which were confirmed by FE-SEM and DLS measurements). For both luminogens, the emission peaks were red-shifted from THF to water (99%), for DT1NC 35 nm red-shifted from 540 nm to 575 nm and for DT2NC it was 112 nm red-shifted from 490 nm to 602 nm because of the formation of J-type aggregation.

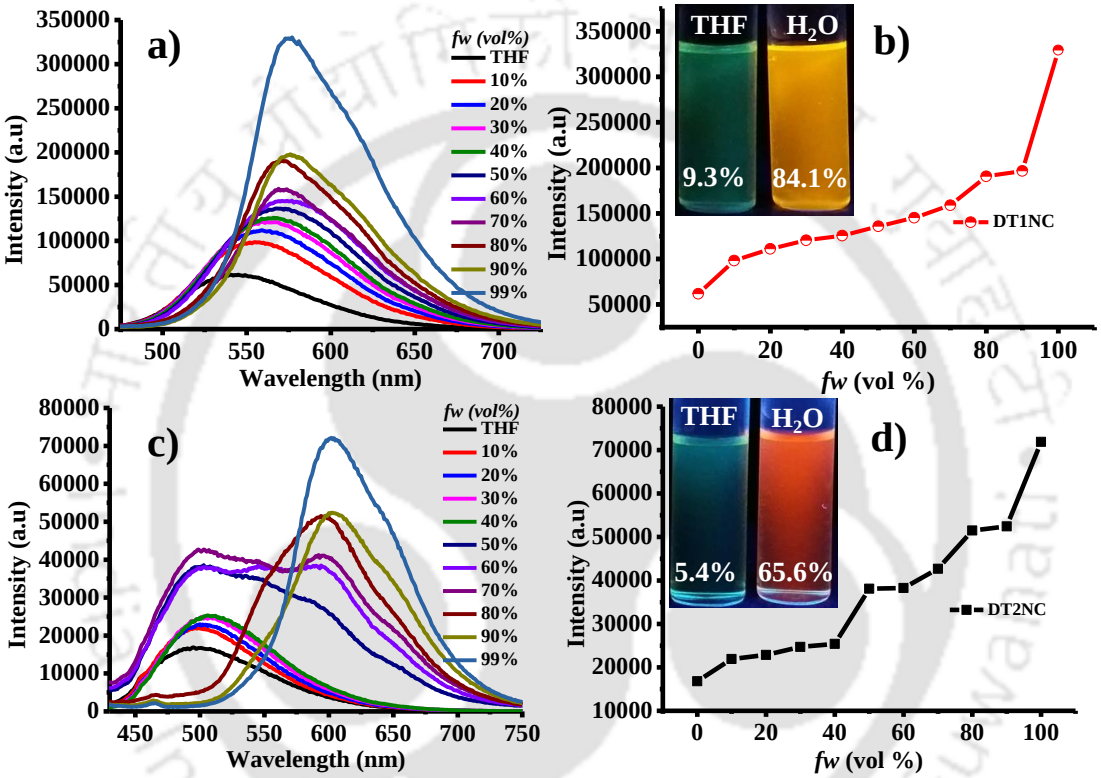

Figure 6.4: PL spectra and PL relative intensity of DT1NC (a) & (b) and DT2NC (c) & (d) in THF and Water mixtures. The photographs were taken under 365 nm UV lamp; the number indicates the calculated quantum yields using an integrating sphere of the luminogens.

Such remarkable red-shifts were also observed in the absorption spectra. The maximum emission intensities were observed when *fw* reached 99%. This was because of RIR and red-shift of emissions was attributed to intramolecular planarization of nanoparticles leading to the formation of J-type aggregation. On comparing both the luminogens in THF and water, it was found that DT2NC was blue-shifted (50 nm) in THF and red-shifted (27 nm) in 99% *fw*. As already explained earlier, the two bromine atoms, present at the 2,7 positions on the DBF moiety of the DT2NC, are responsible for such a drastic blue-shift in the THF solution and red-shift in 99% *fw*. But unexpectedly, both DPNC luminogens

showed a relatively opposite behavior compared to the DTNC luminogens, i.e., these luminogens exhibited a strong blue fluorescence with high quantum yields 74.19% and 71.92% for DP1NC and DP2NC, respectively in THF. As shown in Figure 6.5, on increasing the *fw* in THF from 0% to 70%, the emission intensity of the DP1NC increased with 20 nm red-shift because of the formation of nanoparticles. On increasing the *fw,* the emission intensity decreases. This might be due to the agglomeration of nanoparticles in the higher *fw,* leading to reduced effective fluorescence emission (4.5% quantum yield in 99% *fw*).

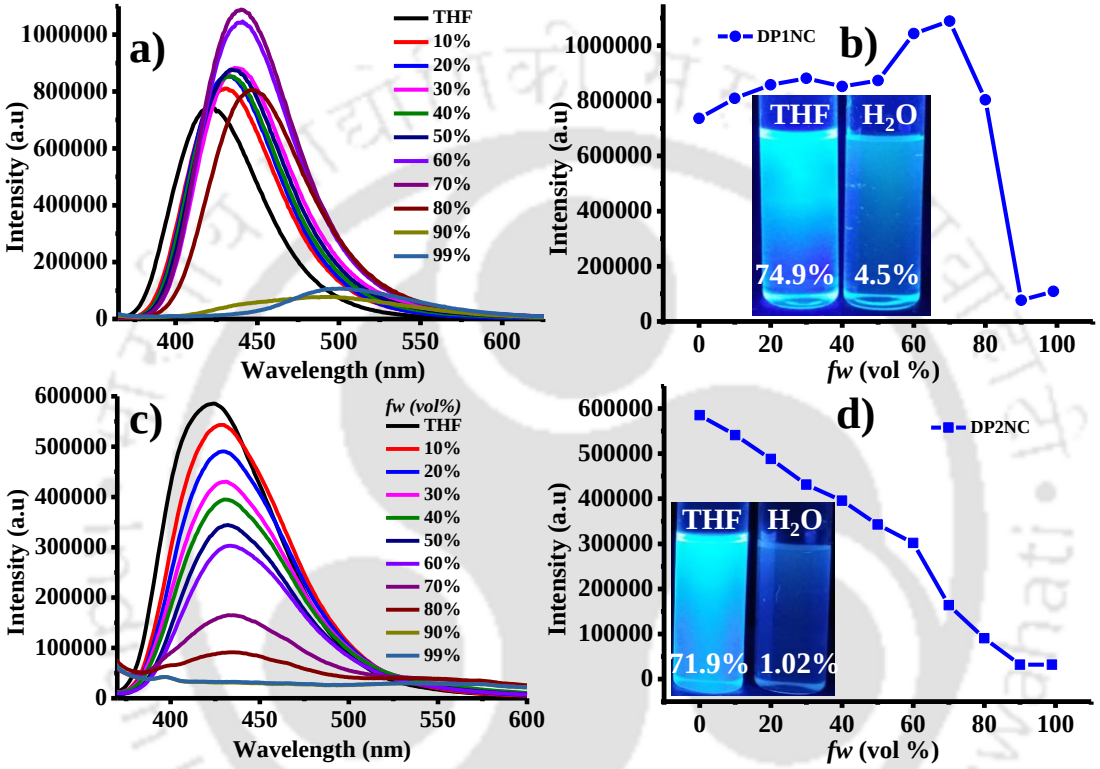

Figure 6.5: PL spectra and PL relative intensity of DP1NC (a) & (b) and DP2NC (c) & (d) in THF and Water mixtures. The photographs were taken under 365 nm UV lamp; the number indicates the calculated quantum yields using an integrating sphere of the luminogens.

Similarly, the DP2NC luminogen exhibited a strong emission in the THF. The emission intensity gradually decreased when the *fw* was varied from 0% to 99% (1.02% quantum yield in 99% *fw*). This might be due to the strong intermolecular π-π interactions of DP2NC in the aggregated state. The DP2NC emission was almost completely quenched in the aggregated state, compared to DP1NC. These results indicate that DP2NC molecules might be strongly packed in the aggregated state (which was confirmed by the single crystal X-ray studies and explained in later sections). These two DPNC luminogens are structurally similar to DTNC luminogens with only difference being the phenyl (DPNC) or thiophene (DTNC)

bridge between the NC and DBF moieties. Thus, it can be concluded that the thiophene moiety plays a crucial role to achieve weak emission in THF in the DTNC luminogens. Using FE-SEM and DLS measurements, it was confirmed that DT1NC and DT2NC (Figure 6.6) formed nano-aggregates in 99% water. The FE-SEM images confirmed the presence of nanoparticles (~160 nm for both luminogens) that were further confirmed by DLS studies in 99% water. These results gave the size distribution of ~180 nm for DT1NC and ~175 nm for DT2NC. The geometry and crystal packing of the DPNC luminogens were obtained from the single crystal X-ray measurements. These results were utilized to explore the AIEE active or inactive nature of the luminogens. Unfortunately, single crystals of the DTNC luminogens were not obtained, but DPNC luminogens single crystals

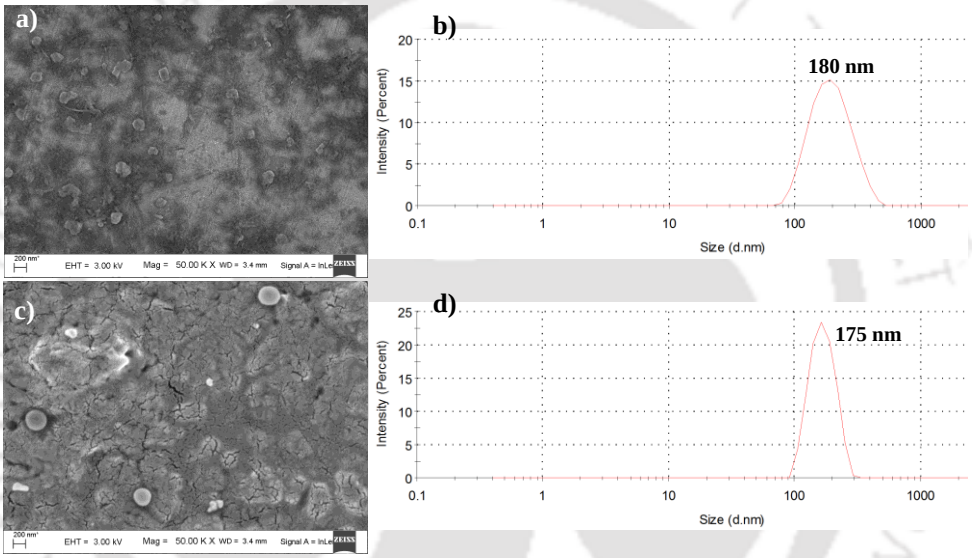

Figure 6.6: FE-SEM images and Dynamic Light Scattering (DLS) curves of DT1NC (a) & (b) and DT2NC (c) & (d).

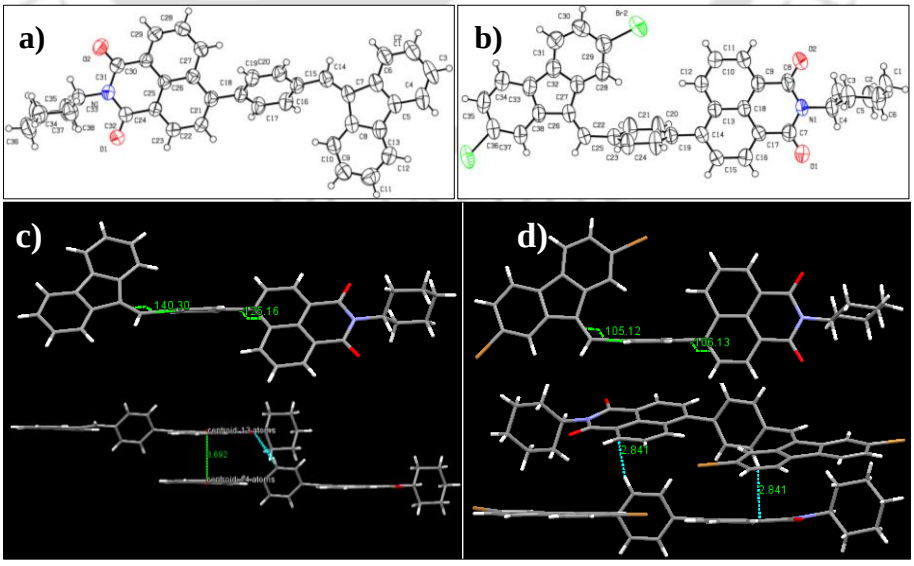

Figure 6.7: ORTEP diagrams a) & b) and crystal packing (c) & (d) of DP1NC and DP2NC.

were obtained by slow evaporation of chloroform. Figure 6.7 shows ORTEP diagrams of the DPNC luminogens, where both the luminogens exhibited non-planarity. In both luminogens the phenyl ring is located in one plane and the remaining two groups (DBF and NC moieties) are in another plane. The torsion angles of both luminogens are almost same, i.e., between DBF and phenyl the angle was 140.30° for DP1NC and 105.12° for DP2NC. Similarly, torsion angles between phenyl and NC are 125.16° for DP1NC and 106.13° for DP2NC. However, the arrangement of the DBF moiety is different compared to that of the NC moiety. The DBF moiety is opposite to NC (like trans to NC) for DP1NC and the same side (like cis to NC) for DP2NC. These slight structural changes likely occurred because of the bromine atoms. However, these minor structural arrangements highly affected the crystal packing as well as the photophysical properties. As shown in Figure 6.7 the two DP2NC luminogens are strongly packed by the C-H···π (2.841 Å) intermolecular interactions. Similarly, two adjacent molecules of the DP1NC are tightly packed by C-H···O (2.703 Å) intermolecular interactions. This could efficiently quench the fluorescence in the aggregated state, suggesting that DPNC luminogens are AIEE inactive. The crystal studies strongly suggest that C-H···π and C-H···O interactions might be promoting an increase in the non-radiative deactivation.

6.3.4. Density Functional theory (DFT) Calculations

The density functional theory (DFT) calculations were carried out using Gaussian09 A.02 software package[46] B3LYP/6-31g(d,p) basis set[47] to understand the structural property of the luminogens. Figure 6.8 showed the optimized molecular structures of the luminogens. It is clearly visible that all the luminogens are non-planar structures. In the DTNC luminogens, the DBF and thiophene moieties are almost in one plane, with torsion angles of 178.00° for DT1NC and 176.97° for DT2NC, while the non-planar NC moiety had torsion angles of 130.63° between thiophene and NC for DT1NC and 130.71° for DT2NC. Therefore, because of the non-planarity of these luminogens, they cannot come close together. This might be the reason for achieving high fluorescence in the aggregated state. These half planar molecules highly favor their self-arrangement to form ladder-type structures, which is quite common for the J-type aggregation in the solid or aggregated state. This might be the reason for the red-shift in the emission spectra from THF to 99% *fw*. The torsion angles of both DTNC luminogens are nearly similar to each other. On the contrary, in DPNC

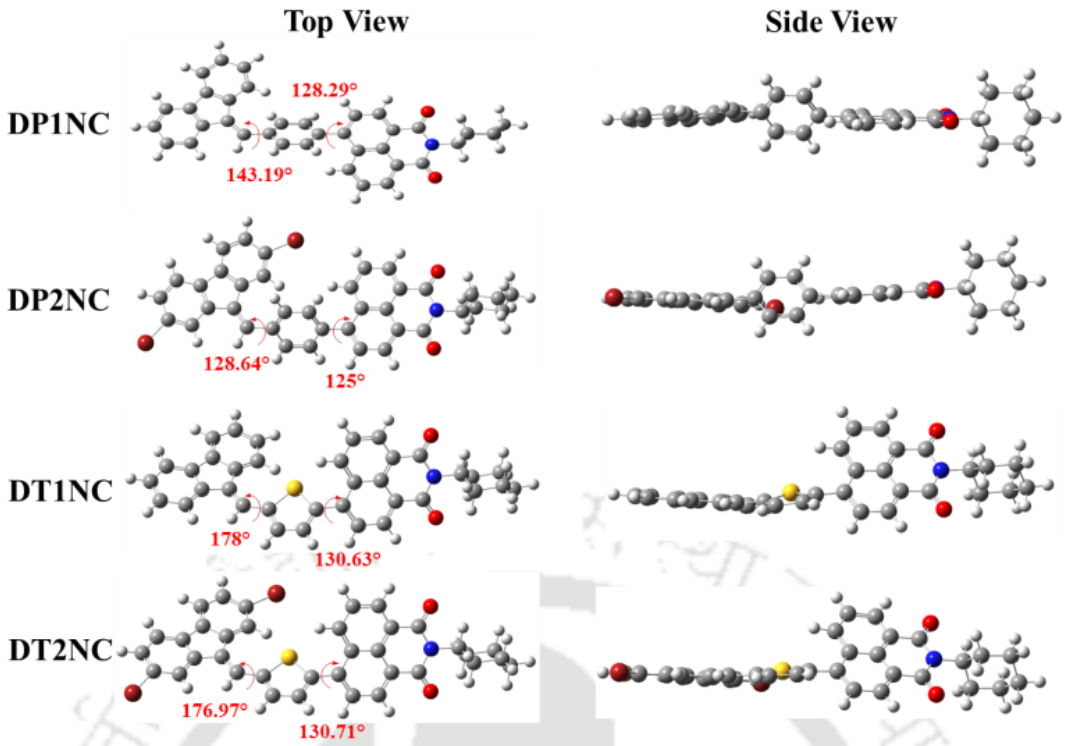

Figure 6.8: Optimized molecular geometries of **DT1NC, DT2NC, DP1NC** and **DP2NC**

luminogens, the DBF and NC moieties are in one plane while the phenyl ring is another. The optimised structures and crystal structures are quite similar to each other. The torsion angels between DBF and phenyl moieties are 143.19° for DP1NC and 128.64° for DP2NC, and the phenyl and NC moieties are 128.29° for DP1NC and 125.00° for DP2NC. In both DPNC luminogens, the torsion angles between phenyl and NC are almost similar. However, surprisingly, the torsion angles between DBF and phenyl are different and the arrangement of DBF moiety is also different with respect to NC moiety. The DBF moiety is arranged trans to NC for DP1NC but in DP2NC the DBF moiety shifted to cis positon. These opposite structural arrangements likely occurred because of the bromine atoms, which are present in DP2NC. On comparing DTNC with DPNC luminogens, it can be observed that the DPNC luminogens have almost planar structures except the phenyl ring, which reduces the emission intensity in the aggregated state. However, as seen in Figure 6.8, the DTNC luminogens are not in plane, and therefore, there is no possibility for them to come closer, which results in high PL emission in the aggregated state. The molecular orbital distributions of HOMO and LUMO structures of the luminogens are given in Figure 6.9 and their energy levels are tabulated in Table 6.3. The HOMO electron clouds are mainly located on DBF and thiophene or phenyl moieties because of their electron donating capacity and the

LUMO electron clouds are dominated on the acceptor (NC) moiety. The time-dependant density functional theory (TD-DFT) calculations were carried out using a CAM-B3LYP/6-31g(d,p) basis set[48] to find out the UV absorption transitions of all luminogens (Figure 6.11 to 6.14). The TD-DFT data suggested two transitions for DTNC luminogens at 302 & 323 and 403& 399 nm for DT1NC and DT2NC, respectively. The peaks at lower wavelength are attributed to π-π* transition and second set of peaks at the higher wavelength region are due to ICT from the donor to acceptor. One major transition observed for both DP1NC and DP2NC at 339 and 328 nm, respectively, is due to the π-π* transition. Compared to the non-brominated samples, the brominated luminogens were blue-shifted. These results strongly supported the notion that bromine atoms acted as the weak electron withdrawing groups in both DT2NC and DP2NC. It is also observed that the ICT peak intensity was increased for DT2NC compared to that of DT1NC. Simultaneously, the π-π* transition decreased for DT2NC compared to that of DT1NC because of the bromine atoms, which are known to reduce electron donating capacity of the DBF moiety.

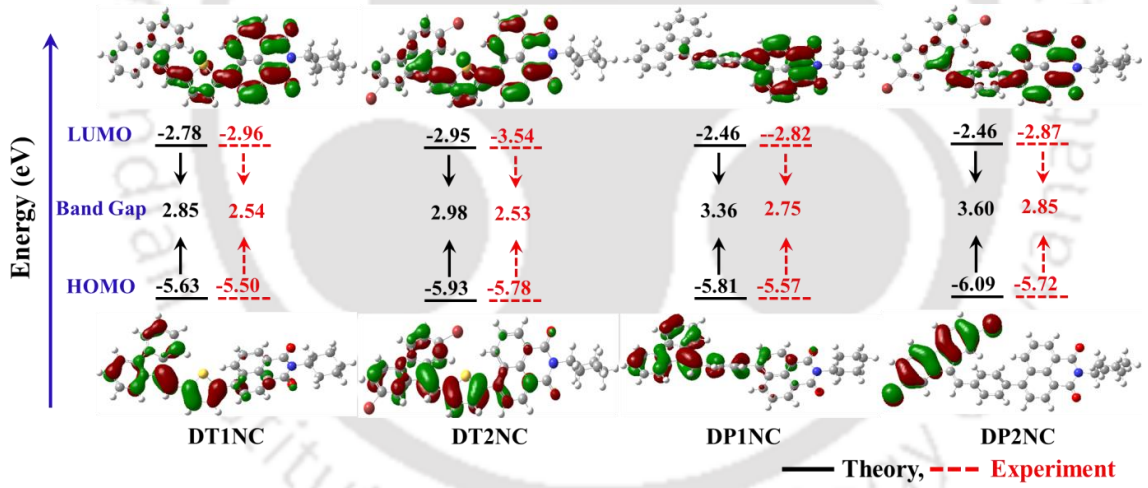

Figure 6.9: The frontier orbital plots of the HOMO and LUMO levels and the comparison energy levels estimated from the theoretical data and electrochemical data of DT1NC, DT2NC, DP1NC and DP2NC

To investigate the highest occupied molecular orbital (HOMO) and lowest unoccupied molecular orbital (LUMO) energy levels of the four luminogens, cyclic voltammetry (CV) was performed in the drop-cast solid films. The CV curves of luminogens are displayed in Figure 6.10 and the electrochemical data are listed in the Table 6.3. As shown in Figure 6.10, all the luminogens displayed two potential peaks and a quasi-reversible reduction waves. This might be due to the electron deficient NC moiety. The HOMO and LUMO energies were estimated by

6.3.5. Electrochemical properties

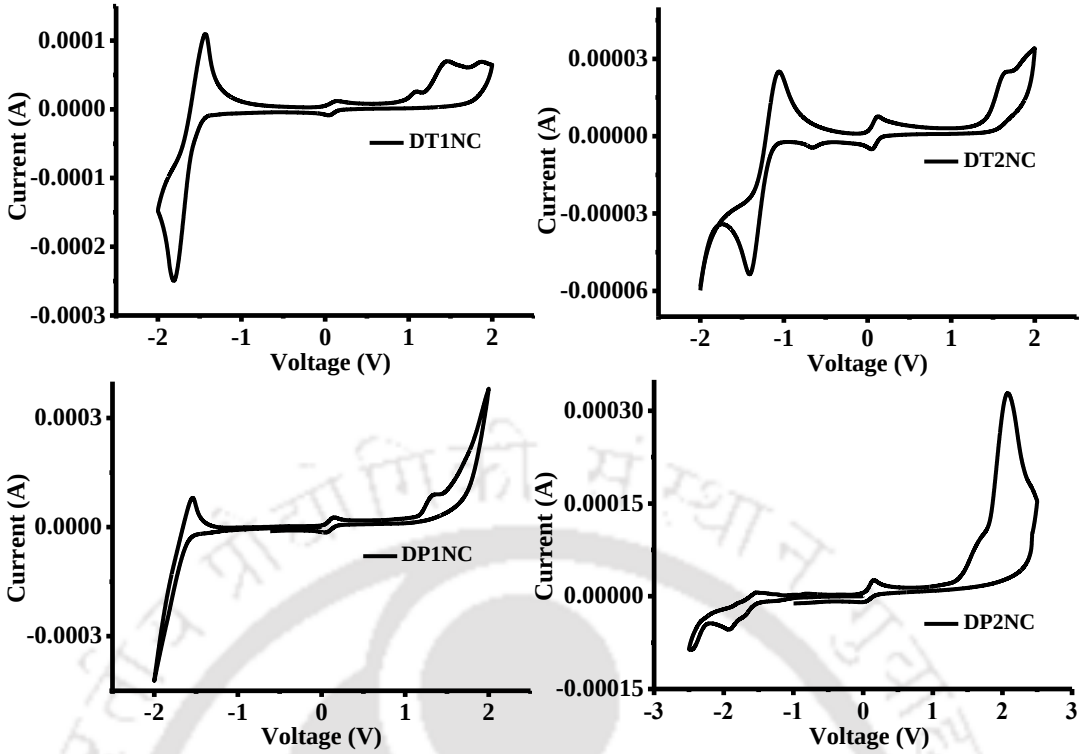

Figure 6.10: Cyclic voltammograms of Luminogens

substituting the onset reduction and onset oxidation peak values in E_{LUMO} = -[(E_{red}- $E_{1/2}$(ferrocene)) + 4.8 eV], E_{HOMO} = -[(E_{ox} -$E_{1/2}$(ferrocene)) + 4.8 eV]. The CV and theoretical calculations revel that the band gaps between HOMO and LUMO are less in DTNC luminogens than in DPNC luminogens. This is due to the greater electron donating capacity of the thiophene bridge-substituted DBF moiety.

Table 6.3: The Comparison of energy levels estimated from electrochemical studies and DFT theoretical.

Monomer	Electrochemical Potentials and Energy Levels					DFT data (eV)		
	E_{ox}/V	E_{red}/V	E_{HOMO}/eV	E_{LUMO}/eV	E_g/eV	HOMO	LUMO	H-L Gap
DT1NC	0.92	-1.44	-5.5	-2.96	2.54	5.63	2.78	2.85
DT2NC	1.38	-1.14	-5.78	-3.54	2.53	5.93	2.95	2.98
DP1NC	1.17	-1.58	-5.57	-2.82	2.75	5.81	2.46	3.36
DP2NC	1.32	-1.53	-5.72	-2.87	2.85	6.09	2.46	3.60

Table 6.4: TD-DFT calculations of the luminogens

Monomers	TD-DFT		
	λ_{theory} (nm)	f	Composition
DT1NC	302 ($S_0 \rightarrow S_{11}$)	0.11,	H→L+1 (72.13%) = π-π*
	403 ($S_0 \rightarrow S_5$)	1.17	H→L (84.19%) = π-π* (ICT)
DT2NC	323 ($S_0 \rightarrow S_9$)	0.09,	H→L+1 (65.45%) = π-π* H-2→L (25.0%)
	399 ($S_0 \rightarrow S_5$)	1.23	= π-π*, H→L (89.65%) = π-π* (ICT)
DP1NC	339 ($S_0 \rightarrow S_6$)	1.26	H→L (60.05%) = π-π* H→L+1 (16.83%) = π-π*
DP2NC	328 ($S_0 \rightarrow S_8$)	1.04	H→L+1 (55.77%) = π-π* H→L (23.43%) = π-π*

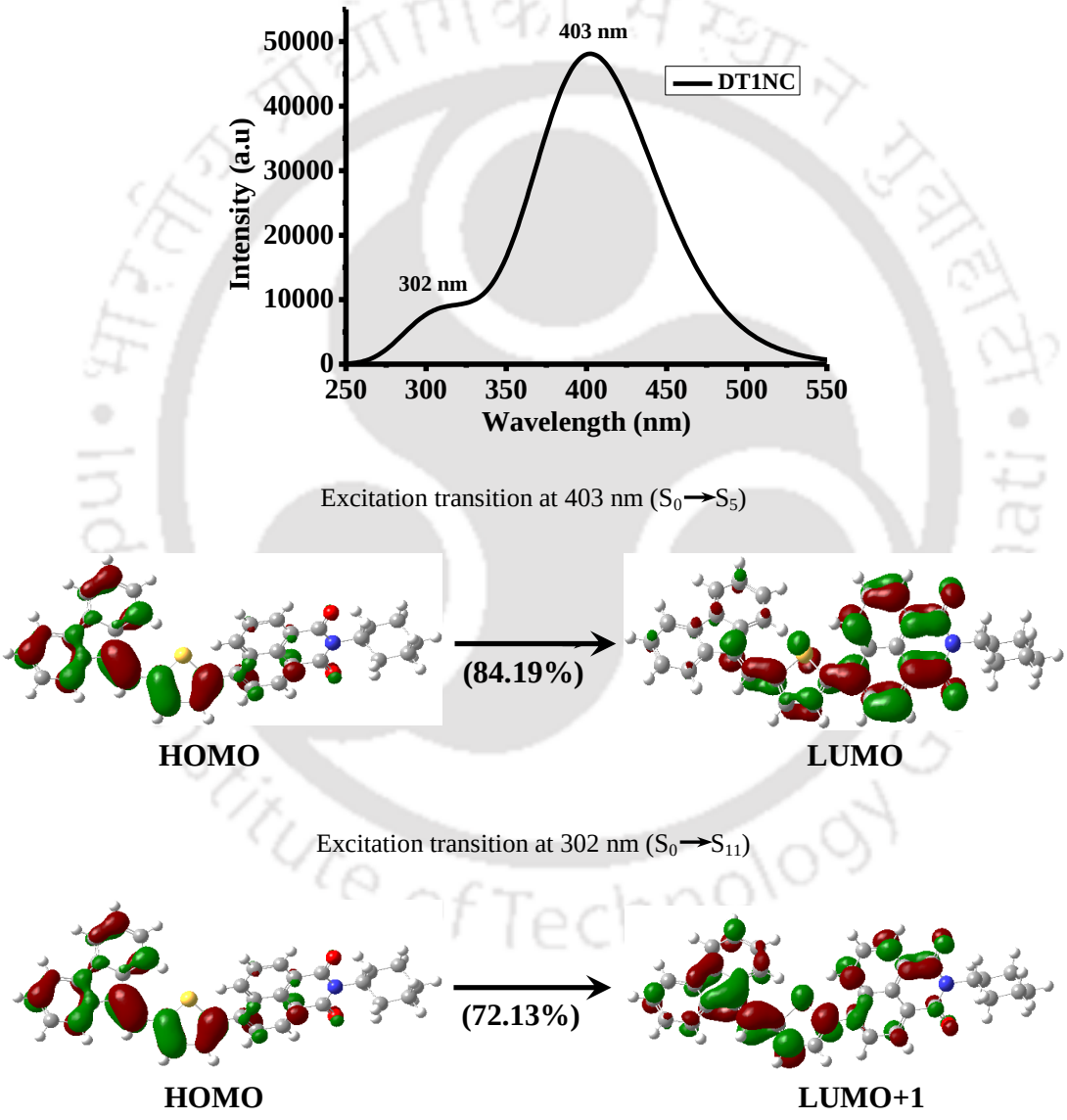

Figure 6.11: TD-DFT simulated absorption spectra and contributing orbitals at each excitation of **DT1NC** luminogen

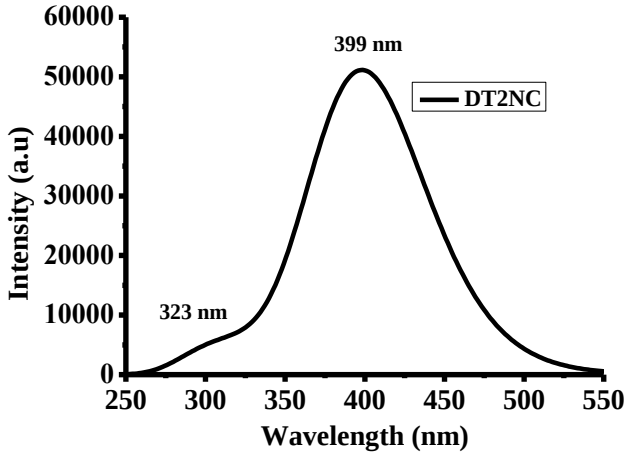

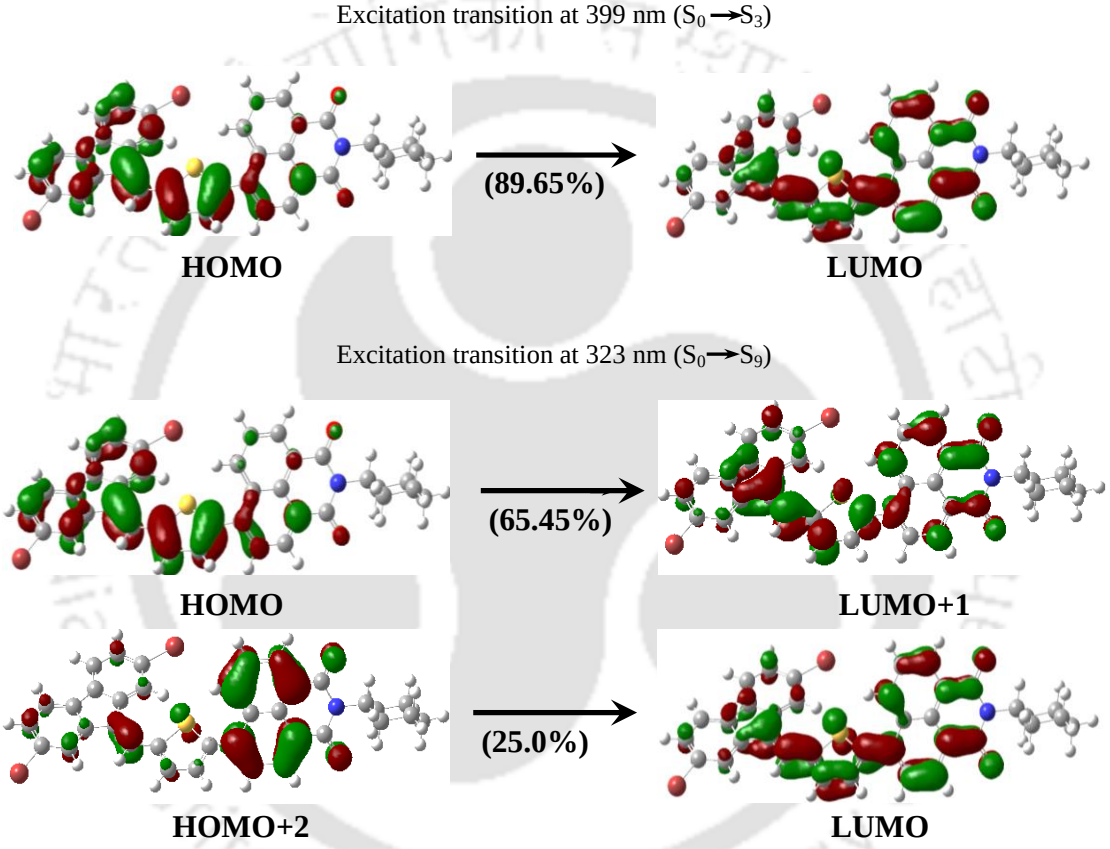

Figure 6.12: TD-DFT simulated absorption spectra and contributing orbitals at each excitation of **DT2NC** luminogen

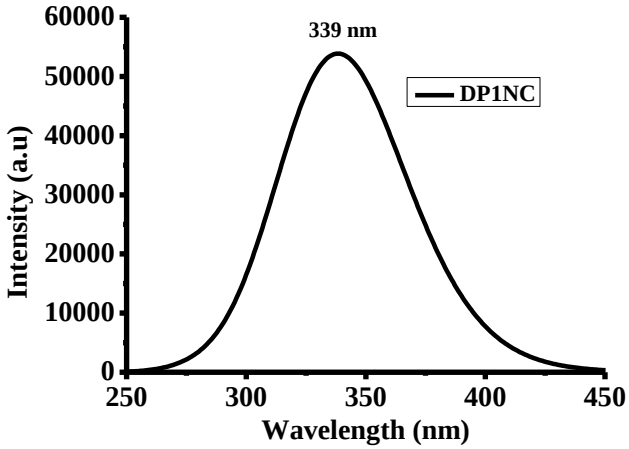

Excitation transition at 339 nm ($S_0 \rightarrow S_6$)

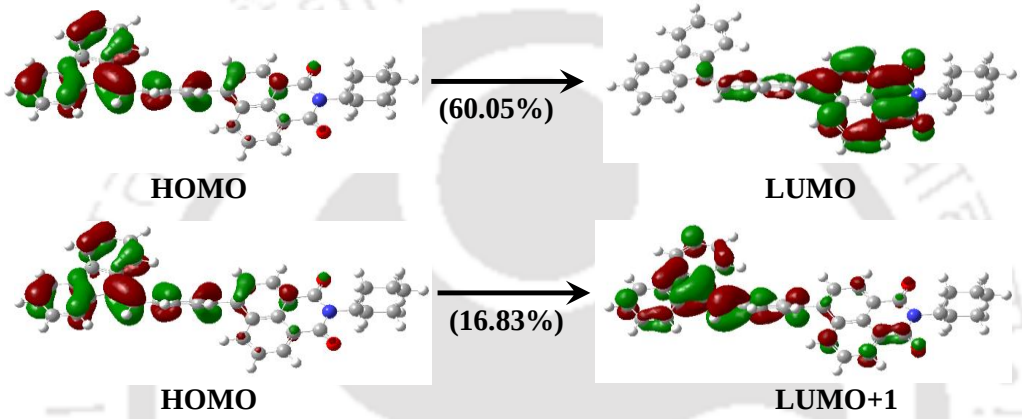

Figure 6.13: TD-DFT simulated absorption spectra and contributing orbitals at each excitation of **DP1NC** luminogen

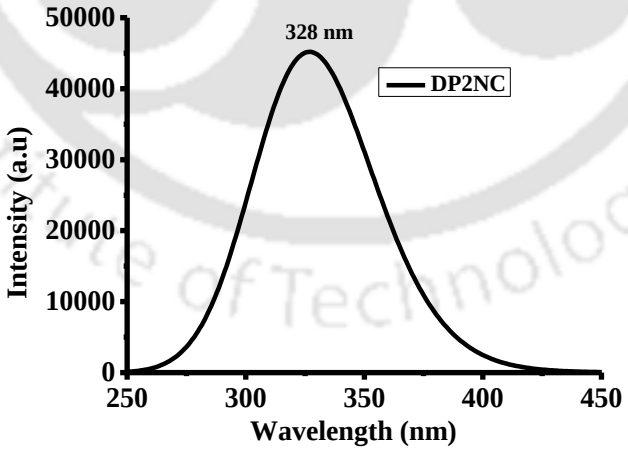

Excitation transition at 328 nm ($S_0 \rightarrow S_8$)

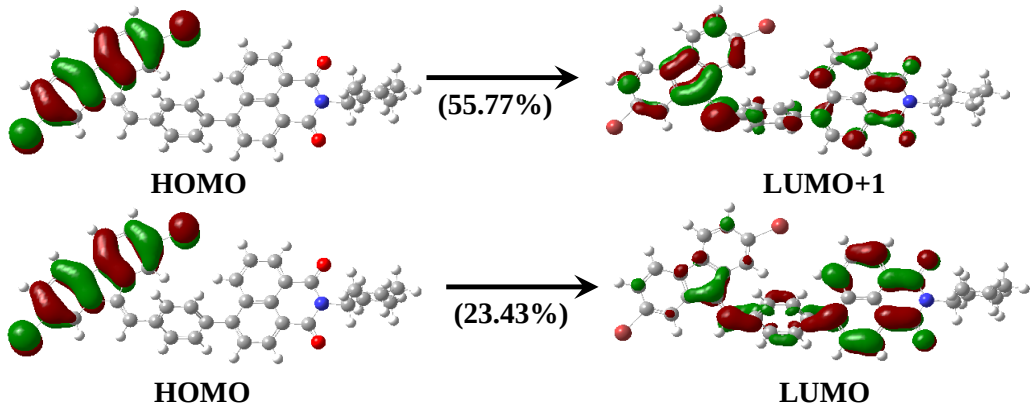

Figure 6.14: TD-DFT simulated absorption spectra and contributing orbitals at each excitation of **DP2NC** luminogen.

6.3.6. Thermal Properties of the Luminogens

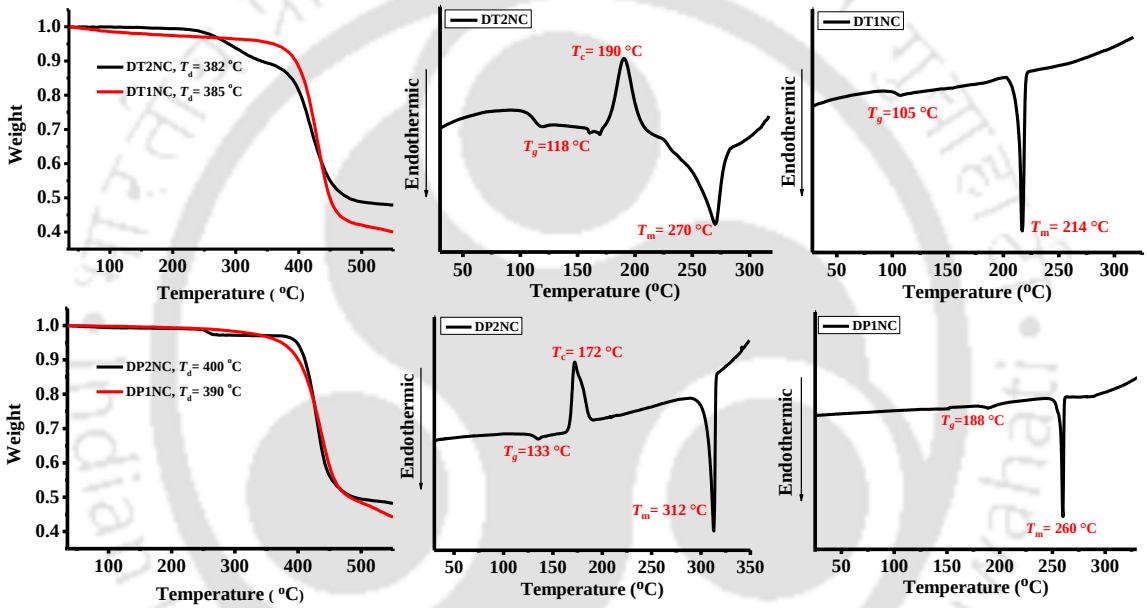

Figure 6.15: TGA and DSC curves of luminogens.

The thermal properties of the four luminogens were studied by thermogravimetric analysis (TGA) and differential scanning calorimetry (DSC), and the curves are shown in Figure 6.15. Both the experiments were performed under nitrogen atmosphere with a 10 °C min^{-1} heating rate. According to the TGA study, all the luminogens exhibited good thermal stability up to 380-400 °C, i.e., no weight loss at low temperatures. The brominated luminogens (i.e., DT2NC and DP2NC) showed the two step degradation, first degradation step for the bromine moiety loss and second for the aromatic backbone. The remaining two luminogens (i.e., DT1NC and DP1NC) showed a single step degradation. The DSC analysis revealed that all the luminogens exhibited high melting points (T_m) at 312 °C, 270 °C, 214 °C and 260 °C for DP2NC, DT2NC, DT1NC and DP1NC, respectively.

The glass transition temperatures (T_g) during the second heating scan for all the luminogens at 133 °C, 118 °C, 105°C and 188 °C for DP2NC, DT2NC, DT1NC and DP1NC, respectively. Similarly, during the second heating scan the crystallization temperatures (T_c) were observed for brominated luminogens at 172 °C for DP2NC and 190 °C for DT2NC. These results strongly suggest that the four luminogens exhibited good morphological stability.

6.4. Summary

To summarize, it was demonstrated that the photophysical and the thermal properties of the organic materials are highly dependent as well as precisely controlled by their core structures. Two novel thiophene bridge substituted AIEE active (DT1NC and DT2NC) and two phenyl substituted inactive bridge (DP1NC and DP2NC) luminogens based on the 1,8-naphthalimde and mono-substituted dibenzofulvene derivatives were reported. Thiophene bridge substituted luminogens exhibited strong emission with high fluorescence quantum yields 84.10% and 65.65% and a large bathochromic shift 35 nm and 112 nm for DT1NC and DT2NC, respectively, in their aggregated state because of the ladder type J-aggregation. The theoretical and experimental results concluded that both DP1NC and DP2NC luminogens are AIE inactive. All the luminogens are structurally similar, yet the photophysical properties of the luminogens predominantly depended on the bridge between DBF and NC. In addition, the fluorescence emission color could be precisely tuned through the entire visible range (blue to red) by changing the bridge between DBF and NC. The thiophene bridge moiety played a major role in achieving such a unique phenomenon. Furthermore, the heavy atom effect was successfully studied on novel donor-acceptor luminogens by introducing bromine atoms on the DBF moiety. All luminogens exhibited excellent positive solvatochromism. The experimental and theoretical studies strongly supported that these color-tenable luminogens could contribute significantly in the field of OLEDs and multicolor bio-imaging applications.

6.5. References

1. Shimizu, M.; Kaki, R.; Takeda, Y.; Hiyama, T.; Nagai, N.; Yamagishi, H.; Furutani, H. *Angew. Chem. Int. Edit.* **2012,** *51*, 4095-4099.
2. Yao, L.; Zhang, S. T.; Wang, R.; Li, W. J.; Shen, F. Z.; Yang, B.; Ma, Y. G. *Angew. Chem. Int. Edit.* **2014,** *53*, 2119-2123.
3. Yuan, W. Z.; Lu, P.; Chen, S. M.; Lam, J. W. Y.; Wang, Z. M.; Liu, Y.; Kwok, H. S.; Ma, Y. G.; Tang, B. Z. *Adv. Mater.* **2010,** *22* (19), 2159-2163.
4. Yuan, W. Z.; Tan, Y. Q.; Gong, Y. Y.; Lu, P.; Lam, J. W. Y.; Shen, X. Y.; Feng, C. F.; Sung, H. H. Y.; Lu, Y. W.; Williams, I. D.; Sun, J. Z.; Zhang, Y. M.; Tang, B. Z. *Adv. Mater.* **2013,** *25*, 2837-2843.
5. Qin, W.; Ding, D.; Liu, J. Z.; Yuan, W. Z.; Hu, Y.; Liu, B.; Tang, B. Z. *Adv. Funct. Mater.* **2012,** *22*, 771-779.
6. Kobayashi, H.; Ogawa, M.; Alford, R.; Choyke, P. L.; Urano, Y. *Chem. Rev.* **2010,** *110*, 2620-2640.
7. Zhang, X. Q.; Zhang, X. Y.; Wang, S. Q.; Liu, M. Y.; Tao, L.; Wei, Y. *Nanoscale* **2013,** *5*, 147-150.
8. Li, K.; Jiang, Y. H.; Ding, D.; Zhang, X. H.; Liu, Y. T.; Hua, J. L.; Feng, S. S.; Liu, B. *Chem. Commun.* **2011,** *47*, 7323-7325.
9. Zhang, M.; Yu, M. X.; Li, F. Y.; Zhu, M. W.; Li, M. Y.; Gao, Y. H.; Li, L.; Liu, Z. Q.; Zhang, J. P.; Zhang, D. Q.; Yi, T.; Huang, C. H. *J. Am. Chem. Soc.* **2007,** *129*, 10322-10323.
10. Gu, X. G.; Yao, J. J.; Zhang, G. X.; Zhang, D. Q. *Small* **2012,** *8*, 3406-3411.
11. Huang, J.; Yang, X.; Li, X. J.; Chen, P. Y.; Tang, R. L.; Li, F.; Lu, P.; Ma, Y. G.; Wang, L.; Qin, J. G.; Li, Q. Q.; Li, Z. *Chem. Commun.* **2012,** *48*, 9586-9588.
12. Liu, X. Y.; Bai, D. R.; Wang, S. N. *Angew. Chem. Int. Edit.* **2006,** *45*, 5475-5478.
13. Jenekhe, S. A.; Osaheni, J. A. *Science* **1994,** *265*, 765-768.
14. Ning, Z. J.; Tian, H. *Chem. Commun.* **2009,** 5483-5495.
15. Verbouwe, W.; Van der Auweraer, M.; De Schryver, F. C.; Piet, J. J.; Warman, J. M. *J. Am. Chem. Soc.* **1998,** *120*, 1319-1324.
16. Luo, J. D.; Xie, Z. L.; Lam, J. W. Y.; Cheng, L.; Chen, H. Y.; Qiu, C. F.; Kwok, H. S.; Zhan, X. W.; Liu, Y. Q.; Zhu, D. B.; Tang, B. Z. *Chem. Commun.* **2001,** 1740-1741.
17. Hong, Y. N.; Lam, J. W. Y.; Tang, B. Z. *Chem. Soc. Rev.* **2011,** *40*, 5361-5388.
18. An, B. K.; Kwon, S. K.; Jung, S. D.; Park, S. Y. *J. Am. Chem. Soc.* **2002,** *124*, 14410-14415.
19. Zhao, L. F.; Lin, Y. L.; Liu, T.; Li, H. X.; Xiong, Y.; Yuan, W. Z.; Sung, H. H. Y.; Williams, I. D.; Zhang, Y. M.; Tang, B. Z. *J. Mater. Chem. C* **2015,** *3*, 4903-4909.
20. Yuan, Y. Y.; Zhang, C. J.; Xu, S. D.; Liu, B. *Chem. Sci.* **2016,** *7*, 1862-1866.
21. Chang, Z. F.; Jing, L. M.; Chen, B.; Zhang, M. S.; Cai, X. L.; Liu, J. J.; Ye, Y. C.; Lou, X. D.; Zhao, Z. J.; Liu, B.; Wang, J. L.; Tang, B. Z. *Chem. Sci.* **2016,** *7*, 4527-4536.
22. Tang, B. Z.; Chen, H. Z.; Xu, R. S.; Lam, J. W. Y.; Cheuk, K. K. L.; Wong, H. N. C.; Wang, M. *Chem. Mater.* **2000,** *12*, 213-221.

23. Chen, J. W.; Law, C. C. W.; Lam, J. W. Y.; Dong, Y. P.; Lo, S. M. F.; Williams, I. D.; Zhu, D. B.; Tang, B. Z. *Chem. Mater.* **2003,** *15*, 1535-1546.
24. Li, Z.; Dong, Y.; Mi, B. X.; Tang, Y. H.; Haussler, M.; Tong, H.; Dong, Y. P.; Lam, J. W. Y.; Ren, Y.; Sung, H. H. Y.; Wong, K. S.; Gao, P.; Williams, I. D.; Kwok, H. S.; Tang, B. Z. *J. Phys. Chem. B* **2005,** *109*, 10061-10066.
25. Du, X. B.; Wang, Z. Y. *Chem. Commun.* **2011,** *47*, 4276-4278.
26. Jiang, Y. H.; Wang, Y. C.; Hua, J. L.; Tang, J.; Li, B.; Qian, S. X.; Tian, H. *Chem. Commun.* **2010,** *46*, 4689-4691.
27. Zhang, G. H.; Sun, J. B.; Xue, P. C.; Zhang, Z. Q.; Gong, P.; Peng, J.; Lu, R. *J. Mater. Chem. C* **2015,** *3*, 2925-2932.
28. Gopikrishna, P.; Iyer, P. K. *J. Phys. Chem. C* **2016,** *120*, 26556-26568.
29. Liu, J.; Tu, G. L.; Zhou, Q. G.; Cheng, Y. X.; Geng, Y. H.; Wang, L. X.; Ma, D. G.; Jing, X. B.; Wang, F. S. *J. Mater. Chem.* **2006,** *16*, 1431-1438.
30. Tu, G. L.; Mei, C. Y.; Zhou, Q. G.; Cheng, Y. X.; Geng, Y. H.; Wang, L. X.; Ma, D. G.; Jing, X. B.; Wang, F. S. *Adv. Funct. Mater.* **2006,** *16*, 101-106.
31. Gopikrishna, P.; Das, D.; Iyer, P. K. *J. Mater. Chem. C* **2015,** *3*, 9318-9326.
32. Lin, H. H.; Chan, Y. C.; Chen, J. W.; Chang, C. C. *J. Mater. Chem.* **2011,** *21*, 3170-3177.
33. Li, Y. H.; Wu, Y. Q.; Chang, J.; Chen, M.; Liu, R.; Li, F. Y. *Chem. Commun.* **2013,** *49*, 11335-11337.
34. Meher, N.; Chowdhury, S. R.; Iyer, P. K. *J. Mater. Chem. B* **2016,** *4*, 6023-6031.
35. Meher, N.; Iyer, P. K. *Nanoscale* **2017,** *9*, 7674-7685.
36. Zhang, G. F.; Aldred, M. P.; Gong, W. L.; Li, C.; Zhu, M. Q. *Chem. Commun.* **2012,** *48*, 7711-7713.
37. Mukherjee, S.; Thilagar, P. *Chem. Commun.* **2013,** *49*, 7292-7294.
38. Duke, R. M.; Veale, E. B.; Pfeffer, F. M.; Kruger, P. E.; Gunnlaugsson, T. *Chem. Soc. Rev.* **2010,** *39*, 3936-3953.
39. Hua, Q. X.; Xin, B.; Liu, J. X.; Zhao, L. X.; Xiong, Z. J.; Chen, T.; Chen, Z. Q.; Li, C.; Gong, W. L.; Huang, Z. L.; Zhu, M. Q. *Faraday Discuss* **2017,** *196*, 439-454.
40. Mei, C. Y.; Tu, G. L.; Zhou, Q. G.; Cheng, Y. X.; Xie, Z. Y.; Ma, D. G.; Geng, Y. H.; Wang, L. X. *Polymer* **2006,** *47*, 4976-4984.
41. Hedstrom, S.; Henriksson, P.; Wang, E.; Andersson, M. R.; Persson, P. *Phys. Chem. Chem. Phys.* **2014,** *16*, 24853-24865.
42. Pastore, M.; Mosconi, E.; De Angelis, F.; Gratzel, M. *J. Phys. Chem. C* **2010,** *114*, 7205-7212.
43. Cho, D. W.; Cho, D. W. *New. J. Chem.* **2014,** *38*, 2233-2236.
44. Wintgens, V.; Valat, P.; Kossanyi, J.; Biczok, L.; Demeter, A.; Berces, T. *J. Chem. Soc. Faraday T* **1994,** *90*, 411-421.
45. Xue, P. C.; Yao, B. Q.; Sun, J. B.; Xu, Q. X.; Chen, P.; Zhang, Z. Q.; Lu, R. *J. Mater. Chem. C* **2014,** *2*, 3942-3950.
46. Frisch, M. J.; Trucks, G. W.; Schlegel, H. B.; Scuseria, G. E.; Robb, M. A.; Cheeseman, J. R.; Scalmani, G.; Barone, V.; Mennucci, B.; Petersson, G. A.; et al. Gaussian 09, revision D.01; Gaussian, Inc.: Wallingford, CT, 2013.
47. Becke, A. D. *J. Chem. Phys.* **1993,** *98*, 1372-1377.
48. Yanai, T.; Tew, D. P.; Handy, N. C. *Chem. Phys. Lett.* **2004,** *393*, 51-57.

Appendix

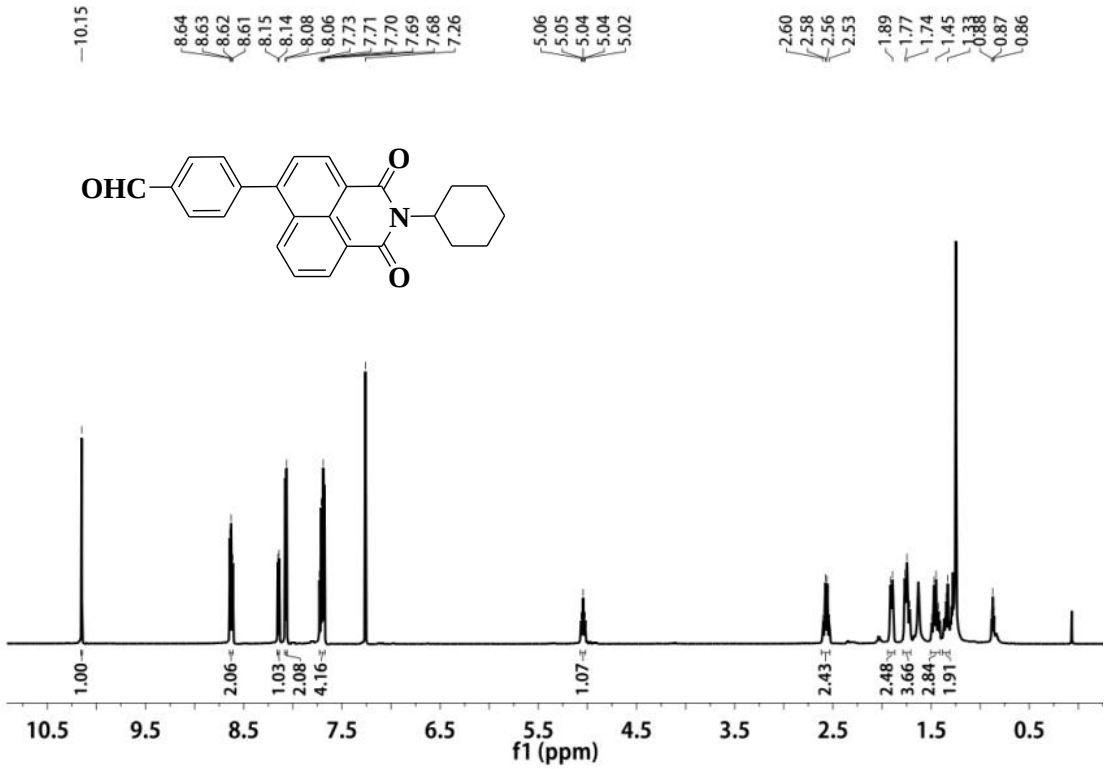

Figure 6.16: The ^{1}H NMR of the **Compound-1** in $CDCl_3$

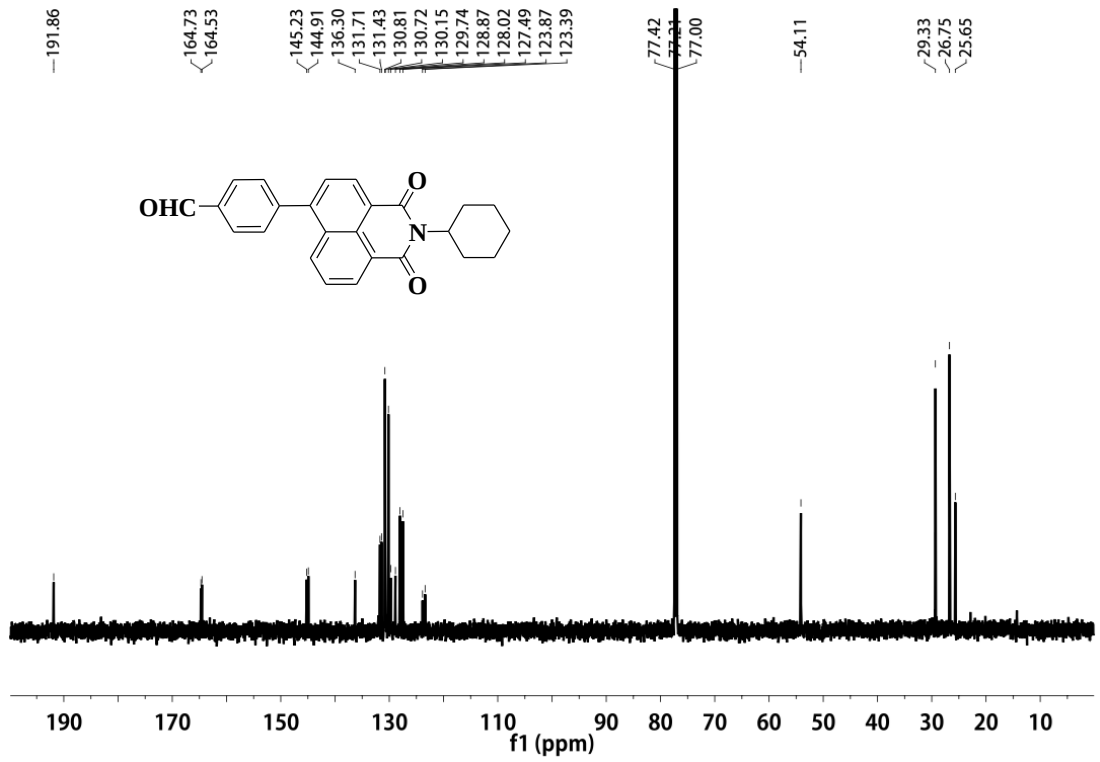

Figure 6.17: The ^{13}C NMR of the **Compound-1** in $CDCl_3$

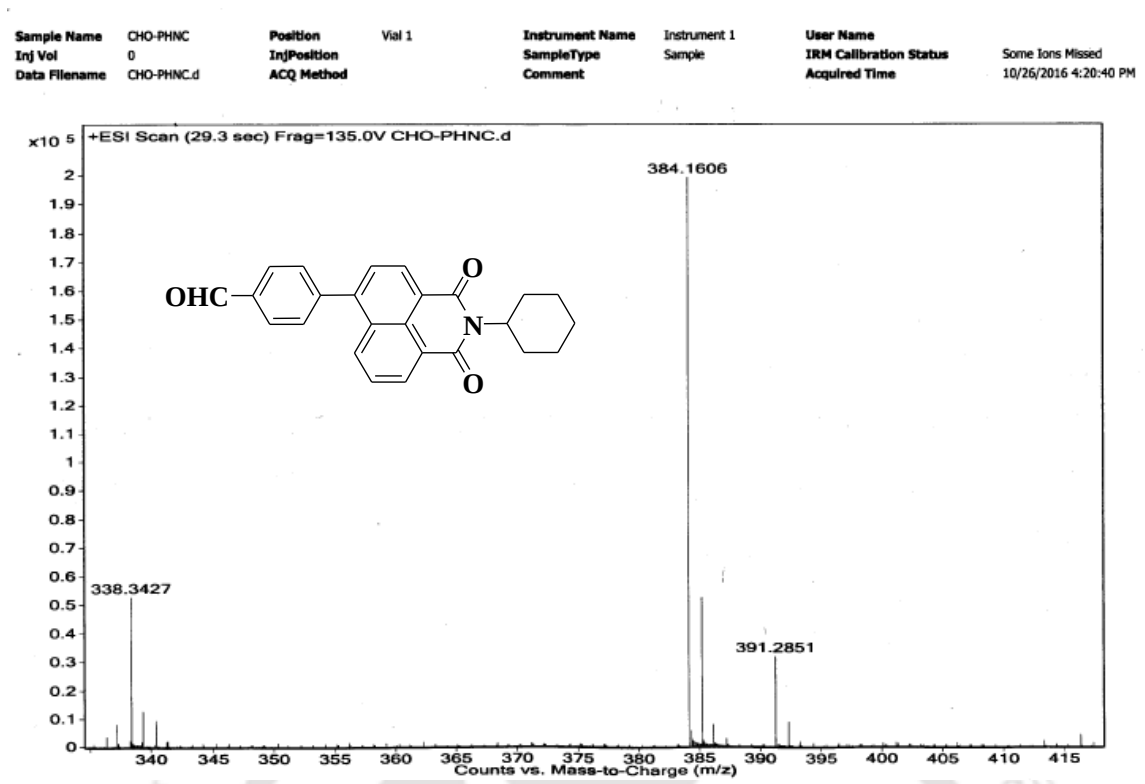

Figure 6.18: HRMS of the **Compound-1**

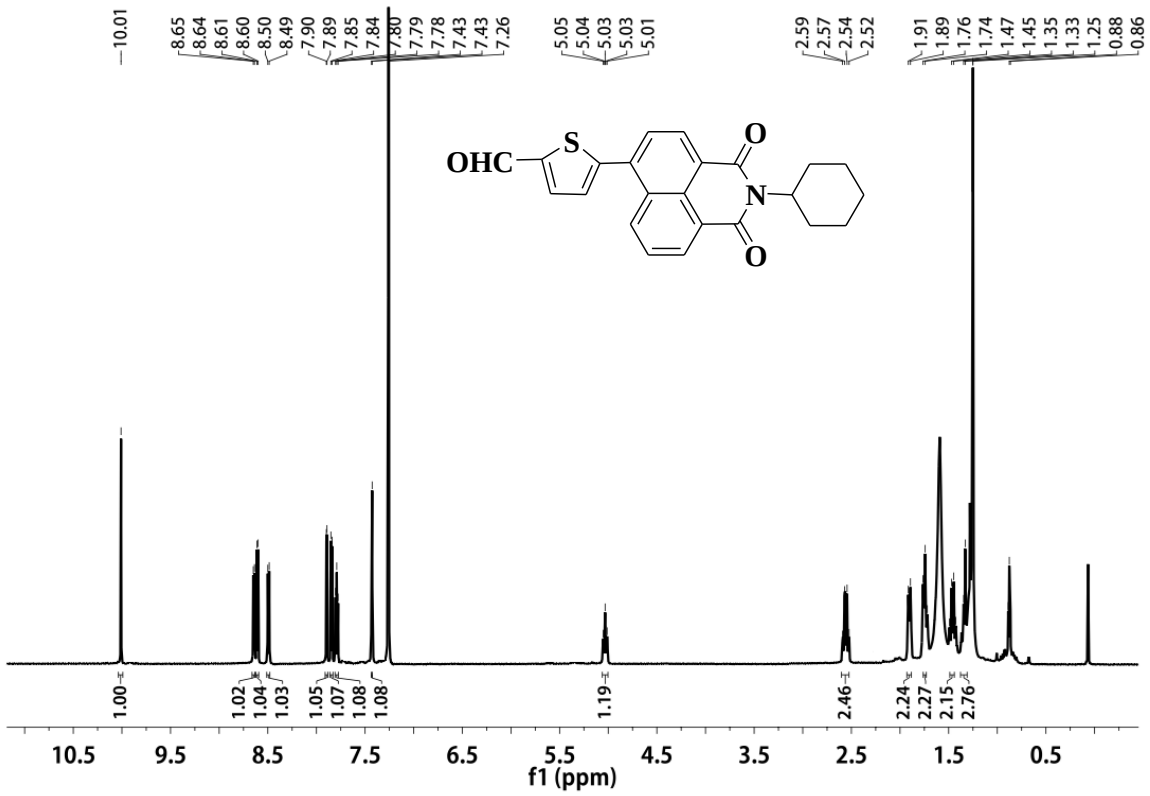

Figure 6.19: The ^{1}H NMR of the **Compound-2** in $CDCl_3$

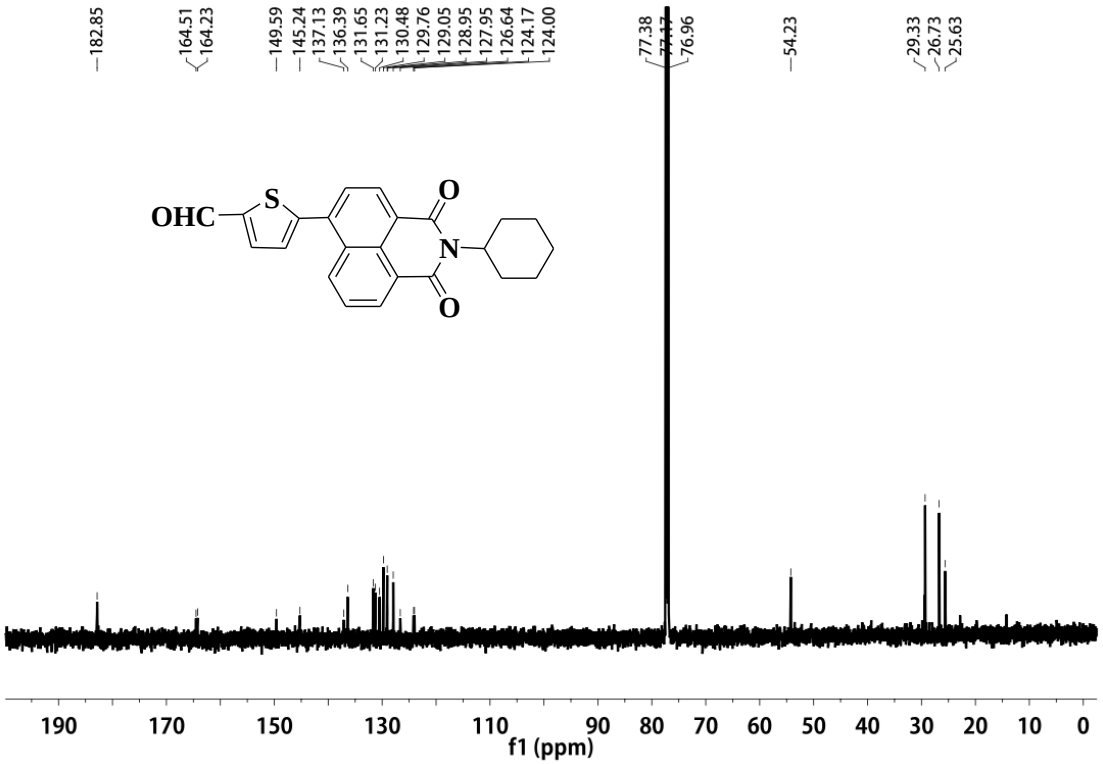

Figure 6.20: The ^{13}C NMR of the **Compound-2** in $CDCl_3$

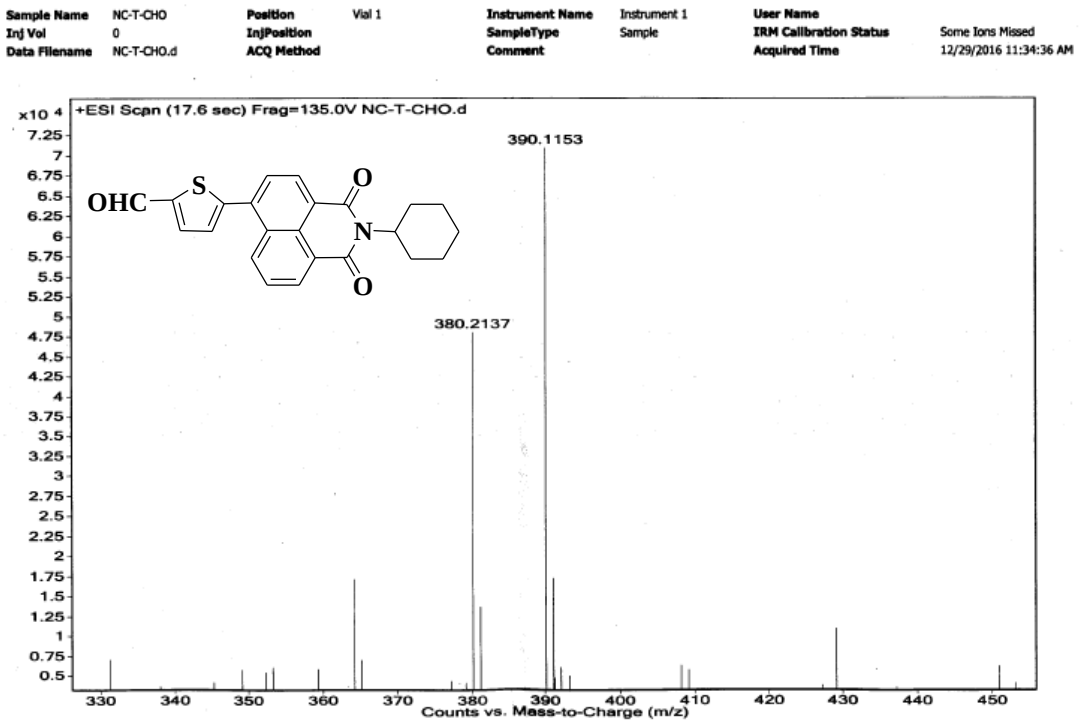

Figure 6.21: HRMS of the **Compound-2**

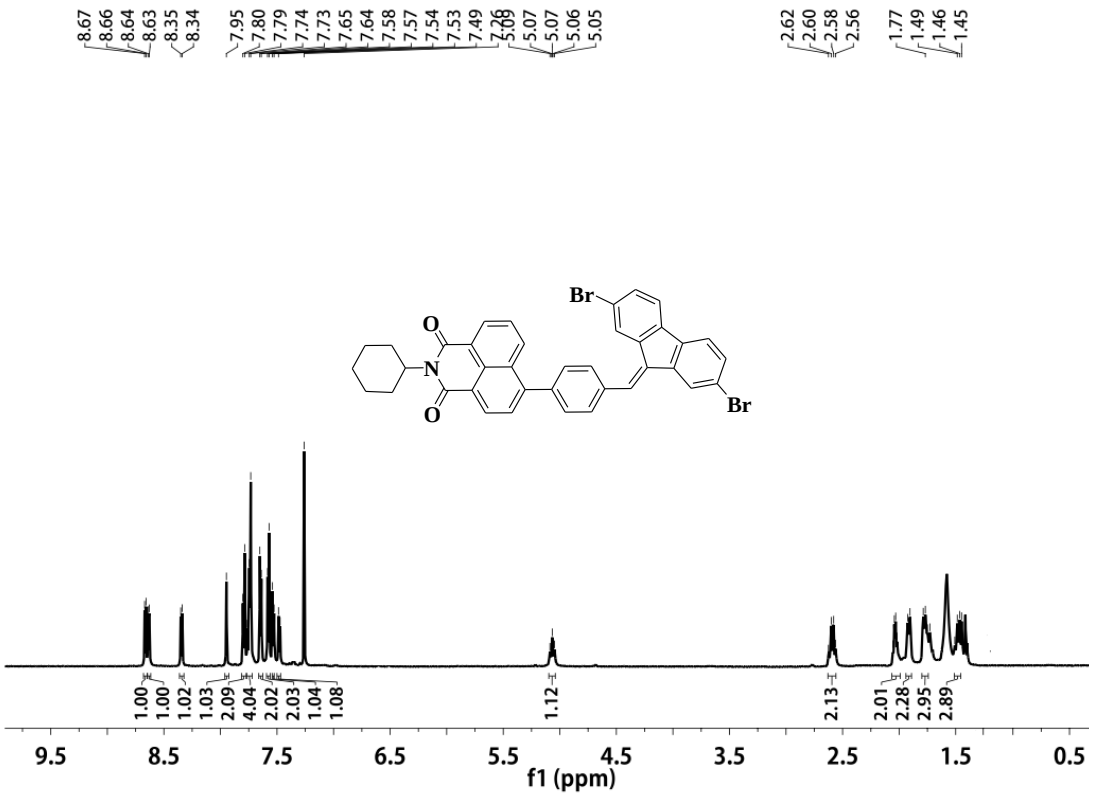

Figure 6.22: The ^{1}H NMR of the **DP2NC** in $CDCl_3$

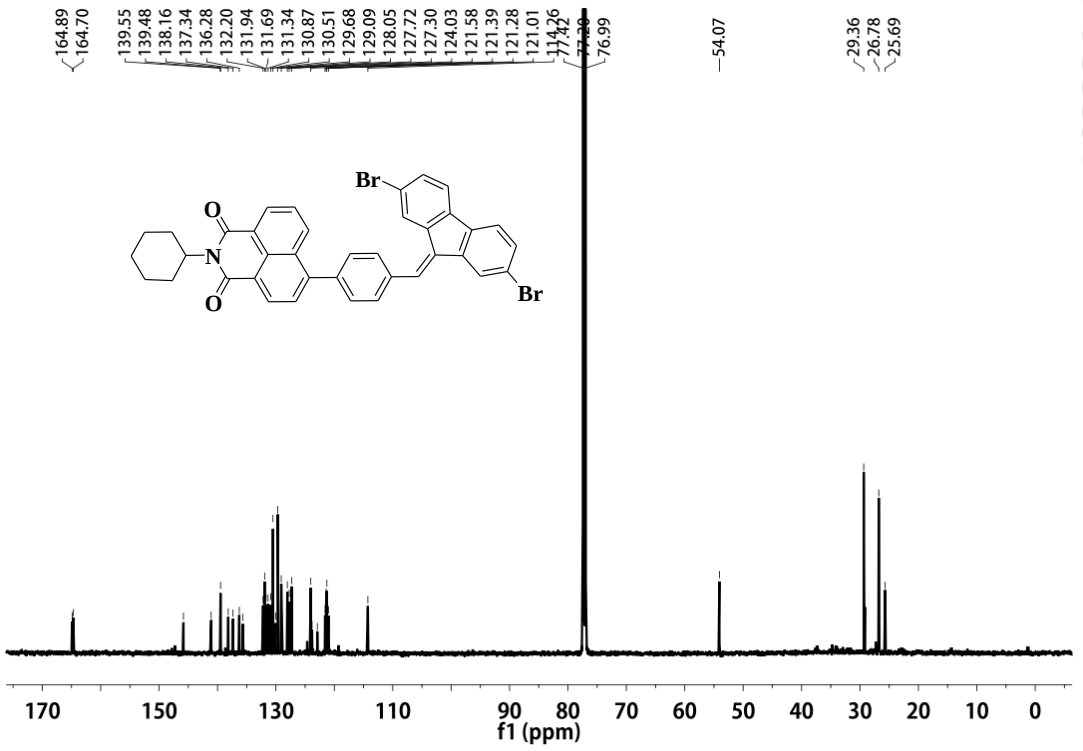

Figure 6.23: The ^{13}C NMR of the **DP2NC** in $CDCl_3$

Sample Name	Unavailable	**Position**	Unavailable	**Instrument Name**	Unavailable	**User Name**	Unavailable
Inj Vol	Unavailable	**InjPosition**	Unavailable	**SampleType**	Unavailable	**IRM Calibration Status**	All Ions Missed
Data Filename	DP2-NC-1.d	**ACQ Method**		**Comment**	Sample information is unavailable	**Acquired Time**	Unavailable

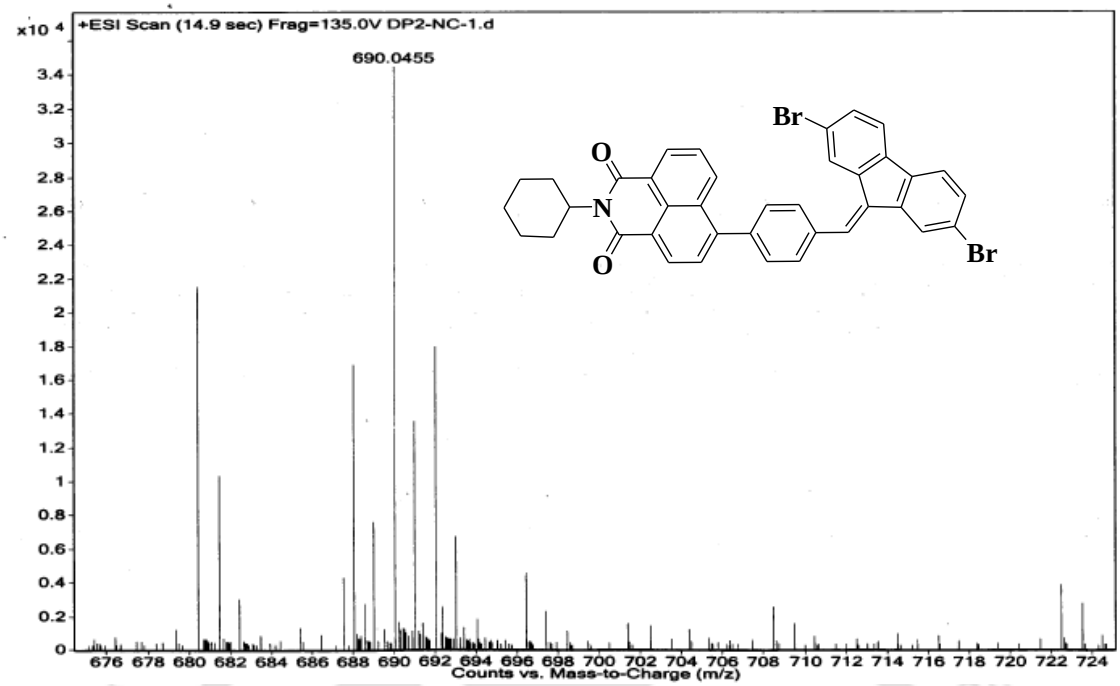

Figure 6.24: HRMS of the **DP2NC**

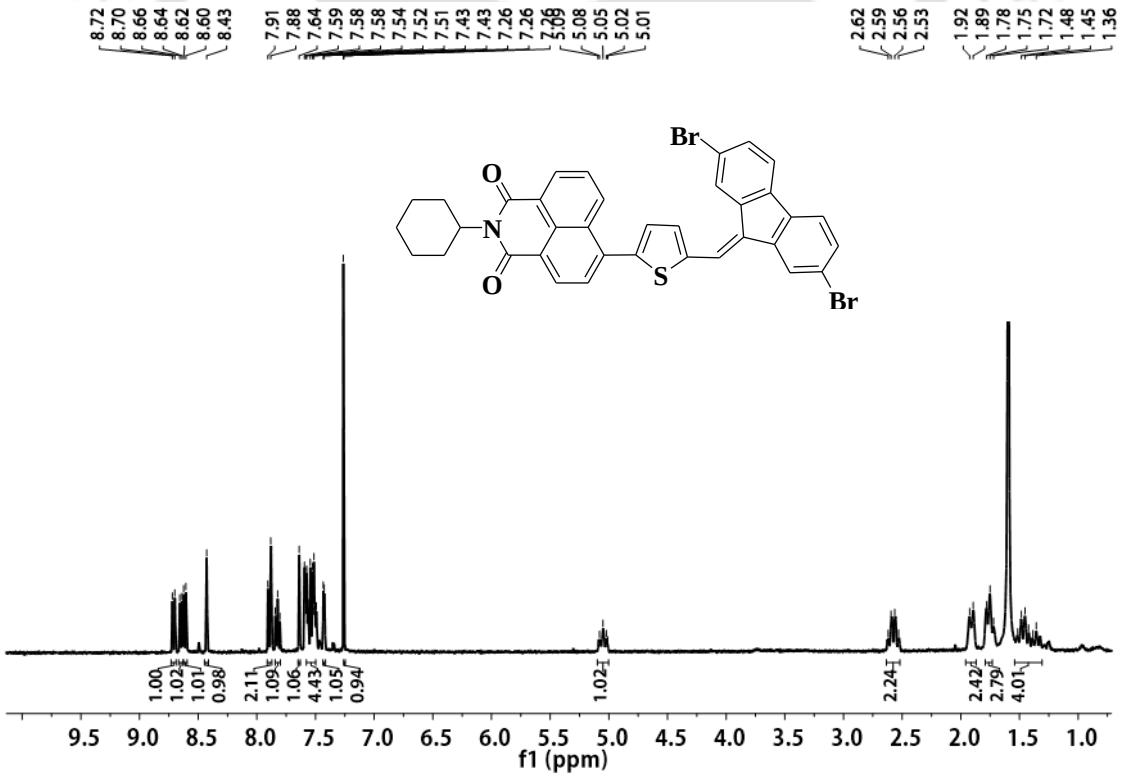

Figure 6.25: The ^{1}H NMR of the **DT2NC** in $CDCl_3$

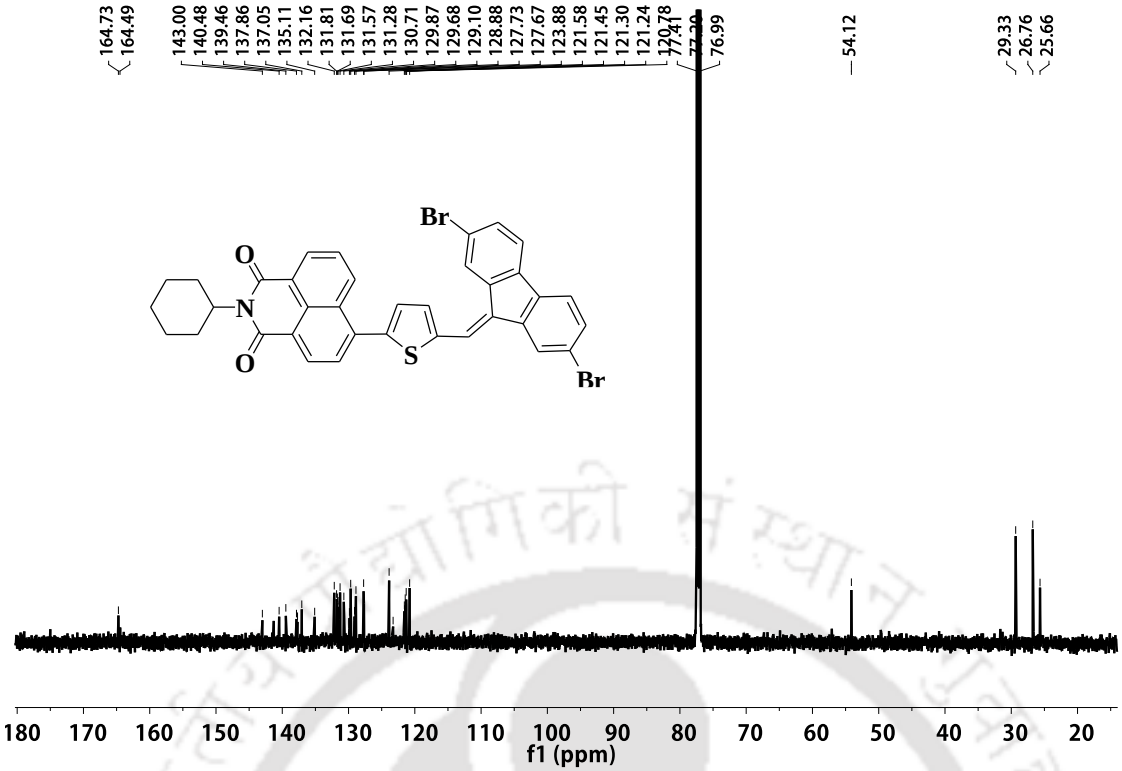

Figure 6.26: The ^{13}C NMR of the **DT2NC** in $CDCl_3$

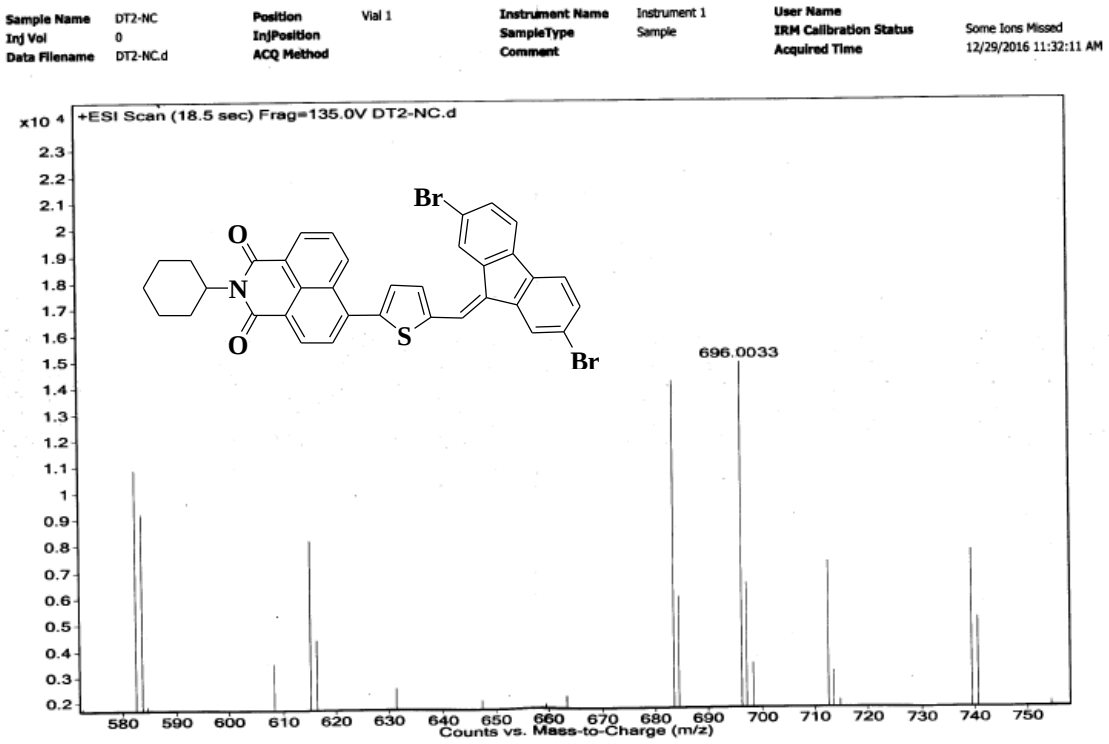

Figure 4.27: HRMS of the **DT2NC**

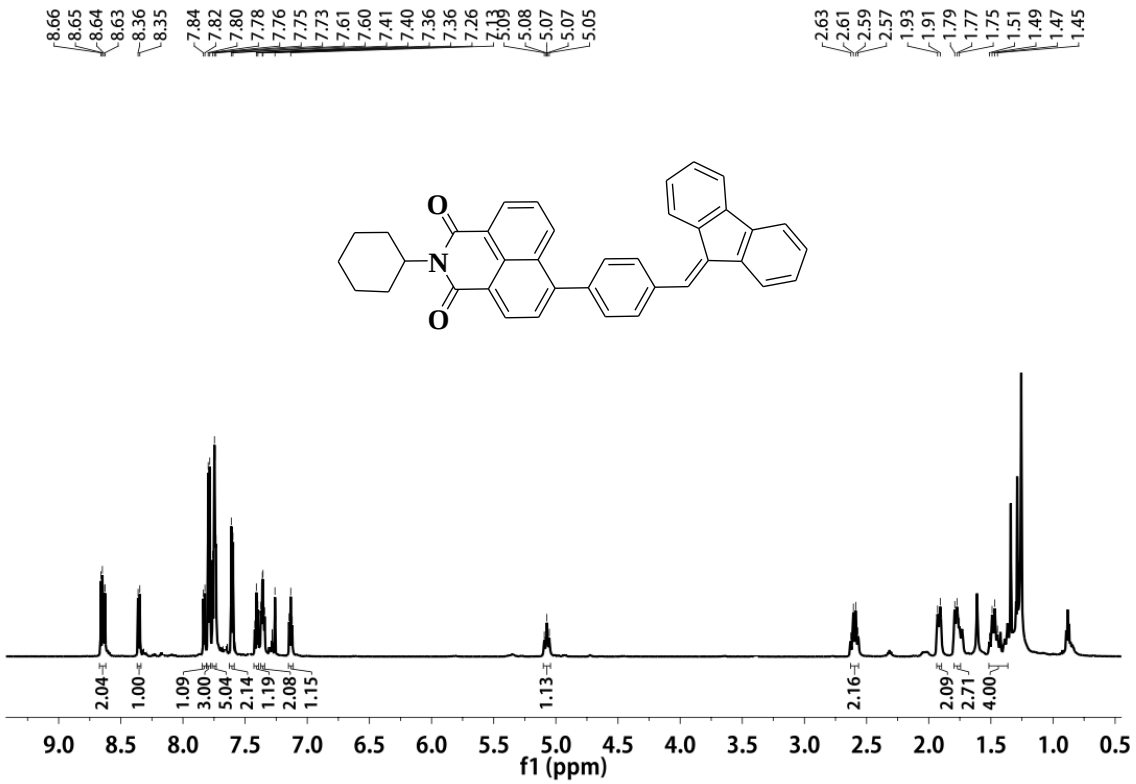

Figure 6.28: The ^{1}H NMR of the **DP1NC** in $CDCl_3$

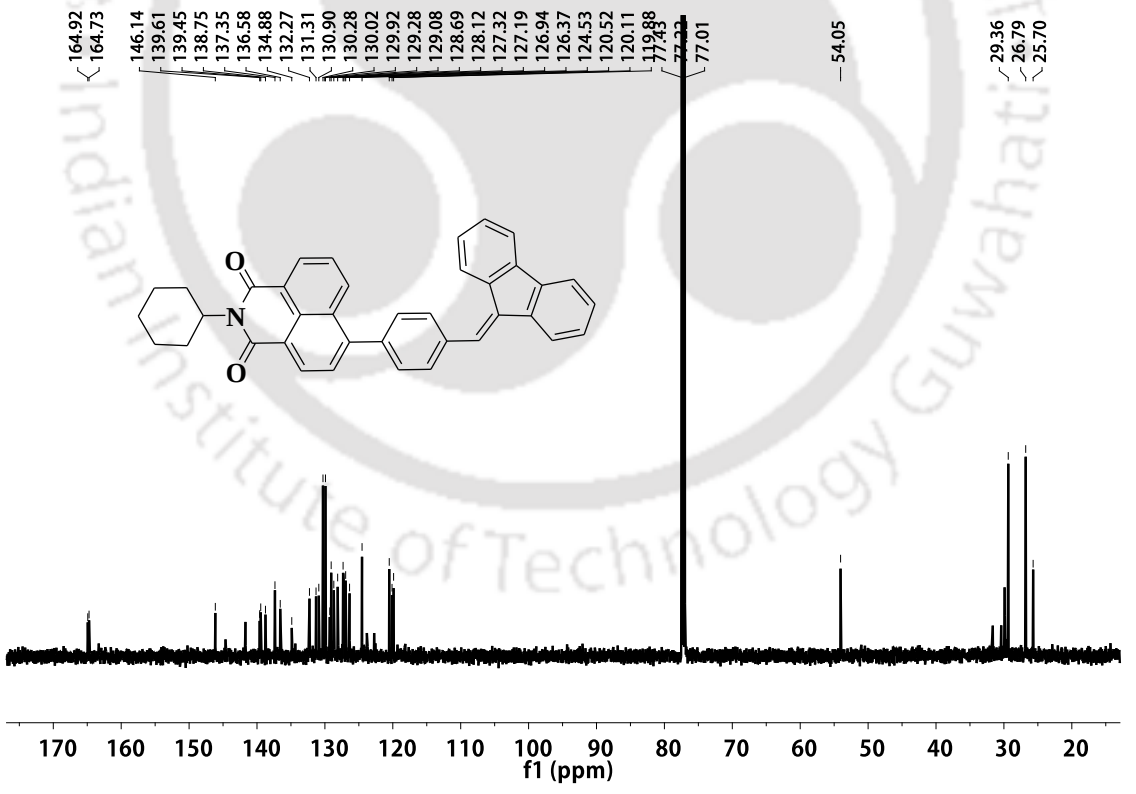

Figure 6.29: The ^{13}C NMR of the **DP1NC** in $CDCl_3$

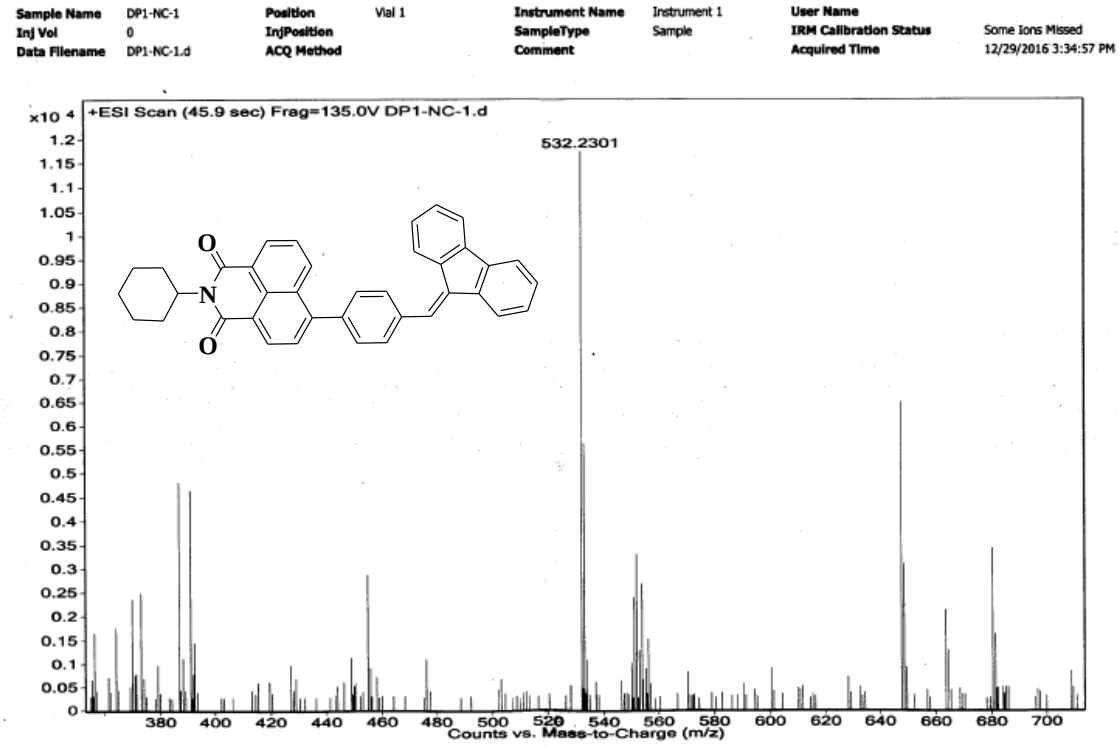

Figure 6.30: HRMS of the **DP1NC**

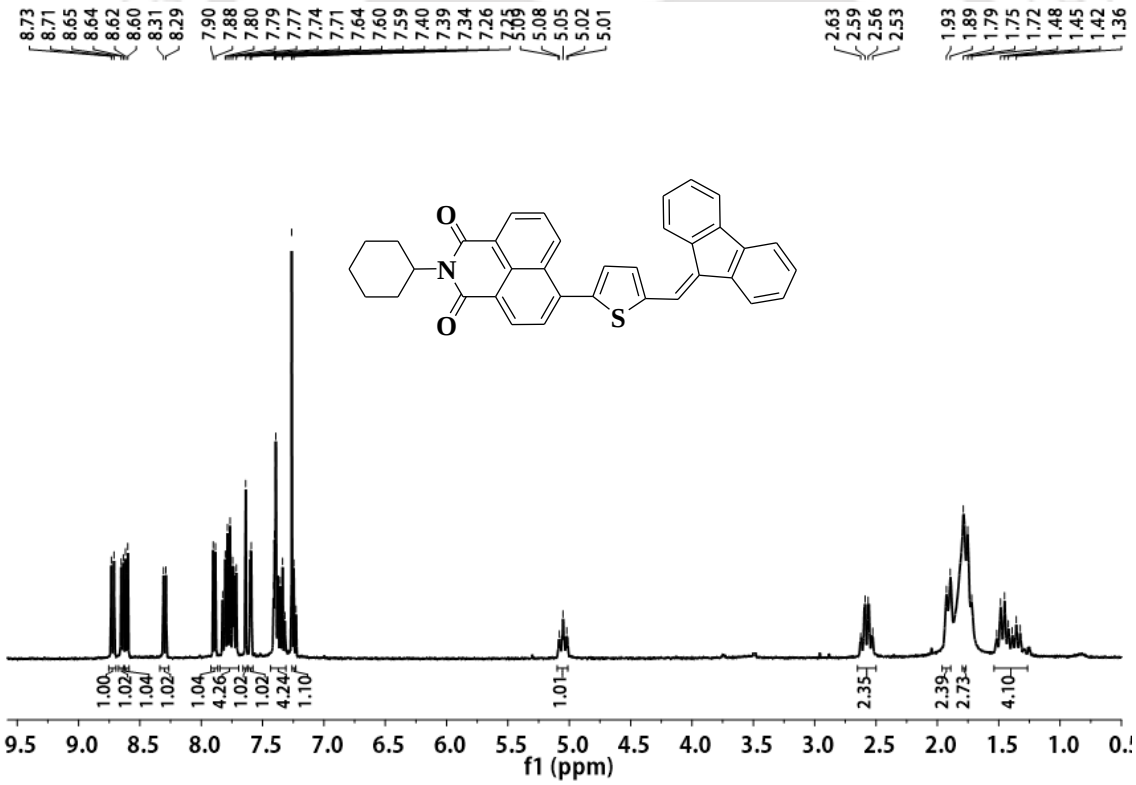

Figure 6.31: The ^{1}H NMR of the **DT1NC** in $CDCl_3$

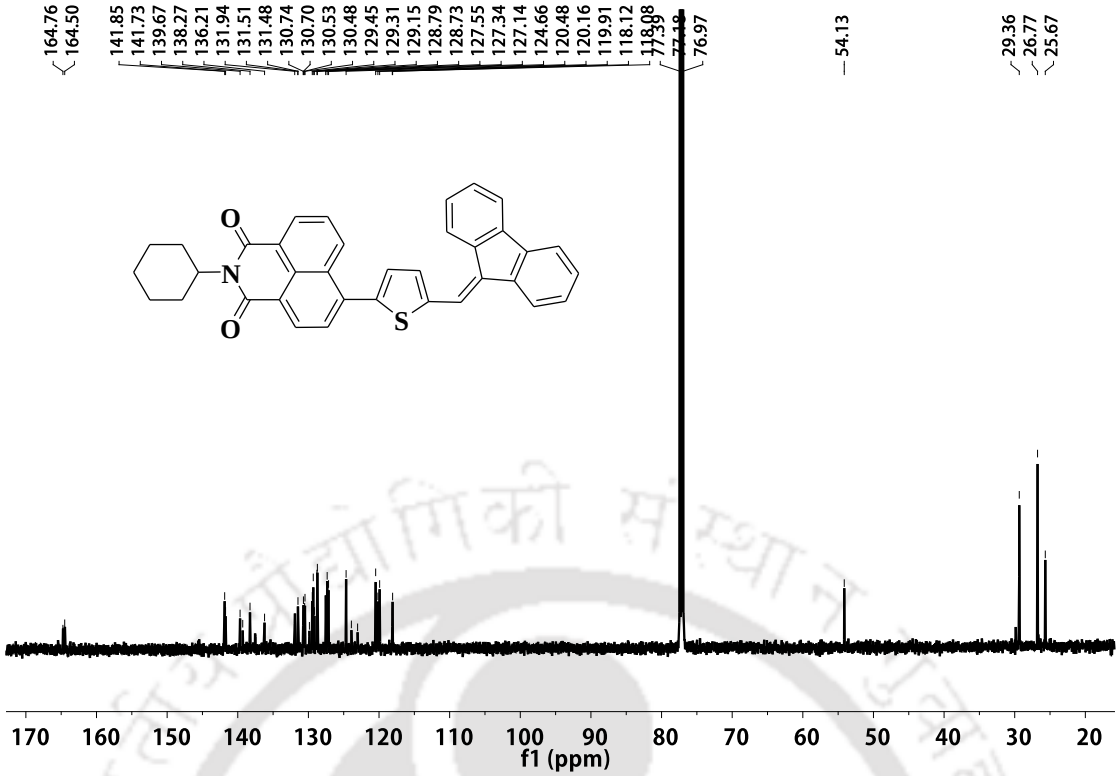

Figure 6.32: The ^{13}C NMR of the **DT1NC** in $CDCl_3$

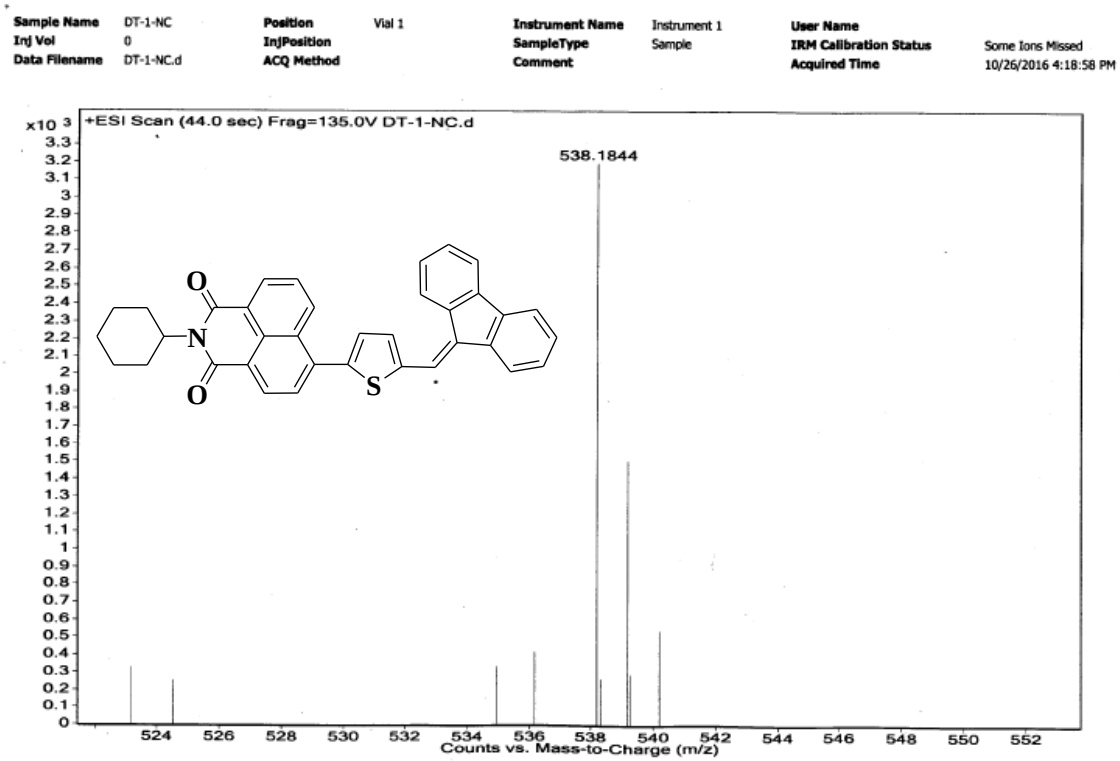

Figure 6.33: HRMS of the **DT1NC**

Summary

Chapter 1 details brief introduction of organic semiconductors materials, history of electroluminescence, basic structure of organic light emitting diode and its working principle. Recent developments conjugated materials including monomer and polymers and their OLED fabrication, followed by some most commonly used hole and electron transporting materials and brief introduction of AIE active materials and their device performances.

Chapter 2 provides a series of six new donor-acceptor electroluminescent copolymers were synthesised using Suzuki polymerization from 9,9'-dioctylfluorene (DOF) as donor and N-phenyl-1,8-naphthalimide (NPN) as acceptor. These copolymers exhibited excellent thermal stability with an onset decomposition temperature (T_d) in the range of 340-405 °C and a glass transition temperature (T_g) in the range of 123-134 °C. All the copolymers are highly fluorescent and soluble in common organic solvents, such as chlorobenzene, chloroform, dichloromethane, THF, etc. allowing their processing from desired solvent. The electroluminescence (EL) properties of the copolymers were also studied by fabricating single layer devices with ITO/PEDOT:PSS/PFONPN/Ca:Al configuration. The emission color of the copolymers have tuned from blue to green with Commission International de l'Echairage (CIE) coordinates being (0.17, 0.22) to (0.24, 0.49) by changing the feed ratios from 0% to 50% of NPN. This color tuning can be attributed to the strong energy transfer from the fluorene to NPN unit in the polymer backbone. The devices made using these copolymers are found to be very bright with PFONPN01 giving the highest brightness of 5236 cd m^{-2} with a luminous efficiency of 3.52 cd A^{-1}.

Chapter 3 mainly presents a series of novel color tunable donor-acceptor conjugated copolymers (CPs) which were developed from N-octylcarbazole (Cz-O) and N-phenyl-1,8-naphthalimide (N-PN) with a combination of feed ratios of Cz-O and N-PN (50:50, 65:35, 75:25, 90:10, 95:05 and 99:01). The copolymers exhibit desirable solubility in organic solvents, color tunability from blue to orange and desired electrochemical properties and are utilized for PLED fabrication. The PL emissions of the CPs are red shifted steadily with increase in the N-PN content in the CP main chains. PLEDs are fabricated using these newly developed CPs as emissive layer (EML) in ITO/PEDOT:PSS/PCzN-PN/BCP/LiF/Al configuration. Among all devices, PLEDs using PCzN-PN05 copolymer as EML is found to give the best device performance with maximum brightness of 309 cd m^{-2} and 0.451 cd A^{-1} luminous efficiency.

Chapter 4 discusses the aggregation-induced emission enhancement (AIEE) phenomenon in the deep red wavelength region, dual state emission, and intramolecular charge transfer of dibenzofulvene (DBF) derivatives is described. These consist of a series of newly synthesized donor-acceptor based M-DBF molecules (DT1, DT2, DP1, and DP2) with their cores comprising DBF molecules. The photophysical properties reveal that thiophene-substituted at the ninth position of DBF, viz. DT1 and DT2, displayed AIEE with predominant J-type aggregation. On the other hand phenyl substituted DP1 and DP2 luminogens, an extra phenyl ring was inserted at the ninth position of DBFs (between thiophene and DBF) that resulted in a blue-shift (~60 nm) as compared to the DT derivatives and exhibited a unique dual state emission with good quantum yields. This additional phenyl moiety reduces the effective conjugation length toward 2,1,3-benzothiadiazole from DBF and simultaneously interrupts the head to tail interaction and also prevents the J-type aggregation. All the four luminogens exhibited distinctive solvent-dependent photoluminescence (PL) behavior (solvatochromism) because of the efficient intramolecular charge transfer. The DT2 and DP2 luminogens showed heavy atom effect due to the presence of two bromine atoms. These new AIEE active luminogens are likely to stimulate interest in academic research as well as industry with applications in bio-imaging, organic light emitting diodes and other optical applications due to their high quantum yields even in aggregated form.

Chapter 5 highlights two class of new electroluminescent copolymers were synthesised and WPLED fabricated based on polyfluorene and aggregation-induced emission enhancement (AIEE) active or dual state emitting, mono-substituted dibenzofulvene (M-DBF) derivatives. The mol % of M-DBF monomer based small π-systems have been optimized as low as 0.0003, 0.0006, and 0.001%. Here, the utilization of "dual emission" peaks from PFO and M-DBFs in the blue and orange region that enabled the fabrication of bias-independent WPLEDs which is fundamentally very important and highly challenging in the case of linear polymers has been reported. These copolymers showed excellent solubility in organic solvents viz. $CHCl_3$, THF, toluene, p-xylene, etc. WPLEDs with ITO/PEDOT:PSS/WDP or WDT/TPBi/LiF/Al configurations were also fabricated to study their electroluminescence (EL) properties. Partial energy transfer has been achieved by adjusting the PFO and DT or DP concentrations in the single polymer main chain leading to the white emission in a facile manner. The copolymers WDP-1 and WDT-1 gave saturated white emission with CIE coordinates of (0.31, 0.33) and (0.35, 0.34) between 8-14 voltages and exhibiting excellent voltage independent emission. The

highest luminous efficiencies of 7.82 and 4.57 cd A^{-1} were achieved for WDP and WDT polymers with the highest brightness values of 9753 and 7436 cd m^{-2}, respectively. This unique approach is provides to generate stable white emission from linear single layer copolymers by incorporating AIE active and dual state emitting small π-system luminogen materials in a polymer main chain.

Chapter 6 provide D-π-A AIEE active and inactive materials were synthesized based on 1,8-naphthalimide (NC) and mono-substituted dibenzofulvene. The photophysical and thermal properties were highly dependent on the bridge between donor and acceptor. Two luminogens were substituted by thiophene bridge (DT1NC and DT2NC) while the two other luminogens substituted by phenyl bridge (DP1NC and DP2NC) between NC and dibenzofulvene (DBF) units. DT1NC and DT2NC displayed aggregation induced emission enhancement (AIEE) behaviour. They also showed orange and red emission (575 nm and 602 nm), respectively with large bathochromic shifts (35 nm and 112 nm) and high quantum yields (84.10% and 65.65%) in the aggregated state due to ladder type J-aggregation. DP1NC exhibited weak AIEE behaviour in blue region while DP2NC showed AIE inactive nature due to the strong C-H···π intermolecular interactions. All luminogens showed positive solvatochromism caused by intramolecular charge transfer (ICT). The DT2NC and DP2NC luminogens were substituted with two extra bromine atoms at 2,7 positions of DBF moiety, but unexpectedly the DT2NC showed strong heavy atom effect. All luminogens displayed excellent thermal stabilities. The experimental and theoretical studies strongly supported that these color-tunable luminogens could contribute significantly in the field of OLEDs and multicolor bio-imaging applications

List of Publications

1. **Gopikrishna, P.;** Meher, N.; Iyer, P. K. Functional 1,8-Naphthalimide AIE/AIEE Based Materials: Recent Advances and Prospects. *ACS Appl. Mater. Interfaces* **2018**, *10*, 12081-12111.

2. **Gopikrishna, P.;** Adil, L. R.; Iyer, P. K. Bridge-Driven Aggregation control in Dibenzofulvene-Naphthalimide Based Donor-Bridge-Acceptor Systems: Enabling Fluorescence Enhancement, Blue to Red Emission and Solvatochromism, *Mater. Chem. Front.* **2017,** *1*, 2590-2598.

3. **Gopikrishna, P.;** Das, D.; Adil, L. R.; Iyer, P. K. Saturated and Stable White Electroluminescence from Linear Single Polymer Systems based on Polyfluorene and Mono-Substituted Dibenzofulvene Derivatives, *J. Phys. Chem. C* **2017**, *121*, 18137-18143.

4. **Gopikrishna, P.;** Das, D.; Iyer, P. K. Color Tunable Donor-Acceptor Electroluminescent Copolymers: Synthesis, Characterization, Photophysical Properties and PLED Fabrication, *ChemistrySelect*, **2017,** *2*, 7044-7049.

5. **Gopikrishna, P.;** Iyer, P. K. Monosubstituted Dibenzofulvene-Based Luminogens: Aggregation-Induced Emission Enhancement and Dual-State Emission, *J. Phys. Chem. C* **2016**, *120*, 26556-26568.

6. **Gopikrishna, P.;** Das, D.; Iyer, P. K. Synthesis and Characterization of Color Tunable, Highly Electroluminescent Copolymers of Polyfluorene By Incorporating the N-Phenyl-1,8- Naphthalimide Moiety into the Main Chain, *J. Mater. Chem. C.* **2015,** *3*, 9318-9326.

7. **Gopikrishna, P.;** Das, S.; Mukherjee, S.; Patra, C. R.; Iyer, P. K. Mono-Substituted Dibenzofulvene based AIEE and Dual State Emitting Luminogens for Cell Imaging. (***Communicated***)

8. Das, D.; **Gopikrishna, P.;** Singh, A.; Dey, A.; Iyer, P. K. Solution Processed WPLEDs with Good Color Stability and High Color Rendering Index via a Phosphor-Sensitized System, *ChemistrySelect*, **2017**, *2*, 3184-3190.

9. Das, D.; **Gopikrishna, P.;** Narasimhan, R.; Singh, A.; Dey, A.; Iyer, P. K. White Polymer Light Emitting Diodes based on PVK: the Effect of the Electron Injection Barrier on Transport Properties, Electroluminescence and Controlling the Electroplex Formation, *Phys. Chem. Chem. Phys.* **2016,** *18*, 33077-33084.

10. Das, D.; **Gopikrishna, P.;** Ashish Singh.; Anamika Dey.; Iyer, P. K. Efficient Blue and White Polymer Light Emitting Diodes based on a Well Charge Balanced, Core Modified Polyfluorene Derivative, *Phys. Chem. Chem. Phys.* **2016**, *18*, 7389-7394.

11. Das, D.; **Gopikrishna, P.;** Singh, A.; Dey, A.; Iyer, P. K. Influence of Emissive Layer Thickness on Electrical Characteristics of Polyfluorene Copolymer based

Polymer Light Emitting Diodes, *Journal of Physics: Conference Series.* **2016**, *704*, 012016.

12. Raju, B. T.; **Gopikrishna, P.;** Iyer, P. K. Highly Efficient and Facile Alkylation of 4Hcyclopenta-[2,1-b:3,4-b']dithiophene in Water, *RSC Adv.* **2014,** *4*, 37738-37745.

13. Narasimhan, R .; **Gopikrishna, P.;** Das, D.; Iyer, P. K. Solution Processed Bistable Electrical Memory Device Containing Tunable Single Chain Donor-Acceptor Polymer Exhibits Remarkably High Ion/Ioff Ratio at Ambient Conditions. (***Communicated***)

14. Raju, T. B.; **Gopikrishna, P.;** Vaghasiya, J. V.; Soni, S. S.; Iyer, P. K. The Solvatochromism and Aggregation-Induced Enhance Emission of Triphenylamine Substituted Styrene Derivatives and its Application in Dye Sensitized Solar Cells. (***Communicated***)

Conferences

1. Yong Scientists Colloquium held on 11th October, 2017 at IIEST Shibpur, India.
2. International Conference on Sophisticated Instruments in Modern Research from 30th June -1st July, 2017 at Central Instruments facility IIT Guwahati India.
3. 3rd National Workshop on MEMS/NEMS and Theranostic Devices held during 21st to 23rd February, Centre for Nanotechnology 2017 IIT Guwahati India.
4. Research Conclave from 16th-19th March, 2017, at IIT Guwahati, Assam, India.
5. Fourth International Symposium on Semiconductor materials and Devices (ISSMD-4) 8th -10th, March, 2017 School of materials Science and Nanotechnology, Jadavpur University Kolkata, India. **(Selected for best poster presentation)**
6. 20th CSRI National Symposium in Chemistry (CSRI NSC-19) from 3rd -5th February, 2017, organized by Department of Chemistry, Gauhati University, Guwahati, India.
7. 19th CSRI National Symposium in Chemistry (CSRI NSC-19) from 14th -16th July, 2016 at University of North Bengal, India.
8. 2nd National Workshop on MEMS/NEMS and Theranostic Devices held during 21st to 22nd February, Centre for Nanotechnology 2017 IIT Guwahati, India.
9. Research Conclave from 23rd -26th March, 2015, at IIT Guwahati, Assam, India.
10. International Conference on Advanced Nanomaterials and Nanotechnology (Nanos-2015) held at GITAM University from 14th -17th Dec 2015, Visakhapatnam, India.
11. 4th International Conference on Advanced Nanomaterials and Nanotechnology (ICANN-2015) held at IIT Guwahati, Guwahati, during Dec 8th -10th, 2015.
12. 2-Day Familiarization Workshop on Nanofabrication Technologies, from 25th -26th April, 2015, at Tezpur University, Assam, India.
13. National Workshop on MEMS/NEMS and Theranostic Devices (NWNTD), from March 16th-17th, 2015, at IIT Guwahati, Assam, India.
14. 3rdInternational Conference on Advanced Nanomaterials and Nanotechnology (ICANN-2013) held at IIT Guwahati, Guwahati, during Dec 1st -3rd, 2013.